U.PORTO

Doutoramento
Ciências Biomédicas

Mechanisms of actin cytoskeletal dynamics in oligodendrocyte biology and myelin formation

Maria Manuela Azevedo

D
2018

U.PORTO

Maria Azevedo

Mechanisms of actin cytoskeletal dynamics in OLs biology and myelin formation

D.ICBAS **2018**

Mechanisms of actin cytoskeletal dynamics in OLs biology and myelin formation

Maria Manuela Azevedo

INSTITUTO DE CIÊNCIAS BIOMÉDICAS ABEL SALAZAR

Maria Manuela Coutinho Alves de Azevedo

MECHANISMS OF ACTIN CYTOSKELETAL DYNAMICS IN OLIGODENDROCYTE BIOLOGY AND MYELIN FORMATION

Tese de Candidatura ao grau de Doutor em Ciências Biomédicas submetida ao Instituto de Ciências Biomédicas Abel Salazar da Universidade do Porto.

Orientador – Doutor João Carlos Bettencourt de Medeiros Relvas

Categoria – Investigador Principal

Afiliação – Instituto de Biologia Molecular e Celular; Instituto de Investigação e Inovação em Saúde - Porto

Co-orientadora – Doutora Ana Isabel Barreira Seixas

Categoria – Investigadora

Afiliação – Instituto de Biologia Molecular e Celular; Instituto de Investigação e Inovação em Saúde – Porto

Co-orientadora Tutora – Doutora Maria do Rosário Almeida

Categoria – Professora Associada

Afiliação – Instituto de Biologia Molecular e Celular; Instituto de Investigação e Inovação em Saúde; Instituto de Ciências Biomédicas Abel Salazar – Porto

Foi utilizado nesta tese o artigo publicado:

*__Azevedo, M. M.__, *Domingues, H. S., Cordelières, F. P., Sampaio, P., Seixas, A. I., & Relvas, J. B. (2018). Jmy regulates oligodendrocyte differentiation via modulation of actin cytoskeleton dynamics. *Glia*, 1-19. doi:10.1002/glia.23342

*Maria M. Azevedo e Helena S. Domingues são co-primeiras autoras.

This thesis was written based on the published manuscript:

*__Azevedo, M. M.__, *Domingues, H. S., Cordelières, F. P., Sampaio, P., Seixas, A. I., & Relvas, J. B. (2018). Jmy regulates oligodendrocyte differentiation via modulation of actin cytoskeleton dynamics. *Glia*, 1-19. doi:10.1002/glia.23342

*Maria M. Azevedo and Helena S. Domingues are co-first authors.

Este trabalho foi co-financiado pela Fundação para a Ciência e Tecnologia (FCT), Portugal, através de uma bolsa de doutoramento (SFRH/BD/90301/2012) e do projecto PTDC/SAU/NMC/119937/2010.

The work presented in this thesis was co-funded by Fundação para a Ciência e Tecnologia (FCT), Portugal, through a doctoral fellowship (SFRH/BD/90301/2012) and grant PTDC/SAU/NMC/119937/2010.

Acknowledgements / Agradecimentos

Chegado o final desta viagem, resta agradecer a todas as pessoas que, de alguma forma, foram intervenientes e permitiram que tal acontecesse:

Ao meu orientador, Doutor João Relvas, gostaria de agradecer a oportunidade que me deu, de me juntar à sua equipa de investigação. Sem qualquer dúvida ou hesitação aceitou-me como sua aluna de doutoramento, o que para mim significou muito. Obrigada João pela partilha de conhecimento e pelo voto de confiança.

À Professora Maria do Rosário gostaria de agradecer por toda a disponibilidade que sempre mostrou para ajudar em qualquer situação. A sua simpatia e positividade sempre tornaram a burocracia e os pequenos sobressaltos mais fáceis de resolver. O meu muito obrigada Professora Rosário.

À minha co-orientadora, Doutora Ana Seixas (ou mais facilmente AS), gostaria de agradecer pelo acompanhamento, pela ajuda, pela confiança, por ter partilhado comigo o conhecimento que tem, por me ter puxado para fora da minha zona de conforto... obrigada pelas brincadeiras no laboratório que ajudaram a tornar as longas horas de trabalho um pouco mais leves... obrigada pelo chili maravilhoso!!! Obrigada por teres estado ao meu lado, por te teres tornado uma amiga sempre disponível e sempre presente... Sei que não é fácil lidar com o "Sino" mas tu lá conseguiste. Muito obrigada querida AS!

À Joana Paes o meu obrigada pela constante presença e disponibilidade para ajudar. Obrigada por todas as palavras de motivação e incentivo... Obrigada pela ajuda nos momentos em que de facto estava como um "Sino"!!! Obrigada pelos momentos descontraídos de fofocas do mundo dos famosos. Obrigada pela confiança e por te teres tornado, também tu, numa grande amiga sempre disponível (pessoalmente porque por telemóvel é outro assunto =p). Muito obrigada querida Pães de Farinha!

À Lígia Tavares (LT) obrigada por teres aceite ser minha co-orientadora em primeiro lugar =). Apesar de os planos terem mudado, sempre estiveste pronta para tudo! Sempre tiveste uma palavra de incentivo, de desdramatização (porque também consigo ser uma "Drama Queen" às vezes), de força... Obrigada pela boa energia... Obrigada por me chibares ao grupo... Obrigada pelo sorriso e por me ouvires. Obrigada pela amizade!

À Doutora Paula Sampaio, ou querida PS/guru da microscopia/Professora, tenho imenso a agradecer... para começar muito obrigada por me ATURARES! Obrigada por me teres mostrado a beleza da microscopia! Obrigada por me teres ensinado tudo que sei sobre os ditos microscópios e imagem! Obrigada por todas as ajudas na definição de "focu", e intensidades de luz, e marcações intermináveis de microscópios, e no STED, e na análise de imagem... obrigada por me teres apresentado o Fábrice... e posso continuar a agradecer por

mais mil coisas diferentes, mas tu sabes que agradeço mesmo muito tudo o que fizeste por mim, e o facto de seres uma amiga que está sempre disponível para tudo... mesmo para responder a perguntas de “Sino”! Obrigada por não teres desistido de mim Paulinha!
A ti Raquel Silva (aka Cassandra), muito obrigada pela boa disposição matinal, pela partilha de soluções, pela constante disponibilidade para ajudar e claro, obrigada pelo apoio moral nas fases mais “artísticas” deste percurso!
Às “Sofias dos cabelos aos caracóis”, querida Sofia Domingues e Sofia Santos, gostaria de agradecer todo o companheirismo e a disponibilidade para ajudarem em qualquer situação! Obrigada pelas palavras de força e motivação!
À Carolina Lemos, obrigada por partilhares os teus conhecimentos comigo! Obrigada pela enorme ajuda na estatística... obrigada por me teres ensinado como usar o “bicho” do SPSS... obrigada por toda a paciência... muito obrigada Carolina!
À Cristina Ferrás, obrigada por todo o companheirismo e positividade! Foi graças ao Frankenstein, aka AxioVert, que os nossos caminhos se cruzaram e nos tornamos próximas! Quem diria xD.... Obrigada por teres tido sempre paciência para me ouvir e uma palavra amiga para me dizer! Obrigada pelas tuas doses de loucura! Obrigada por teres estado presente!
À Andreia Carvalho (querida Pipa!), muito obrigada por me teres ensinado algumas coisas de bioquímica... incluindo a fazer os famosos saquinhos! Obrigada por toda a ajuda fora do lab! Obrigada por estares sempre disponível! Devias continuar a ser a nossa vizinha da frente porque tenho saudades tuas!!!
À Ana Abreu, obrigada por todos os momentos que partilhamos no lab e fora dele! Obrigada por seres uma grande maluca que tem sempre uma palavra amiga para dizer! Fazes falta!
A ti minha querida Médica (aka Catarina Carolina Alanis Morissette), obrigada por toda a amizade! Obrigada por seres uma querida que está sempre disponível para dar apoio e para dar uma consulta grátis (sei que às vezes, se fosse possível, fugias dessas consultas xD)!!!
A ti querida Ana Keating, obrigada por seres a pessoa maravilhosa que és. Obrigada por toda a força e positividade que sempre transmites!
Aos queridos “ex-Nervos”, Tiago Silva (aka GFP) e Rita Malheiro (aka Ritinha), muito obrigada pela vossa amizade, pela boa disposição, pelas conversas... pela ajuda a nível científico que sempre passou pela recetividade para: 1) desenrascar qualquer tipo de material e/ou reagentes, 2) desenrascar uma câmara de fluxo 3) ensinar técnicas de dissecação fantásticas tipo “a técnica da sardinha” xD, entre muitas outras... muito obrigada aos dois por tudo!
Aos eternos queridos vizinhos Cláudia Grou, “Manel”, Tony e Tânia, obrigada por toda a simpatia, ajuda, partilha de reagentes entre muitas outras coisas... obrigada por tudo queridos vizinhos!
À Paula Magalhães, obrigada por toda a simpatia, boa disposição e ajuda ao longo destes anos! Apesar das minhas “queixinhas” nunca me expulsaste do serviço =). Obrigada!

À Dona Isabel (Isabel Duarte), obrigada por toda a ajuda em relação ao biotério! Obrigada por ter estado sempre disponível para os meus pedidos com "pressões" associadas, por ter estado sempre disponível para solucionar os pequenos problemas que surgiam. Obrigada Isabel!

A ti Susana Sampaio, muito obrigada por teres estado sempre disponível para me ouvir e teres tido sempre uma palavra de conforto! Obrigada por seres uma amiga presente! Mesmo longe estás sempre perto!

A ti Renata Costa, minha querida Vet, muito obrigada por teres sido companheira nesta aventura, mesmo que à distância! Obrigada pelos momentos de alegria e boa disposição que passamos juntas! Obrigada por estares sempre presente!

A ti, querida Vanessa Machado, muito obrigada por tudooooooooo... por ouvires as queixas e as parvoíces que não fazem qualquer sentido... obrigada por opinares sobre os meus gostos musicais (NOT!)... obrigada por apesar da distância e das tuas coisas estares sempre disponível! Miss you!

A vocês Paula Rolo, Pedro Cardante, Fatinha, obrigada por não desistirem de mim! Apesar da ausência constante vocês são o meu suporte! Sei que estão sempre disponíveis para tudo o que eu precisar! Recebem-me sempre de braços abertos e procuram sempre perceber como é que eu estou! Vocês são únicos e fazem-me imensa falta! Estou ansiosa por termos um jantar para matar todas as saudades e pôr a conversa em dia!!!

A ti Pedro Meira, obrigada pela constante presença. Obrigada por me fazeres sorrir mesmo nos momentos mais difíceis.

Ao meu irmão e madrinha, obrigada por estarem sempre presentes e por sempre terem ajudado para que tudo isto fosse possível! Obrigada pelo ano fantástico que vivi com vocês! Obrigada por serem os melhores!

A ti Mãe, obrigada por tudo. Sim, a ti devo tudo! Obrigada por todos os esforços que fizeste por mim... obrigada por teres lutado sempre por mim e me teres dado sempre força para continuar! Foi graças a ti que cheguei até aqui e, é a ti que dedico esta conquista. Obrigada!

Tenho a certeza que muito fica por dizer... Assim, acabo por agradecer em geral a todas as pessoas do meu laboratório e aos "outsiders" que fizeram parte desta viagem de alguma forma... não se faz ciência sozinho... o meu muito obrigada a TODOS!

Table of Contents

ABSTRACT / RESUMO

Abstract

During central nervous system (CNS) development, oligodendrocytes form structurally and functionally distinct actin-rich protrusions that, upon axonal contact, transform into flat sheets that spread and wrap around axons to generate a multilayered stack of membranes. The resulting myelin sheath acts as an insulator, facilitating the rapid saltatory conduction of electrical signals along axons. The morphological differentiation of oligodendrocytes is a pre-requisite for myelination. From a less complex morphology, characterized by a mainly bipolar shape, to an extremely complex architecture, necessary for the establishment and stabilization of axonal contacts, oligodendrocytes undergo successive morphological changes with the extension of multiple dynamic protrusions. Establishment of axonal contact is a limiting step in myelination that relies on the oligodendrocyte's ability to locally coordinate cytoskeletal rearrangements with myelin production, under the control of a transcriptional differentiation program. mRNAs encoding proteins related to cytoskeleton dynamics are enriched in newly-formed protrusions of oligodendrocyte progenitor cells (OPCs), supporting the idea that morphological plasticity is important for differentiation. Failure to differentiate or to establish axonal contact compromises myelination and, ultimately, results in delayed or disrupted signal transmission, illustrated in the CNS by the severe neurological consequences of dysmyelinating diseases. Despite the importance of oligodendrocyte differentiation for myelination, the molecules that provide fine-tuning of actin dynamics during this biological process remain largely unidentified.

The junction mediating and regulatory protein (Jmy), initially reported as a cofactor of the transcriptional regulator p300/CBP involved in the p53 response, is a multifunctional regulator of actin polymerization, highly expressed in brain and testis. *Jmy* is found ubiquitously but, in the brain, it has higher expression in endothelial cells and newly-formed oligodendrocytes. Interestingly, *Jmy* transcripts were found to be enriched in newly-formed protrusions of OPCs. Therefore, we sought to study how actin dynamics regulates oligodendrocyte differentiation and establishment of axonal contact, and how such events are controlled by the actin regulator Jmy.

Firstly, we examined the expression of Jmy *in vivo* during myelination of the developing CNS, using tissue from wild-type mice. We also assessed the expression profile of Jmy during oligodendrocyte differentiation *in vitro*. The histological characterization of Jmy expression in white matter tracts during developmental myelination showed that Jmy is: 1 - expressed by oligodendrocytes, and 2 - co-expressed with markers of pro-myelinating oligodendrocytes during the active phase of myelination. Moreover, the *in vitro* characterization of the expression profile of Jmy, in primary cultures of OPCs that were induced to differentiate, showed an upregulation of Jmy expression at the onset of differentiation, which was maintained as

oligodendrocytes matured further. Additionally, we found that Jmy is mainly located in the cytoplasm of oligodendrocytes, which suggests that, unlike in other cells, Jmy is probably regulated by expression levels and not only by subcellular localization.

To investigate the role of Jmy in oligodendrocyte differentiation, we performed a functional analysis by knocking down its expression. Morphological analysis revealed that Jmy is required for the assembly of actin filaments and protrusion formation during oligodendrocyte differentiation, since oligodendrocytes lacking expression of Jmy: 1) form less protrusions; 2) do not acquire an arborized morphology; 3) have an overall small area; 4) show decreased content of F-actin; and 5) show defects in the organization and displacement of actin filaments. Additionally, the ability of oligodendrocytes to form myelin-like sheath membranes was impaired, most likely due to the defects found in morphological differentiation, as the antigenic differentiation was not found to be affected upon Jmy knockdown. Furthermore, in a myelinating co-culture system, oligodendrocytes depleted of Jmy showed to be less efficient in contacting neurites and in forming myelin wraps.

For a better understanding of the real-time dynamics involved in oligodendrocyte differentiation, we followed this biological process using time-lapse microscopy. As expected, oligodendrocyte differentiation proved to be an extremely dynamic process that requires high protrusion remodeling, and during which cells undergo profound cytoskeleton rearrangements that follow a stereotypical “cellular shaping” program. Moreover, Jmy was found to be essential for morphological plasticity in oligodendrocytes, and for cells to follow the stereotypical “cellular shaping” program of differentiation.

The application of time-lapse imaging to our studies led to the acquisition of a large amount of data to be analyzed. As there is no available software for the analysis of phase-contrast images of such dynamic and complex cells, we developed an open source semi-automated ImageJ macro-toolset, which was able to follow oligodendrocyte dynamics at the spatiotemporal scale and extract quantitative parameters.

In summary, our study reveals an essential role of Jmy as a regulator of actin cytoskeleton dynamics in oligodendrocyte differentiation, contributing for a better understanding of the molecular machinery involved in this process.

Resumo

Durante o desenvolvimento do sistema nervoso central (SNC), os oligodendrócitos estendem protrusões ricas em actina, estrutural e funcionalmente distintas que, ao entrarem em contacto com o axónio, formam uma membrana que o envolve formando múltiplas camadas. A bainha de mielina resultante atua como isolante, facilitando a rápida condução de sinais elétricos ao longo dos axónios de uma forma saltatória. A diferenciação morfológica dos oligodendrócitos é um pré-requisito para a mielinização. A transição de uma morfologia menos complexa, caracterizada por uma forma bipolar, para uma arquitetura extremamente complexa que permite o contacto axonal, implica que os oligodendrócitos sofram sucessivas alterações morfológicas, caracterizadas pela extensão de múltiplas protrusões extremamente dinâmicas. O estabelecimento de contacto com o axónio é um passo limitante na mielinização que depende da capacidade do oligodendrócito coordenar localmente alterações do citoesqueleto com a produção de mielina, sob o controlo de um programa de diferenciação transcripcional. mRNAs que codificam proteínas relacionadas com a dinâmica do citoesqueleto encontram-se enriquecidos nas recém-formadas protrusões das células progenitoras de oligodendrócitos (OPCs), evidenciando a extrema importância de uma correta diferenciação morfológica. A falha deste processo biológico e consequente falha na mielinização resultam em alterações na transmissão dos sinais elétricos, que podem ser atrasados ou totalmente interrompidos, levando a graves consequências neurológicas, como o caso das doenças desmielinizantes. Apesar da elevada importância destes processos biológicos, as moléculas que regulam a dinâmica da actina durante a diferenciação de oligodendrócitos e o revestimento dos axónios permanecem, em grande parte, não identificadas.

A proteína *junction mediating and regulatory protein* (Jmy), inicialmente descrita como cofator do complexo regulador transcripcional p300/CBP, envolvida na resposta da via p53, é também um regulador multifuncional da polimerização da actina, altamente expressa no cérebro e nos testículos. O Jmy é expresso em diferentes células, sendo que no cérebro é maioritariamente expresso em células endoteliais e oligodendrócitos recém-formados. Igualmente interessante, o Jmy apresenta uma expressão enriquecida nas protrusões recém-formadas em OPCs. Neste trabalho, foi colocada a hipótese de que o Jmy poderá estar envolvido na regulação da dinâmica de actina durante a diferenciação de oligodendrócitos. O nosso objetivo passou por entender se a dinâmica do citoesqueleto de actina é importante durante a diferenciação de oligodendrócitos e no contacto/envolvimento dos axónios, e em que medida o Jmy, como regulador da polimerização de actina, pode estar envolvido neste processo.

Começámos por examinar a expressão de Jmy *in vivo* durante a mielinização do SNC ao longo do desenvolvimento, usando tecido de murganhos *wild-type*. Além disso, também determinámos o perfil de expressão do Jmy durante a diferenciação dos oligodendrócitos *in vitro*. A caracterização histológica da expressão de Jmy, ao longo dos tratos ricos em mielina durante o desenvolvimento, mostrou que o Jmy é: 1 – expresso em oligodendrócitos e, 2 - co-expresso com marcadores de oligodendrócitos *pro-myelinating* na fase ativa da mielinização. Além disso, a caracterização *in vitro* do perfil de expressão do Jmy, em culturas primárias de OPCs induzidas a diferenciar, mostrou uma sobre-expressão de Jmy nos primeiros dias de diferenciação, que se manteve ao longo da diferenciação. O estudo da localização subcelular do Jmy nos oligodendrócitos revelou que este está maioritariamente localizado no citoplasma destas células o que indica, contrariamente ao descrito para outras células, que o Jmy é provavelmente regulado através dos seus níveis de expressão e não pela sua localização subcelular.

De forma a investigar a função do Jmy na diferenciação dos oligodendrócitos, uma análise funcional foi feita por disrupção da expressão de Jmy. Através de uma avaliação morfológica, verificou-se que o Jmy é necessário para a formação de filamentos de actina e protrusões durante a diferenciação dos oligodendrócitos, uma vez que oligodendrócitos sem expressão de Jmy: 1) formam menos protrusões; 2) não adquirem morfologia arborizada; 3) têm uma área, em geral, pequena; 4) contêm menos F-actina; e 5) apresentam defeitos na organização e distribuição dos filamentos de actina. Além disso, a capacidade de os oligodendrócitos formarem membranas semelhantes à bainha de mielina está diminuída após a disrupção da expressão de Jmy, muito provavelmente devido às alterações morfológicas observadas, uma vez que não foram encontradas evidências de que a diferenciação antigénica dos oligodendrócitos seja afetada pela disrupção da expressão de Jmy. Adicionalmente, os oligodendrócitos depletados de Jmy mostraram ser menos eficientes no contacto com as neurites e na formação de mielina, quando em contacto com neurónios dos gânglios dorsais (DRGs).

Para uma melhor compreensão da dinâmica envolvida na diferenciação dos oligodendrócitos, experiências de *live cell imaging* foram realizadas, de forma a seguirmos este processo biológico em tempo real. Como esperado, a diferenciação de oligodendrócitos provou ser um processo extremamente dinâmico que requer elevada remodelação das protrusões, e onde as células passam por rearranjos profundos do citoesqueleto, seguindo um programa estereotipado de "modelação celular". Além disso, o Jmy mostrou ser essencial para a dinâmica dos oligodendrócitos, e para que as células sigam o programa estereotipado de "modelação celular", característico da diferenciação dos oligodendrócitos.

A aplicação da tecnologia de *live cell imaging* ao nosso estudo resultou na aquisição de uma grande quantidade de dados de imagem a serem analisados. Devido à não existência

de um software que permite a análise de imagens de contraste de fase de células dinâmicas e complexas, como os oligodendrócitos, desenvolvemos uma macro semiautomática para o ImageJ, com código disponível, que foi capaz de acompanhar a dinâmica morfológica dos oligodendrócitos ao longo do tempo.

Em resumo, o nosso estudo revela que o Jmy desempenha uma função preponderante como regulador da dinâmica do citoesqueleto de actina durante a diferenciação dos oligodendrócitos, o que contribui para uma melhor compreensão da maquinaria molecular envolvida no processo de diferenciação.

ABBREVIATIONS

Abbreviations

ABP - Actin-binding protein

ADF - Actin depolymerization factor

ADP - Adenosine di-phosphate

Arp - Actin-related protein

ATP - Adenosine tri-phosphate

BAB - Boric acid buffer

BBB - Blood brain barrier

BSA - Bovine serum albumin

CARMIL - Capping protein regulator and myosin-I linker homology 1

CNP - 2',3'-cyclic nucleotide 3' phosphodiesterase

CNS - Central nervous system

DAPI - 4’,6-diamidino-2-phenylindole

DIV - Days *in vitro*

DMEM - Dulbecco’s modified Eagle’s medium

DNA - Deoxyribonucleic acid

DOD - Days of differentiation

DRG - Dorsal root ganglia

E [number] - Embryonic day

ECM - Extracellular matrix

EdU - 5-Ethynyl-2´-deoxyuridine

EGFP - Enhanced GFP

EM - Electron microscopy

ENPP6 - Ectonucleotide pyrophosphatase/phosphodiesterase 6

ER - Endoplasmic reticulum

F-actin - Filamentous actin

FA - Focal adhesions

FACS - Fluorescence-activated cell sorting

FBS - Fetal bovine serum

FGF - Fibroblast growth factor

G-actin - Globular actin

GalC - Galactosylceramidase C

GC - Galactocerebroside

GDP - Guanosine diphosphate

GFP - Green fluorescence protein

GPR - G-protein regulatory

GSH2 - Genomic screened homeobox2
GTP - Guanosine triphosphate
HEK - Human embryonic kidney
HSP90 - Heat shock protein 90
ICC - Immunocytochemistry
IHC - Immunohistochemistry
Ilk - Integrin-linked kinase
Jmy - Junction mediating and regulatory protein, p53 cofactor
kDa - Kilodalton
Mag - Myelin associated glycoprotein
Mbp - Myelin basic protein
MEF - Mouse embryonic fibroblast
MGC - Mixed glial culture
Mog - Myelin oligodendrocyte glycoprotein
mRNA - messenger RNA
MS - Multiple Sclerosis
N-WASP - Neural Wiskott-Aldrich syndrome protein
NG2 - Chondroitin sulfate proteoglycan
NGF - Nerve growth factor
NGS - Normal goat serum
NLS - Nuclear localization sequence
NPF - Nucleation promoting factor
NSC - Neural stem cells
OL - Oligodendrocyte
ON - Optic nerve
OPC - Oligodendrocyte progenitor cell
P [number] - Post-natal day
PBS - Phosphate buffered saline
PDGFRα - Platelet-derived growth factor receptor α
PDL - Poly-D-lysine
Plp - Proteolipid protein
pMN - Motor neuron progenitor domain
RNA - Ribonucleic acid
RNAi - RNA interference
ROCK - Rho-associated kinase
ROI - Region of interest
RT-PCR - Real-time polymerase chain reaction

SC - Spinal cord
SEM - Standard error mean
shRNA - Short hairpin RNA
SiR - Silicon rhodamine
siRNA - Small interference RNA
STED - Stimulated emission depletion
TBS - Tris buffered saline
TEMED - N,N,N'N'-tetramethylethylene diamine
TUNEL - Terminal deoxynucleotidyl Transferase (TdT) dUTP Nick-End Labeling
U2OS - Human bone osteosarcoma epithelial cells
VASP - Vasodilator-stimulated phosphoprotein
VEGF - Vascular endothelial growth factor
WASP - Wiskott–Aldrich syndrome protein
WAVE - WASP family verprolin-homologous protein
WH2 - WASP homology 2
WHAMM - WAS Protein Homolog Associated with Actin, Golgi Membranes and Microtubules
WIP - WASP-interacting protein

GENERAL INTRODUCTION

Cells of the central nervous system

The central nervous system (CNS), consisting of the brain (including the optic nerve) and the spinal cord, is a complex system built up of neurons and glial cells. The two main subsets of glia in the CNS are the microglia and macroglia, which includes astrocytes and oligodendrocytes. Neurons and macroglia arise from neuroepithelial cells that line the lumen of the embryonic neural tube. Development of CNS neurons relies on a series of chronological events: regional proliferation of undifferentiated cells in different areas; cellular migration from the sites of origin; aggregation of cells to form different functional areas; differentiation of neurons; formation of connections between neurons giving rise to the so-called tracts; selective cell death; and elimination of some connections with parallel stabilization of others (Lazzarini, 2003). Glial precursors, with the exception of microglia, are generated in the ventricular regions from brain and spinal cord, migrating from these sites of origin toward their final destinations in response to external cues. Then, *in situ* maturation of glial precursors takes place, being followed by the establishment of connections between glia and newly formed neurons, the basis for the formation of specific brain regions.

Neurons are well known for their function in the propagation and transmission of electrical signals to other neurons or cells. Glia includes structurally and functionally distinct cellular populations that outnumber neurons in the brain: oligodendrocytes (OLs), astrocytes and microglia (Figure 1). Astrocytes, the most abundant cells in the CNS, play important roles in homeostatic functions, such as the formation and maintenance of the blood brain barrier (BBB) and nearby blood capillaries, and nutrient provision and maintenance of extracellular homeostasis. With complex morphology, astrocytes may exhibit branched or long fiber-like protrusions according their location in grey or white matter, respectively (Sofroniew & Vinters, 2010). Microglia, which originate in the yolk sac, are the mononuclear resident “macrophages” of CNS tissues. During development, microglia are involved in the phagocytosis of dead cells, and refine the developing neural circuits by pruning synapses (Kierdorf & Prinz, 2017; Nayak et al., 2014). These cells act as sentinels to detect the first signs of invasion/inflammation/injury, acting as scavengers that remove cell debris, and as producers of inflammatory signaling molecules (i.e. cytokines). Considered the most versatile cells in the body, microglia have the capacity to morphologically adapt to their surroundings by changing their morphology from an amoeboid to a more ramified form characterized by the presence of elongated and extremely dynamic protrusions (Nimmerjahn et al., 2005). Oligodendrocytes are the specialized cells responsible for forming the myelin sheath that insulates axons, being also important for neuronal survival/protection and trophic support (Griffiths, 1998; Rushton, 1951).

The myelinated areas of the CNS, called white matter, consist mainly of myelinated axons, and are devoid of neuronal somas, whereas the gray matter regions are composed

mainly of neuronal somas and dendrites. Originated in neural stem cells (NSCs), oligodendrocytes suffer a differentiation process from oligodendrocyte precursor cells (OPCs) into immature premyelinating oligodendrocytes (pre-OLs) and finally, into mature oligodendrocytes that are able to contact and myelinate axons. This differentiation process requires heavy changes in the morphology of oligodendrocytes, which go from a mostly bipolar to a highly ramified and multiple branched shape that enable deposition of the myelin membrane.

As previously mentioned, all cells from CNS have an extremely complex and exuberant morphology on which cellular functions depend on. Consequently, the dynamic cytoskeleton is a key feature that dictates both CNS development and the individual cellular functions of its cellular components.

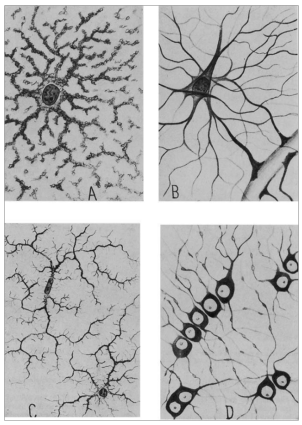

Figure 1 - Pío del Río Ortega described 4 types of glia: A) gray matter protoplasmic glia, B) white matter fibrous glia, C) microglia and D) oligodendrocytes. From Somjen, 1988.

The actin cytoskeleton

In eukaryotic cells, the actin cytoskeleton is a well-known feature that conveys structure and organization, resistance and stress sensing, and drives changes in shape and motility. In fact, morphological plasticity, through rearrangements of the actin cytoskeleton, are the basis for several important biological processes such as cell motility (Mitchison & Cramer, 1996; Pollard & Borisy, 2003; Ridley et al., 2003), cell adhesion (Alexandrova et al., 2008; Hu et al., 2007; Mitchison & Cramer, 1996), endocytosis (Engqvist-Goldstein & Drubin, 2003; Mooren et al., 2012), and cell division (Heng & Koh, 2010).

Cellular actin filament networks

Actin filaments (polymerized globular actin), can be organized into distinct networks (Figure 2). These networks are the key elements that provide dynamics to cell movement and cell shape. Resistance or deformation of actin filaments in response to force or chemical signals dictates the dynamic nature of a cell. For instance, force production capacity requires stiff actin networks to resist compression, but for cell contraction the actin networks need to be flexible enough to deform, which shows the striking balance needed between resistance and deformation of actin networks to convey specific cellular functions (Bendix et al., 2008).

Based on tight regulation of actin remodeling, the local organization of actin filaments in the networks can vary. These distinct architectures mostly depend on the action of different actin filament connectors (crosslinkers) that by pulling actin filaments tightly together may form different structures that can hold various degrees of stiffness (Lecuit et al., 2011). The different networks that can be formed with the filaments include crosslinked, bundled or branched actin networks, and stress fibers (Figure 2).

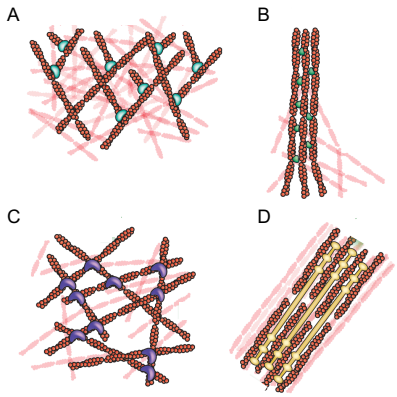

Figure 2 - Scheme of different actin network architectures. From Fletcher & Mullins, 2010. A) Branched actin network formed by the Arp2/3 complex with the crosslinks at an angle of 70º. B) Bundled actin network with orthogonal crosslinks found in the filopodia. C) Crosslinked networks with a flexible and extensible mesh mostly found in the cell cortex. D) Stress fibers are formed from bundled actin filaments with long orthogonal crosslinks.

In the whole cell unit, those different actin networks confer the structural basis for specific functional cellular structures such as lamellipodia, filopodia and the cell cortex (discussed ahead).

Actin dynamics

Actin dynamics is a process that relies on the transition between monomeric (ATP-G-actin) and filamentous actin (F-actin), which in turn is intimately associated with the asymmetry of the formed filament. In fact, the newly-formed actin filaments are polar structures with opposite ends called “barbed” (or plus) and/or “pointed” (or minus) ends (Huxley, 1963). At the barbed end, the fast-growing end, actin polymerization is favored by the presence of ATP-G-actin whereas at the pointed end, the opposite site of the filament, depolymerization takes place stimulated by the presence of ADP-actin (Carlier et al., 1987; Korn et al., 1987) (Figure 3).

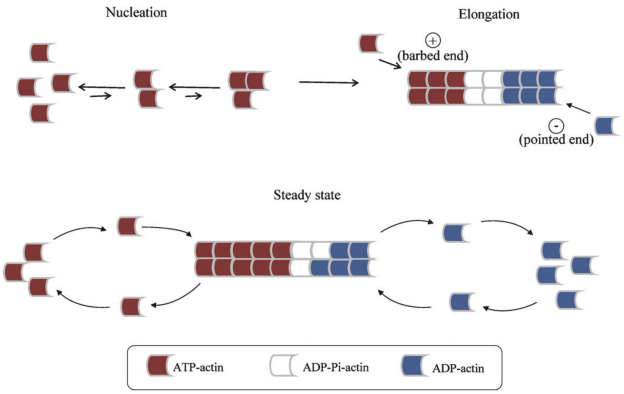

Figure 3 - Representative scheme of actin polymerization. From Kustermans et al., 2008. Nucleation - is the limiting step in *de novo* filament formation, due to unfavorable kinetics of actin oligomer formation and instability of actin dimers. Once an actin nucleus (composed of a trimer of actin monomers) is formed, the assembly of additional monomers proceeds. Elongation - A favorable and rapid step characterized by the successive and preferential addition of monomers at the barbed end. Treadmilling - The polymerization process reaches a steady state phase where an equilibrium between monomer disassembly at the pointed end and polymerization at the barbed end is established and maintained by a critical concentration of free monomers in the cytosol.

The actin polymerization process is highly controlled by a broad cohort of proteins called actin-binding proteins (ABPs). These proteins may exert their role by controlling nucleation, elongation, depolymerization, severing, capping, crosslinking and/or by sequestration of actin monomers (Pollard & Borisy, 2003; Rafelski & Theriot, 2004; Zigmond, 2004) (Figure 4).

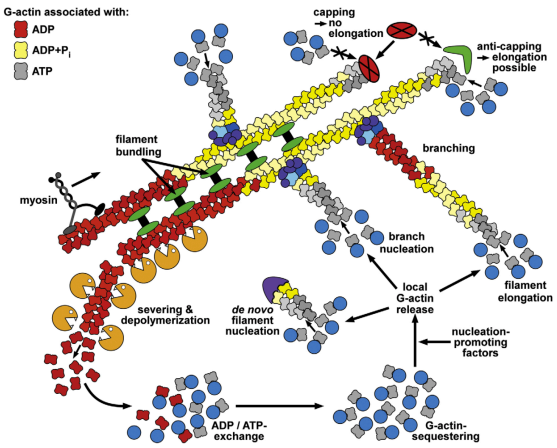

Figure 4 - Regulation of actin dynamics. From Witte & Bradke, 2008. There are several mechanisms that contribute to the regulation of actin polymerization. Actin polymerization can be driven by nucleation-promoting factors while anti-capping proteins can promote filament elongation. On the other hand, to avoid uncontrolled actin polymerization, sequestering proteins can interact with monomeric actin whereas capping proteins can interact with filamentous actin avoiding aberrant filament elongation. Furthermore, the severing and depolymerization proteins can stimulate the increase in the dynamics of actin, and the crosslinking proteins can be used to bundle of previously formed actin filaments.

The correct interplay between all regulatory molecules during actin polymerization is crucial for appropriate remodeling of the actin cytoskeleton and formation of the different actin cytoskeletal networks (Blanchoin et al., 2014).

Actin-binding proteins

Seven main groups of ABPs have been characterized (Figure 5): 1) Monomer-binding proteins (bind to G-actin being able to promote as well as inhibit polymerization); 2) Filament-depolymerizing proteins (induce the conversion of F-actin into G-actin); 3) Filament end-binding proteins (promote capping of actin filaments end preventing the exchange of monomers at the pointed and barbed ends); 4) Filament severing proteins (promote the shortening of the filaments length by binding to the side of the filament and cutting it into two pieces); 5) Cross-linking proteins (bring the actin filaments together, facilitating the formation of actin filament bundles, branched actin filaments, and three-dimensional networks); 6) Stabilizing proteins (prevent depolymerization of actin filaments); 7) Motor proteins (use actin filaments as tracks to move) (dos Remedios et al., 2003). Interestingly, some ABPs are not restricted to one functional group, which means that they can have different functions and be redundant among them.

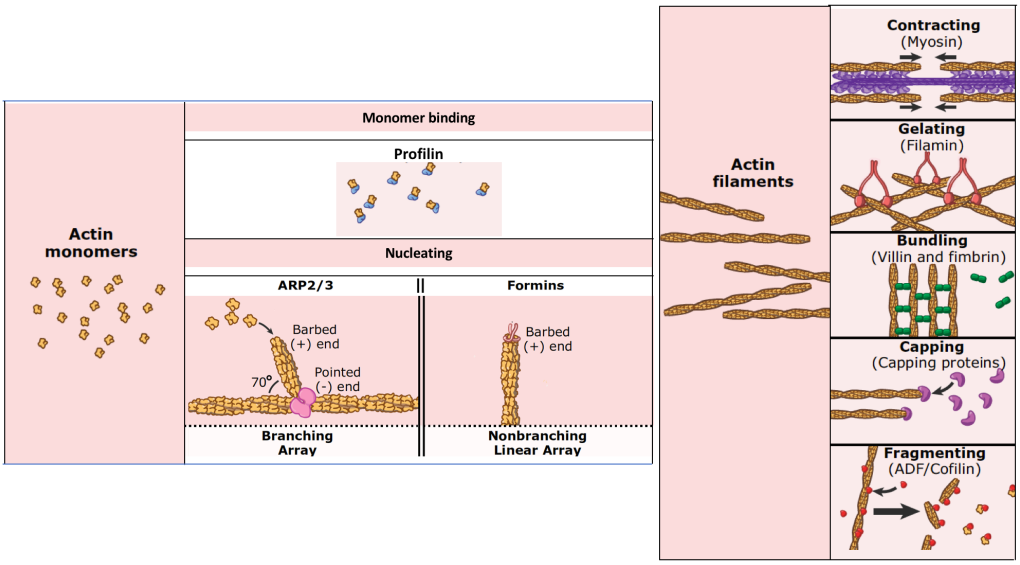

Figure 5 - Actin binding proteins. From Plopper et al., 2013. Representation of some ABPs that regulate the dynamics of actin polymerization and the organization of filaments by direct binding to monomers or to filaments. Nucleating proteins: Arp2/3 complex and formins; Monomer binding: profiling; Motor protein: myosin; Crosslinking proteins: filamin, villin and fimbrin; Capping proteins: CapZ; Severing and depolymerizing proteins: ADF/cofilin family.

Remodeling of the actin cytoskeleton can be triggered by extracellular signals. Different molecules, such as growth factors, chemoattractants, and chemorepellants, and extracellular matrix (ECM) proteins can bind to the cell´s transmembrane receptors, triggering specific responses that can go from migration, proliferation, to changes in cell shape. The activation of these transmembrane receptors leads to the activation of specific signaling pathways. The major pathways regulating the actin cytoskeleton in response to extracellular stimuli involve the Rho family of monomeric G proteins that will act on downstream effectors, such as the promoters of actin polymerization (WASP/Scar and WAVE proteins that activate the Arp2/3 complex). Because different cell surface receptors can be activated, different Rho family proteins can also be recruited and/or activated (Figure 6).

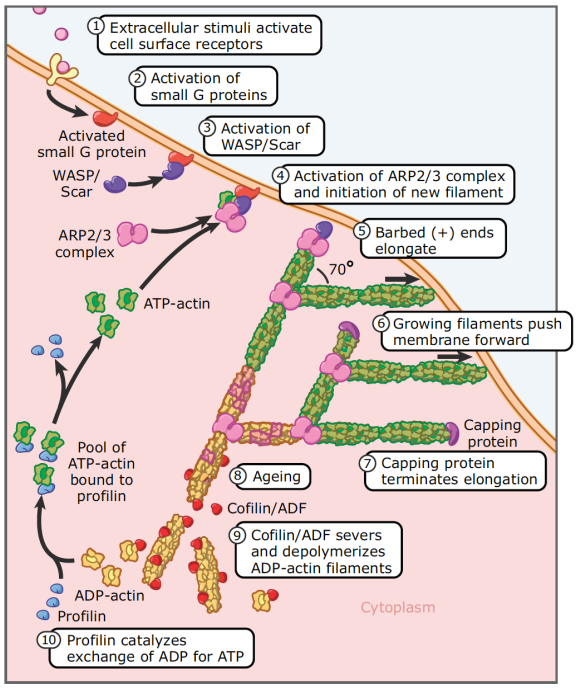

Figure 6 - Representation of the dendritic nucleation model. From Pollard et al., 2000. Extracellular stimulus leads to the rearrangement of the actin cytoskeleton of the cells through Rho GTPase activation of downstream targets, the actin polymerization factors.

Rho proteins are GTPases, members of the Ras family that are activated upon exchange of GDP for GTP. Rho GTPases can be classified into different subfamilies. The most well studied are the classical Rho GTPases RhoA, Rac1 and Cdc42. Several studies have established a critical role of these molecular switches in the regulation of cytoskeleton remodeling. Of note is the contribution of Allan Hall and colleagues who, using constitutively active forms of the proteins injected into cells, first showed that: RhoA induces contractile actin and myosin filament assembly, forming stress fibers; Rac1 leads to the formation of actin-enriched surface protrusions named lamellipodia (Ridley & Hall, 1992; Ridley et al., 1992); and Cdc42 promotes the formation of thin actin-enriched protrusions on the membrane surface, called filopodia (Nobes & Hall, 1995) (Figure 7).

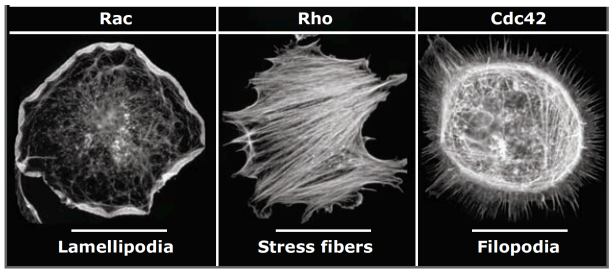

Figure 7 - Formation of different actin structures upon activation of different Rho GTPases families namely Rac, Rho and Cdc42. From Gielen et al., 2006; Hall, 1998. Constitutive active forms of the proteins were injected into Swiss 3T3 fibroblasts. Activation of Rac induces lamellipodia, Rho activation leads to the formation of stress fibers, and Cdc42 activation leads to the formation of filopodia.

Rho GTPase signaling determines the activity of downstream effectors such as ABPs. Of particular interest are the ABPs responsible for controlling the availability of actin monomers and the polymerization process, considering that this is the limiting factor for rapid actin cytoskeleton rearrangement. Formins (unbranched actin filaments) (Chesarone et al., 2010), the Arp2/3 complex plus its activators (branched actin filaments) (Campellone & Welch, 2010; Chesarone & Goode, 2009) and the harboring tandem actin monomer binding proteins (unbranched actin filaments) (Renault et al., 2008) are the three major classes of proteins involved in this process.

The Arp2/3 Complex and its nucleation promoting factors

The Arp2/3 complex was the first actin nucleator to be identified (Machesky et al., 1994). It is made up of 7 subunits, some of which can interact directly with actin monomers, while others form branching points on pre-existing filaments (Machesky et al., 1997; Mullins et al., 1997; Welch, Matthew D. et al., 1997; Welch, M. D. et al., 1997). The newly formed actin filaments grow from the mother filament at an angle of around 70º, giving origin to the Y-branched network (Blanchoin et al., 2000).

The ability of Arp2/3 to form new branched actin filaments from pre-existing ones depends on nucleation promoting factors (NPFs) that activate the complex (Table 1) (Robinson et al., 2001).

Table 1 - Arp2/3 complex nucleation promoting factors (NPFs). Adapted from Welch & Mullins, 2002.

Abbreviation	Description
WASP/N-WASP	Wiskott-Aldrich syndrome protein/neural-WASp
WAVE 1-3	WASP family verprolin-homology protein
WASH	WASP and Scar homology protein
WHAMM	WASP homolog associated with actin, membranes, and microtubules
JMY	Junction-mediating and regulatory protein
GMF	Glia maturation factor
WIP	WASP-interacting protein
CARMIL	Capping protein, Arp2/3, and myosin I linker

The branched actin network formed by the Arp2/3 complex, together with its NPFs, is the force generator involved in several cellular processes that require membrane remodeling. In the case of NPFs specifically, several lines of evidence highlight their important role in a range of biological processes: membrane remodeling during lamellipodia (Yamazaki et al.,

2005) and filopodia formation (Higgs & Pollard, 2000; Miki, Suetsugu, et al., 1998); formation and extension of specialized cellular protrusions (such as in the case of neurite outgrowth, growth cone and spines formation, and during protrusions extension in oligodendrocytes) (Dahl et al., 2003; Kim et al., 2006; Soderling et al., 2007); cell migration (Sossey-Alaoui et al., 2005; Suetsugu et al., 2003); and vesicle trafficking (Campellone et al., 2008; Derivery et al., 2009; Duleh & Welch, 2010). Several NPFs, including WASP, N-WASP, WAVE1-3, WASH, WHAMM and Jmy, have in their structure a WCA domain (W region binds to the actin monomer, and the CA region binds to the Arp2/3 complex), that allows for Arp2/3 activation. Since the WCA region by itself can activate the Arp2/3 complex, in a preventive form, this region is folded in the protein, or protein complexes, to avoid uncontrolled association with the Arp2/3 complex. For N-WASP and WAVE family proteins, the regulation mechanism through autoinhibition are well studied: N-WASP depends on the Cdc42 activity to expose the VCA region (Miki, Sasaki, et al., 1998), whereas WAVE family proteins rely on Rac1 activity to unmask the VCA region (Chen et al., 2010). The regulation of WASH, WHAMM and Jmy is still not understood.

Junction-mediating and regulatory protein - Jmy

Junction-mediating and regulatory (Jmy) is a 110 kDa protein, only found in vertebrates, that was originally reported as a cofactor for the p300 protein, being involved in the p53-dependent apoptosis (Shikama et al., 1999; Zuchero et al., 2009). Jmy is mainly localized in the nucleus of mouse embryonic fibroblasts (MEFs), B16-F10 mouse melanoma cells, NIH 3T3 cells and primary neurons (Zuchero et al., 2009), and cells depleted of Jmy have compromised p53 activity (Coutts et al., 2007). In this context, Mdm2, a well-known regulator of p53, was shown to interact and negatively regulate Jmy under physiological conditions, partially by targeting it for degradation (Coutts et al., 2007).

Interestingly, Jmy can act as multifunctional regulator of actin nucleation: dependent on the Arp2/3 complex activity, giving rise to branched actin filaments, or as nucleator itself, originating unbranched actin filaments (Figure 8 B) (Zuchero et al., 2009). These multiple functions are only possible due to Jmy's C-terminal region composed of three actin-binding WH2 domains (WWW), an actin and Arp2/3 binding connector (C), and an Arp2/3 acidic region (A) (Figure 8 A) (Zuchero et al., 2009). *In vitro* studies have shown that Jmy is able to increase the rate of actin polymerization independently of its binding to the Arp2/3 complex, which is a unique characteristic of this actin regulator (Zuchero et al., 2009).

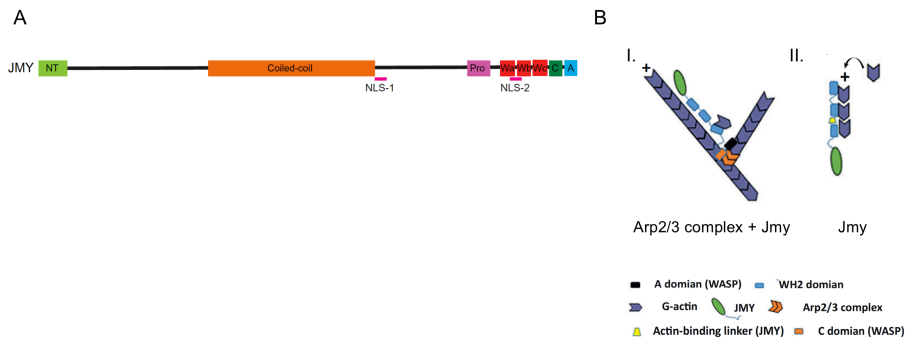

Figure 8 - A) Domain structure of Jmy protein showing the putative NLSs. From Zuchero et al., 2012. (B) Arp2/3 and Jmy-dependent actin nucleation. I - Branched actin nucleation driven by the Arp2/3 complex, with Jmy as a NPF. II - Jmy promoting actin nucleation by itself, giving rise to unbranched actin filaments. From Siton-Mendelson & Bernheim-Groswasser, 2017.

As for its subcellular localization, Jmy is mainly found in the nucleus of, for example, mouse embryonic fibroblasts and primary rat neurons (Zuchero et al., 2009). However, in highly motile cells, such as primary human neutrophils, Jmy appears to be excluded from the nucleus and co-localizes with actin filaments at the leading edge of the cell. This observation suggested a direct role for Jmy in cell motility. This hypothesis is further supported by experiments where Jmy overexpression resulted in increased migration of human bone osteosarcoma epithelial cells (U2OS), as well as by the observation that Jmy depletion leads to decreased migration of U2OS and human embryonic kidney cells (HEK293) (Zuchero et al., 2009). The decreased cell migration capacity observed upon Jmy depletion was accompanied by an overall decrease in the cell's F-actin content, suggesting that Jmy promotes cell motility through the regulation of actin polymerization (Zuchero et al., 2009). The WH2 domain region, for Arp2/3 binding, is the structural element important for the function of Jmy in cell motility (Coutts et al., 2009). Coutts and colleagues have also suggested that besides promoting motility by direct control of actin polymerization, Jmy may also regulate adhesion by changing expression levels of cadherins (Figure 9) (Coutts et al., 2009).

Jmy has a bipartite NLS that partially overlaps with the WH2 domain (Figure 8 A) (Zuchero et al., 2012), which suggests that its subcellular localization is important to regulate its function. Complementary experiments have shown that when preventing actin binding to the WH2 domains Jmy completely localizes to the cytoplasm of the cells, indicating that the subcellular regulation of Jmy activity is in part actin-dependent (Zuchero et al., 2012). Another interesting aspect is that translocation of Jmy to the nucleus does not occur by diffusion through the nuclear pore, but instead, is regulated by importins α/β, which compete with actin monomers for binding to the overlapping WH2 and NLS-2 regions (Zuchero et al., 2012).

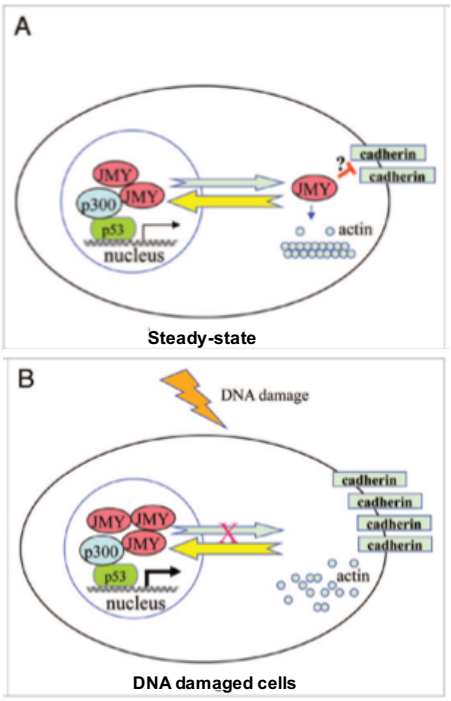

Figure 9 - Proposed model of Jmy's function in steady-state vs. DNA damaged conditions. From Wang, 2010. (A) Under steady-state conditions Jmy, shuttles between the cytoplasm and the nucleus. The fraction of Jmy that is in the cytoplasm of the cell promotes actin polymerization and changes in cell adhesion by affecting cadherin levels, via a still unidentified mechanism. (B) Upon DNA-damage, Jmy is translocated to the nucleus where it participates in the p53 response. As a result, cell motility is affected due to stabilization of cadherin levels that leads to increased adhesion. Actin polymerization is also affected, which contributes for the decrease in cell motility.

Jmy has also been shown to be important to establish polarization during asymmetric division and cytokinesis in the mouse oocytes (Sun et al., 2011). More recently, Schluter and colleagues reported that Jmy is expressed in the endomembrane compartment of several cell lines (Schluter et al., 2014). These authors propose that Jmy is involved in the formation of endomembrane tubules, a function that is dependent of its WH2 domains. Moreover, Jmy is shown to binds to VAP-A, a connector of ER membranes to other cellular membrane compartments and regulates anterograde vesicle traffic in the Cos-7 African green monkey kidney fibroblast-like cell line (Cos-7 cells) (Schluter et al., 2014).

Jmy is ubiquitously expressed in mammalian tissues and various cell lines. It is found at higher levels in brain and testis (Firat-Karalar et al., 2011). Aside from its complex functional domain structure and multifunctional potential, the studies performed to date suggest that its activity may be cell context-dependent. For instance, its role in cell motility (Coutts et al., 2009; Zuchero et al., 2009) is not seen in mouse embryonic fibroblasts (MEFs) and NIH 3T3 cells (Firat-Karalar et al., 2011). Likewise, overexpression of Jmy in U2OS and Cos7 cells did not induce any alterations in the F-actin content of these cells, which suggest that Jmy is inhibited in its ability to promote actin polymerization through mechanisms that are still not understood (Firat-Karalar et al., 2011).

A cell type-specific RNA-seq analysis of the mouse cerebral cortex showed that Jmy is expressed in all the brain cells examined (glia, neurons and vascular cells), but at higher levels in newly formed oligodendrocytes and endothelial cells (Zhang et al., 2014). The function of Jmy in brain cells is unknown. The only information available is regarding Jmy function in a

neuroblastoma cell line (N2A), where it is described as a negative modulator of neurite outgrowth (Firat-Karalar et al., 2011).

Actin structures in the cell

The dynamic and flexible actin filament organization in a cell is associated with the recruitment of different actin-related proteins to different subcellular domains, giving rise to distinct cytoskeletal structures, such as lamellipodia, filopodia, the cell cortex and stress fibers (Blanchoin et al., 2014). The correct spatiotemporal assembly of these structures in the cell is determinant for the regulation of specific biological processes. Even if each cellular structure is localized in different regions in the cell, the individual dynamics of each one can influence the dynamics of the others (Figure 10).

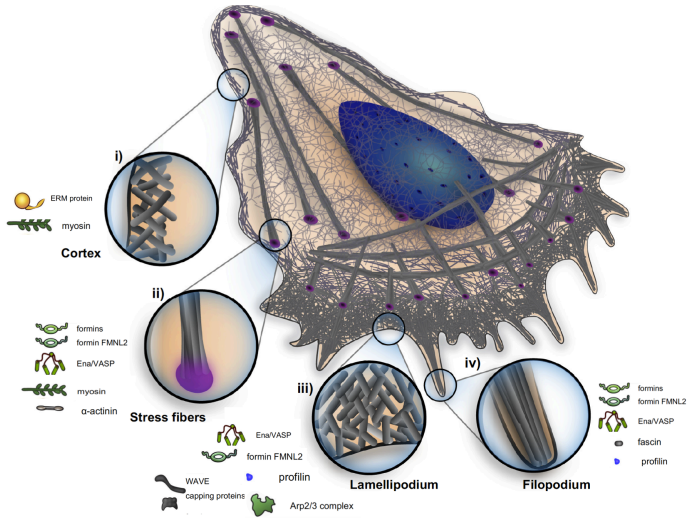

Figure 10 - Schematic representation of actin organization with reference to the four main actin cellular structures and their main actin regulators. From Blanchoin et al., 2014. i) Cell cortex; ii) Stress fibers as an example of contractile fibers; iii) Lamellipodia and iv) Filopodia.

Lamellipodium

The lamellipodium is a leading-edge structure devoid of microtubules that has a complex branched actin network beneath its ruffling membrane (Theriot & Mitchison, 1991; Vinzenz et al., 2012). The actin network in lamellipodia is responsible for force generation that pushes the plasma membrane forward, for example, during cell migration (Pollard & Borisy, 2003). In neurons, lamellipodia can work as sensors for extracellular signals, driving growth cone movement and axonal guidance (Gomez & Letourneau, 2014). Mechanistically, lamellipodia formation is mainly regulated by the Arp2/3 complex, which is activated by WAVE and the Rho GTPase Rac1.

Filopodium

The filopodium is a finger-like actin projection, found at the front of many different cell types. Filopodia can be involved in cell migration, cell-cell communication (Karp & Solursh, 1985; Malinda et al., 1995), and operate as sensors for external cues, for example in nerve growth cones and macrophages (Allen et al., 1998), and also function as tracks for protein transport (Zhuravlev et al., 2012). These structures are abundant in neuronal dendrites where they play an important role in dendritic spine development (Jontes & Smith, 2000).

The filopodia actin network is composed of bundles of parallel actin filaments with orthogonal crosslinkers. Formins and Ena/Vasodilator-stimulated phosphoprotein (VASP) are the main proteins known to link and maintain the growing barbed end of filaments at the cell membrane, thus increasing filament growth at the tip of filopodia (Lewis & Bridgman, 1992). The mechanisms behind filopodia formation remain unclear. The most popular model proposes that filopodia assemble by 'convergent elongation' of lamellipodial filaments (Blanchoin et al., 2014; Mellor, 2010). Briefly, filopodia that extend deep into the lamellipodia are formed by reorganization of the Arp2/3-mediated dendritic network into bundles. This arrangement is achieved when the barbed ends of actin filaments at the leading edge associate with proteins as VASP and formins, which protect the barbed ends from capping and allow the elongation of actin filaments. Finally, bundling proteins such as fascin would bundle the contacting actin filaments and eventually generate the filopodia at the leading edge of plasma membrane.

The cell cortex

The cell cortex is a thin contractile crosslinked actin network located beneath the surface of the plasma membrane. The contractility of this structure derives from the presence of the motor protein myosin. The cortical actin network confers resistance to extracellular stresses, mechanical work, and drives changes in shape. Formins, among other actin regulators, grow cortical actin filaments at the plasma membrane (Fritzsche et al., 2013). Cortical contractility is important in, for example, maintenance of the round shape of cells before mitosis (Stewart et al., 2011), and to drive the formation of blebs (membrane bulbs extruded at the cell surface) (Charras et al., 2008; Charras et al., 2005).

Stress fibers

Stress fibers are contractile fibers formed by bundles of unbranched actin filaments that contain myosin. These structures are ventrally located in the cell, with a parallel orientation towards the direction of movement, promoting the connection of the cell cytoskeleton to the ECM via focal adhesion sites. The interaction of these structures with myosin is crucial for their role in cell-substrate adhesion, mechanosensing, and in adhesion. The actin network found in

stress fibers is dependent on the activity of formins, Ena/VASP proteins and possibly the Arp2/3 complex (Kanchanawong et al., 2010; Tojkander et al., 2011). Moreover, Rho signaling is also involved in the formation of stress fibers by activating nonmuscle myosin, and stabilization of myosin-containing filaments.

Myelination in the central nervous system

Myelin

The vertebrate CNS is characterized by the presence of myelin, a specialized glial membrane produced by oligodendrocytes that ensheaths axons. Interestingly, each oligodendrocyte is able to extend several protrusions that will contact and myelinate multiple axons (Hildebrand et al., 1993). Myelin has three main functions: (1) electrical insulation of axons, (2) increasing the speed of nervous impulse conduction, and (3) to provide axonal trophic support (Funfschilling et al., 2012; Morrison et al., 2013; Nave, 2010). This specialized membrane is composed of 70-80% lipids, including cholesterol, phospholipids, galactolipids and plasmalogens, and around 20-30% of proteins, specifically proteolipid protein (Plp), myelin basic protein (Mbp) (the two main protein constituents), cyclic nucleotide phosphodiesterase (Cnp), myelin oligodendrocyte glycoprotein (Mog), myelin-associated glycoprotein (Mag), sirtuin 2 (Sirt2) and claudin 11 (Cldn11) (Richard H. Quarles, 2005).

Biogenesis of myelin

Myelination results in stretches of myelinated axonal segments - internodal segments or internode - separated by unmyelinated regions, the nodes of Ranvier, that allow for the rapid propagation of action potentials (Tasaki, 1939). How is the myelin membrane formed around axons has been investigated for a long time (Bunge et al., 1961; De Robertis et al., 1958; Ioannidou et al., 2012; Luse, 1956; Pedraza et al., 2009; Sobottka et al., 2011). The current accepted model has been proposed by Snaidero and colleagues where, based on observations made using *in vivo* live-imaging experiments in zebrafish and 3D EM reconstructions of the mouse optic nerve, the authors showed that myelin emerges as a single triangle-like shaped membrane that wraps the leading edge around the axon, underneath previously deposited membrane. Simultaneously, lateral extension of myelin membrane layers occurs, towards the nodal regions (Figure 11) (Snaidero et al., 2014). Additionally, an equilibrium of Mbp and Cnp levels was showed to be essential for proper speed of compaction early in myelination, occurring first in the outermost layers and moving inwards with time (Snaidero et al., 2014).

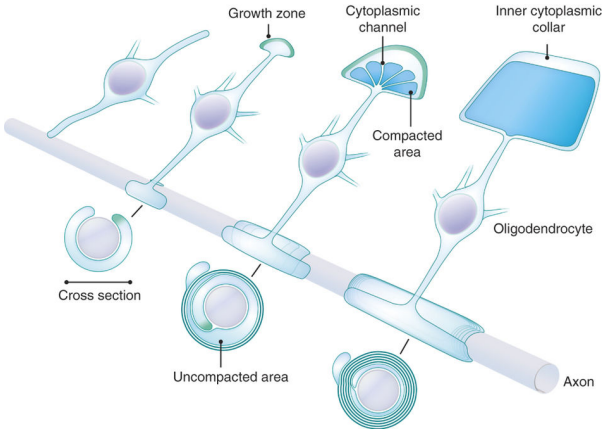

Figure 11 - Schematic representation of the currently accepted model of myelination in the CNS. From Chang et al., 2016. A differentiated oligodendrocyte extends a protrusion towards an unmyelinated axon and, upon contact, starts wrapping by spreading its membrane. The myelin membrane extends radially and longitudinally. After several myelin membrane layers are formed, compaction occurs from the outermost to the inner layers.

Mbp, the second major myelin constituent, has an important role in the formation of myelin and compaction, as well as in the organization of formed internodes. Present in the soma of oligodendrocytes, Mbp mRNA is then gradually redistributed to oligodendrocyte protrusions where it can be locally translated (Ainger et al., 1993; Amur-Umarjee et al., 1990; Colman et al., 1982). Mbp neutralizes membrane phospholipids, allowing for the tight apposition of two myelin membrane layers in so-called “nucleation sites”. After the bilayers are formed, Mbp will attach to and bring them into close contact, giving rise to compact myelin (Aggarwal et al., 2013; Readhead et al., 1987) (Figure 12).

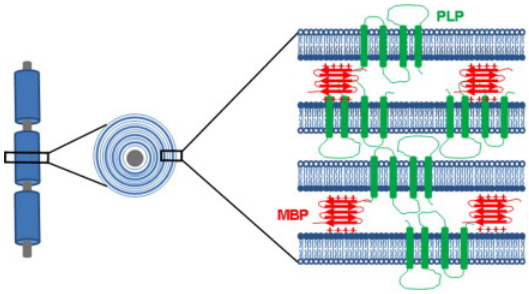

Figure 12 - Schematic representation of the myelin sheath structure in the CNS. From Baron & Hoekstra, 2010. Compact myelin requires Mbp-mediated apposition of the myelin membrane bilayers as well as the abundant expression of others structural proteins such as Plp.

Mbp is also important to modulate the molecular composition of the myelin membrane. By creating a physical barrier that filters proteins with large cytoplasmic domains, Mbp keeps proteins such as Cnp and Mag in the right cellular compartment, inducing the polarization of membranes. The extrusion of such proteins from the myelin membranes is translated into the low protein-to-lipid ratio of myelin (Aggarwal et al., 2011; Fitzner et al., 2006).

Formation of myelin is a tightly controlled process, regulated by a lineage-specific transcriptional program that initiates, in a developmentally-regulated manner, the

differentiation of oligodendrocytes (Emery, 2010; Li et al., 2009). During this process, there are numerous events tightly coordinated in the myelinating oligodendrocyte, such as synthesis of lipids and proteins, and cytoskeletal modifications.

Myelin in disease

Myelin is an essential feature of a functioning nervous system in vertebrates. Failure to properly form myelin membranes is associated with dysmyelinating diseases, including leukodystrophies, which result from an inherited condition that causes abnormal formation and function of myelin. In humans, these diseases can arise from defects in the synthesis of particular myelin proteins, such as in Pelizaeus-Merzbacher disease in which Plp synthesis is compromised, or in the 18q-syndrome, characterized by deficiency in Mbp (Kolodny, 1993).

Additionally, disruption of compact myelin after development is the hallmark of demyelinating diseases. The classic example of a demyelinating disease is multiple sclerosis (MS). MS, characterized by damage induced to the myelin sheaths (Franklin & Ffrench-Constant, 2008), is an autoimmune disease of significant incidence. In Europe, the incidence of MS is 10,8/10.000 (Leray et al., 2016), and in Portugal is of around 5,62/10.000 (Correia et al., 2016).

The natural regenerative response to myelin disruption, characterized by *de novo* synthesis of myelin sheaths on exposed axons - remyelination - is very limited in the adult CNS. Often, and for reasons that are not completely clear, OPCs in the demyelinated lesion are unable to differentiate and/or mature properly (Chang et al., 2000; Chang et al., 2002; Kuhlmann et al., 2008; Sim et al., 2002; Wolswijk, 1998). Additionally, even when new myelin is formed, the sheaths are generally thinner and the internodes shorter, features that may impact neuronal function recovery (Blakemore, 1974; Duncan et al., 2017; Smith & Koles, 1970). Promotion/improving oligodendrocyte differentiation is a possible strategy to use in remyelination. However, the molecular mechanisms that govern the differentiation process in oligodendrocytes and the interaction with axons have not been fully dissected, which limits the development and application of potential strategies that aim at improving remyelination in humans.

Oligodendrocytes: from birth to differentiation

Rudolf Virchow first described oligodendrocytes in 1854, even though at the time he did not recognized them as a distinct macroglial subpopulation. Only in 1921, Pio del Rio Hortega divided a “third element”, previously described by Santiago Ramon y Cajal in 1913, into 2 types of cells: microglia and oligodendrocytes (Scolding, 2004). In 1858, Virchow introduced the term “myelin”, with the description of sheaths found around nerve fibers. Others also contributed to the association of oligodendrocytes and myelin: Hardesty, in 1904, depicted

neuroglia as myelin producing cells; in 1928, Hortega illustrated spiral projections from oligodendrocytes; and Penfield, in 1932, concluded that oligodendrocytes indeed elaborate and maintain myelin sheaths. Later, Bunge and co-workers visualized, using electron micrographs, developing white matter with detailed oligodendrocyte protrusions (Bunge et al., 1961). Peters, Butt and Ramson further corroborated these observations by showing that a single oligodendrocyte is able to form internode segments in 30-50 axons (Butt & Ransom, 1989; Peters, 1964). Although oligodendrocytes are mainly linked with myelin sheath formation and proper insulation of axons, several lines of evidence have shown that they also provide trophic support to neurons (Nave, 2010; Nave & Trapp, 2008).

Oligodendrocyte progenitor cells: origin

OPCs are derived from neural precursor cells localized in specialized domains of the developing spinal cord and brain. OPCs are formed within the motor neuron progenitor domain (pMN) region of the ventricular zone of mouse spinal cord, after motor neuron production, through the simultaneous expression of Olig2 and Nkx6.1. (Figure 13 A). Two temporally distinct waves take place from different regions within the spinal cord: first wave - starts about E12.5 from the ventral ventricular zones, and the second wave - at about E15, from more dorsal regions (Figure 13 B). In the developing brain, it was also shown that oligodendrocytes arise from both ventral and dorsal regions of the ganglionic eminences in three distinct waves. In the first wave - the ventral-most OPCs are generated from the medial ganglionic eminence (MGE) (around E12.5), express Nkx2.1, and migrate to the forebrain (entering in the region after E16) (Kessaris et al., 2006); in the second wave - that takes place a few days later, OPCs are generated from the lateral and/or caudal ganglionic eminence(s) (LGE, and CGE), express the of genomic screened homeobox2 (Gsh2), and migrate towards the cortex (Kessaris et al., 2006); and in the third wave - OPCs are generated in the cortex itself, express Emx1, and migrate from the dorsal subventricular zone (SVZ) and outer SVZ towards the developing corpus callosum (Kessaris et al., 2006) (Figure13 C). Interestingly, MGE-derived OPCs (first wave) disappear after birth, being replaced first by OPCs originated in the LGE and CGE regions (second wave), and later by endogenous Emx1-positive cortical OPCs (third wave). Besides their different origins, there is no evidence of functional heterogeneity among the different OPC lineages in the forebrain (Kessaris et al., 2006). However, in the spinal cord it was shown that dorsally- and ventrally-derived oligodendrocytes show preferences to myelinate specific tracts (dorsally derived OPCs are better adapted to myelinate dorsal axons)

despite having similar electrical properties (Tripathi et al., 2011), which shows the complexity around CNS colonization by oligodendrocytes and their functions.

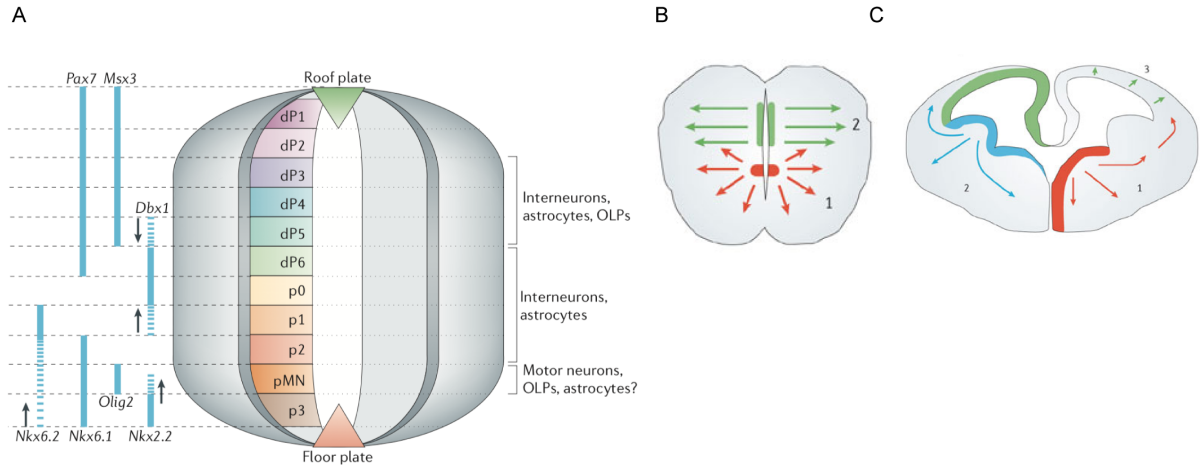

Figure 13 - Origin of OPCs and their migratory path in the spinal cord and ventricular telencephalon. From Richardson et al., 2006. (A) Representation of the progenitor domains in the embryonic spinal cord with indication of the transcription factors expressed. dP1-dP6, dorsal progenitor domains; Msx3, a homeobox gene, Olig2, oligodendrocyte lineage gene 2; Pax7, paired box gene 7; pMN and p0-p3, ventral progenitor domains. (B) Representation of the two migratory waves of OPCs that will populate the spinal cord. The first wave has origin in the ventral ventricular zone (1), and the second has origin in the dorsal regions of the neural tube (2). (C) Representation of the three distinct migratory waves of oligodendrocyte progenitor cells in the telencephalic ventricular regions, with reference to the transcription factors characteristic of the different regions.

The timing of colonization of different CNS regions by OPCs differs. For instance, OPCs start to appear in the cerebellum at E11.5 (first wave), but only after birth the region is entirely populated (Reynolds & Wilkin, 1988; Zhang & Goldman, 1996). In the spinal cord, the first wave of OPCs arises after E12.5, and the region is evenly populated by the time of birth (Fogarty et al., 2005; Vallstedt et al., 2005). In the optic nerve (ON), OPCs are generated at E12.5 (Ono et al., 2017) however only at birth (P0) the presence of OPCs is detectable at the retinal end of the nerve, and the distribution is homogenous at about P5 onwards (Small et al., 1987).

Oligodendrocyte progenitor cells: migration

OPCs are cells with a highly proliferative and motile profile, migrating from regions of origin towards their final destination in response to different extracellular cues (Ffrench-Constant et al., 1988; Small et al., 1987), including ECM proteins, secreted growth factors, mitogens, hormones, and neurotransmitters (Decker et al., 2000; Dubois-Dalcq & Murray, 2000; Rogister et al., 1999). For example, the action of chemorepellant gradients of netrin-1 and semaphorins are thought to be involved in the dispersal of OPCs in the optic nerve (Armendariz et al., 2012; Sugimoto et al., 2001) and the spinal cord (Miller, 2002). Recently, OPCs were shown to migrate along the vasculature by crawling or jumping on vessels, being the orphan G protein-coupled receptor 24 (GPR 24) essential for this process (Kuhnert et al.,

2010; Tsai et al., 2016). Migration towards the cortex was shown to be driven by molecules from the mesenchymal Tgf β family that act as chemorepellents in ventral niches (Choe et al., 2014). OPC migration is also controlled by the adhesion receptors integrins, which are developmentally regulated and interact with ECM proteins such as laminins and fibronectin (Milner & Ffrench-Constant, 1994). *In vitro* studies have shown that both basic fibroblast growth factor (bFGF2) and platelet-derived growth factor (PDGF) regulate OPC proliferation, survival and differentiation (Calver et al., 1998; Fruttiger et al., 1999), but also migration, acting as chemoattractant molecules (Fruttiger et al., 1999). Moreover, vascular endothelial growth factor (VEGF), a soluble signaling molecule known to regulate angiogenesis, has been recently reported to promote OPC migration *in vitro*, by inducing reorganization of the actin cytoskeleton at the leading-edge of the cell's protrusions (Hayakawa et al., 2012).

At their final destination, OPCs are distributed in a uniform and non-overlapping way in order to occupy white and grey matter regions (Hughes et al., 2013; Zhang & Miller, 1996). At this time, OPCs exit the cell cycle and begin differentiation (Kessaris et al., 2008).

Oligodendrocyte progenitor cells: differentiation

The development of OPCs requires exceptional morphological plasticity and the sequential expression of markers under the control of a lineage-specific transcriptional program. Bipolar-shaped OPCs, which express PDGFRα (Levine et al., 1993; Nishiyama et al., 1996; Pringle et al., 1992), ganglioside A2B5 (Dubois et al., 1990), and proteoglycan NG2 (Chittajallu et al., 2004), give rise to pre-oligodendrocytes characterized morphologically by the presence of multipolar short protrusions, and additional expression of 3'-sulfogalactosylceramide recognized by the O4 antibody (Sommer & Schachner, 1981) and GPR 17 protein (Boda et al., 2011). Immature oligodendrocytes are post-mitotic cells that do not express A2B5 or NG2 but retain the O4 marker, and begin to express galactocerebroside C (GalC) (Yu et al., 1994). Morphologically, these cells are multipolar with multi-branched protrusions (Armstrong et al., 1992; Gard & Pfeiffer, 1989). The final step of differentiation, to generate mature oligodendrocytes capable of extending membranes that will wrap axons, involves the expression of several proteins such as Mbp, Plp, Mag and Mog, which are main components of myelin sheaths (Reynolds & Wilkin, 1988; Scolding et al., 1989) (Figure 14).

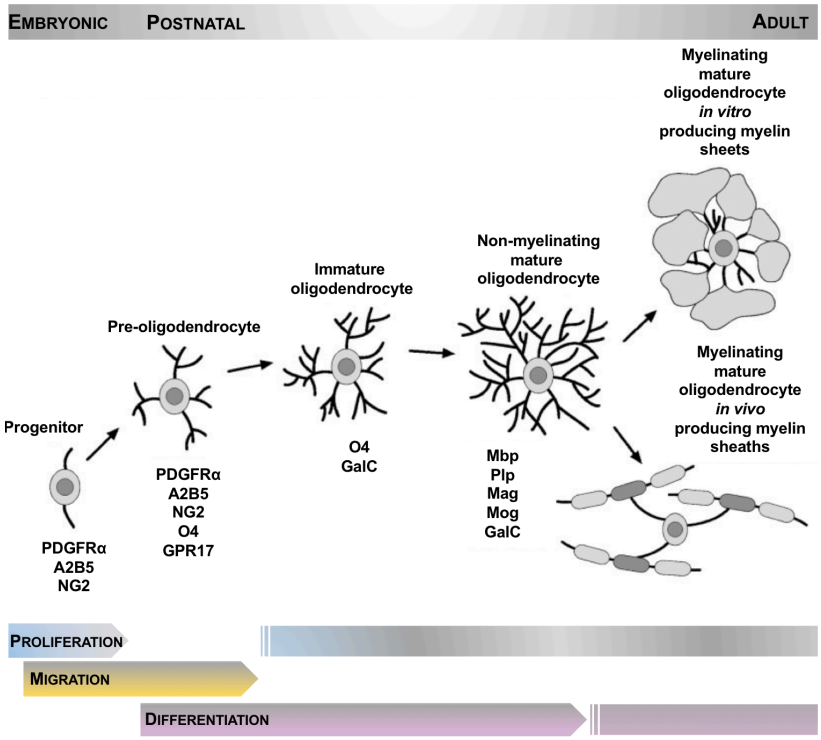

Figure 14 - Overview of oligodendrogenesis. From Gielen et al., 2006. The morphological states of oligodendrocytes during differentiation with timed specification of different antigenic markers.

In the mouse, spinal cord and brain myelination starts at birth (Foran & Peterson, 1992), being complete in most white matter tracts at around 40-60 days postnatally. In the ON however, myelination only starts after P6 (Foran & Peterson, 1992). In humans, myelination starts during the second half of fetal life, peaks during the first postnatal year, and continues until 20 years of age in some cortical fibers (Yakovlev & Lecours, 1967) (Figure 15).

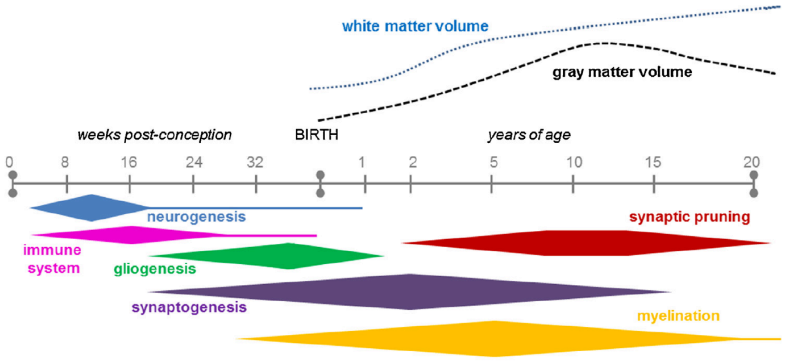

Figure 15 - Time course of key neurodevelopmental processes in humans (not to scale). From Semple et al., 2013. Changes in white and gray matter volumes over time are depicted.

Of note, after birth and in the adult brain, OPCs are continuously produced, in small numbers, in the SVZ. Adult generated OPCs were shown to be able to myelinate continuously throughout normal adult life (reviewed in Bergles et al., 2010). The presence of these adult OPCs capable of differentiating into myelinating oligodendrocytes may be linked with myelin

plasticity and/or repair. Myelin remodeling by replacement of dying myelinating oligodendrocytes or by introduction of additional myelin internodes (Young et al., 2013), also occur during adulthood. Although the presence of adult OPCs is thought to be of extreme importance, further research is required to better understand the functional consequences of myelin plasticity in the adult brain.

The actin cytoskeleton in oligodendrocytes

The cytoskeleton of oligodendrocytes is composed of microtubules, microfilaments but devoid of intermediate filaments (Kachar, Behar, & Duboisdalcq, 1986; Wilson & Brophy, 1989). The multiple protrusions extending from the oligodendrocyte cell body are characterized by growing tips that resemble the growth cone in axons: highly motile with the typical actin-rich filopodia and lamellipodia structures (Fox et al., 2006). The oligodendrocyte protrusions also have long bundles of actin filaments that radiate from the leading edge towards the central area of the lamellipodia, a typical and unique structural organization of growth cones. The ability of the protrusion tips to integrate cues from the extracellular environment and cell:cell interaction directs its extension and is crucial for the proper establishment of oligodendrocyte-axon contact (Fox et al., 2006; Kirby et al., 2006; Michalski et al., 2016).

Microtubules are found in the cell body and stable primary processes (Lunn et al., 1997), and serve as “tracks” for transport of organelles and macromolecules during differentiation (Carson et al., 1997; Lunn et al., 1997; Smith & Li, 2004). As for actin-based microfilaments, they are present in the cortical region and throughout the protrusions (Nawaz et al., 2015; Song et al., 2001). An interesting aspect of this organization is the fact that microtubules do not invade the most distal regions of the protrusion leading edge, but instead use the F-actin “trails” to occupy the center of the oligodendrocytes protrusions (Song et al., 2001).

As oligodendrocytes mature, there is a shift from protrusion remodeling to membrane formation, a process that also depends on actin dynamics.

Regulation of actin dynamics during oligodendrocyte differentiation and myelination

Actin regulators driving differentiation

During oligodendrocyte differentiation, polymerization of F-actin acts as the driving force to induce membrane deformation during protrusion extension and branching (Nawaz et al., 2015). The Arp2/3 complex has been identified as a driver of F-actin assembly necessary for protrusion extension in oligodendrocytes (Zuchero et al., 2015). Accordingly, loss of WAVE1, an Arp2/3 activator, in OPCs *in vitro* leads to defects in protrusion extension and impaired formation of lamellipodia structures, associated to defects in oligodendrocyte

maturation (Kim et al., 2006). N-WASP, another Arp2/3 activator, was also shown to be important for protrusion extension in oligodendrocytes (Bacon et al., 2007).

Control of the actin cytoskeleton is dependent on multiple extracellular signals that can activate different signaling pathways, which in turn can act on different downstream effectors, leading to changes in the actin network of oligodendrocytes. For instance, the integrin-linked kinase (Ilk), a focal adhesion protein that mediates signaling transduction from the ECM, was shown to be essential for proper protrusion branching and outgrowth during *in vitro* differentiation (Michalski et al., 2016; O'Meara et al., 2013). Additionally, studies showed that RhoA acts as a negative regulator of oligodendrocyte differentiation *in vitro* through its downstream effector Rho-associated kinase (ROCK) (Liang et al., 2004; Rajasekharan et al., 2010; Wolf et al., 2001). Possibly, it activates myosin II and induces hyper-contractility inhibiting oligodendrocyte morphological plasticity. Consequently, downregulation of RhoA/ROCK activity decreases actomyosin contractile forces, favoring protrusion extension. (Bauer, N. G. et al., 2009; Rajasekharan et al., 2010; Wang et al., 2012).

Interestingly, Mbp is reportedly a linker for F-actin specific on the plasma membrane (resembling focal adhesion contacts) and in new membrane ruffles (Boggs et al., 2014). *In vitro* studies show that Mbp promotes F-actin bundling and the binding of microtubules to F-actin (Boggs et al., 2011). In line with this, analysis of *Shiverer* mutant mice - which carry an autosomal recessive trait that results in a deficiency of CNS myelination due to absence of Mbp (Chernoff, 1981) - revealed that in the absence of Mbp, F-actin bundles are not formed and the connection between microtubules and F-actin is lost, resulting in smaller cell protrusions associated with larger cell bodies (Dyer et al., 1995; Dyer et al., 1997). The interaction between Mbp and the actin cytoskeleton seems to be determinant for protrusion formation, as well as for myelination.

Actin regulators driving myelination

The subcellular distribution of F-actin in oligodendrocytes changes during differentiation. *In vitro* studies show that extension of myelin-like membranes is accompanied by a delocalization of F-actin towards the outermost region of the forming sheets. Accordingly, live-imaging in zebrafish showed that, as soon as oligodendrocyte protrusions embrace the axon, the same pattern of F-actin delocalization takes place (Nawaz et al., 2015). Interestingly, previous studies have suggested that as oligodendrocytes undergo maturation, actin cytoskeleton elements start to be removed from the structure that will give rise to the compact myelin (Boggs & Wang, 2001; Dyer & Benjamins, 1989).

More recently, it was shown that myelination requires actin disassembly (Nawaz et al., 2015; Zuchero et al., 2015). *In vitro* experiments revealed that depolymerization of F-actin induces a decrease in surface tension at the leading edge of protrusions, which allows the

lateral spreading of the membrane and, consequently, the growth of the sheath as it wraps around the axon (Figure 16) (Nawaz et al., 2015). Accordingly, genes that encode actin depolymerization proteins are highly expressed in myelinating oligodendrocytes (Zhang et al., 2014), and *in vivo* studies, using a oligodendrocyte conditional knockout mouse model for ADF/Cofilin1, show defects in the leading edge/inner tongue of oligodendrocyte protrusions, as well as a decrease in myelin thickness, reinforcing the key role of actin depolymerization for proper myelination (Nawaz et al., 2015). However, how is actin depolymerization activated in the inner tongue of oligodendrocyte protrusions? Mbp expression by oligodendrocytes and in myelin sheaths occurs at the same time of actin disassembly (Zuchero et al., 2015), suggesting Mbp as a good candidate for triggering actin disassembly in order to promote myelin wrapping. Furthermore, *in vitro* studies showed that lack of Mbp in mature oligodendrocytes leads to an abnormal accumulation of F-actin (Zuchero et al., 2015). But, what is the mechanism used by Mbp to control actin disassembly during myelination *in vivo*? The cellular mechanism for regulation of actin disassembly is based on the binding of disassembly factors to membrane phospholipids, where they are kept in an inactive state. For example, cofilin and gelsolin remain inactive when in association with PI(4,5)P2, and become active when released from the membrane (Hilpela et al., 2004). Interestingly, Mbp also binds to PI(4,5)P2 in oligodendrocyte membranes, ensuring the stable attachment of membrane layers and their compaction (Nawaz et al., 2009). Indeed, *in vitro* experiments show that Mbp directly competes with actin disassembly proteins for binding to membrane PI(4,5)P2, providing a link between actin disassembly and myelin wrapping (Zuchero et al., 2015).

In conclusion, recent studies highlight the critical role of the actin dynamics in myelination. Actin polymerization is needed to drive protrusion extension and establish axonal contact, interaction and ensheathment, whereas actin disassembly promotes wrapping and compaction. Despite the last contributions in the field, the molecular mechanisms that regulate actin dynamics in oligodendrocytes remain to be fully characterized. A better understanding of the actin cytoskeleton role in oligodendrocytes biology, and the possible implication of other actin-related proteins in the process needs to be clarified.

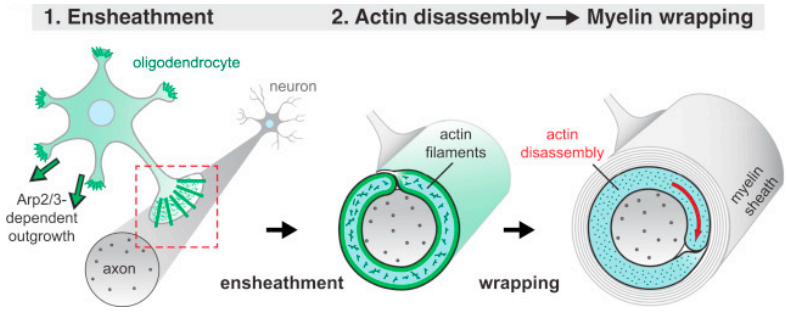

Figure 16 - The two-step model of actin dynamics in developmental myelination. From Zuchero et al., 2015. (1) Ensheathment of axons by oligodendrocyte protrusions requires F-actin polymerization that is driven by the Arp2/3 complex. (2) Actin disassembly occurring in the inner tongue facilitates myelin wrapping and compaction.

AIMS

Aims

Myelination is an essential feature of the nervous system of vertebrates. The importance of myelin is illustrated by the severe neurological conditions resulting from dysmyelination and demyelination in humans. We still lack good understanding of how developmental myelination takes place, and exactly how the different steps of this intricate process, specifically the morphological and antigenic differentiation of oligodendrocytes, a pre-requisite for axonal contact and ensheathment, are regulated. We hypothesize that actin cytoskeleton dynamics, and particularly actin-related proteins that are spatio-temporally restricted to or enriched within oligodendrocyte progenitor cells protrusions, are likely to be important to convey morphological plasticity to oligodendrocyte progenitor cells and oligodendrocytes, thus regulating protrusion extension, axon contact and wrapping.

The aim of this work was to study and characterize in detail the actin-dependent cellular events leading to the first stages of protrusion extension and axonal contact. For that, the function of the actin-related protein Jmy was analyzed both in oligodendrocyte differentiation and myelination *in vitro*. The following tasks were performed to characterize:

1. Expression of Jmy in:
    - White matter tracts of the mouse CNS;
    - Oligodendrocyte differentiation *in vitro*.
2. The role of Jmy in:
    - The morphological and antigenic differentiation of oligodendrocytes *in vitro*;
    - The establishment of the oligodendrocyte:axon unit.
3. Morphodynamics of oligodendrocytes during *in vitro* differentiation using a semi-automated macro specifically developed for this task.

Together, this complementary set of experiments allowed us to explore the role of the actin cytoskeleton dynamics in oligodendrocyte differentiation and axonal contact, and to further elucidate how actin dynamics regulates oligodendrocyte myelination capacity.

RESULTS

CHAPTER 1

Jmy, a multifunctional actin regulator expressed in oligodendrocytes

Introduction

The nervous system of vertebrates is characterized by the presence of an insulator membrane, the myelin sheath, that wraps axons and allows for rapid and efficient saltatory conduction of the action potential. In the CNS, oligodendrocytes are the specialized cells responsible for producing and depositing myelin.

Oligodendrocyte development follows a stereotypical sequence of events. Migration of OPCs, from their sites of origin towards the different developing white matter regions throughout the CNS, is the first event to take place (Kessaris et al., 2006). This migratory phase is then followed by proliferation and expansion of the OPC pool, and by differentiation of OPCs into myelinating oligodendrocytes that will contact and myelinate axons. Establishment of this functional interaction requires the oligodendrocyte to extend multiple protrusions that survey the surrounding environment, followed by membrane deposition and axonal wrapping (Sherman & Brophy, 2005). Like in humans, myelination is timely and spatially coordinated in the mouse nervous system, starting at birth in the spinal cord and brain and later, at around P6, in the ON (Foran & Peterson, 1992).

Oligodendrocytes respond to different extracellular stimuli and neuron-derived signals by activating pathways that drive both the morphological alterations needed for myelination to occur and the expression of myelin genes that will give rise to the major structural components of mature sheaths (Simons & Nave, 2015). In fact, the extraordinary morphological plasticity intrinsic to oligodendrocytes during differentiation is a pre-requisite for myelin sheath formation (Azevedo et al., 2018). However, the molecular machinery linking and controlling this aspect of oligodendrocyte biology is still poorly understood.

Primary cultures of OPCs recapitulate to a great extent the *in vivo* developmental program: *in vitro* OPCs are motile and proliferate in the presence of mitogens (Fruttiger et al., 1999; McKinnon et al., 1990; Noble et al., 1988; Raff et al., 1988; Richardson et al., 1988), and can be induced to differentiate into mature oligodendrocytes upon withdrawal of the mitogen factors. Oligodendrocyte differentiation *in vitro* is also driven by a cell-autonomous transcriptional program that regulates the morphological changes (cells form a complex network of membrane protrusions and assemble myelin-like sheaths) and the concomitant expression of myelin proteins (Kachar, Behar, & Dubois-Dalcq, 1986), which make primary cultures of OPCs a good experimental model to study oligodendrocyte biology and differentiation.

Different studies have looked at the transcriptional program that governs differentiation in oligodendrocytes (Cahoy et al., 2008; Dugas et al., 2006; Nielsen et al., 2006; Zhang et al., 2014). Among the most heavily regulated genes, aside from those encoding for myelin proteins, are the ones involved in cell cycle and motility, adhesion, and cytoskeletal

remodelling. Additionally, recent data from our group shows that there is a spatial enrichment of specific transcripts at the membrane protrusions of OPCs (Azevedo et al., 2018). We found that transcripts encoding for proteins related to cellular component assembly and cytoskeleton organization, and particularly actin-related molecules, were found to be the most abundant in the protrusion-enriched pool of mRNAs. In fact, 64% of the transcripts are functionally related to the actin network and 28% are microtubule function related (Azevedo et al., 2018). These results provided additional evidence to support a major role for actin-related proteins in the regulation of oligodendrocyte differentiation and myelination.

One of the asymmetrically distributed transcripts in OPCs is Jmy, displaying higher expression in membrane protrusions during the initial phase of extension, compared to the soma (Azevedo et al., 2018). Interestingly, however, Jmy was not found enriched in protrusion-like structures of other cells such as fibroblast pseudopodia, axons and neurites (Azevedo et al., 2018), suggesting a possible functional role of Jmy in protrusion extension specifically in OPCs.

Jmy, the junction-mediating and regulatory protein, is a multifunctional actin regulator that can act as a pro-nucleating factor for the Arp2/3 complex, thus forming branched actin filaments, or it can promote nucleation of unbranched filaments by itself (Zuchero et al., 2009). Ubiquitously expressed, in the mouse brain Jmy is found at higher levels in newly formed oligodendrocytes and endothelial cells (Zhang et al., 2014). Jmy is required for regulation of fast actin rearrangements at the cell leading edge, an important feature for cell migration (Coutts et al., 2009; Zuchero et al., 2009). However, in neuroblastoma cells it acts as a negative regulator of neuritogenesis (Firat-Karalar et al., 2011).

Based on a possible function of Jmy in protrusion extension specifically in OPCs, we decided to study if Jmy is involved in controlling actin dynamics during oligodendrocyte differentiation. Since Jmy had not been previously studied in brain cells, different aspects needed to be addressed in the particular context of oligodendrocyte biology. Therefore, we addressed: 1) expression of Jmy during developmental myelination as well as during oligodendrocyte differentiation *in vitro*; 2) subcellular localization of Jmy, which is known to be determinant for its functions (Zuchero et al., 2012); and 3) distribution of Jmy in actin-rich structures. By making use of CNS mouse tissue, we showed that Jmy is expressed in myelin-rich areas during developmental myelination and present specifically in pro-myelinating oligodendrocytes. Additionally, and taking advantage of primary cultures of OPCs, we also showed that Jmy expression is upregulated during oligodendrocyte differentiation *in vitro,* being mainly expressed in regions of higher F-actin content in OPCs membrane protrusions, and in the perinuclear region of both OPCs and myelinating oligodendrocytes.

Results

Developmental expression of Jmy in the mouse central nervous system

The expression of Jmy *in vivo* was assessed in white matter areas of the mouse CNS during developmental myelination, which occurs in the early postnatal period. Double immunofluorescence analysis showed that, during developmental myelination, Jmy is predominantly expressed in cells positive for CC1 (Figure 17 A, C and E), a marker of pro-myelinating and mature oligodendrocytes (Bhat & Zhang, 1996). Quantification of the number of cells positive for both Jmy and CC1 showed a significantly increase during active myelination in the mouse spinal cord (at P5), cerebellum (from P5 to P14) and optic nerve (around P14) (Figure 17 B, D and F). An important aspect to highlight is the fact that approximately 25-30% of CC1-posititve oligodendrocytes transiently co-express Jmy in the first 14 postnatal days (Figure 17), which points for a possible role of Jmy during a specific time window of differentiation in pro-myelinating and/or myelinating oligodendrocytes.

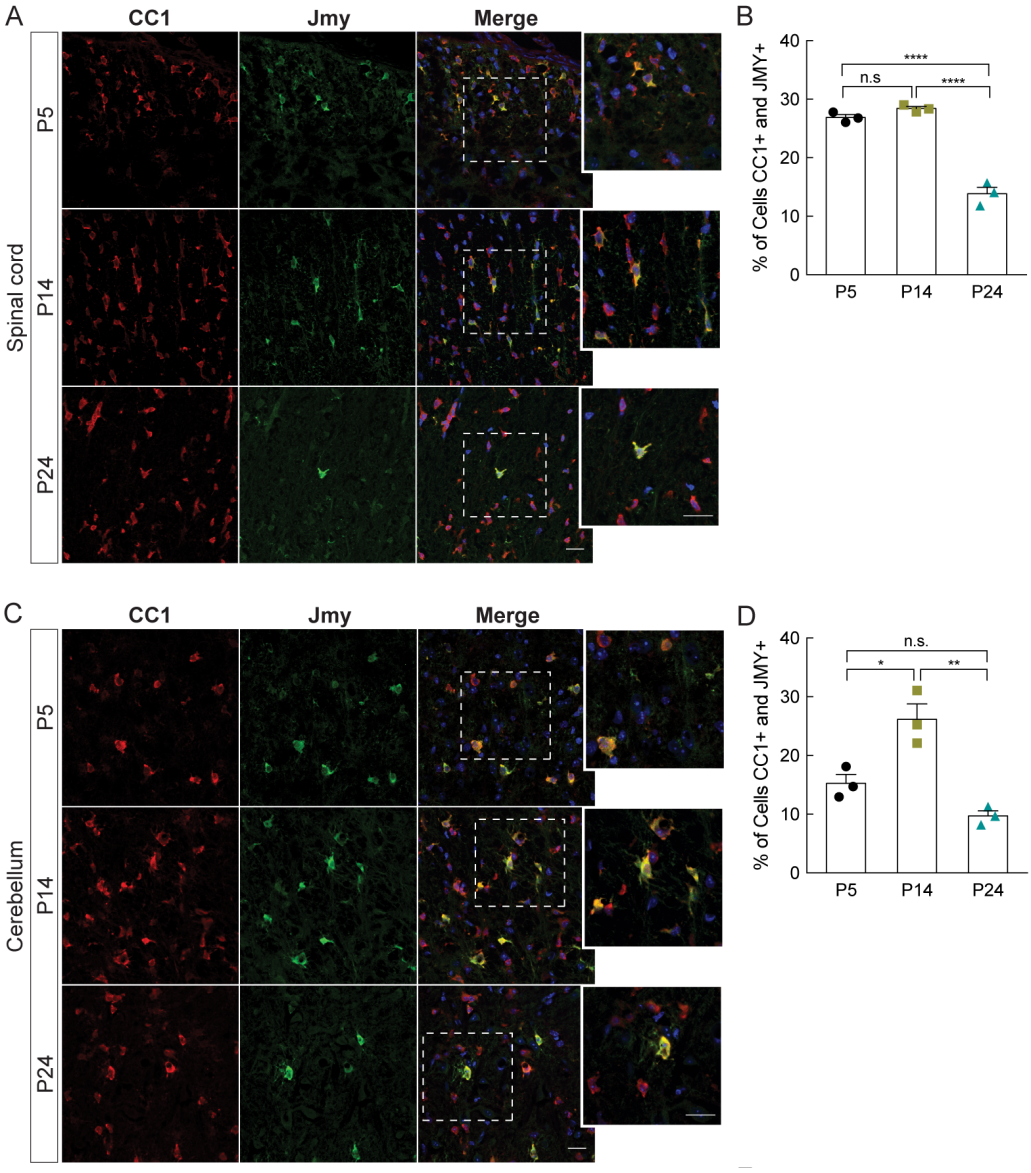

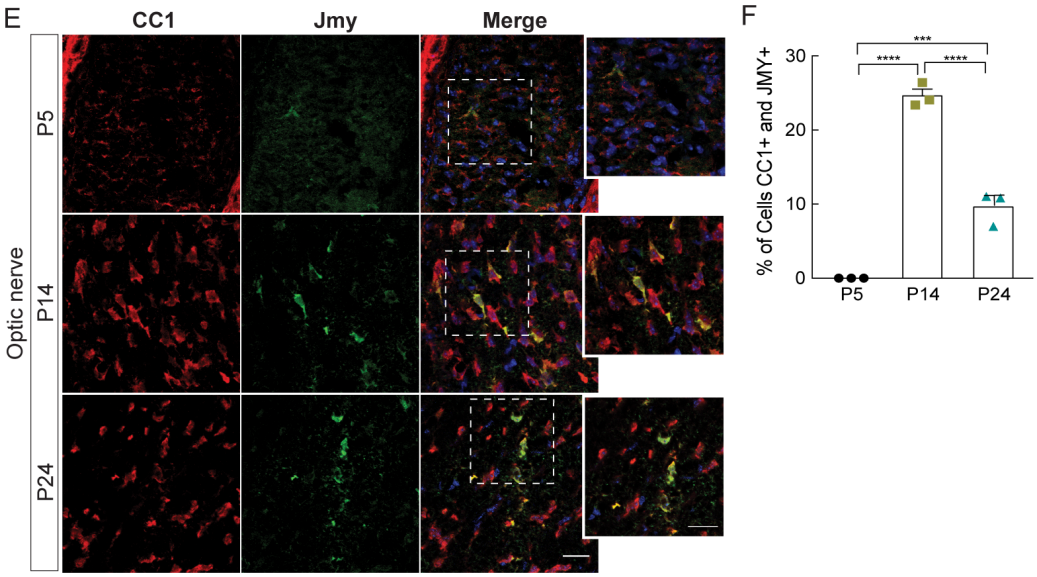

Figure 17 - Jmy is predominantly expressed in oligodendroglia during postnatal development in the mouse CNS. Representative single plane confocal images of immunohistochemistry (IHC) of transversal sections of mouse (A) spinal cord, (C) cerebellum and (E) optic nerve to label oligodendrocytes (CC1, red), Jmy (green) and nuclei (DAPI, blue), with zoomed in detail of the areas indicated by the white frames. Scale bars 20 µm. Quantification of oligodendrocytes co-expressing CC1 and Jmy in CNS regions (B, D and F, correspond to spinal cord, cerebellum and optic nerve, respectively). Three whole, non-consecutive sections per animal were used for quantification. Data represented as mean ± SEM of 3 animals (n.s.=p>0.05, *p<0.05, **p<0.01, ***p<0.001, ****p<0.0001, calculated using one-way ANOVA followed by Tukey's multiple comparisons test).

Assessment of the expression levels of Jmy by immunoblot revealed a similar trend in myelin-rich CNS regions during developmental myelination (Figure 18 A and B).

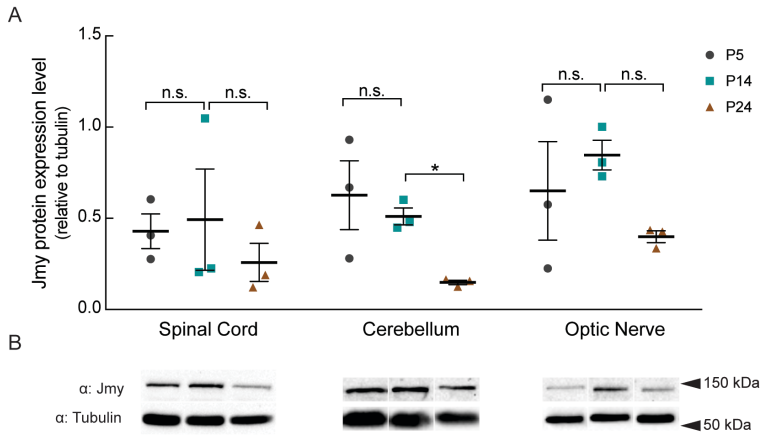

Figure 18 - Expression levels of Jmy during developmental myelination. Immunoblot analysis (A and B) of Jmy in total extracts from spinal cord, cerebellum and optic nerve at P5, P14 and P24. Data represented as mean of the normalized relative densities ± SEM of n=3, (n.s.=not significant, *p<0.05, calculated using one-way ANOVA followed by Tukey's multiple comparisons test (for cerebellum and optic nerve) or Friedman test followed by Dunn's multiple comparisons test (for spinal cord)).

In order to understand if Jmy localizes to myelin sheaths in myelinated tracts, we assessed its co-expression in the spinal cord, cerebellum and optic nerve during developmental myelination. Mbp was used as a marker for myelin sheaths. We found no

evidence of co-localization of Jmy and Mbp in myelinated tracts, suggesting that Jmy is not present in the sheaths (Figure 19 A, B and C).

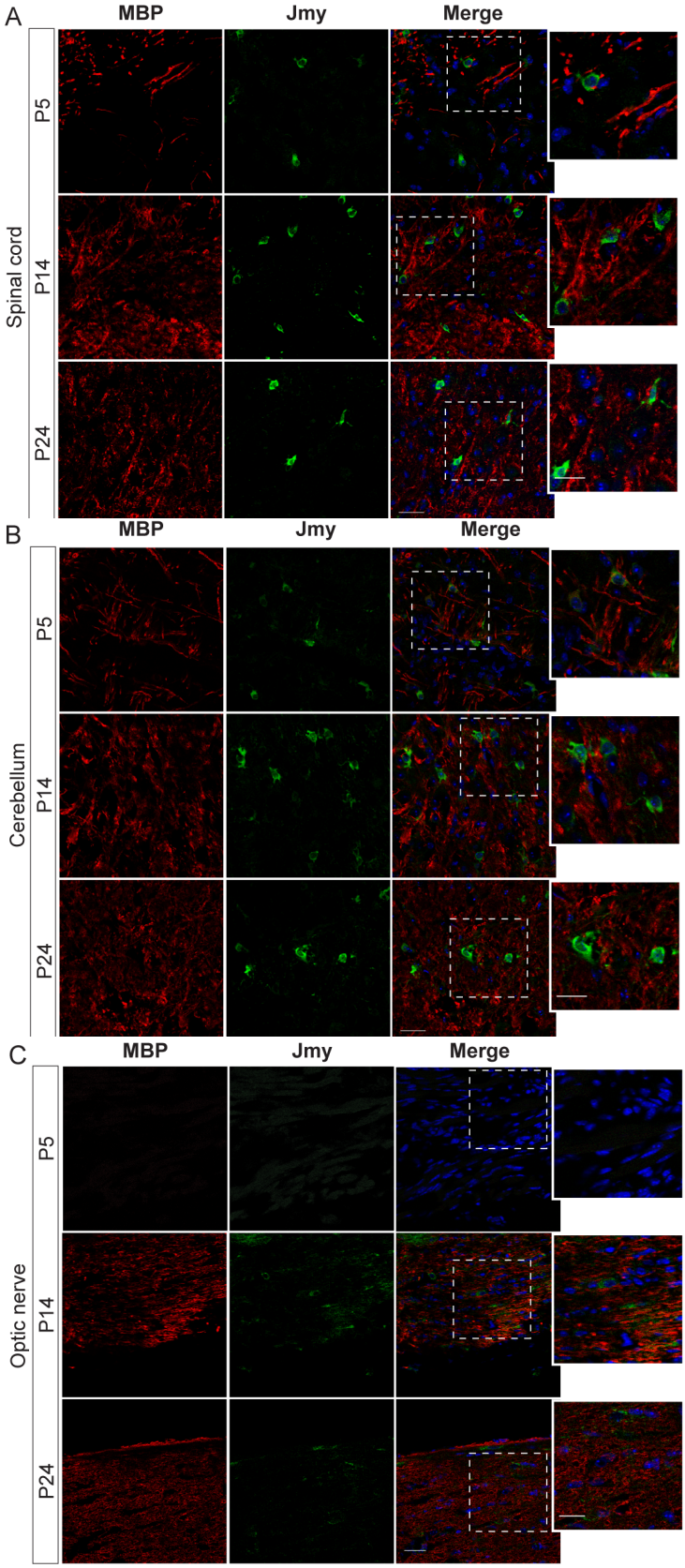

Figure 19 - Jmy is not found in myelin sheaths. IHC of transversal sections of mouse spinal cord (A), cerebellum (B) and longitudinal optic nerve sections (C) to label Mbp (red), Jmy (green) and nuclei (DAPI, blue). Scale bars 30 µm. Detail of the framed areas are shown in the inset images for each panel - scale bars 20 µm.

Expression of Jmy during oligodendrocyte differentiation *in vitro*

The expression profile of Jmy during oligodendrocyte differentiation was characterized using *in vitro* cultures of OPCs obtained from neonate rat brains. The analysis of Jmy transcript levels by qPCR showed an upregulation during oligodendrocyte differentiation (Figure 20 A). In line with that, protein levels showed an increase of approximately 4-fold in the first 3 days of differentiation (DOD), an increase that was sustained as oligodendrocytes differentiated further (Figure 20 B).

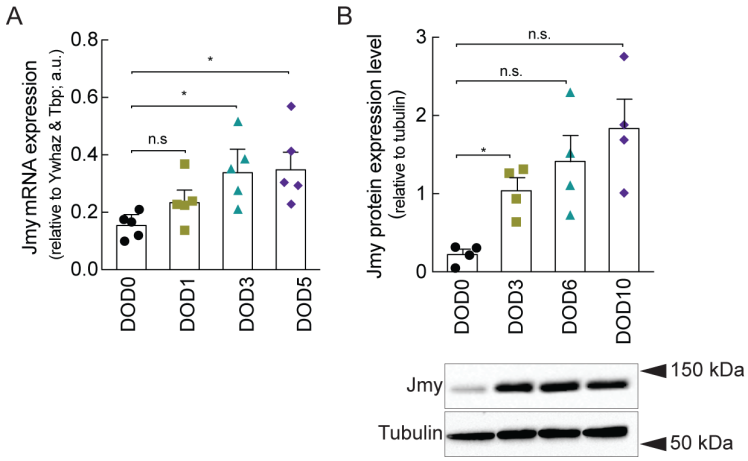

Figure 20 - Expression of Jmy is upregulated during differentiation. Expression levels of Jmy mRNA (A) and protein (B) were assessed by qPCR and immunoblotting, respectively, in primary rat OPCs (DOD0) and differentiating oligodendrocytes (DOD3, 5, 6 and 10). (A) Relative transcript expression levels calculated as $2^{-\Delta Ct}$ (**p<0.01, calculated using one-way ANOVA followed by Tukey's multiple comparisons test on $2^{-\Delta Ct}$ values of n=5 biological replicates collected from independent experiments). (B) Data represented as mean of the normalized relative densities ± SEM of n=4 biological replicates collected from independent experiments (*p<0.05, calculated using one-way ANOVA followed by Tukey's multiple comparisons test). Tubulin was found to be stably expressed during oligodendrocyte differentiation and was used as a loading control in all immunoblots performed.

Jmy was initially described as a p300 transcription cofactor, active in the p53 response to cellular stress (Shikama et al., 1999), being present in both the nucleus and the cytosol of human leukemic (HL)-60 cells, U2OS and fibroblast cells (Zuchero et al., 2012; Zuchero et al., 2009). However, in motile cells, such as neutrophils, Jmy is enriched in the cytoplasm and found at the leading edge of cells (Zuchero et al., 2009). The mechanism of Jmy translocation from the cytoplasm into the nucleus was shown to be dependent on the levels of monomeric actin in the cytoplasm. A nuclear localization sequence (NLS) was found in the structure of Jmy, partially overlapping with the WH2 domains. Additionally, translocation of Jmy to the nucleus was shown to be regulated by the importin machinery (Zuchero et al., 2012). A mechanism for how actin dynamics directs the nuclear import of Jmy was suggested based on the spatial overlap of the NLS and the actin-binding WH2 domains: the binding of monomeric actin to the WH2 domains blocks the access of the importin α/β complex to the NLS region, which blocks the translocation of Jmy to the nucleus (Zuchero et al., 2012). A competition

between actin and importins for direct binding to Jmy is the proposed mechanism that regulates its cellular localization. We assessed the subcellular localization of Jmy in oligodendrocytes at different stages of differentiation by immunofluorescence analysis. Jmy was mainly detected in the cytoplasm, showing a punctate staining pattern with widespread cytosolic distribution in both OPCs and oligodendrocytes. Additionally, a prominent localization in the perinuclear region of the cell soma is also visible (Figure 21 A). Of particular interest, we noticed that during early differentiation (at DOD1 to 3), when oligodendrocytes are undergoing extension and branching of membrane protrusions, Jmy was detected in discrete sites of strong F-actin labelling throughout the protrusions (Figure 21 A and B arrows). F-actin was stained with phalloidin, a phallotoxin produced by the mushroom *Amanitaphalloides*, used as a probe that selectively binds F-actin and prevents its depolimerization (Dancker et al., 1975).

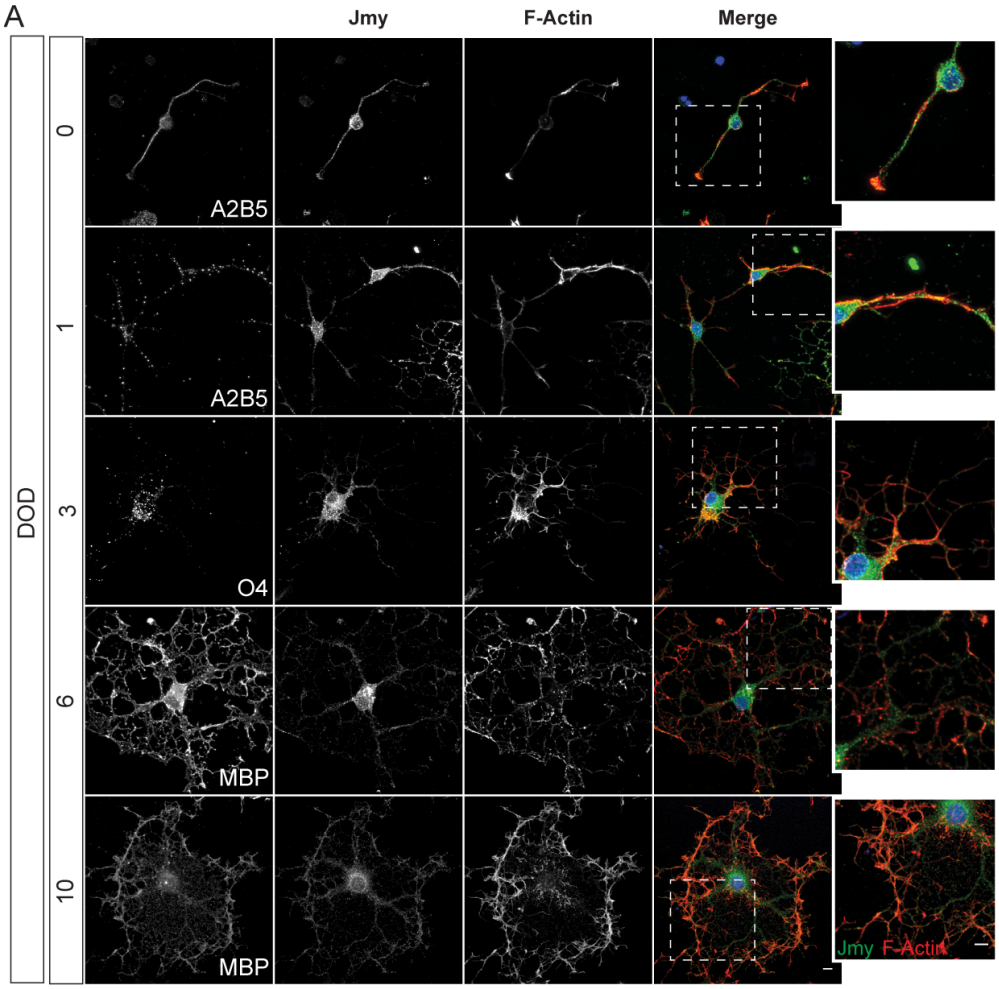

B

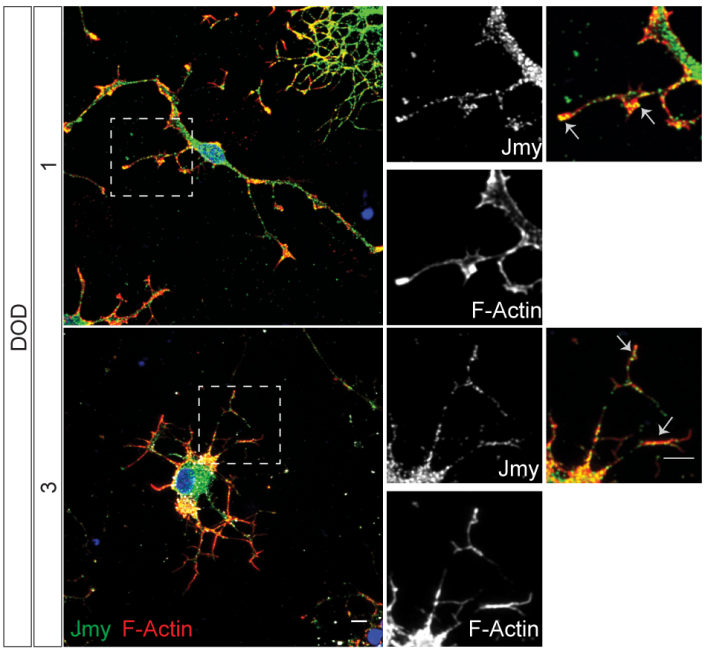

Figure 21 - Jmy localizes to the perinuclear region and membrane protrusion of oligodendrocytes. (A) Representative images of confocal deconvoluted Z-projections showing the cellular distribution of Jmy at different stages of oligodendrocyte differentiation. Immunofluorescence (IF) labelling was performed for an oligodendrocyte lineage marker (A2B5, O4, or Mbp), Jmy (green), F-actin (phalloidin, red), and nuclei (DAPI, blue). Scale bars 5 µm. (B) Representative images of confocal deconvoluted Z-projections showing Jmy in sites of F-actin enrichment in oligodendrocyte protrusions (arrows) early in differentiation, at DOD1 and DOD3. IF labelling was performed for an oligodendrocyte lineage marker (A2B5 or O4), Jmy (green), F-actin (phalloidin, red), and nuclei (DAPI, blue). Scale bars 5 µm.

Since Jmy can shuttle between the cytoplasm and the nucleus of the cells (Coutts et al., 2007; Zuchero et al., 2012; Zuchero et al., 2009), we decided to further investigate if in oligodendrocytes Jmy is regulated by its subcellular localization. For that, expression levels of Jmy were analyzed by immunoblot in subcellular fractions of oligodendrocytes at different stages of differentiation. Jmy was mainly detected in cytoplasm-enriched fractions containing heat shock protein (HSP) 90, a predominantly cytosolic protein, compared to nuclear-enriched fractions, containing histone H3, a nuclear protein (Figure 22 A). Taking advantage of the fluorescence images of oligodendrocytes double stained for Jmy and DAPI, we measured the relative intensities of both Jmy and DAPI across the nucleus, which showed little overlap of fluorescence signals (Figure 22 B). Together, these observations suggest that Jmy is expressed and transcriptionally upregulated during oligodendrocyte differentiation, particularly during stages of intense actin filament assembly. Furthermore, its role in oligodendrocytes biology is probably independent of its nuclear function as a transcription co-factor: although Jmy was not completely excluded from the nucleus, we found significant enrichment in the cytoplasm during all stages of differentiation.

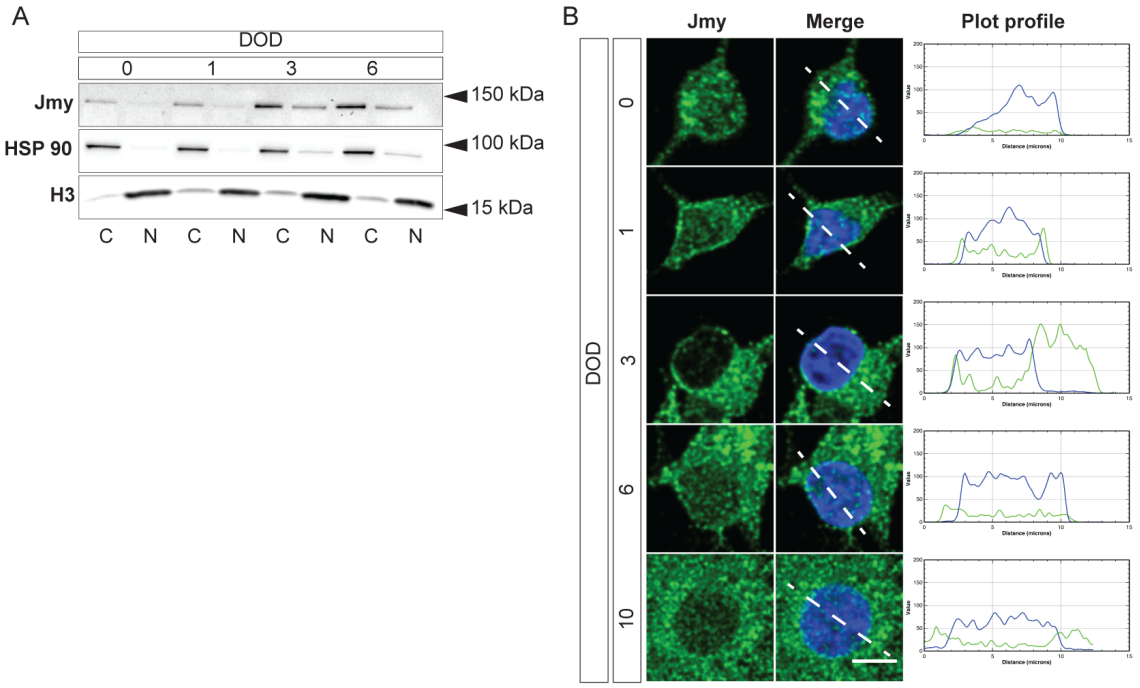

Figure 22 – Jmy mainly localizes to the cytoplasm of oligodendrocytes. (A, B) Relative subcellular distribution of Jmy in oligodendrocytes assessed by: (A) immunoblotting of sub-fractionated OPCs and oligodendrocytes lysates collected during differentiation. Both cytoplasmic and nuclear samples were immunoblotted against Jmy, HSP90 (a cytoplasmic-enriched protein) and histone H3 (a nuclear protein). (B) Middle plane representative images of high magnification of the oligodendrocyte soma that were used to determine DAPI and Jmy intensities that were plotted as a function of position across a line (shown in the images as an overlay). Scale bar is 5 μm.

Discussion

During development, OPCs need to proliferate and migrate to reach their final destinations, where they will differentiate into myelinating oligodendrocytes capable of contacting and wrapping axons. Morphological differentiation relies on extreme remodeling of the oligodendrocyte architecture, which requires an enrichment of specific mRNAs in the protrusions (Azevedo et al., 2018). The junction mediating and regulatory protein (Jmy), a multifunctional actin regulator that was found to be asymmetrically distributed, shows higher expression of it transcripts in membrane protrusions than in soma during the initial phase of protrusion extension in OPCs. Of interest, Jmy was only found to be enriched in membrane protrusions of OPCs, which point to a specific role of Jmy in oligodendrocytes (Azevedo et al., 2018).

To assess the expression of Jmy in myelinated tracts of the CNS, we have analyzed myelin-rich areas of the mouse CNS, including the optic nerve, spinal cord and cerebellum, during developmental myelination. Furthermore, expression of Jmy was also assessed during oligodendrocyte differentiation *in vitro.* Our results show that Jmy is enriched in pro-myelinating oligodendrocytes in the mouse CNS during developmental myelination, and its expression is upregulated during oligodendrocyte differentiation *in vitro*. Interestingly, it was already showed that other NPFs are expressed in the CNS. Transcripts of WAVE1, WASP and N-WASP were detected in mouse brain, with the expression of WAVE1 shown to be developmentally regulated and temporally linked to the onset of myelination (Kim et al., 2006). Isolated oligodendrocytes were also shown to express several actin-related proteins: formins, WASP, WHAMM, WIP, and the Arp2/3 complex are expressed mainly by OPCs, whereas CARMIL and WAVE are highly expressed in newly formed oligodendrocytes (Zhang et al., 2014). Indeed, actin-related proteins seem to be important for oligodendrocyte biology, particularly in the initial phase of differentiation, which is in line with our results.

The analysis of Jmy co-expression with CC1 in different myelin-rich areas of the mouse CNS showed that expression profile of Jmy accompanied the different rates of oligodendrocyte lineage progression and myelination (Foran & Peterson, 1992). Jmy is detected first in the spinal cord and later in the optic nerve and cerebellum, because oligodendrocytes first colonize the spinal cord and then, the optic nerve and cerebellum (Foran & Peterson, 1992). Moreover, Jmy has its highest expression at 14 postnatal days, a developmental time window that in the optic nerve, for example, represents the period of axon ensheathment (Dangata & Kaufman, 1997). This observation suggest that Jmy plays a role during a specific time window of differentiation, in pro-myelinating and/or myelinating oligodendrocytes. Because only 25-30% of CC1 positive oligodendrocytes are positive for Jmy during active myelination, it would be interesting to use a different antigenic marker to understand the difference between the double

and single-CC1 labelled cells. It is likely that oligodendrocytes double-positive for CC1 and Jmy have the antigenic machinery already seated to initiate myelination, but still bearing morphology of a less mature oligodendrocyte. The need for further actin cytoskeleton rearrangements, in order to reach a fully mature morphology, would explain the expression of Jmy in a such specific population of oligodendrocytes. ENPP6, a choline-specific phosphodiesterase, was recently described as a new marker of early oligodendrocyte differentiation (Morita et al., 2016). Expressed before Mbp and Mag, and after Pdgfrα, ENPP6 overlaps with the onset of CC1 expression (ENPP6^{high}), but it is downregulated in more mature myelinating oligodendrocytes (ENPP6^{low}) (Xiao et al., 2016). Therefore, the use of ENPP6 could allow us to understand if CC1 and Jmy double positive oligodendrocyte are earliest formed CC1 positive cells or more mature myelinating oligodendrocytes. Jmy was not found localized in the myelin sheaths. In fact, actin nucleators were not found in the proteomic analysis of CNS myelin (Jahn et al., 2009), which is in line with our observation that Jmy is absent from myelin sheaths.

When analyzing the expression of Jmy during oligodendrocyte differentiation *in vitro*, our results showed that transcript levels of Jmy, as well as its protein expression levels, are upregulated. Particularly, Jmy was found significantly upregulated during stages characterized by intense actin filament assembly, at the transition from DOD0 to DOD3, and found in areas enriched in phalloidin staining, which strongly point for a role of Jmy in the assembly of F-actin. Interestingly, Jmy is described to co-localize with actin filaments at: the leading edge of B16-F10 mouse melanoma cells, U2OS cells and primary neutrophils, and at the cell cortex of differentiated HL-60 cells, driving actin nucleation (Zuchero et al., 2009). So, it would not be surprising that Jmy has a role in driving actin polymerization in oligodendrocytes.

Our *in vitro* results regarding oligodendrocyte differentiation seem to be in line with the ones obtained in the *in vivo* analysis. *In vitro*, Jmy is highly expressed in oligodendrocytes that are undergoing extensive cytoskeleton remodeling, and the same is probably happening *in vivo* since Jmy has its higher expression when active myelination is occurring, being expressed in a particular subpopulation of CC1 positive cells that. We propose that they are in a more immature state of morphological differentiation.

The role of Jmy in oligodendrocyte biology is probably independent of its nuclear function as a transcription co-factor. Although Jmy was not completely excluded from the nucleus, we found significant enrichment in the cytoplasm during all stages of oligodendrocyte differentiation. Additionally, assessment of Jmy subcellular localization by immunofluorescence showed its localization in the cytoplasm, mainly in the perinuclear region, exhibiting a punctate staining. This specific localization in the perinuclear region may suggest: 1 - inhibition of nuclear import due to the binding of actin to Jmy's WH2 domain or, 2 - a role

for Jmy in the formation/maintenance of perinuclear actin structures in oligodendrocytes. Since the actin binding domain partially overlaps with the putative NLS region of Jmy (Zuchero et al., 2012), it is conceivable that actin is retaining Jmy in the cytoplasm of oligodendrocyte by masking the putative NLS. Actin cytoskeleton remodeling is a steady feature of oligodendrocyte differentiation, which means that constant changes between both G- and F-actin states can increase, transiently, the pool of G-actin available for binding to Jmy's WH2 region. In this situation, translocation of Jmy to the nucleus is inhibited and its role as nucleator in the cytoplasm of oligodendrocytes can be favored. However, the preferential location of Jmy in the perinuclear region of oligodendrocytes may also suggests an involvement in the formation/reorganization of perinuclear actin structures important for nuclear protection in case of cellular mechanical stimulation and cell migration (Shao et al., 2015; Skau et al., 2016; Thiam et al., 2016). Oligodendrocytes are cells with migratory capacity that constantly perceive the surrounding environment and adapt to the external cues, so it is possible that they have such actin perinuclear structures for nuclear protection, and Jmy may be playing a major role in their formation. Further studies are necessary to confirm the presence of such actin structures in the perinuclear region of oligodendrocytes and investigate the role of Jmy in their assembly.

Collectively, our data showed that Jmy is expressed and transcriptionally upregulated during oligodendrocyte differentiation, particularly during stages of intense actin filament assembly, highlighting its possible involvement in oligodendrocyte differentiation. In line with what is already known in cells with high rates of actin cytoskeleton remodeling such as highly motile neutrophils (Zuchero et al., 2009), in oligodendrocytes Jmy localizes mainly in the cytoplasm, which further stresses its function as an actin nucleator with a specific function in oligodendrocyte biology.

CHAPTER 2

Jmy is required for oligodendrocyte differentiation and establishment of axonal contact

Introduction

Oligodendrocyte differentiation involves extraordinary morphological plasticity, which is a critical requirement for proper myelination of axons. From a less complex morphology characterized by a mainly bipolar shape, oligodendrocytes undergo successive morphological alterations characterized by the extension of multiple and extremely dynamic protrusions. In a coordinated fashion, oligodendrocytes express different proteins that are specific of each stage of differentiation. The combination of both elements is used to assess the degree of maturation of oligodendrocytes *in vivo* as well as *in vitro* (Baumann & Pham-Dinh, 2001). Moreover, taking in consideration both factors, oligodendrocytes can be included into four different categories that represent the different maturation stages: OPCs; pre-oligodendrocytes; immature oligodendrocytes and mature oligodendrocytes.

The extension of specialized cellular protrusions is a hallmark of oligodendrocyte differentiation. These highly dynamic cellular protrusions are responsible for surveying the surrounding environment and integrate different extracellular cues, also being determinant for the establishment of contact with the axons that will be myelinated (Buttery & ffrench-Constant, 2001). Once axons are selected, the oligodendrocyte protrusion establishes contact and myelination starts by deposition of flat sheaths that wrap around the axons, a process that is accompanied by the lateral extension of these membranes in a non-adhesion depend manner (Snaidero et al., 2014).

The precise control of the actin cytoskeleton coordinates the morphological changes characteristic of oligodendrocyte differentiation. Recently, it was shown that protrusive forces generated through F-actin assembly are needed to promote membrane formation at the leading edge of oligodendrocyte protrusions prior to axonal contact and ensheathment. Subsequently, actin depolymerization is necessary for the lateral extension of myelin-like sheaths during wrapping and compaction (Nawaz et al., 2015; Zuchero et al., 2015). Interestingly, myelin basic protein, Mbp, was pointed out as a trigger factor to initiate the disassembly of actin polymers. By direct binding to membrane PI(4,5)P2, Mbp drives the release of actin disassembly proteins that stimulate myelin wrapping (Zuchero et al., 2015).

Several studies have shown the involvement of different actin regulators in oligodendrocyte differentiation. Among others, *in vitro* studies have shown that in OPCs: inhibition of N-WASP blocks protrusion extension (Bacon et al., 2007); downregulation of WAVE blocks protrusion formation (Kim et al., 2006); and depletion of integrin-linked kinase (Ilk) result in loss of their capacity to form complex protrusion networks (O'Meara et al., 2013). In addition, the major actin nucleator, the Arp2/3 complex, was shown to be necessary for oligodendrocyte protrusions outgrowth and for the initiation of myelination (Zuchero et al., 2015). Rho GTPases also play an important role in myelination, as deletion of Cdc42 and Rac1

results in defects in myelin sheath formation (Thurnherr et al., 2006). However, and despite the existing information, how the actin network machinery regulates oligodendrocyte differentiation, and consequently myelination, is still not fully understood.

We showed that Jmy is expressed in myelin rich areas of the mouse CNS during developmental myelination and during oligodendrocyte differentiation *in vitro*. We hypothesized that Jmy may be a major player in oligodendrocyte differentiation, controlling actin dynamics during this process. Functional studies assessing the role of Jmy were conducted by knocking down levels of Jmy in OPCs in culture. We found that Jmy is necessary for morphological plasticity in oligodendrocytes: oligodendrocytes lacking Jmy extend and branch fewer protrusions, resulting in a deficiently arborized morphology associated with decreased F-actin trails along the protrusions. Moreover, oligodendrocyte capacity to form myelin-like sheaths was impaired upon Jmy loss, a defect also seen in oligodendrocyte:axon co-cultures system, where oligodendrocytes with decreased levels of Jmy fail to establish contact with neurites efficiently, and to form myelin segments. Furthermore, Jmy seems to be essential for OPC survival and proliferation.

Results

The role of Jmy in actin filament organization and protrusion extension in oligodendrocytes

Jmy is essential for morphological plasticity during oligodendrocyte differentiation

Control of actin rearrangement is a requirement for normal oligodendrocyte differentiation. To investigate the role of the actin regulator Jmy in this process, a functional analysis was performed using RNAi in order to knockdown Jmy. Two different short hairpin RNAs (shRNAs) were designed, *Jmy*-shRNA construct #1 and #2, and cloned into the lentiviral pSicoR vector, that allows the delivery of shRNAs into mammalian cells through transduction (Ventura et al., 2004). This technique allows for stable integration of shRNAs into the DNA, leading to a long-lasting knockdown of the target genes (Moore et al., 2010) Moreover, primary cultures of OPCs are not transfectable with reasonable efficiency, requiring the use of lentiviral-based shRNAs for successful delivery of RNAi. Knockdown efficiency was tested for both *Jmy*-shRNAs by immunoblot analysis. Similar reduction in the protein levels was obtained for both constructs (Figure 23 A). On average, *Jmy*-shRNA construct #1 showed a knockdown efficiency of 55% and was used in all the experiments reported here. pSicoR lentiviral vector has a second promoter driving expression of EGFP, which was used as a marker of successful lentiviral transduction.

The morphological differentiation of oligodendrocytes was followed using phalloidin staining. Actin labelling of the entire oligodendrocyte allowed us to follow fine changes in cell shape and assess morphological states in oligodendrocytes transduced with *Jmy*-shRNA (sh*Jmy*-OLs) or a non-targeting shRNA (shCtr-OLs). As expected, during differentiation shCtr-OLs suffer a dramatic morphological transformation: from a multipolar state at DOD3, characterized by the extension of new protrusions associated with branching, oligodendrocytes successively increase their complexity, by augmenting the number of branched protrusions (DOD6), until they reach a highly arborized morphology that precedes the flattening of protrusions to form membranous sheaths characteristic of mature oligodendrocytes *in vitro* (DOD10) (Figure 23 B). However, differentiating sh*Jmy*-OLs did not form a complex arborization, but instead displayed less membrane protrusions and decreased branching (Figure 23 B). To further investigate these discrepancies in morphological differentiation, total cytoskeletal area of shCtr-OLs and sh*Jmy*-OLs was measured based on the cells F-actin staining. Interestingly, when compared to shCtr-OLs, sh*Jmy*-OLs were

generally smaller during all stages of differentiation, although the difference in cell area did not reach statistical significance at DOD10 (Figure 23 C).

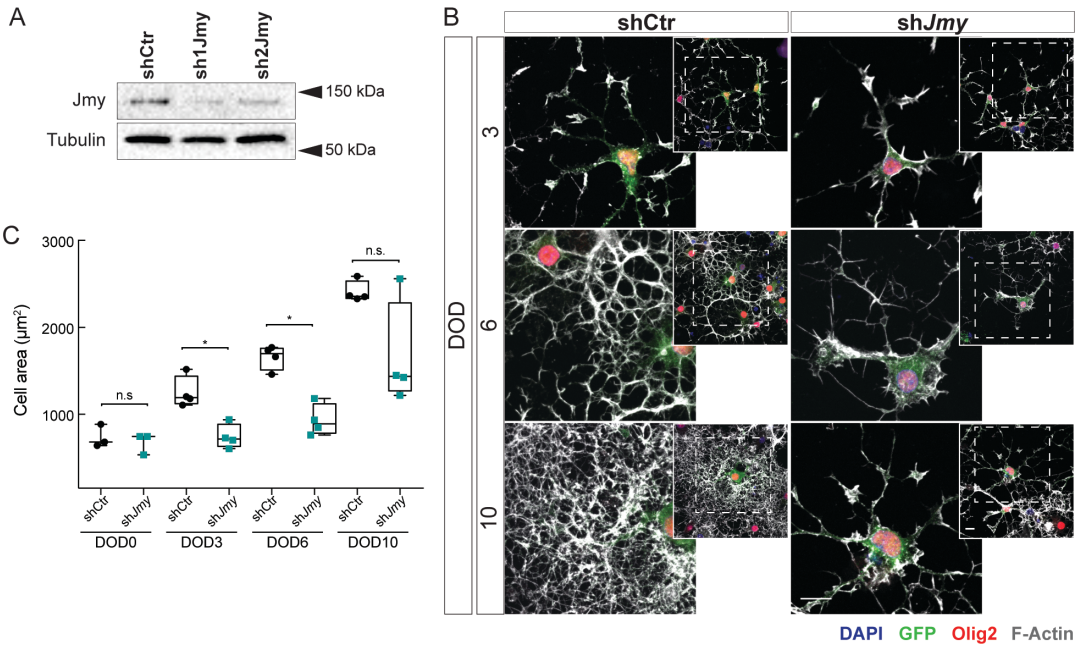

Figure 23 - Jmy is required for normal morphological differentiation of oligodendrocytes. (A) Immunoblot analysis to assess knockdown efficiency of Jmy in OPCs after transduction with two different shRNA sequences. Tubulin was used as loading control. (B) Representative single plane confocal images showing morphological differentiation of transduced shCtr- or sh*Jmy*-OLs. IF labeling was performed for an oligodendrocyte lineage marker (Olig2, red), F-actin (phalloidin, grey), and nuclei (DAPI, blue), and GFP was used as a reporter of transduction. A zoomed out view of the framed areas is shown for each image. Scale bar is 20 µm. (C) F-actin staining of $GFP^+/Olig2^+$ cells was used to determine the total area of the cell. Data represented as median area ± min and max values of n=4 independent experiments, with at least 30 $GFP^+/Olig2^+$ cells in each condition analyzed per experiment (n.s.= not significant; **p<0.01, calculated using the Mann Whitney test).

It is well established that the maturation state of oligodendrocytes can be correlated with different levels of protrusion branching (Bauer, Nina G. et al., 2009; Thurnherr et al., 2006). We classified oligodendrocytes into four different morphological branching stages (from stage I to stage IV) based on their degree of morphological complexity during differentiation. At DOD3, we observed more sh*Jmy*-OLs arrested in a more immature morphology (stage II), showing mainly primary protrusion (Figure 24 A). In line with this, Sholl analysis at the same day of differentiation revealed that sh*Jmy*-OLs protrusions have significantly less intersections per Sholl ring compared to shCtr-OLs, which means that sh*Jmy*-OLs display a decreased morphological complexity (Figure 24 B). At DOD6, sh*Jmy*-OLs persisted as multipolar or arborized cells (stage II and III), and very few formed lamellar structures or membranous sheaths (stage IV), comparing to shCtr-OLs (Figure 24 A). Importantly, even after 10 days of differentiation, most sh*Jmy*-OLs still as stage III cells presenting a less mature morphology, indicating that defects in branching earlier in differentiation lead to a partial arrest, and not a delay, in the timing of morphological differentiation. Overall, during differentiation sh*Jmy*-OLs

showed a less complex morphology when compared to shCtr-OLs, which suggests that Jmy is essential for normal morphological differentiation.

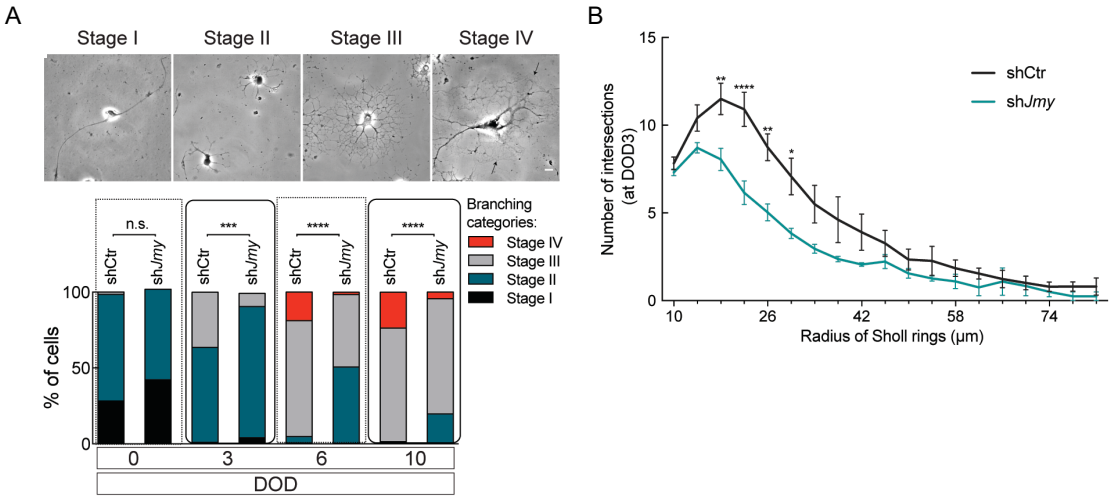

Figure 24 - Depletion of Jmy leads to arrested morphological differentiation of oligodendrocytes. (A) Representative phase-contrast images of oligodendrocytes morphological categories during differentiation, which were used to classify the differentiation stage of shCtr- and sh*Jmy*-OLs. Morphology of GFP$^+$/Olig2$^+$ cells was assessed using images of stained F-actin and phase contrast. Data are represented as the percentage of cells counted in each morphological category at different times of differentiation. The total cells analyzed were pooled from 3 independent experiments, with at least 70 GFP$^+$/Olig2$^+$ cells in each condition collected per experiment. A significant association was found at DOD3 ($\chi^2_{(2,\ N=700)}$=17.42, ***p<0.001), DOD6 ($\chi^2_{(2,\ N=827)}$=50.83, ****p<0.0001) and DOD10 ($\chi^2_{(2,\ N=695)}$=30.51, ****p<0.0001), calculated using the Chi-square test. (B) Sholl analysis was performed in shCtr- and sh*Jmy*-OLs to measure complexity and length of protrusions at DOD3. The analysis was performed using images of stained F-actin. The number of intersections between protrusions and the concentric rings was determined and plotted as a function of distance from the cell body (starting radius: 10 µm; step size: 4 µm; end radius: 82 µm). Data represented as mean ± SEM of n=4 independent experiments, with at least 40 GFP$^+$/Olig2$^+$ cells in each condition analyzed per experiment (*p<0.05, **p<0.01 ****p<0.0001, calculated using two-way ANOVA followed by Sidak's multiple comparisons test).

Jmy is involved in actin filament assembly during early protrusion extension in oligodendrocytes

Jmy is capable of promoting actin nucleation by itself, or through activation of the Arp2/3 complex working in this case as an actin nucleation promoting factor (Zuchero et al., 2009). We decided to investigate if disrupting the expression of Jmy affects the F-actin content during early oligodendrocyte differentiation. Super-resolution microscopy of live differentiating oligodendrocytes was used in combination with the fluorogenic probe SiR-actin (a silicon-rhodamine (SiR) derivative, fluorogenic upon interaction with polar proteins, conjugated with desbromo-desmethyl-jasplakinolide, which binds specifically to F-actin (Lukinavicius et al., 2014)) to label the oligodendrocyte actin cytoskeleton. Early in differentiation, star-shaped and arborized shCtr-OLs have abundant, thick, bundles of F-actin visible in the many protrusions that characterize cells in this stage of differentiation (Figure 25, arrows). In contrast, sh*Jmy*-

OLs showed “hollow” protrusions (Figure 25, arrowheads) void of actin trails, suggesting that less F-actin was present in these structures. These results indicate that Jmy is necessary for F-actin filament assembly in the early oligodendrocyte differentiation.

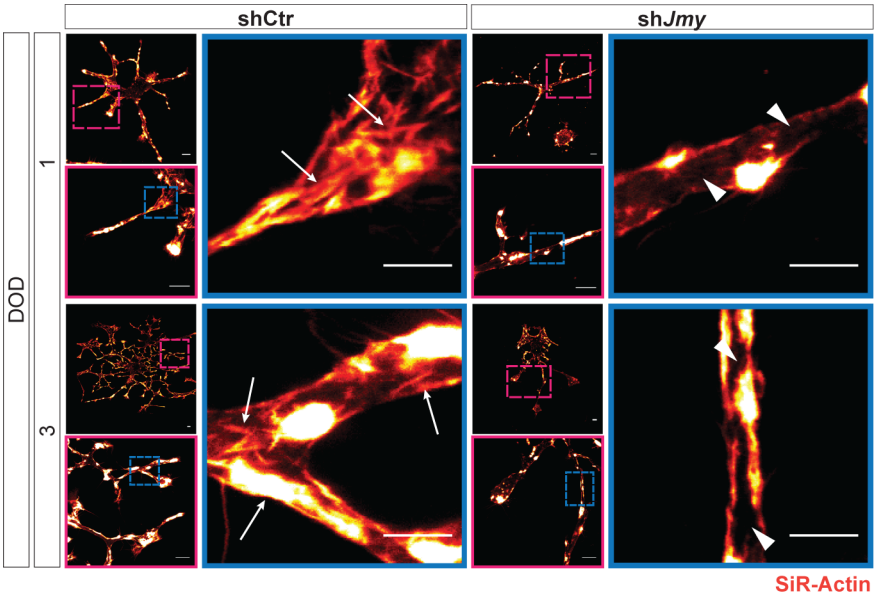

Figure 25 - Morphological differentiation of oligodendrocytes requires Jmy-dependent assembly of F-actin. (A) Representative live STED super resolution microscopy images of shCtr- and sh*Jmy*-OLs at DOD1 and 3. Shown are thick bundles of F-actin (arrows) found in the many protrusions of star-shaped shCtr-OLs early in differentiation, which are not seen in the “hollow” protrusions (arrowheads), void of actin cables, of sh*Jmy*-OLs. Scale bar is 5 µm on the left upper and lower panels, and 2 µm on the panels to the right.

F-actin distribution during oligodendrocyte differentiation

To further investigate how actin remodeling occurs during oligodendrocyte morphological differentiation, we used the probe SiR-Actin to label F-actin in live oligodendrocytes. Analysis with SiR-Actin was performed in sh*Jmy*- and shCtr-OLs. Live-cell imaging of actin cytoskeleton dynamics showed that during the initial extension of protrusions, levels of F-actin in shCtr-OLs were highly increased at the leading edge of the growth cone-like structures (Figure 26 and Supporting Information Movie S4). As oligodendrocytes progress to the stage of arborization, high levels of F-actin are seen in newly-formed secondary and tertiary branches, away from primary processes and the cell body (Figure 26 and Supporting Information Movie S4). This is in sharp contrast with what was seen in sh*Jmy*-OLs, which

exhibit a permanent strong labeling of F-actin around the cell body and in primary protrusions, and very little F-actin in the protrusion tips (Figure 26 and Supporting Information Movie S5).

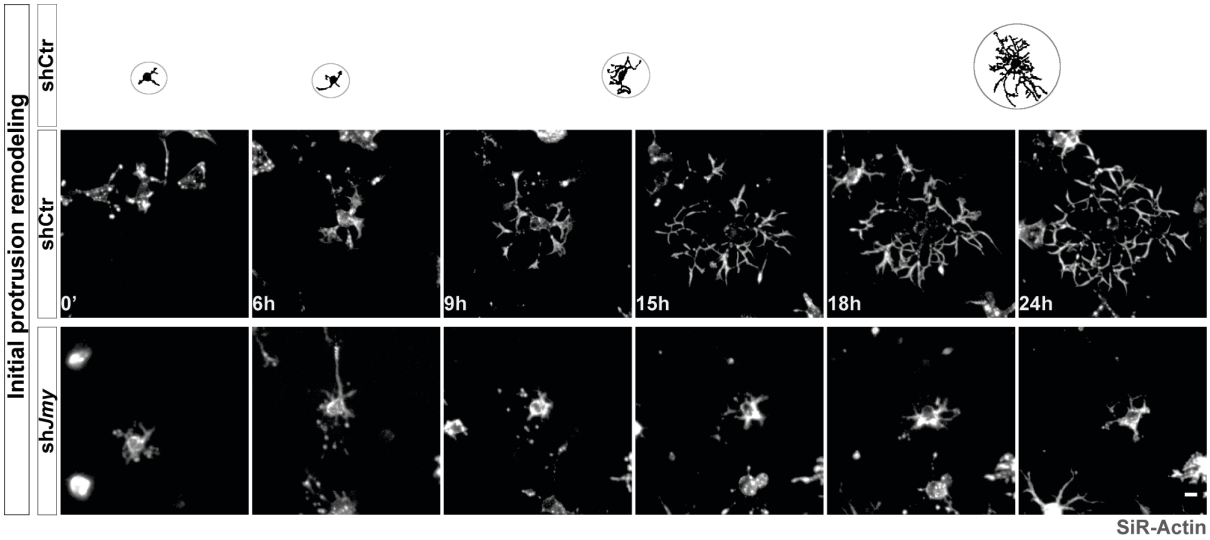

Figure 26 - Representative images of shCtr and sh*Jmy*-OLs from time-lapse videomicroscopy of the initial protrusion remodeling, using SiR-Actin. In shCtr-OLs, top row, there is active extension and remodeling of actin-rich protrusions during the initial phase of differentiation as the cell arborizes. sh*Jmy*-OLs display an aberrant distribution of F-actin towards the cell soma not following the normal protrusions dynamics. Images were processed using a nonlinear gamma change of 0.45. Scale bar is 10μm.

As previously mentioned, some shCtr-OLs occasionally formed membranous sheaths and we used SiR-actin to follow actin cytoskeleton dynamics during this process. Formation of this specialized structure, limited in its border by an actin ring, is accompanied by a drastic decrease in F-actin levels in the inner region of the forming lamella, which occurs simultaneously with the collapse of secondary and tertiary protrusions (Figure 27 and Supporting Information Movie S6). As differentiation progresses, sh*Jmy*-OLs were not able to remodel protrusions and arborize and failed to redistribute F-actin away from the cell soma (Figure 27 and Supporting Information Movie S7).

Altogether, our results suggest that Jmy is necessary for the precise organization and displacement of actin filaments during oligodendrocyte morphological differentiation, which is critical for the timely acquisition of the different morphological states that direct oligodendrocyte maturation.

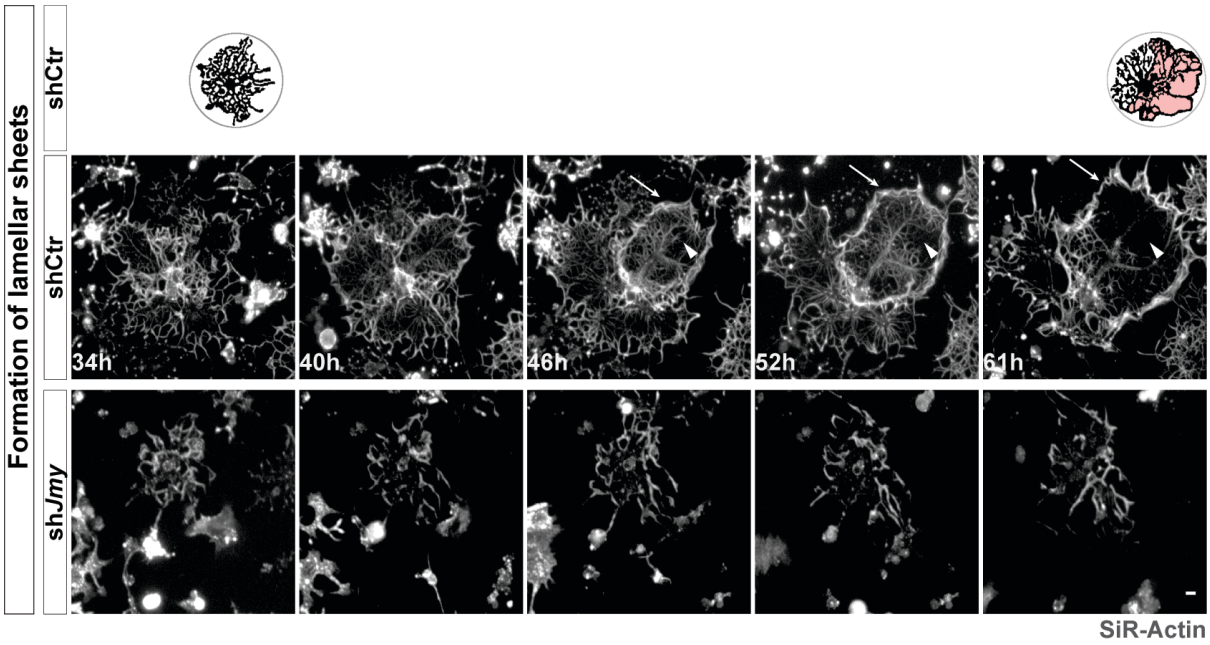

Figure 27 - Representative images of shCtr and sh*Jmy*-OLs from time-lapse videomicroscopy during the formation of lamellar sheaths, using SiR-Actin. Top row shows pro-myelinating oligodendrocytes forming lamellar sheaths, delimited by an actin ring (arrows) that grows simultaneously with retraction of fine protrusions in the inner area (arrowheads). Differentiating sh*Jmy*-OLs have shorter and thinner protrusions, and an overall abnormal actin profile. Images were processed using a nonlinear gamma change of 0.45. Scale bar is 10µm.

Jmy depletion seems to slightly increase the expression of Arp2/3 complex

To further understand if knocking down expression of Jmy would lead to changes in other actin related proteins we started by assessing the levels of Arp2/3 complex. The Arp2/3 complex is expressed in oligodendrocytes and can be directly linked with Jmy, which can promote activation of the complex. We have analyzed the levels of Arp3, an essential subunit of the complex, during sh*Jmy*-OLs differentiation. Interestingly, we found a slightly increase in the Arp3 protein levels in sh*Jmy*-OLs during differentiation, compared to shCtr-OLs (Figure 28 A and B), which may suggest the activation of a compensatory mechanism.

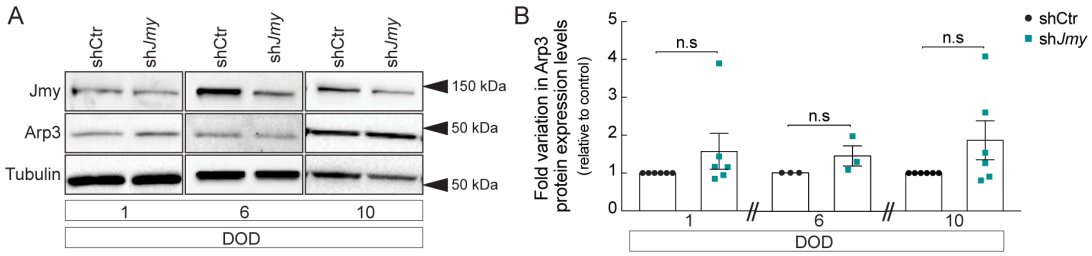

Figure 28 – (A) Immunoblot analysis and (B) relative quantification of Arp3 expression in total extracts of shCtr-sh*Jmy*-OLs at DOD 1, 6 and 10. Levels of tubulin were used as a loading control. Data represented as mean of the fold variation to control of the relative densities ± SEM of n=4 and n=6 biological replicates collected from independent experiments for DOD6 and DOD1 and 10, respectively (n.s.= not significant, calculated with the one sample t test).

We also tried to analyze the levels of formins upon Jmy knockdown. Formins are described as being required for diverse roles in the cytoskeletal reorganization including: the assembly of filopodia, lamellipodia, stress fibers and cytoplasmic actin networks used for long-range vesicle transport (Breitsprecher & Goode, 2013). We were unable to obtain conclusive results due to technical difficulties.

The role of Jmy in the assembly of Mbp sheaths and myelin segments

Jmy is essential for the normal assembly of Mbp sheaths *in vitro*

Oligodendrocyte differentiation depends on both antigenic and morphological alterations, which are timely coordinated and intimately linked. Based on the morphological defects observed upon Jmy depletion in oligodendrocytes, we wondered whether Jmy was also required for normal antigenic differentiation. We assessed the expression of Mbp, one of the earliest myelin-specific components to arise and a marker of mature oligodendrocytes. RT-PCR analysis of the mRNA levels of Mbp at DOD3 revealed similar transcript levels between sh*Jmy*- and shCtr-OLs (Figure 31 A). Additionally, immunofluorescence analysis showed comparable numbers of sh*Jmy*- and shCtr-OLs expressed Mbp, both at DOD6 and 10 (Figure 29 A, B). However, when we looked at the capacity of Mbp-positive oligodendrocytes to form myelin-like sheaths, we observed significantly less sh*Jmy*-OLs forming Mbp positive sheaths after 6 and 10 days of differentiation (Figure 29 A, arrows, and 29 C). In line with this, a significantly decrease in total protein levels of Mbp was detected upon Jmy knockdown (Figure 31 E, F).

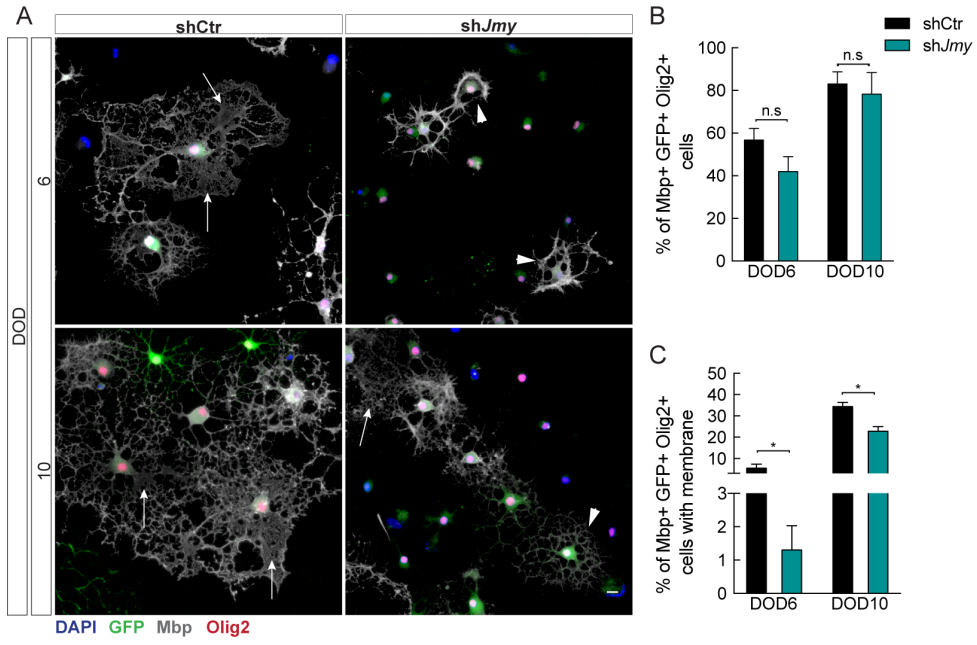

Figure 29 - Jmy is required for the formation of Mbp-like sheaths by mature oligodendrocytes. (A) Representative widefield images of immunocytochemistry (ICC) on shCtr- and sh*Jmy*-OLs during differentiation, labeled for Mbp (red), Olig2 (grey) and nuclei (DAPI, blue). Mature oligodendrocytes (seen at DOD6 and 10) form membranous-like sheaths containing Mbp (arrows) that are rarely seen in sh*Jmy*-OLs, which display an immature morphology with a simple protrusion network (arrowheads). Images were processed using a nonlinear gamma change of 0.5. Scale bar is 10 µm. (B) Percentage of $Mbp^+/GFP^+/Olig2^+$ cells and (C) sheath-forming oligodendrocytes was determined at DOD6 or 10. Cells were labeled for Mbp (red), Olig2 (grey), and nuclei (DAPI, blue). Data represented as mean ± SEM of n=6 or n=3 independent experiments for DOD6 and DOD10, respectively (n.s.=not significant, *p<0.05, calculated using unpaired t-test).

We have also analyzed the percentage of $NG2^+/GFP^+$ and $O4^+/Olig2^+/GFP^+$ cells at both DOD6 and 10. NG2 is a marker of OPCs that precedes the expression of O4, a marker of pre-myelinating oligodendrocytes. A reciprocal change between both markers, with a decrease in the NG2 positive population and an increase in O4 positive, reflects the normal progression of oligodendrocyte antigenic differentiation.

Similar numbers of $NG2^+/GFP^+$ cells were found in both conditions at the two timepoints analyzed (Figure 30 A). As expected, and because NG2 is an antigen characteristic of immature oligodendrocytes, the percentage of NG2-positive cells is drastically decreased at DOD6 and DOD10 decreases even more (Figure 31 A). The analysis of $O4^+/Olig2^+/GFP^+$ cells showed no differences between shCrt- and sh*Jmy*-OLs (Figure 30 B), and almost all $Olig2^+/GFP^+$ cells are also $O4^+$ (Figure 30 B). Both results were in line with the developmental onset of Mbp not being affected upon Jmy depletion.

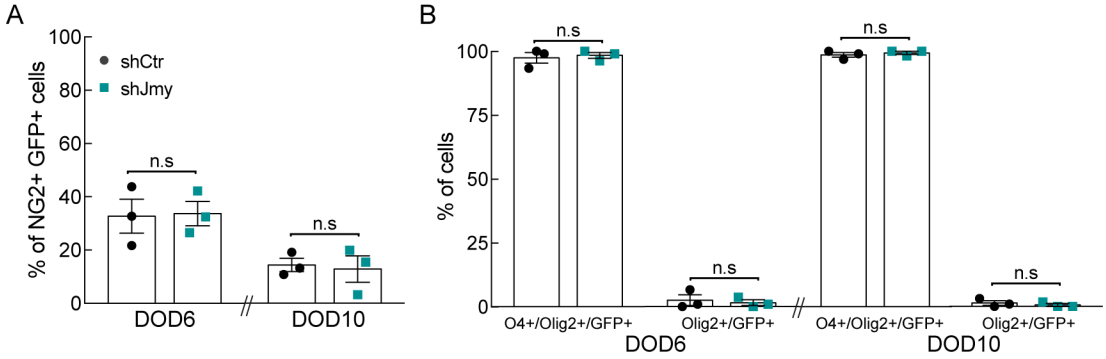

Figure 30 - Jmy depletion does not interfere with oligodendrocyte antigenic differentiation. A) Percentage of $NG2^+/GFP^+$, (B) $O4^+/Olig2^+/GFP^+$ and $Olig2^+/GFP^+$ cells was determined at DOD6 and 10., with at least 80 cells in each condition analyzed per experiment. Data represented as mean ± SEM of n=3 independent experiments (n.s. = not significant, calculated using unpaired t-test).

Comparable levels of expression of Mag, a component of periaxonal myelin that is not required for initial myelination (Li et al., 1994), were found between sh*Jmy*- and shCtr-OLs (Figure 31 E and F). In a complementary analysis, we have looked at the mRNA levels of Plp, Mog and Cnp. Surprisingly, the mRNA levels of Plp and Mog were found significantly decreased in sh*Jmy*-OLs (Figure 31 B and C), while no significant changes were detected for Cnp mRNA levels (Figure 31 D). Depletion of Jmy seems to result in a selective decrease of myeli-specific mRNAs.

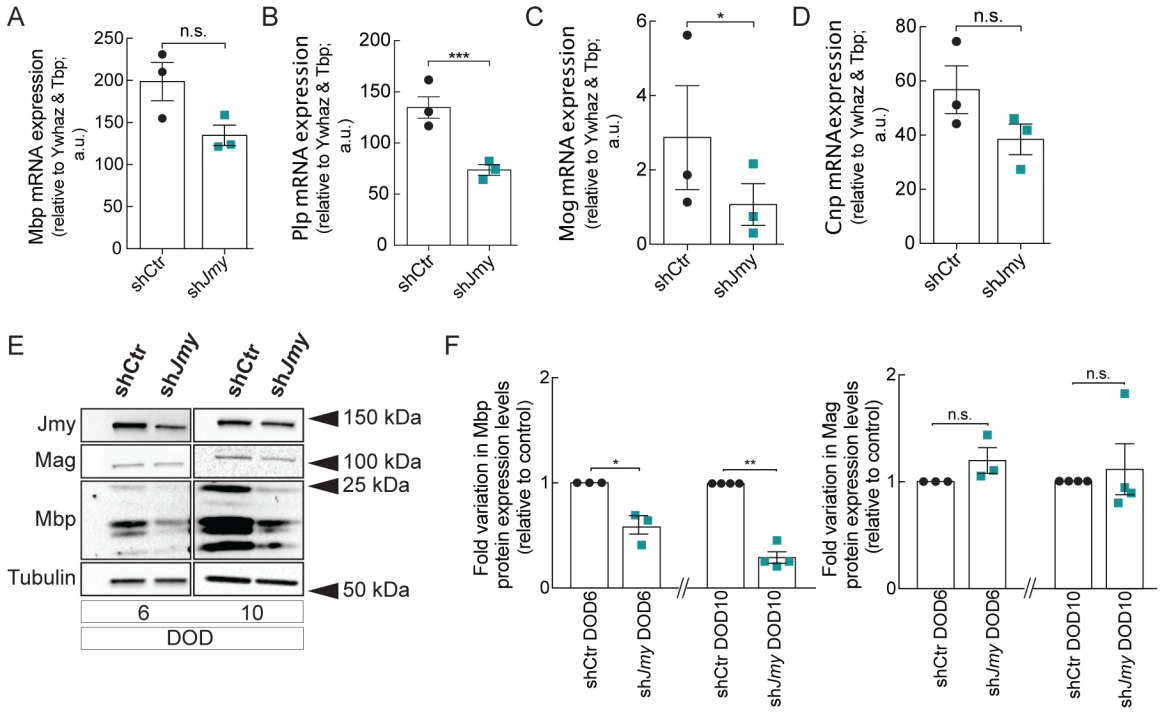

Figure 31 - Depletion of Jmy results in a selective decrease in myelin proteins and RNAs. (A, B, C, D) Expression levels of *Mbp*, *Plp*, *Mog* and *Cnp* mRNA were assessed by qPCR, in primary rat oligodendrocytes at DOD3. Relative transcript expression levels calculated as $2^{-\Delta Ct}$ (n.s. = not significant, p>0.05, *p<0.05, ***p<0.001, calculated using one-sample t test on $2^{-\Delta Ct}$ values of n=3 biological replicates collected from independent experiments). (E) Immunoblot analysis and (F) quantification of Mbp and Mag expression in total extracts from shCtr- and sh*Jmy*-OLs after 6 and 10 DODs. Data represented as mean of the fold variation to control of the relative densities ± SEM of n=3 or n=4 independent experiments for DOD6 and DOD10, respectively (n.s.=not significant, *p<0.05, **p<0.001, calculated using one-sample t test (for Mbp) or Wilcoxon signed rank test (for Mag)).

Jmy is necessary for the assembly of myelin segments in myelinating co-cultures

Our observations that Jmy is required for the acquisition of an arborized morphology in oligodendrocytes and for the assembly of lamellar sheaths led to the question of whether their myelinating capacity would be affected. Co-cultures of purified OPCs and dorsal root ganglia neurons (DRGs) were used as *in vitro* model of myelination. First, we analyzed the capacity of oligodendrocytes to contact neurites, to wrap neurites and finally to form myelin segments. Our analysis showed that, after 18 days of co-culture, less than 60% of Mbp positive sh*Jmy*-OLs

had formed myelin segments, compared to 80% of Mbp positive shCtr-OLs (Figure 32 A). Moreover, sh*Jmy*-OLs showed to be less efficient in contacting and ensheathing neurites as most cells extended membrane protrusions that were not contacting (Figure 32 A).

Additionally, we measured the myelin segments, corresponding to internodes, on the neurites. sh*Jmy*-OLs formed shorter myelin segments comparing to the ones in shCtr-OLs (Figure 32 B). As we found no defects on the developmental onset of Mbp expression upon Jmy downregulation (Figure 29 B and Figure 31 A, E and F), the shorter segments observed in co-cultures with sh*Jmy*-OLs likely resulted from either a delay in the initiation of myelination, or an impairment in lateral membrane extension during wrapping (Figure 32 B). Another curious aspect was that the significantly higher number of Mbp positive sh*Jmy*-OLs displaying multiple, disperse and aberrant accumulations of Mbp that appear to overlap with neurites, comparing to shCtr-OLs (Figure 32 C).

To further characterize the dynamics of early oligodendrocytes-neurite contact we performed live-imaging of the co-cultures in real time. DRG neurons were kept in culture for 21 days and transduced OPCs were seeded on top of them. The co-cultures were immediately moved to the microscope and imaged at a frame rate of 10 min. Interestingly, we observed that shCtr-OLs actively surveyed the neighboring neurites extending and retracting membrane protrusions very rapidly (Supporting Information Movie S8, initial 16 hours in co-culture). We further observed that shCtr-OLs often formed membranous lamellipodia-like structures to stabilize the interaction with neurites (Supporting Information Movie S9, 16—68 hours in co-culture). In contrast, sh*Jmy*-OLs sustained a constant and almost stochastic extension and retraction of their membrane protrusions, only forming short-lasting neurite-oligodendrocyte contacts (Supporting Information Movie S10, 46 hours in co-culture).

Thus, our data strongly suggest that Jmy-dependent regulation of oligodendrocyte morphological differentiation does not affect the developmental timing of Mbp expression but impairs the extension of Mbp membranous-like sheaths *in vitro*, which translates into defects on the myelination capacity.

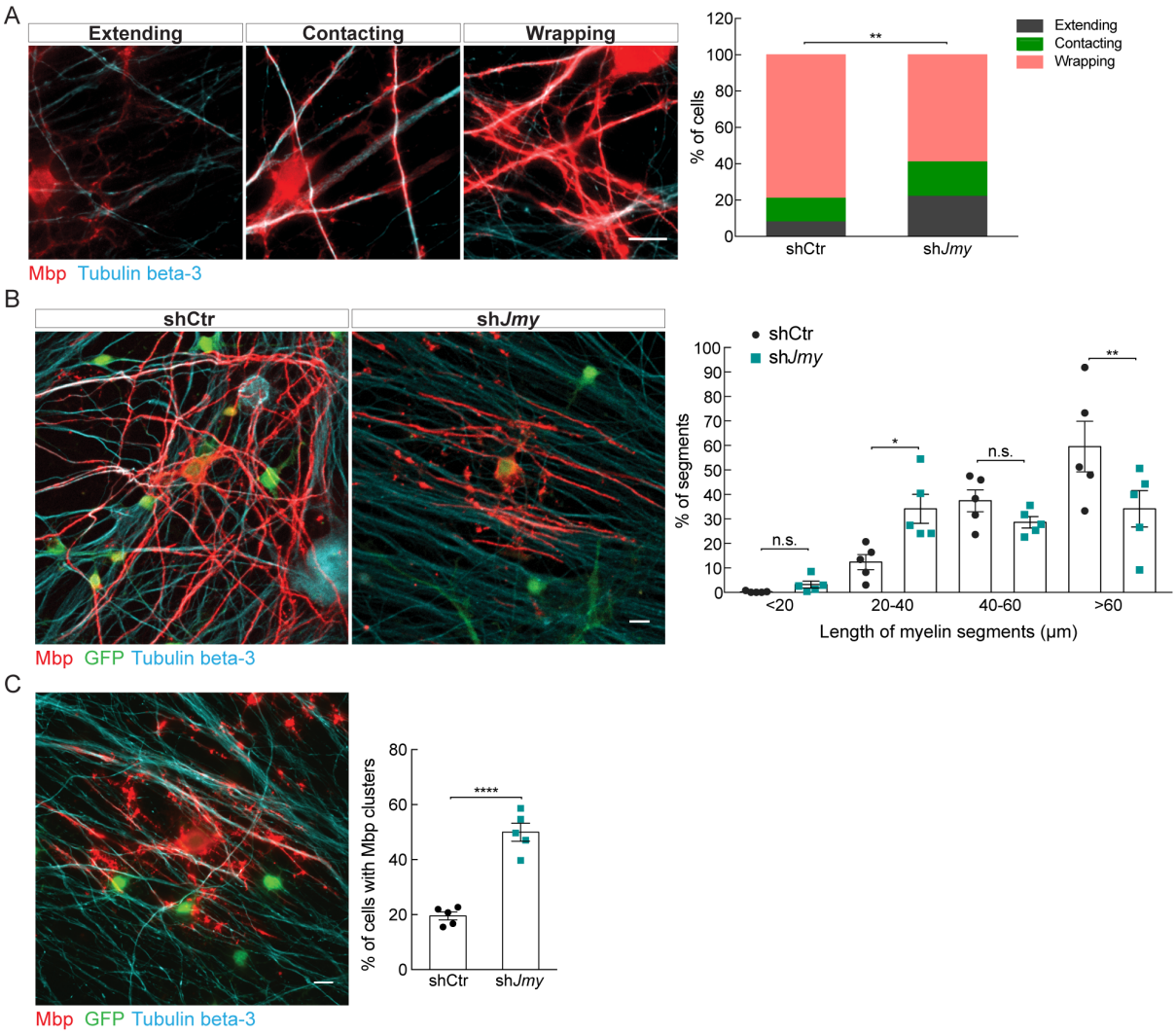

Figure 32 - Jmy is required for neurite wrapping and formation of Mbp segments in a myelinating co-culture. (A) Myelinating co-cultures of DRG neurons and shCtr- or sh*Jmy*-OLs that were previously FACS for GFP. Mbp$^+$ oligodendrocytes were grouped into three different categories of morphological maturity, as shown in the representative images. After 18 days, co-cultures were fixed and ICC was performed for Olig2 (blue), Mbp (red), and Tubulin beta-3 (cyan), a neuronal marker. Data are represented as the percentage of cells counted in each category. The total cells analyzed were pooled from 5 independent experiments, with an average of 100 Mbp$^+$ cells in each condition collected per experiment. A significant association was found between the shRNA and the stage of OL-neurite interaction ($\chi^2_{(2, N=1062)}$ = 10.56, p=0.0051, calculated using the Chi-square test). Scale bar is 10 µm. (B) Length distribution of Mbp segments used as a readout for the ability of oligodendrocytes to form internodes in a myelinating co-culture. Length measurement was performed in co-cultures of shCtr- or sh*Jmy*-OLs and binned into four groups. Data represented as mean ± SEM of n=5 independent experiments (n.s.= not significant, **p<0.01, calculated using one-way ANOVA followed by Sidak's multiple comparisons test). Scale bar is 10 µm. (C) Percentage of shCtr- or sh*Jmy*-OLs in co-culture with aberrant Mbp clusters. Data represented as mean ± SEM of n=5 independent experiments (****p<0.0001, calculated using the unpaired t test). Scale bar is 10 µm.

The role of Jmy in OPCs viability and proliferation

Jmy may be associated with the survival and proliferation of OPCs

Changes in actin dynamics and alterations in the expression of several ABPs can mediate apoptosis (Desouza et al., 2012). Moreover, the same molecules can also induce alterations in the proliferative capacity of cells. For instance, conditional genetic ablation of *Arpc2*, a subunit of the Arp2/3 complex, in radial glial cells leads to decreased proliferation and increased apoptosis in the Arpc2-deficient cortex (Wang et al., 2016), whereas conditional knockout of N-WASP in mouse fibroblasts induced hyper proliferation (Jain et al., 2016). As Jmy is an actin-related protein, able to function as an actin nucleator or as an actin NPF, we decided to investigate the role of Jmy in oligodendrocyte survival and proliferation capacity.

We performed cell death assays using the Terminal deoxynucleotidyl Transferase (TdT) dUTP Nick-End Labeling (TUNEL) system, for detection of apoptotic cells. This method relies on the ability of TdT to bind and label blunt ends of fragmented DNA (Kyrylkova et al., 2012). Our analysis revealed a significant increase in the percentage of TUNEL-positive OPCs upon Jmy loss (Figure 33), suggesting that Jmy is important for OPCs survival.

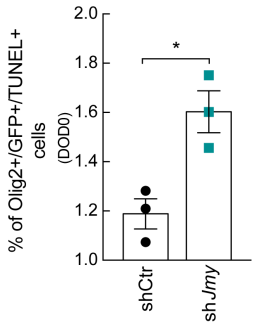

Figure 33 - Jmy depletion induces cell death in oligodendrocytes. Percentage of TUNEL positive OPCs 48 hours after transduction, with at least 100 $GFP^+/Olig2^+$ cells in each condition analyzed per experiment. Data represented as mean ± SEM of n=3 independent experiments (*$p<0.05$, calculated using unpaired t-test).

We also investigated whether there were differences in the rate of proliferation between sh*Jmy*- and shCtr-OPCs. We assessed OPC proliferation using the EdU incorporation assay, which has been previously used to assess oligodendrocyte proliferation (Zuchero et al., 2015). This assay is based on the incorporation of 5-ethynyl-2'-deoxyuridine (EdU), a thymidine analogue, into cellular DNA detected by a reaction of EdU with a fluorescent azide. Compared to other methods, EdU detects DNA synthesis without need for DNA denaturation making it less armful for samples, allowing preservation of physical integrity and antigenicity of various proteins markers (Zeng et al., 2010). We observed a significant two-fold increase in the

percentage of sh*Jmy*-OPCs positive for EdU (Figure 34), which indicate that knocking down Jmy leads to an increase in OPC proliferation.

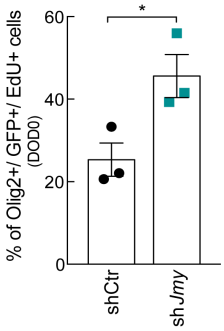

Figure 34 - Jmy depletion induces oligodendrocytes proliferation. Percentage of EdU positive OPCs 48 hours after transduction, with at least 32 GFP$^+$/Olig2$^+$ cells in each condition analyzed per experiment. Data represented as mean ± SEM of n=3 independent experiments (*p<0.05, calculated using unpaired t-test).

Signaling pathways regulating Jmy in oligodendrocytes

There are few studies looking at the signaling pathways regulating Jmy. We performed a small screen, using the OLN93 cell line - which spontaneously transformed from primary rat brain glial cultures and show continuous division capacity and expression of antigenic markers of mature oligodendrocytes (Richter-Landsberg & Heinrich, 1996) - to search for potential regulators of Jmy. Signaling pathways involved in the regulation of actin dynamics are the rational targets to follow. Moreover, some of these signaling molecules regulating actin dynamics were already shown to be also important for oligodendrocyte differentiation and myelination, including the integrin signaling pathway (Brakebusch & Fassler, 2003) and Rho GTPases (Ridley, 2006). In oligodendrocytes, Jmy appears to be at least in part regulated by expression levels. So, we knocked down the expression of RhoA, Rac1 and integrin-linked kinase (Ilk) and assessed the levels of Jmy. Although we did not find any significant changes in Jmy protein expression level upon depletion of RhoA (Figure 35 A), depletion of Rac1 and Ilk lead to a significant decrease in Jmy expression (Figure 35 B and C).

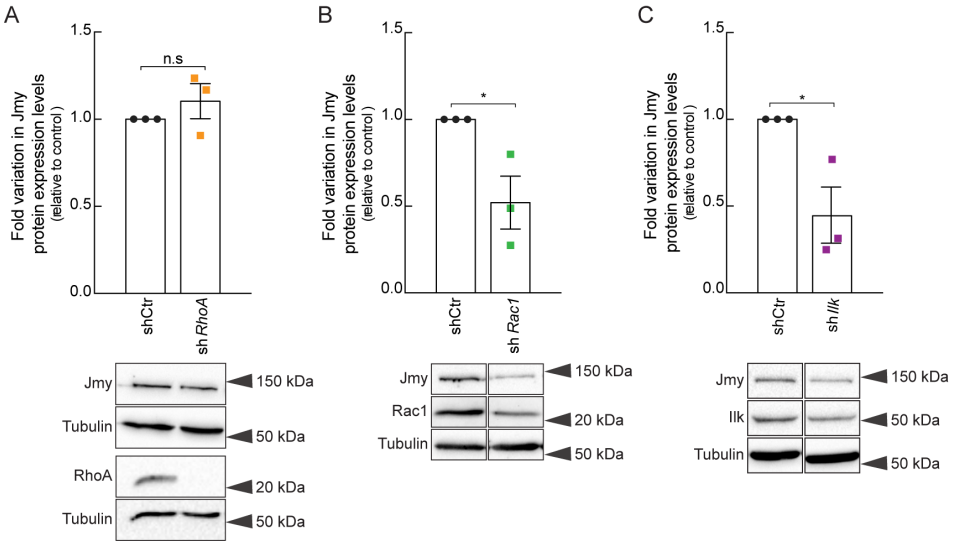

Figure 35 - Mini-screen to identify signaling pathways regulating Jmy's expression. Immunoblot analysis and relative quantification of Jmy expression upon (A) RhoA, (B) Rac1 and (C) Ilk depletion in OLN93 cells. Levels of tubulin were used as a loading control. Data represented as mean of the fold variation to control of the relative densities ± SEM of n=3 biological replicates (n.s.= not significant, *p<0.05, calculated with the unpaired t test).

Based on the results obtained in our mini-screen, we sought to validate such findings in a conditional Rac1 mutant mice where the loss of Rac1 is targeted to myelinating cells, including oligodendrocytes (Thurnherr et al., 2006). Protein lysates obtained from the optic nerve of oligodendrocyte-conditional mutant P14 mice - the developmental window that corresponds to axon ensheathment in the optic nerve - were used to assess expression levels of Jmy. However, no significant differences in Jmy protein levels were found between control and mutant optic nerves (Figure 36 A).

Ilk is a focal adhesion protein that binds to the cytosolic C terminus of β1 integrin (Hannigan et al., 1996), mediating signaling transduction between the ECM and the cell interior at the focal adhesions (FA). Ilk with Parvin and Pinch proteins form the IPP complex at the FA, which functions as a signaling node between integrin signaling and the cytoskeleton (Brakebusch & Fassler, 2003). In mammalians, Pinch is encoded by two genes, Pinch1 and 2, that bind exclusively to IPP. The stability of Ilk, Parvin and Pinch depends on their recruitment into the IPP complex. Only a complex consisting of all three proteins is able to assemble at the FA allowing integrin signaling transduction (Legate et al., 2006). So, to further validate the results obtained in our *in vitro* system upon Ilk knockdown, we have used protein lysates obtained from optic nerves of conditional Pinch1/Pinch2 double mutant mice. In the absence of these two proteins, the IPP complex is not formed causing disruption of the integrin signaling cascade. Recombination and ablation of both Pinch1 and Pinch2 conditional allele was targeted to oligodendrocytes using the Cre-lox system. We did not observe significant changes in the protein levels of Jmy between lysates obtained from optic nerves of Pinch1/Pinch2 double mutant, and those obtained from control animals (Figure 36 B).

These results suggest that at least *in vivo* both, Rac1 and the IPP-dependent signaling, are probably not directly involved in the regulation of Jmy expression during axon ensheathment.

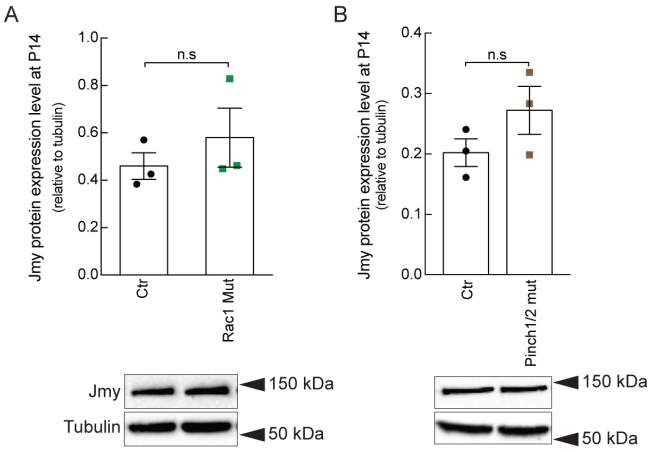

Figure 36 - Pinch1/Pinch2 and Rac1 signaling does not seem to be involved in the regulation of the expression of Jmy. Immunoblot analysis and relative quantification of Jmy expression in optic nerve total extracts of P14 (A) Rac1 and (B) Pinch1/2 mutant mice. Levels of tubulin were used as a loading control. Data represented as mean of the fold variation to control of the relative densities ± SEM of n=3 biological replicates (n.s.=not significant, calculated with the unpaired t test).

Discussion

Oligodendrocyte differentiation is characterized by dramatic morphological changes that follow antigenic differentiation. So far, the decoupling between both events has not been reported: alteration of molecules involved in the control of oligodendrocyte actin dynamics also lead to defects in oligodendrocyte antigenic differentiation (Kim et al., 2006; Liang et al., 2004; O'Meara et al., 2013). However, we found that Jmy, an actin related protein, is crucial for normal oligodendrocyte morphological differentiation but not for antigenic differentiation.

Upon Jmy depletion differentiation of oligodendrocytes is impaired. We observed a marked decrease in morphological complexity characterized by the extension of fewer and shorter protrusions, and consequently smaller cell area in Jmy-depleted oligodendrocytes. The observed effects were not due to a delay in the differentiation because even after 10 days of differentiation the majority of oligodendrocytes depleted of Jmy were not able to reach the typical morphology of fully mature oligodendrocytes. Moreover, Jmy depletion resulted in a clear decrease in the F-actin content in oligodendrocyte protrusions, demonstrating that the defects observed in protrusions extension and branching probably derive from deficient F-actin polymerization.

Arp2/3-dependent actin polymerization was shown to be the driving force for oligodendrocyte protrusion extension and ensheathment of axons (Zuchero et al., 2015). Interestingly, we found that the Arp2/3 complex, which was still found at normal expression levels in oligodendrocytes, did not compensate for defects in the morphological differentiation of oligodendrocytes depleted of Jmy. These results strongly support the idea of Jmy being a key regulator of actin polymerization during oligodendrocyte differentiation. Jmy is a unique molecule in the sense that can mediate actin polymerization through activation of the Arp2/3 complex working as a nucleation promoting factor, or directly by itself (Zuchero et al., 2009). So, further studies would be needed to determine the precise mechanism by which Jmy is acting and controlling F-actin polymerization during oligodendrocyte differentiation. For example: 1 - To further understand how Jmy is regulated, a comparison of the relative activity of full-length Jmy and its WWWCA domain may be assessed, which can provide information regarding a possible regulation through conformational autoinhibition; 2 - To further investigate Jmy's capacity to nucleate F-actin by itself, a mutation of the conserved tryptophan residue (W981) in the A region, that is implicated in Arp2/3 complex binding and activation, could be generated to block the Jmy - Arp2/3 nucleating activity; 3 - to assess whether the effect of Jmy on oligodendrocyte protrusion extension requires its actin polymerization activity, a mutant of Jmy missing the WWWCA domain could be generated to try to rescue the observed phenotype.

We did not observe any direct effect of Jmy depletion on the antigenic differentiation of oligodendrocytes in culture. mRNA levels of Mbp were not significantly affected and the number of Mbp positive sh*Jmy*-OLs were similar to those in control cells. Similar results were observed for oligodendrocytes depleted of Scribble, a polarity protein that has been shown to be essential for oligodendrocyte morphological differentiation but does not induce alterations in the number of Mbp positive cells (Jarjour et al., 2015). However, we did find reduced capacity of oligodendrocytes to form and extend myelin-like sheaths, which can explain the decreased levels of Mbp protein found. Most likely, formation of complex morphological structures is a pre-requisite for subsequent myelin-like sheaths formation, which is probably compromised as a result of the morphological defects caused by Jmy depletion. According to recent studies, extension of multiple protrusions that branch forming a highly complex morphology is followed by active depolymerization that allows for the lateral membrane spreading during myelination (Nawaz et al., 2015; Zuchero et al., 2015). As loss of Jmy compromises normal oligodendrocyte morphological differentiation resulting in less content of F-actin, most probably due to defects on F-actin polimerization, it is plausible that less depolymerization may be occurring. If in fact depolymerization is affected in Jmy-depleted oligodendrocytes, this could explain the decreased ability of Jmy depleted oligodendrocytes to form membranous sheaths even in the presence of normal Mbp transcript levels. Moreover, the failure in the extension of myelin-like membranes may explain the decreased levels of Plp and Mog, which are expressed latter and are involved in the formation and maintenance of myelin (Baumann & Pham-Dinh, 2001; Williams & Deber, 1993). Interestingly, no changes were observed in the mRNA levels of Cnp, a constituent of myelin, which has been recently implicated in the maintenance of intact cytoplasmic regions in the myelin sheath by associating and organizing the actin cytoskeleton (Snaidero & Simons, 2017). This suggests that the machinery for proper myelin-like sheaths organization is not affected upon Jmy depletion. As we did not find changes in the mRNA levels of Mbp and Cnp, both essential for myelin sheaths assembly, and the analysis of the NG2 and O4 positive cells indicate that oligodendrocyte development is normal, our results suggest that the machinery needed for myelin-like sheaths extension is not affected upon Jmy depletion.

We followed in real-time the dynamics of the actin cytoskeleton in live oligodendrocytes, which highlighted that a proper distribution of F-actin within the cell is a critical step for normal oligodendrocyte differentiation and myelin membrane formation. Indeed, knocking down Jmy compromises the normal F-actin distribution in oligodendrocytes, which culminates with aberrant displacement of F-actin to the cell soma compromising the differentiation process and formation of myelin-like membranes

Our *in vitro* model of myelination has shown that oligodendrocytes lacking Jmy are less prone to contact and wrap neurites, and when they succeed the myelin segments formed are

shorter. These results suggest that the defects in protrusion extension in Jmy-depleted oligodendrocytes, directly impact in the oligodendrocyte:axon interaction, probably because Jmy is involved in the formation of a specific actin network that is determinant for proper targeting of neurites. The defects observed in the extension of membranous myelin-like sheaths were also observed in our co-culture model as Jmy depleted oligodendrocytes were inefficient in forming myelin segments when in the presence of neurons. Similar findings were reported for mice in which oligodendrocytes lack the basal polarity protein Scribble (Jarjour et al., 2015). Establishment of intracellular polarity is critical for oligodendrocyte differentiation and myelination, being this process dependent on actin-based nucleation. As we report here, Jmy depletion leads to alterations in F-actin content in oligodendrocytes, probably due to defects in actin polymerization.

The decreased levels of Plp and Mog can explain the presence of a higher number of Mbp clusters instead of normal myelin segments observed in our co-culture system with sh*Jmy*-OLs. Since the two proteins are involved in the maintenance of myelin structure and function (Williams & Deber, 1993), oligodendrocytes lacking Jmy able to form myelin did not have the molecular machinery necessary to maintain the integrity of formed membranes, resulting in the loss of their normal appearance, and consequent function. However, further *in vivo* studies are necessary to clarify to which extent myelination is dependent on Jmy function.

Concerning the regulation of Jmy, the molecular pathways regulating its function are poorly understood. Recently, however Jmy was classified as a member of the WASP family (Alekhina et al., 2017). WASP proteins can interact with Cdc42, Rac, the lipid phosphatidylinositol 4, 5-bisphosphate, many SH3-containing proteins, and can also be phosphorylated, to induce a structural rearrangement that changes the WCA domain from the autoinhibitory conformation (Higgs & Pollard, 2000; Kim et al., 2000; Miki, Sasaki, et al., 1998; Prehoda et al., 2000; Rohatgi et al., 2000; Rohatgi et al., 1999; Tomasevic et al., 2007). Therefore, putative upstream candidates regulating Jmy function could include integrins and the GTPases of the Rho subfamily, particularly Cdc42 and Rac1, both well known for their involvement in the reorganization of the actin cytoskeleton in other cell types (Hall, 1998; Longhurst & Jennings, 1998), and myelin formation (Relvas et al., 2001; Thurnherr et al., 2006). Out of the Rho GTPase family, RhoA was shown to inhibit oligodendrocyte process extension in culture (Liang et al., 2004), and Cdc42 to regulate developmental myelination *in vivo* (Thurnherr et al., 2006). Interestingly, and as Cdc42 appears not to regulate oligodendrocyte morphological differentiation, it is possible that Jmy function depends, at least partially, on other molecules besides Cdc42. Furthermore, Rac1 was shown to be important for myelination (Thurnherr et al., 2006). However, its role during oligodendrocyte differentiation *in vitro* was not studied. Moreover, Rac1 is known to be involved in the formation of lamellipodia (Bosco et al., 2009), a cellular structure present at the growth-cone like-tips of

oligodendrocyte protrusions, and essential for the contact of oligodendrocytes with axons (Michalski et al., 2016; O'Meara et al., 2013). Our results showed that knocking down of Rac1 and Ilk causes a significant decrease in the levels of Jmy. However, to our surprise, when we moved to the *in vivo* models, Rac1 deletion and integrin signaling pathway disruption did not induced significant alterations in Jmy expression levels. These results suggest that, specifically at 14 postnatal days during axonal ensheathment, these signaling pathways are not directly regulating Jmy levels. However, we cannot exclude the possible existence of compensatory mechanisms that may be regulating Jmy levels in the absence of Rac1 and the integrin signaling pathway. Moreover, a detailed study of the influence of both signaling pathways in Jmy levels at different developmental stages would be useful to clarify if our observations are specific to this time point.

We also assessed the possible involvement of Jmy in oligodendrocyte survival and proliferation. We observed that upon Jmy depletion the percentage of TUNEL- and EdU-positive oligodendrocytes was significantly increased. Several lines of evidence have shown that alterations in the actin dynamics may mediate apoptosis. For instance, F-actin stabilization in Jurkat T- and HL-60 cells, by the use of jasplakinolide, was shown to be responsible for apoptosis induction (Odaka et al., 2000; Posey & Bierer, 1999), whereas active actin depolymerization in T-cells triggers apoptosis (Rao et al., 1999). Based on this knowledge, we can speculate that the alterations induced in the actin dynamics following Jmy depletion are the trigger for oligodendrocyte apoptosis. With the increased apoptosis we have observed a significantly increase in oligodendrocytes proliferation. This phenomenon may be a consequence of oligodendrocyte cell death. As a result of the impairment of actin dynamics, we may be in the presence of an apoptosis-induced proliferation phenomenon, a cellular process by which apoptotic cells secret mitogens that promote proliferation of surrounding living cells (Mollereau et al., 2013; Ryoo & Bergmann, 2012). Interestingly, the induction of apoptosis specifically in mature oligodendrocytes was showed to result in an increase in the number of proliferating OPCs (Caprariello et al., 2012). However, this biological process need to be further characterized in oligodendrocytes, particularly to understand to which extent the apoptosis is the trigger for proliferation.

Altogether, our observations show that Jmy is required for morphological differentiation of oligodendrocytes by controlling F-actin polymerization. We also showed that oligodendrocyte morphology clearly impacts on the biological function of these cells and its tight regulation is critical for normal myelination. Moreover, we could decouple morphological from antigenic differentiation, with Jmy being mostly involved in the regulation of oligodendrocyte morphological differentiation.

CHAPTER 3

OligoMacro - a new tool for morphodynamics analysis of oligodendrocyte differentiation

Introduction

In response to different intra- and/or extracellular stimuli, the actin cytoskeleton undergoes fast remodeling to form localized and highly organized protrusions that trigger membrane deformation. The actin cytoskeleton conveys dynamics to the cell. This structure is the basis of many physiological processes, including cell growth, proliferation and migration, differentiation, and apoptosis (Bezanilla et al., 2015; Pollard & Cooper, 2009).

Actin dynamics is critical during CNS development. A clear example is oligodendrocyte development, a complex and dynamic process involving extensive morphological changes that require actin remodeling. Characterized by the extension of multiple protrusions that branch and form a highly arborized morphology, the morphological differentiation of oligodendrocytes often involves continuous cycles of protrusion extension and retraction, being some very thin, small, and transient, which makes the analysis of such dynamic process very difficult (Kirby et al., 2006). Interestingly, oligodendrocyte protrusions were described to have at the distal tips a structure similar to the growth cone of axons (Fox et al., 2006; Michalski et al., 2016). Furthermore, oligodendrocyte growth cones were shown to guide oligodendrocyte protrusions in response to extracellular cues, and to change their motility according to the differentiation state of the cell - less motile as oligodendrocytes mature (Fox et al., 2006). Since the morphological plasticity of oligodendrocytes is important in the context of development, remyelination, as well in cases of injury, it is important to understand the normal dynamic of protrusions as they are responsible for the morphological plasticity of these cells.

In most cells, membrane protrusions influence changes in cell shape and motility during development and disease. For example: filopodia are known mediators of attractant and repellent guidance cues sensed by growth cones (McConnell et al., 2016; Zheng et al., 1996), and key elements of axonal guidance during early CNS development (Bentley & Toroian-Raymond, 1986; Chien et al., 1993; O'Connor et al., 1990), but cell protrusions are also important for migration in primary tumors during metastasis (reviewed in Machesky, 2008). Both lamellipodia and filopodia are used to generate shape changes and drive motility, and understanding how the dynamics of both structures are regulated is of extreme importance.

Although live cell imaging will probably not completely replace static imaging, recent advances in the field of optical imaging techniques, through the introduction of highly sensitive digital cameras associated with improved microscope designs and new labeling methods are revealing the dynamics of the cytoskeleton in live cells with unprecedented detail. However, the computational methods dedicated to image processing and analysis remains a limiting step in live cell time-lapse microscopy. The application of such powerful imaging techniques leads to the extraction of large amounts of data, and the manual analysis of such information is time consuming, prone to “operator bias”, and poor in terms of quantitative data extraction, which

makes the development of software for semi-automated or fully automated analysis of cell dynamics an urgent need.

Several programs have been developed to perform quantitative analysis of cellular morphologies and dynamics: for example CellGeo and ADAPT (Barry et al., 2015; Tsygankov et al., 2014). However, the majority of these tools require proprietary software, use complex code sources, are primarily developed to work with datasets of fluorescence microscopy images, mainly directed for single cell analysis, and are not easily adaptable to follow morphodynamic events over time. Moreover, such image analysis tools are not able to follow highly complex cellular morphodynamics, such as in the case of oligodendrocyte differentiation.

So far, very few time-lapse studies of oligodendrocyte differentiation have been reported, and the data generated mainly result in qualitative analysis (Suzuki et al., 2017; Zuchero et al., 2015), showing the need for new analytic tools adaptable to support large image data sets of cells with complex morphology. With the purpose of addressing these limitations, we have developed a new ImageJ - (Schneider et al., 2012) based workflow called OligoMacro (Azevedo et al., 2018). OligoMacro can perform semi-automated analysis of large phase contrast time-lapse videos over time. Such analysis allows for quantification of cellular protrusions as well as the extraction of the number of branching points, which gives the user a readout of oligodendrocyte morphological complexity in culture. OligoMacro also performs tracking of cell movement during the time of analysis.

Early oligodendrocyte differentiation was assessed by phase contrast time-lapse imaging in order to characterize the process in real time. Oligodendrocytes were transduced with three different shRNAs: shCtr, sh*Jmy* and sh*Rnd2*, already known to result in different oligodendrocyte differentiation patterns. The ability of OligoMacro to follow and analyze the different cell behaviors was tested by the analysis of early oligodendrocyte differentiation in the three experimental conditions mentioned above. Early oligodendrocyte differentiation analysis using OligoMacro showed that oligodendrocytes follow a specific “cellular shaping” program during differentiation. Furthermore, OligoMacro was able to follow and extract quantifiable data from oligodendrocytes that present different differentiation capacities compared to the shCtr-OLs. Indeed, OligoMacro proved to be versatile in following fine changes independently of the overall oligodendrocyte differentiation capacity.

Results

OligoMacro - an ImageJ tool for oligodendrocyte morphodynamics analysis

Lack of adaptable informatics tools appropriated for semi- or full-automated analysis of biological digital imaging data is a current, unresolved problem. The problem is even more significant with analysis of live cell imaging, due to the large digital datasets that need to be processed. To overcome these limitations, we collaborated with Fabrice Cordelières (Bordeaux Imaging Centre, UMS 3420 CNRS, CNRS-INSERM, University of Bordeaux, France), who developed a new macro toolset for ImageJ, which we called OligoMacro. OligoMacro is suitable for the analysis of phase-contrast microscopy images, of time-lapse experiments with live cells with highly complex morphology. OligoMacro is composed of 5 different tools that work in an independent, although sequential, way (Figure 37).

Figure 37 - ImageJ tool bar displaying the OligoMacro toolset (highlighted by the red line). First icon is the “Build stacks” option, second is “Detect and track cells”, third is “Cut out cells” and the last two are for connecting to R software and build graphs.

For all stage positions defined by the user, individual images from the same coordinates are saved as individual tiff files. The first OligoMacro tool, called “Build stacks”, allows for the assembly of all individual tiff images, acquired during a given time period, into a stack. This step generates one stack for each stage position imaged. With the stack built, OligoMacro can then start working on detecting and tracking cells over time by activation of the “Detect and Track cells” function. At this point the user is asked to define three different tracking parameters that will determine the tracking accuracy. After several steps of image segmentation, the user has the possibility of reviewing the detected cells, to delete or add cells, before initiating tracking. Once the cells to be analyze are defined by the user, tracking takes place, and the output data generated (including x,y coordinates, distance moved, and velocity) is saved in a table format. Quality control images are generated, which gives the user the opportunity to revise the OligoMacro tracking performance. To further validate the tracked cells and proceed to their isolation, the “Cut out cells” function needs to be activated, and the user is asked to define both the cell body and the cell outline regions. After successive steps of image processing, the table of results is updated to include: the number of branching points, new protrusions, and cytoskeleton length, for each cell over time. Additionally, each cell analyzed will have a quality control image where the user can verify the detections made by

OligoMacro. The last two functions of OligoMacro take advantage from the R software (Team, 2011) to create graphical representations of collected data, for each individual cell, and/or to group the data, for subsequent analysis. Moreover, the link with R software allows for the immediate calculation of averages and standard deviation of all collected data.

Building OligoMacro involved successive trials based on the extensive debugging of the source code. Of note, the segmentation of phase-contrast images proved to be particularly challenging with images of oligodendrocyte differentiation (Figure 38 A). A compromise in the efficiency of segmentation was achieved in order to follow fine changes in oligodendrocyte morphology minimizing the presence of artifacts (Figure 38 B). The OligoMacro source code is open, which allows other users to easily change the parameters and optimize OligoMacro to be efficiently applied to live-imaging of other cell types and images with different characteristics.

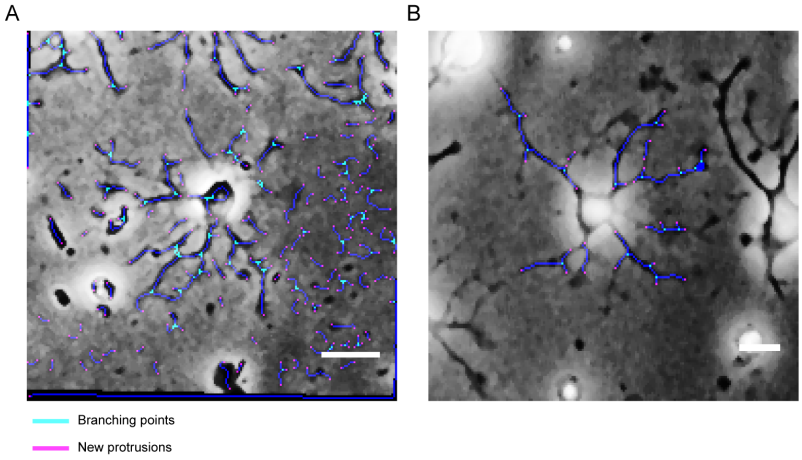

Figure 38 - Results of image segmentation with OligoMacro. (A) Representation of results obtained with the first OligoMacro version. The segmentation process was poorly adapted to phase-contrast images of oligodendrocyte. The cell body was not excluded for the analysis of protrusions, and background pixels were being counted as branching points (cyan), and new protrusions (pink). (B) After successive trials and optimizations, OligoMacro parameters for segmentation were adjusted to accurately follow fine changes in oligodendrocyte morphology with the minimal introduction of artifacts. Scale bars is 20 μm.

To validate OligoMacro, we performed morphodynamics analysis of FACS - EGFP-positive sh*Jmy*-, sh*Rnd2*- and shCtr-OLs. Cells were imaged by phase contrast microscopy over a period of 3.5 days, with frames acquired every 5-minutes. We knockdown the expression of two proteins known to be actin-related: Jmy (see chapter 2) and Rnd2. Rnd2 is an atypical small GTPase involved in migration of newborn cortical neurons in the embryonic mouse brain (Hand et al., 2005; Pacary et al., 2011) and, interestingly, is highly expressed in newly formed oligodendrocytes (Zhang et al., 2014). Additionally, we have shown that Rnd2 is important for oligodendrocyte differentiation (unpublished results from our lab). Our previous results from manual analysis of morphology in fixed cells showed that, upon depletion of Jmy, oligodendrocytes show dramatic defects morphological progression during differentiation.

Because a quantitative readout of oligodendrocyte morphological differentiation is of extreme value - is faster, provide detailed information regarding morphological alterations during time, is less prone to operator bias -, we have decided to test OligoMacro in our live cell imaging data. Our preliminary results show that sh*Jmy*- and sh*Rnd2*-OLs behave differently from shCtr-OLs, and from each other, which turn these conditions ideal to assess the adaptable capacity of OligoMacro to different cellular behaviours.

Morphodynamics analysis of oligodendrocyte differentiation

The use of OligoMacro to study morphological differentiation of oligodendrocytes provided significant advantages over the analysis of fixed cells at pre-determined timepoints. So, we decided to apply OligoMacro to extract quantitative parameters of our live-cell imaging data and address two important aspects of oligodendrocyte biology: first, whether morphological differentiation follows a specific pattern that can be extracted by morphometric analysis; and second, how the differentiation program is affected by the disruption of actin dynamics.

An initial qualitative assessment of the movies showed that in shCtr-OLs differentiation is an extremely dynamic process requiring high protrusion remodeling, with cells undergoing profound cytoskeleton rearrangements that follow a stereotypical “cellular shaping” program (Figure 39 A and B; Supporting Information Movie S1).

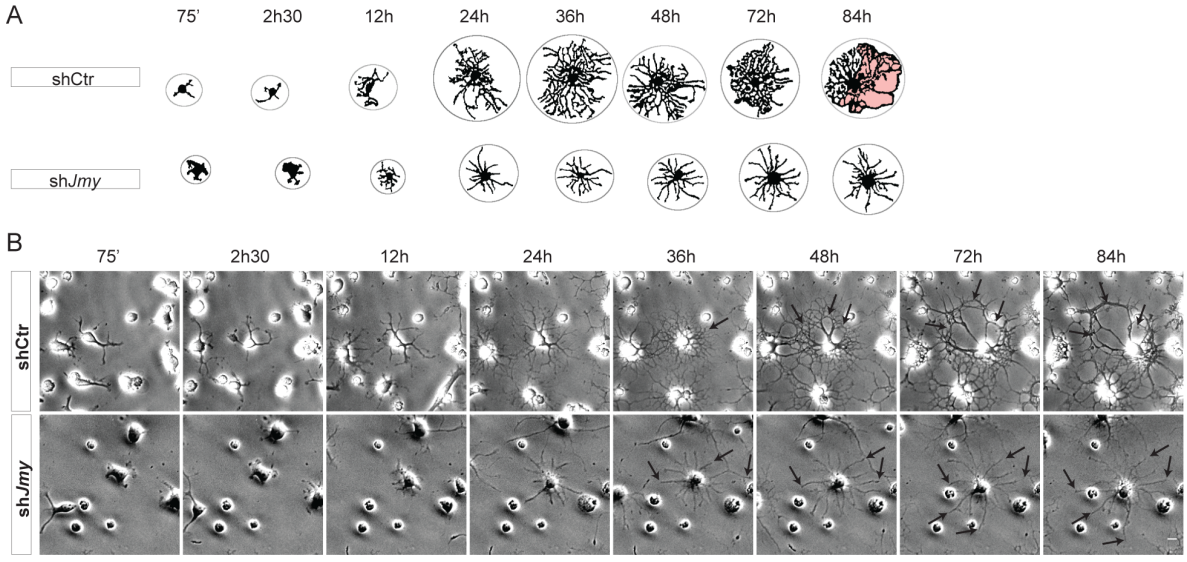

Figure 39 - Morphodynamics of early oligodendrocyte differentiation. (A) Cartoon depicting the morphological states that characterize a stereotypical “cellular shaping” program in shCtr-OLs: protrusion formation, extension and remodeling, arborization (secondary branching), and retraction on sites where lamellar sheaths will begin to assemble (shown as a pink shade). sh*Jmy*-OLs remain in an immature morphology, with fewer and unbranched protrusions, and do not arborize. The circle lines denote the total space occupied by the cell’s protrusion network, sketched after tresholded, representative images of shCtr- and sh*Jmy*-OLs from the time-lapse videomicroscopy shown in (B). Scale bar is 10 μm).

Using OligoMacro for a quantitative analysis of morphological changes in oligodendrocytes during differentiation proved to be effective, extracting with high accuracy the number of new protrusions formed over time, as well as, the number of branching points. The analysis showed that shCtr-OLs undergo an initial phase of intense formation of new protrusions that slows down after 48h into differentiation (Figure 40 A). After 24h of differentiation, a rapid increase in branching points was observed (Figure 40 B), corresponding to the addition of secondary and tertiary branches, which results in widespread arborization of the cells. An important aspect observed was that arborization is followed by retraction/collapse of secondary membrane protrusions, which translates into a plateau or even a decrease in the number of added protrusion or branches in the graphical representation (Figure 40 A and B), and maintenance of a steady morphology roughly after day 3 of differentiation. We could occasionally observe some lamellipodial structures, characteristic of pro-myelinating oligodendrocytes, and noticed that formation of these membranous sheaths was always seen in localized sites where retraction of secondary oligodendrocyte protrusions occurred (Movie S2). In contrast, we found that sh*Jmy*-OLs were, in general, less dynamic (Movie S3), showing an impairment in protrusion formation (Figure 40 A), and in the addition of new branching points (Figure 40 B). A general look at sh*Jmy*-OLs showed that they are not able to acquire complex arborization (Figure 39 A and B) and do not follow the “cellular shaping program” timeline that we identified in shCtr-OLs (Figure 39 A and B). Regarding oligodendrocytes depleted of Rnd2, they also showed impaired formation of new protrusions almost immediately (Figure 40 C). Additionally, sh*Rnd2*-OLs showed a significantly decreased capacity to form branching points that would contribute for the oligodendrocyte arborized structure (Figure 40 D).

Our results from manual morphological categorization (Chapter 2, Figure 1 D regarding shCtr- and sh*Jmy*-OLs; data not shown for sh*Rnd2*-OLs) validated the results obtained with the use of OligoMacro. Both analyses indicate that Jmy is essential for normal oligodendrocyte morphological differentiation.

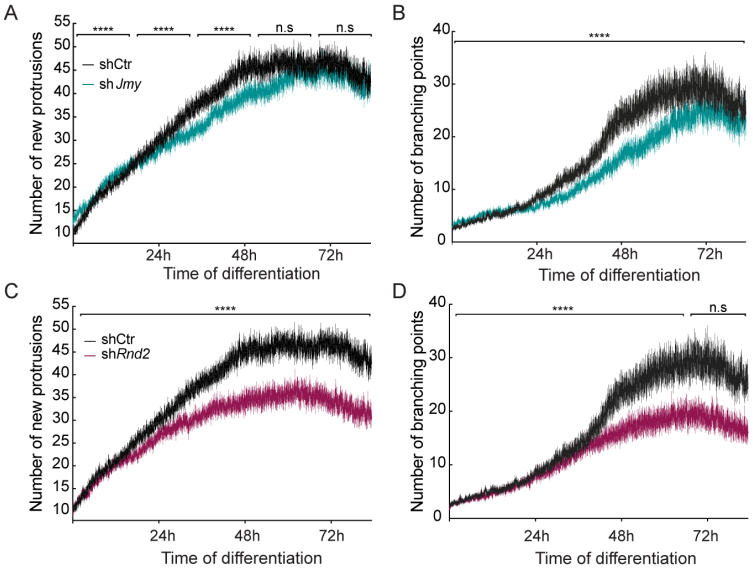

Figure 40 - Quantitative morphodynamics analysis of early oligodendrocyte differentiation. Quantitative analysis of morphological complexity in oligodendrocytes performed with OligoMacro on 5000 images acquired by videomicroscopy of shCtr-, sh*Jmy*- and sh*Rnd2*-OLs, measuring the: (A), (C) number of new protrusions. A two-way ANOVA, to examine the effect of time of differentiation and knockdown, showed a statistically significant interaction between both factors on the number of new protrusions, both for sh*Jmy*- and sh*Rnd2*-OLs ($F_{4,\ 1990}$ = 84.97, ****p<0.0001) and ($F_{4,\ 1990}$ = 329.935, ****p<0.0001), respectively. shCtr-OLs formed significantly more new protrusions than sh*Jmy*- and sh*Rnd2*-OLs, during differentiation ($F_{1,\ 1990}$ = 370.83, ****p<0.0001) and ($F_{1,\ 1990}$ = 3980.676, ****p<0.0001), respectively. A multiple comparisons analysis of time intervals, followed by Tukey's test, showed a significant effect of time on the number of new protrusions only during the first 50h of differentiation, upon Jmy knockdown (****p<0.0001). The same analysis upon Rnd2 knockdown showed a significant effect of time on the number of new protrusions during all differentiation (****p<0.0001). Data represented as mean ± SEM of n=55 cells per condition, randomly sampled from 3 independent experiments; and (B), (D) branching points per cell. A two-way ANOVA showed a statistically significant interaction between: time of differentiation and Jmy knockdown on the number of branching points ($F_{4,\ 1990}$ = 198.94, ****p<0.0001); and time of differentiation and Rnd2 knockdown on the number of branching points ($F_{4,\ 1990}$ = 536.701, ****p<0.0001). sh*Jmy*- and sh*Rnd2*-OLs had decreased ability to form protrusion branches during differentiation when compared to shCtr-OLs ($F_{1,\ 1990}$ = 1331.91, ****p<0.0001) and ($F_{1,\ 1990}$ = 3041.588, ****p<0.0001), respectively. A multiple comparisons analysis of time intervals, followed by Tukey's test, showed a significant effect of time on formation of branching points during differentiation (****p<0.0001) upon Jmy depletion, effect that was observed after Rnd2 depletion only in the first 66h of differentiation. Data represented as mean ± SEM of n=55 cells per condition, randomly sampled from 3 independent experiments.

Analysis of motility during oligodendrocyte differentiation

Once the OligoMacro function "Detect and Track cells" is activated, the user needs to define the "cell body" area. The created region of interest (ROI) is then used to track cell movement over time. Due to the high sensitivity of OligoMacro, small changes in cell shape can be mistaken for movement. To avoid quantification of "false movements", after several hand-made measurements of the displacement generated between two consecutive frames,

we established a minimum of 10 μm as a threshold for what we considered to be the most adequate value of cell motility.

Tracking analysis of oligodendrocytes over time showed that sh*Jmy*-OLs present a larger displacement from their point of origin when compared to the shCtr-OLs (Figure 41 A, B). Interestingly, sh*Rnd2*-OLs showed a displacement pattern similar to the one of shCtr-OLs, characterized by movements near the point of origin (Figure 41 A, C).

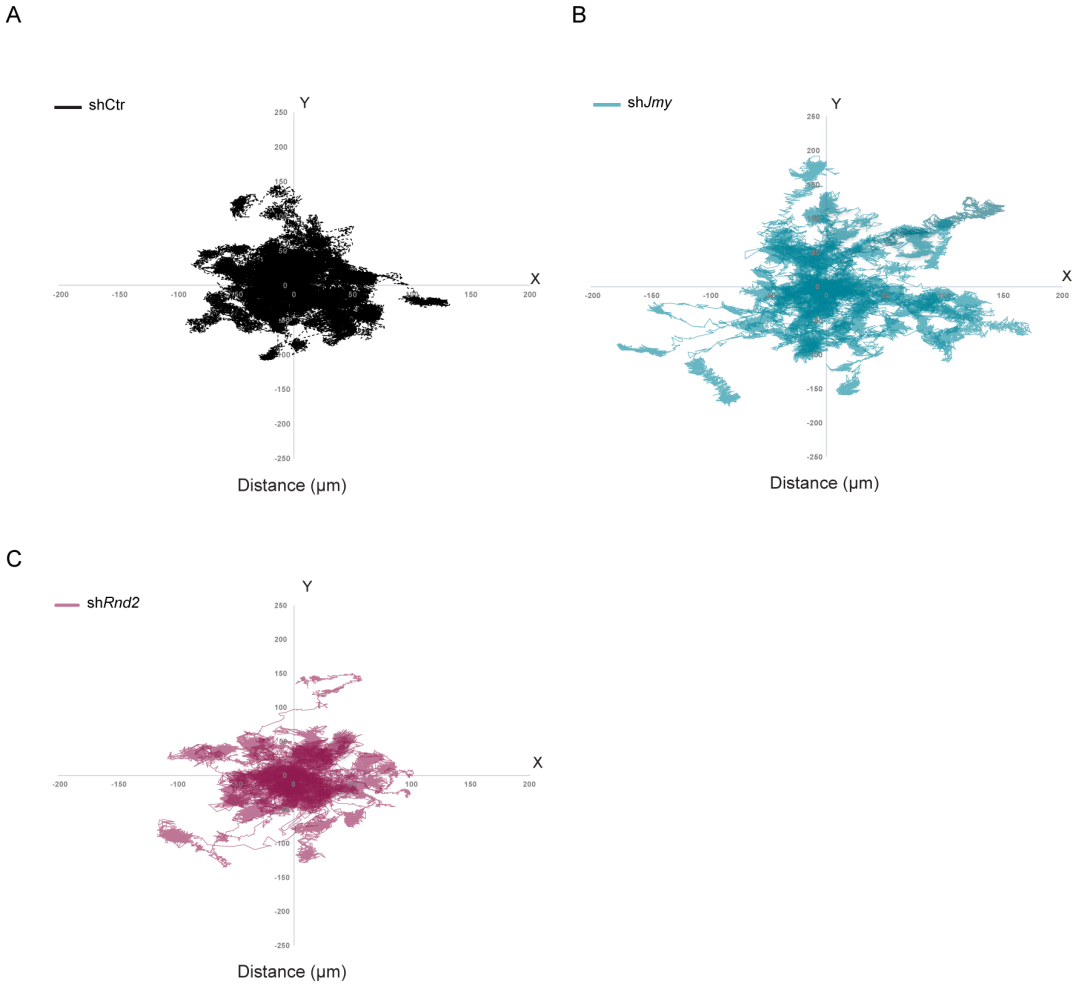

Figure 41 - Analysis of motility during oligodendrocyte differentiation. Graphical representation of individual trajectories of (A) shCtr-, (B) sh*Jmy*- and (C) sh*Rnd2*-OLs from their point of origin at the start of differentiation (n=55 in each group).

Interestingly, besides having larger displacement from the point of origin, sh*Jmy*-OLs moved significantly slower than shCtr-OLs (Figure 42 A). Similar results were obtained when we looked at the oligodendrocyte distance moved over time after knockdown of Rnd2 (Figure 42 B).

From our observations, we concluded that OligoMacro is effective in the simultaneous tracking of multiple cells with different motility profiles.

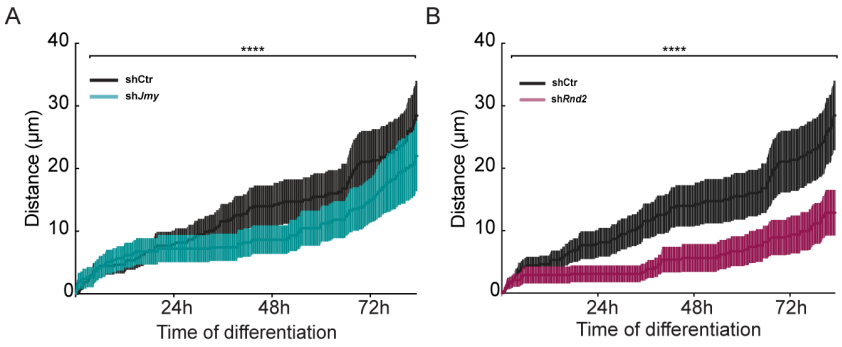

Figure 42 - Cumulative cell body movement during oligodendrocyte differentiation. Plot of the cumulative cell body movement in time of (A) sh*Jmy*- and (B) sh*Rnd2*-OLs in function of control. A two-way ANOVA showed a statistically significant interaction between time of differentiation and gene knockdown, on the movement of cell body: sh*Jmy*-OLs ($F_{4,\ 1992}$ = 331,454, ****p<0.0001); sh*Rnd2*-OLs ($F_{4,\ 1992}$ = 2053,173, ****p<0.0001). A multiple comparisons analysis of time intervals followed by Tukey's test showed a significant effect of time on the cells travelled distance during differentiation (****p<0.0001). Data represented as mean ± SEM of n=55 cells per condition, randomly sampled from 3 independent experiments.

Discussion

Here, we describe the development of OligoMacro, an ImageJ macro toolset, designed to perform semi-automated analysis of oligodendrocyte morphodynamics using large datasets of time lapse phase-contrast images. OligoMacro relies on ImageJ built-in functions to do the image processing and data extraction (with direct connection with R software to plot the data), to track isolated cells, quantify cellular membrane protrusions remodeling along time, output the extracted numerical data and plot it. With interactive manual options, OligoMacro allows the user to fine-tune several parameters to improve its performance as, for example, the tracking parameters (max displacement and max jump between frames). OligoMacro showed to be efficient in extracting quantitative data from highly complex morphodynamics in oligodendrocytes. Indeed, OligoMacro allowed us to show in a quantitative way that oligodendrocytes follow a stereotypical "cellular shaping" program.

OligoMacro allows tracking of cell movement, and quantification of cellular protrusions, which are important features of the behavior of many cells in culture. OligoMacro presents an alternative to the typical requirement of workflows designed for fluorescence images of a labeled actin cytoskeleton (Jacquemet et al., 2017; Tsygankov et al., 2014) and cellular membrane labelling, by working with phase-contrast images and suitable for large image datasets. The requirement for fluorescence images can turn out to be a problem when primary, hard to transfect, cells are to be studied.

OligoMacro is written as an ImageJ macro with scripts in R, and the entire code is freely available. Because it runs on ImageJ, the use of proprietary software that the majority of researchers have no access to is overcome, which presents a great advantage comparing to other image analysis tools (Billeci et al., 2013; Tsygankov et al., 2014; Yu et al., 2009). The fact that the entire code is available allows the user to see exactly how the functions and algorithms were implemented, which can increase reproducibility. Another important aspect of having an open source code is the continuous improvement and the possible extension of the original code to other experimental situations. The use of part of the original code or the introduction of new code modules, can improve OligoMacro performance or can prepare it to other applications increasing its "usability".

OligoMacro showed a good performance on tracking oligodendrocyte motility, and in the extraction of quantitative data regarding the morphological changes that take place during differentiation. Tracking motility of cells depends on several aspects such as the frame rate in relation to the speed of movement, and the presence of an uncluttered environment with relatively disperse cells. Oligodendrocytes are demanding cells in terms of culture conditions. Optimal cell density, where the cells are not extremely confluent but still not to disperse, is needed for oligodendrocytes to be healthy and differentiate. To adjust the analysis to different

cell confluences, OligoMacro gives the user the option to adjust specific parameters and ensure that all cells are tracked. At the end of the tracking analysis, reviewing of the quality control images is important. This action allows for the detection of incorrect tracking, and deletion of wrongly extracted data. For example, tracking cell motility is still a big challenge (Chenouard et al., 2014), with increased difficulties in case of phase-contrast images, and clearly there is not one single solution to deal with this problem. The application of this analysis to the early stages of oligodendrocyte differentiation gives us information regarding oligodendrocyte motility from which we can infer migration capabilities. The results obtained from OligoMacro tracking capacity revealed that sh*Jmy*-OLs move slower, move randomly away from the origin site, and show large displacement rates, suggesting that sh*Jmy*-OLs may have an impaired migratory profile. Cell motility is dependent on adhesion: extremes of too little or too much adhesion result both in low motility, while mid-range adhesion allows for maximum cell displacement rates (DiMilla et al., 1993; Palecek et al., 1997). Because oligodendrocyte depleted from Jmy show larger displacement, we may speculate that Jmy is also playing a role in controlling oligodendrocyte adhesion, and therefore controlling motility. Jmy was shown to regulate cell motility by inducing alterations in the expression levels of the adhesion molecules E- and N-cadherin. Both E- and N-cadherin were upregulated upon Jmy depletion in MCF-7 and, U2OS and SAOS2 cell lines, respectively (Coutts et al., 2009). As oligodendrocyte express both E- and N-cadherin (Payne et al., 1996; Zhang et al., 2014), we can wonder that upon Jmy depletion an alteration in the cadherin levels takes place, which results in the phenotype observed. Further experiments looking at the possible influence of Jmy on cadherin expression levels and at adhesion capacity are needed.

Oligodendrocyte differentiation is characterized by heavy morphological changes that involve the extension of multiple primary protrusions that branch to give rise to an “arborized” morphology. Some of the protrusions and branches formed can be very transient and present different thickness, shape and length. The majority of software programs developed so far to quantify morphological alterations are not able to follow the dynamics of complex cells and require fluorescence images (Barry et al., 2015; Tsygankov et al., 2014; Urbancic et al., 2017). To date, the analysis of morphological differentiation in oligodendrocytes in culture is rarely done through the use of live cell imaging techniques. To the best of our knowledge, the only study using these technique resorts to reporting a qualitative assessment of the phenotypes observed, with no quantitative data incorporated (Zuchero et al., 2015). The development of OligoMacro can now change the way oligodendrocyte morphodynamics is studied. It has the capacity to quantify the number of new protrusions and branching points formed. Moreover, it has the advantage of working with phase-contrast imaging, which is experimentally less demanding and less harsh on the cells than fluorescence microscopy. In addition, segmentation of oligodendrocyte can be challenging due to the inherent complex morphology

of these cells, which can add an extra level of difficulty when no fluorescence labelling is used. The quality of the input images determines the accurate tracking and detection of morphological alterations of all available image analysis workflows. When we talk about phase-contrast images this is even more important. If the quality of the phase-contrast images is poor, the signal to noise ratio, which directly impacts on image segmentation, may not be good enough and lead to the introduction of some false detections. As OligoMacro was developed to work with phase-contrast images with all its limitations, the introduction of false new protrusions and branching points can be unavoidable. The generation of quality control images is a "checkpoint" where the user can verify if major errors in the segmentation/detection were introduced, and act to remove false detections.

The application of OligoMacro to the analysis of other cells is a possibility. For instance, the analysis of morphological changes of neurons for understanding the behavior of these cells can be assessed with OligoMacro. The use of phase-contrast images is a good feature of OligoMacro, as sometimes fluorescence images can also represent a problem due to high levels of background. In fact, for the study of neuron morphology the use of phase-contrast images is suitable. However, the adaptation of OligoMacro for the analysis of fluorescence images can also be done. Additionally, OligoMacro can be applied to the analysis of morphological changes in other dynamic cells, for example, microglia and fibroblasts, with the advantage that the tracking analysis is in theory applicable to any type of motile cells.

OligoMacro was applied to the analysis of different oligodendrocytes during differentiation in a way of test and validate the performance of the macro. For the first time, we show that morphological oligodendrocyte differentiation follows a specific pattern that can be assessed in terms of morphodynamics through the application of semi-automated analysis with OligoMacro. Besides all the limitations that can be associated with the quality of the used images, the results obtained with OligoMacro validated the previous results obtained with "manual" categorization of fixed cells. Indeed, OligoMacro was able to extract quantitative data from cells with distinct morphological behaviors resulting from loss of two different actin-related proteins.

In summary, we have presented a new bioimage analysis workflow, able to characterize the morphodynamics of highly complex cells. Moreover, and for the first time, we have shown the real-time dynamics of F-actin during oligodendrocyte differentiation, which stresses the important role of the multifunctional actin regulator Jmy in this process.

GENERAL DISCUSSION

General Discussion

The work presented in this thesis allowed us to further understand the role of actin cytoskeleton in the biology of oligodendrocyte differentiation and establishment of oligodendrocyte:axon contact. Several lines of evidence have already proven the actin cytoskeleton dynamics as essential for oligodendrocyte development and function. Our findings not only provide a deeper understanding of actin dynamics during oligodendrocyte differentiation, but also highlight Jmy as a new actin regulator playing a role in this process.

Jmy is a novel regulator of oligodendrocyte differentiation and oligodendrocyte:neurite interaction

The morphological differentiation of oligodendrocytes is a requirement for myelination. This process involves the extension of multiple and highly dynamic protrusions, that over time form several branches, increasing the morphological complexity of the oligodendrocyte. The actin cytoskeleton is the major cytoskeletal element of oligodendrocyte protrusions (Simpson & Armstrong, 1999; Song et al., 2001). However, we still lack good understanding of precisely how actin dynamics is regulated during oligodendrocyte differentiation.

Our results show that Jmy, an actin related protein able to promote actin nucleation by itself or through activation of the Arp2/3 complex that has its mRNA enriched in OPC protrusions (Azevedo et al., 2018), is expressed in oligodendrocytes, both during developmental myelination *in vivo* and differentiation *in vitro*. Additionally, we show that depletion of Jmy severely impairs morphological differentiation of oligodendrocytes, which show deficient protrusion extension and branching, accompanied by decreased F-actin content.

During oligodendrocyte differentiation, Jmy was found to localize in regions of higher F-actin content in the protrusions of oligodendrocytes. Upon Jmy knockdown, the decreased levels of F-actin in those protrusions was accompanied by aberrant accumulation of F-actin in the cell soma of these cells, which clearly showed the importance of Jmy for proper actin dynamics during oligodendrocyte differentiation. By following in real time the early stages of oligodendrocyte differentiation, in association with a quantitative morphodynamics analysis, we have described for the first time a specific program of stereotypical “cellular shaping” that governs morphological differentiation of oligodendrocytes: oligodendrocytes must undergo an initial period of intense protrusion remodeling characterized by multiple extensions and retractions, followed by formation of thin branches, to acquire the extremely complex arborized structure characteristic of pre-myelinating oligodendrocytes. In line with this, the presence of highly dynamic protrusions was described in migratory OPCs and pre-myelinating oligodendrocytes during zebrafish development (Kirby et al., 2006). Moreover, our live imaging analysis showed the need for tight regulation of the content of F-actin along the different

regions of oligodendrocytes: a higher concentration of F-actin is needed at protrusions tip during the first phase of protrusion extension and branching. Interestingly, Jmy depletion completely changed the actin dynamics that is needed for oligodendrocyte differentiation, resulting in impairment of the arborization step of differentiation. Actin polymerization is considered to be the driving force for the extension of membrane protrusions in oligodendrocytes (Nawaz et al., 2015; Zuchero et al., 2015). Indeed, our results are in line with this model, and we speculate that Jmy may be a key molecule in this process. The role of Jmy appears to be cell specific since, in the neuroblastoma cell line Neuro2A, depletion of Jmy results in increased ability of these cells to form neurites. Actin regulators can have different functions depending on cell context: the Arp2/3 complex, a key nucleator of actin networks found in lamellipodia, is required for the formation of filopodia in neurons (Korobova & Svitkina, 2008), but not in melanoma cells (Steffen et al., 2006) (reviewed in Firat-Karalar & Welch, 2011); and different diaphanous-related formins, which nucleate linear actin filaments in filopodial protrusions, are required for the assembly of lamellipodia in specific cell types (reviewed in Bogdan et al., 2013). Regarding Jmy, its function can also be different, according to the cell context: it plays a role in the migration of U2OS epithelial cells (Coutts et al., 2009; Zuchero et al., 2009), but not in mouse embryonic and NIH3T3 fibroblast migration (Firat-Karalar et al., 2011). Jmy can also directly activate the Arp2/3 complex (Zuchero et al., 2009) and, because the Arp2/3 complex is known to be involved in the extension of oligodendrocyte protrusions (Zuchero et al., 2015), further studies should address the interplay between Jmy and the Arp2/3 complex in oligodendrocytes.

The fact that Jmy also acts as a transcriptional co-activator in the p53 response to cellular stress makes it a unique actin-related protein. The nuclear localization signal and actin nucleation domains overlap in Jmy, and translocation of Jmy to the nucleus occurs in response to actin polymerization following DNA damage (Zuchero et al., 2012). However, unlike in other cells, Jmy appears not to localize in the nucleus of OPCs or oligodendrocytes and it is improbable that shuttling between the nucleus and the cytoplasm is a primary mechanism of regulating its function in these cells. Regarding other mechanisms that could regulate Jmy in oligodendrocytes, we further looked at the putative involvement of the well-known actin remodeling pathway via integrin and Rac1 signaling. However, we did not find any evidence *in vivo* that Rac1 and the integrin signaling pathways were involved. So, further studies regarding this question are needed. The classical Rho GTPase Cdc42 would be a good target to follow, as Jmy was recently considered a member of the WASP family (Alekhina et al., 2017).

Actin cytoskeleton remodeling has been recognized as a key factor in the regulation of apoptosis, with several actin monomer sequestration and regulatory proteins implicated in the process. Changes in the actin dynamics and in the expression of actin-related proteins may

trigger apoptosis (reviewed in Franklin-Tong & Gourlay, 2008). As we have reported, Jmy depletion induces changes in F-actin levels in oligodendrocytes, as well as in its localization. We speculate that these alterations in the dynamics and cellular distribution of F-actin can trigger oligodendrocyte cell death. This is in line with what has been reported in other cell types, such as Jurkat and HL-60 cells and T lymphocytes, after drug treatments and disruption of the expression levels of different actin regulator proteins (reviewed in Desouza et al., 2012). However, further studies are needed to confirm a direct link between Jmy depletion and compromised cell survival. Alongside with increased cell death, we also observed increased oligodendrocyte proliferation upon Jmy depletion. Jmy may be involved in regulating proliferation in 1) an indirect way - due to cell death induction, which may be triggering a phenomenon of apoptosis-induced proliferation, as has been seen in *Drosophila*, mice and human cells (reviewed in Fogarty & Bergmann, 2017); or 2) a direct way - by inducing alterations in oligodendrocyte polarization ability, culminating in aberrant cell proliferation. Interestingly, Jmy was reported as essential for oocyte asymmetric division, playing a role in spindle migration and induction of oocyte polarization (Sun et al., 2011). Although in OPCs loss of asymmetric cell division is associated with neoplastic transformation (Sugiarto et al., 2011), it is not known whether Jmy plays a role in OPC proliferation during CNS development by promoting asymmetric cells division. Further studies are needed to clarify Jmy's putative involvement in OPC proliferation.

In conclusion, we have unraveled a key role of Jmy in driving the morphological differentiation of oligodendrocytes. Additionally, we found that Jmy is necessary for oligodendrocyte survival and proliferation.

Morphological differentiation of oligodendrocytes is essential for extension of myelin-like membranes and formation of Mbp segments in myelinating co-cultures

The morphological differentiation of oligodendrocytes is concomitant with the expression of myelin-specific proteins by mature oligodendrocytes. We questioned whether Jmy was required for OPCs to differentiate into myelinating oligodendrocytes. Our results suggest that the normal developmental expression of antigenic markers commonly used to assess oligodendrocyte maturation was unaffected by the depletion of Jmy. However, we observed that Jmy depletion impaired the oligodendrocytes ability to extend myelin-like sheath membranes *in vitro* and to myelinate neurites in a co-culture system.

Our live cell imaging studies of oligodendrocyte differentiation provided additional information on why Jmy impacted the ability of oligodendrocytes to form myelin-like sheath membranes. We found that, after the initial period of fast remodeling of membrane protrusions and acquisition of a densely-arborized morphology, oligodendrocytes need to retract the

protrusions to give rise to the myelin-like membranes, with a concomitant displacement of F-actin towards the outermost ring of the membranes. This observation is in line with a previous study showing that actin depolymerization is needed for the formation of myelin sheaths (Nawaz et al., 2015). Jmy-depleted oligodendrocytes showed impaired arborization, which translated into deficient formation of myelin-like sheaths and arrested maturation. Moreover, our analysis of myelinating co-cultures revealed that oligodendrocytes depleted of Jmy are less effective in forming persistent contact with neurites and, when they do, shorter Mbp segments are formed. As depletion of Jmy led to defects in the F-actin network, it is possible that depolymerization occurs to a lesser extent, which would explain why oligodendrocytes form fewer membranous sheaths *in vitro*, and shorter Mbp segments when in co-culture with neurites. Future *in vivo* studies should be conducted to help clarify which aspects of myelination are dependent on Jmy's function.

In conclusion, we found that the arborization step, where Jmy's actin-nucleation activity is crucial, is a pre-requisite for the extension of myelin-like membranes. Moreover, regulation of the actin network architecture by Jmy was found to be essential for the establishment of contacts with neurites.

OligoMacro, a new tool for oligodendrocyte morphodynamics analysis

Oligodendrocyte differentiation is an extremely dynamic process that we followed in real time. In order to analyze the collected data in a more efficient way, we developed OligoMacro, a semi-automated tool that uses ImageJ built-in functions to process images and extract data, using phase contrast microscopy time-lapse datasets. OligoMacro is able to isolate, track and characterize the morphology of a large number of cells in a shorter period of time.

The development of OligoMacro was a necessity, since we were working with phase-contrast images and the vast majority of the available tools to perform semi-automated or fully-automated analyses of cellular morphology require fluorescence microscopy time-lapse datasets. Moreover, those tools are specifically designed or adapted for cells with a less complex morphology (Carpenter et al., 2006; Tsygankov et al., 2014). Herein, we demonstrated some OligoMacro applications and showed that OligoMacro is a powerful tool that can be adapted and used in different contexts to study diverse cellular processes. As it does not require advanced knowledge of any programming language, OligoMacro can easily be adapted to other cell types or to analyze fluorescence images. OligoMacro is the first semi-automated tool specifically designed to study oligodendrocyte behavior at the spatiotemporal scale.

Overall, we were able to further characterize early oligodendrocyte differentiation by showing that: 1) oligodendrocyte differentiation follows a stereotypical "cellular shaping"

program dependent of actin cytoskeleton dynamics; 2) formation of membrane-like sheaths and oligodendrocyte:neurite contacts depend on the correct stereotypical “cellular shaping” program; and 3) Jmy is a key actin related protein playing a role in early oligodendrocyte differentiation.

MATERIALS AND METHODS

Materials and Methods

Materials

Reagents

Dulbecco`s modified Eagle`s medium (DMEM)–glutamax; DMEM–glutamax/F-12; FluoroBrite -DMEM; 10 000 units/mL of penicillin and 10 000 µg/mL of streptomycin (P/S); nerve growth factor 7S (NGF); B27 supplement (50x); horse serum; Hanks's Balanced Salt Solution (HBSS); 0,25% Trypsin-EDTA (1x); normal goat serum (NGS), and OCT were purchased from ThermoFisher Scientific. Insulin; human transferring; progesterone; putrescine; sodium selenite; N-acetyl-L-cysteine (NAC); D-biotin; thyroxine; thiiodo-L-thyronine; 5-fluoro-2'-deoxyuridine (FUdR); fetal bovine serum (FBS); deoxyribonuclease I (DNAse I); poly-D-lysine (PDL); Dulbecco's Phosphate Buffered Saline (PBS); paraformaldehyde; sucrose; fluoroshield mounting medium; and protease inhibitor cocktail were obtained from Sigma. Bovine serum albumin faction V (BSA) was from Nzytech. Human PDGF-AA and basic FGF were purchased from PeproTech. Matrigel^{TM} basement membrane matrix was from BD Bioscience. TUNEL enzyme and biotin-labeled dUTP were from Roche. SuperSignal West Pico Chemiluminescent Substrate was obtained from Thermo Scientific. SuperScript III Reverse Transcriptase was purchased from Invitrogen. Quick-RNA^{TM} MicroPrep was from Zymo Research. SYBR green qPCR master mix and DC Protein Assay Kit was obtained from Bio-Rad.

Antibodies and probes

For immunoblotting, primary antibodies were used as follows: mouse anti-Arp3 (A-1), diluted 1:1000, Cat. # SC-48344, Santa Cruz Biotechnology (SCBT); rabbit anti-Jmy (M-300), diluted 1:800, Cat # SC-13020, (SCBT); rat anti-MBP, clone 12, diluted 1:100, Cat # MCA409S, Bio-Rad; rabbit anti-MAG, diluted 1:500, Cat # Ab46803, Abcam; mouse anti-αTubulin, clone B-5-1-2, diluted 1:40 000, Cat #T5168, Sigma; rabbit anti-HSP90, diluted 1:2500, Cat # ab13495, Abcam; rabbit anti-Histone H3, diluted 1:1000, Cat # mAb4499, Cell Signaling Technology; anti-Rac1, diluted 1:500, Cat # ab33186, Abcam; anti-ILK, diluted 1:750, Cat # 611802, BD Pharmigen; anti-RhoA (67B9), diluted 1:1000, Cat # 2117, Cell Signaling Technology. Secondary antibodies were goat anti-mouse HRP, diluted 1:15 000, Cat # 115- 035-146, goat anti-rabbit HRP, diluted 1: 10 000, Cat # 111-035-144, and goat anti-rat HRP, diluted 1: 10 000, Cat # 112-035-003, all from Jackson ImmunoResearch.

For IF, primary antibodies were used as follows: rabbit anti-Olig2, diluted 1:500, Cat # AB9610, Merck Millipore; rat anti-MBP, clone 12, diluted 1:100, Cat # MCA409S, Bio-Rad; mouse anti-CC1 (Ab7), diluted 1:250, Cat # OP80, Calbiochem; Merck; rabbit anti-Jmy (M-

300), diluted 1:250, Cat # SC-13020, SCBT; mouse anti-O4, diluted 1:400, Cat # MAB1326, R&D Systems; mouse anti-A2B5, clone 105, diluted 1:250, Cat # MAB1416, R&D Systems; mouse anti-βIII Tubulin, diluted 1:1000, Cat. # 302 302, Synaptic Systems. Secondary antibodies for IF were goat anti-mouse Cy3, diluted 1:1000, Cat # 115-165-146, Jackson ImmunoResearch; and goat anti-rat Alexa568, diluted 1:1000, Cat # A21247, goat anti-rabbit Alexa488, diluted 1:1000, Cat # A-11034, goat anti-rabbit Alexa568, diluted 1:1000, Cat # A11011, goat anti-rabbit Alexa647, diluted 1:1000, Cat # A-31573, goat anti-mouse Alexa647, diluted 1:1000, Cat # A21235, all from ThermoFisher Scientific. The following probes were used: DAPI (4',6'-diamidino-2-phenylindole dilactate), diluted 1:40 000, Cat # D3571, and Alexa Fluor 647 Phalloidin, diluted 1:50, Cat # A22287, both from ThermoFisher Scientific; and Sir-Actin, 50nmol, Cat # SC001, Spirochrome AG, Tebu-Bio.

Methods

Animals

Wistar Hahn rats were used for primary cultures of mixed glial cells (MGCs) and embryonic dorsal root ganglia (DRG). For immunohistochemistry (IHC) analysis, CNS tissue was obtained from wild type C57BL/6 mice at different ages. Before dissection, mice were anesthetized with pentobarbital and transcardially perfused with a 4% paraformaldehyde solution. All animal experiments were performed with the approval and in accordance with the IBMC/i3S Animal Ethics Committee, the Portuguese Veterinary Office and the European Union animal welfare laws and guidelines. All efforts were made to minimize suffering and reduce the number of animals used.

Cell line cultures

OLN93, an oligodendrocytes rat cell line, was used in some experiments. The cell line was obtained spontaneously from transformed cells in a primary rat brain glial culture (Richter-Landsberg & Heinrich, 1996). This cell line shows not only the same morphological characteristics of O2A progenitors or immature oligodendrocytes, but it also expresses late oligodendrocyte markers such as galactocerebroside (GC), myelin basic protein (Mbp), myelin associated protein (Mag) and proteolipid protein (Plp) (Armstrong et al., 1992; Richter-Landsberg & Heinrich, 1996). These cells can be differentiated when kept in low serum medium (1% FBS). Cells were maintained in culture using cell culture dishes coated with PDL, with cDMEM (DMEM-glutamax supplemented with 10% FBS and 1% P/S).

HEK293 cells are a stable cell line derived from human embryonic kidney, however without a defined cell type. This cell line was used since HEK cells are easy to grow and to be transfected. Mainly, this cell line was used to produce viral vectors. Cells were grown in c-DMEM.

Primary cultures of OPCs from rat brains

OPCs were isolated from mixed glial cultures (MGCs) of postnatal day 0-2 (P0-P2) rat brains (Chen et al., 2007; McCarthy & de Vellis, 1980). For MGCs, 10-12 brain cortices were dissected, freed of meninges and mechanically homogenized. The tissue suspension was enzymatically treated with DNase I (0.1mg/mL, Sigma) and 0.25% Trypsin-EDTA (Gibco) for 15 minutes at 37°C. After centrifugation (550g, 15min.), the cell pellet was resuspended in c-DMEM, filtered through a 100 μm nylon cell strainer (BD Falcon), plated on poly-D-lysine (PDL)-coated (Sigma) T75 flasks (Sarstedt) at a cell density of ~2 brains/flask and grown at 37°C in 5% CO_2 for approximately 10 days with fresh medium feeding every 2-3 days. To prepare pure OPCs, MGCs were pre-shaken at 220 rpm for 2h in a INFORS HT Minitron incubator with a radius of 2.5 cm at 37ºC. After addition of fresh c-DMEM, a shake at 240 rpm was performed overnight. The cell suspension obtained after differential adhesion was passed through a 40 μm nylon cell strainer (BD Falcon) and plated onto coated glass coverslips (14 mm) (coated with PDL in boric acid buffer (BAB) at 2500 µg/ml) at a density of 45 000 cells in Sato medium (5 µg/ml insulin, 1 mg/ml human transferring, 1 mg/ml BSA, 600 ng/ml progesterone, 160 µg/ml putrescine, 400 ng/ml sodium selenite, 400 ng/ml thyroxine, 300 ng/ml thiiodo-L-thyronine, 1% P/S), supplemented with growth factors PDGF-AA (10 ng/ml) and basic FGF (10 ng/ml) (proliferation medium), or on 6-well plates with ~$3x10^5$ cells/well. To induce differentiation, PDGF and FGF2 were replaced by 0.5% of FBS.

OPCs were transduced with lentivirus particles carrying the shRNAs of interest at the time of seeding. After 24 hours the medium was changed and the cells were maintained in proliferation medium for more 48 hours. In order to induce differentiation of OPCs, following the 48 hours period, the medium was changed for differentiation medium (Sato medium supplemented with 0,5% of FBS) and the cells were maintained in culture for different times according to the experimental setup. To assess the involvement of our protein of interest in oligodendrocytes differentiation, cells were collected for analysis at day of differentiation (DOD) 0, 3, 6 and 10.

Myelinating co-culture

Myelinating co-cultures were performed according to Laursen et al., with minor modifications (Laursen et al., 2011). Briefly, DRG were isolated from spinal cords of E15 rat embryos and digested with 0.05% Trypsin/EDTA and DNase I (0.4 mg/ml) for 90 minutes at 37 ºC. Dissociated neurons were plated at a density of 90 000 cells per coverslip (14 mm) previously coated with PDL and growth factor-reduced matrigel (BD Bioscience). DRG neurons were grown for 21 days *in vitro* (DIV) in C-DMEM supplemented with NGF (100 ng/ml). The culture was treated twice for 48h with 5-fluoro-2'-deoxyuridine (FUrd, 20 µM), at 1 and 6 DIV. After the first FUrd treatment, FBS was replaced by B27. After 21 DIV, transduced

OPCs were seeded on top of neurons at a density of 8 000 cells per coverslip and myelinating medium was added. Co-cultures were maintained for 18 DIV with media changes every 2-3 days.

Cloning into pSicoR vector

shRNAs specific for *Jmy* (sh1 - 5'-GAAGGCAAGTTTGCTATAA-3' and sh2 - 5'-GGACCTCACTGTCAAATAT-3') and for *Rnd2* (5'-GACATTAGCCGGCCAGAAA-3') were designed with PSICOLIGOMAKER 1.5 software. Oligonucleotides containing the shRNA sequence were synthesized, annealed and cloned into the pSicoR vector (a gift from Tyler Jacks - Addgene plasmid # 11579) (Ventura et al., 2004). Lentiviral particles were produced in HEK293T cells by transiently co-transfecting the plasmids pSicoR-shRNA, psPAX2 and pCMV-VSV-G using JetPrime reagent (Polyplus-transfection). After 48h, the medium was collected and the viral particles were purified and concentrated using a Beckman Coulter Optima L-80XP Ultra Centrifuge following a published protocol (Tiscornia et al., 2006). Lentivirus containing a shRNA sequence (5'-AGTTCCAGTACGGCTCCAA-3') targeting DsRed2, which is not found in mammals (Ozcelik et al., 2010), was used as an experimental control. Viral titers were determined as previously described (Tiscornia et al., 2006) and transduction of OPCs was performed with a MOI of 3.

Cell Sorting

48h after transduction, primary OPCs were detached using 0,05% of Trypsin/EDTA, centrifuged, resuspended in FACS buffer (1x PBS (Ca^+/Mg^+ free), 1mM EDTA, 25mM HEPES and 2% FBS) and passed through a cell strainer. Transduced OPCs were sorted for EGFP in a BD FACS Aria™ cell sorter.

Time-lapse microscopy

Live cell imaging of oligodendrocytes was performed with phase contrast microscopy. Cells were plated on 24-well-PDL-coated plastic bottom dishes after sorting and imaged with 5-minute frame rates for 3.5 days. For visualization of F-actin in live cells, OPCs were plated on PDL-BAB-matrigel-coated glass bottom 2-well u-Slides (Ibidi) and imaged with Sir-Actin (at 100nM, Cytoskeleton) added to the proliferation medium (FluoroBrite DMEM supplemented with sato1x and 0,5% FBS). Images were acquired with 15-minute intervals. For live-cell imaging of co-cultures DRGs, images were acquired at a frame rate of 10 min. All imaging was done under a controlled environment (37°C and 5% CO2) with a Leica DMI6000 epifluorescence microscope equipped with an Orca Flash 4.0 v2.0 camera (Hamamatsu). At least 30 fields of view were set for each condition.

Quantitative image analysis

For categorization of oligodendrocytes morphology, we classified Olig2-positive cells according their complexity (Baer et al., 2009) using phase-contrast and F-actin images. Minimums of at least 35 transduced Olig2 positive cells were analyzed from at least three independent experiments for each time point. For Sholl analysis of oligodendrocytes during early differentiation, a minimum of 50 transduced Olig2-positive cells were analyzed using the Sholl analysis tool (Ferreira et al., 2014) for ImageJ (Schneider et al., 2012) with the following parameters: 10 µm starting radius and 4 µm step size. Numbers of Mbp-positive cells were determined in a minimum of 300 transduced Olig2-positive cells, from images of at least three independent experiments. The total area occupied by F-actin was determined using ImageJ tools and a home-made macro. Measurement of Mbp-segment length in co-cultures was performed using the "segmented line" tool from ImageJ.

For semiautomated analysis of phase-contrast live imaging of oligodendrocyte differentiation, we developed "OligoMacro", an ImageJ toolset. After assembly of individual images, temporal stacks are pre-processed and cells tracked over time, retaining only maximum responses after applying derivative filters in all 8 directions (horizontal, vertical, and two diagonals, in both directions). Individual cells are isolated by connexity analysis after a Gaussian blur and automatic thresholding, and its centroid coordinates are retrieved and logged for all times. Tracking is performed by pairing centroids between time t and t+1 using the nearest neighbors algorithm. Tracking gaps are allowed and appear in the implementation as a user-defined parameter. For protrusion analysis, a region defined by the centroid coordinates is cropped for each individual cell. The resulting image is histogram-based filtered, background corrected, thresholded and skeletonized. The analyze particle function is used to remove protrusions that are either too short or not connected to the cell body. Conditional erosion is used to isolate both the endpoints (pixels from the skeleton lacking 7 neighbors) or branching points (pixels from the skeleton lacking 6 neighbors). Tracking and analysis data are logged into a data table, and a quality control image is also generated by overlaying cell and protrusion detections over the original image. Data formatting and reviewing, including plot and data table generation, is done with a R script directly in OligoMacro.

Immunofluorescence analysis (ICC and IHC)

For OPCs/oligodendrocytes, fixation was performed in 4% MP-PFA for 15 minutes at RT, followed by blocking for 1h in 10% NGS - PBS, and an overnight incubation at 4ºC with primary antibodies diluted in 10% NGS - PBS. Alexa Fluor conjugated (AF-) secondary antibodies (1:1000) and/or 647-Phalloidin (1:50) were diluted in blocking solution and incubated for 1h at RT. The nucleus was stained with 4',6'-diamidino-2-phenylindole (DAPI) for 10 minutes and the preparation was mounted with Fluoroshield mounting medium. For

myelinating co-cultures, we followed a previously published protocol (Barateiro et al., 2013) with minor modifications. Briefly, cells were fixed in 4% MP-PFA for 15 min at RT and then permeabilized/blocked with 1% HEPES, 2.5% Triton X-100, 1% NGS and 1% horse serum in PBS for 30 minutes at RT. Primary (Mbp at 1:100, ß-III Tubulin at 1:1000, and Olig2 at 1:500) and AF-secondary antibodies (1:1000) were diluted in blocking solution and sequentially incubated for 1h at RT.

For IHC, coronal or transversal sections (8-10 um thick) of mouse CNS tissues were cut on a Leica CM 3050S cryostat and recovered directly onto glass slides. Sections were permeabilized with 0.5% TX-TBS for 10 minutes, and incubated with blocking solution (10% NGS, 1% BSA, 0,025% TX, in TBS) for 1.5h. Primary antibodies (CC1 at 1:250, Jmy at 1:250 and MBP at 1:100) were diluted in 1% BSA/0.025% TX in TBS and incubated overnight at 4ºC. AF-secondary antibodies (1:500) were diluted in 1% BSA-TBS and incubated for 2h at RT.

Imaging was performed on a Leica DMI6000 epifluorescence microscope using a 40x/0.60 objective, equipped with an Orca Flash 4.0 v2.0 camera (Hamamatsu) or on a Laser Scanning Confocal Microscope Leica TCS SP5 II with a 63x/1.3 Gly objective. Confocal image z stacks acquired at 1 um Z-step were deconvolved using Huygens Professional software (Scientific Volume Imaging B.V). A Gaussian blur filter was applied and a maximum intensity projection was generated with Fiji software (Schindelin et al., 2012).

STED microscopy

We used an Abberior confocal gated-STED microscope with QUADscanner equipped with a pulsed excitation laser of 640nm at 40MHz repetition rate and, a depletion laser at 775nm, 1ns-long, for STED imaging (60x/1.27water objective). The doughnut profile is generated by dynamic phase modulation on a spatial light modulator (Abberior easySTED module). Detectors are avalanche photodiodes which can be gated to reject confocal baseline.

TUNEL and EdU staining

Apoptotic cell death was analyzed by TUNEL staining using biotin-labeled dUTP and Alexa Fluor 594 streptavidin complex according to the manufacturer's instructions (Roche Diagnostics). Proliferation was measured using the Click-iT EdU (5-ethynyl-2'-deoxyuridine) Alexa Fluor 568 imaging kit (Molecular probes) according to the manufacturer's instructions. Cells were collected for analysis at DOD0.

Subcellular fractionation and Immunoblots

OPCs subcellular fractionation was done according to Firat-Karalar et al. (Firat-Karalar et al., 2011). Briefly, OPCs were washed with cold PBS and lysed directly in the plate using cytosolic lysis buffer [10 mM HEPES, pH 7,9, 10 mM KCl, 0,1 mM EDTA, 0.4% NP-40, and

1x PI] for 15 minutes on ice. With a cell scrapper the lysate was collected and centrifuged at 3 000 g for 3 minutes to sediment nuclei fraction. The supernatant was collected and resedimented at 3 000 g for 5 minutes. The resulting supernatant was the cytosolic fraction. The nuclear pellet was washed with cytosolic lysis buffer, resuspended in nuclear lysis buffer (20 mM HEPES, pH 7,9, 0,4 M NaCl, 1 mM EDTA, 10% glycerol, and PI), sonicated on ice, and sedimented at 15 000 g for 5 minutes. The resulting supernatant was the nuclear fraction.

Total protein extracts from cells and tissue were prepared in lysis buffer [50 mM Tris pH 8.0, 150 mM NaCl, 1% NP-40, 1 mM EDTA, 0,5% sodium deoxycholate, 0,1% sodium dodecyl sulphate (SDS) supplemented, and a cocktail of protease inhibitors (Sigma, ref. 8340]. For ON, each N corresponds to a pool of 3 animals. Protein extracts were resolved by SDS - PAGE in 10% or 12% polyacrylamide gels. For immunoblot analysis, proteins were transferred onto a nitrocellulose membrane. Membranes were blocked for 1 h at room temperature in 5% (w/v) milk - TBS. Membranes were probed overnight at 4ºC, and for 1 h at room temperature for primary and secondary antibodies, respectively. Membranes were incubated for 5 minutes at room temperature with SuperSignal West Pico Chemiluminescent Substrate (Dagma) and, chemiluminescence was analyzed by detection in ChemiDoc XRS System (Biorad). Densitometry of the relative levels of protein expression were carried out using Image lab software (Biorad). The levels of the proteins of interest were normalized to the α-tubulin levels as a loading control.

cDNA synthesis and quantitative real time-PCR (qPCR)

Total RNA of oligodendrocytes, at different DODs, was extracted using Quick-RNA MicroPrep, according with manufacture's recommendations. RNA concentration and quality was measured in a Nanodrop 2000 device. cDNA synthesis was performed from 500ng-1µg of RNA using SuperScript III First-Strand Synthesis Supermix for qPCR Kit (Invitrogen) according to manufacturer's instructions. qPCR was performed using iQ SYBR Green Supermix (Bio-Rad) and an iCycler iQ5 real-time PCR machine (Bio-Rad) using the primers listed in Table 2. The results were normalized to *Ywhaz* and *Tbp* expression.

Table 2 – List of primers

Gene	Primer sense	Primer anti-sense
Selected genes		
Jmy	GCCCCACGTATTCGACGAG	CGTCCGGTTGTGACAGGTTA
Mbp	GCTCCCTGCCCCAGAAGT	TGTCACAATGTTCTTGAAGAAATGG
Plp	TCAGTCTATTGCCTTCCCTAGC	AGCATTCCATGGGAGAACAC
Cnp	GCCAGGTCTTTCTGGAGGAG	GCCTTCCCGTAGTCACAGAA
Mog	CTCATTGCCCTTGTGCCTAT	GCACGGAGTTTTCCTCTCAG
Housekeepers for oligodendrocyte cultures		
Tbp	TGGGATTGTACCACAGCTCCA	CTCATGATGACTGCAGCAAACC
YWHAZ	GATGAAGCCATTGCTGAACTTG	GTCTCCTTGGGTATCCGATGTC

Statistical analysis

Statistical analysis was performed using GraphPad Prism or SPSS software. Data distribution was tested for normality using the Shapiro–Wilk test. Comparisons between groups of measurements that follow a normal distribution and pass the F test to compare variances were performed using the one-sample t-test, unpaired two-tailed Student's t-test, or ANOVA followed by the recommended post-hoc test. For non-normal data, non-parametric tests were used. Analysis of distributions of categorical variables was performed with Pearson's chi-squared (χ^2) test. Significance was set as *p<0.05, **p<0.01, or ***p<0.001.

REFERENCES

Aggarwal, S., Snaidero, N., Pahler, G., Frey, S., Sanchez, P., Zweckstetter, M., Janshoff, A., Schneider, A., Weil, M. T., Schaap, I. A., Gorlich, D., & Simons, M. (2013). Myelin membrane assembly is driven by a phase transition of myelin basic proteins into a cohesive protein meshwork. *PLoS Biol, 11*(6), e1001577.

Aggarwal, S., Yurlova, L., & Simons, M. (2011). Central nervous system myelin: structure, synthesis and assembly. *Trends Cell Biol, 21*(10), 585-593.

Ainger, K., Avossa, D., Morgan, F., Hill, S. J., Barry, C., Barbarese, E., & Carson, J. H. (1993). Transport and localization of exogenous myelin basic protein mRNA microinjected into oligodendrocytes. *The Journal of Cell Biology, 123*(2), 431-441.

Alekhina, O., Burstein, E., & Billadeau, D. D. (2017). Cellular functions of WASP family proteins at a glance. *J Cell Sci, 130*(14), 2235-2241.

Alexandrova, A. Y., Arnold, K., Schaub, S., Vasiliev, J. M., Meister, J. J., Bershadsky, A. D., & Verkhovsky, A. B. (2008). Comparative dynamics of retrograde actin flow and focal adhesions: formation of nascent adhesions triggers transition from fast to slow flow. *PLoS One, 3*(9), e3234.

Allen, W. E., Zicha, D., Ridley, A. J., & Jones, G. E. (1998). A role for Cdc42 in macrophage chemotaxis. *J Cell Biol, 141*(5), 1147-1157.

Amur-Umarjee, S. G., Hall, L., & Campagnoni, A. T. (1990). Spatial distribution of mRNAs for myelin proteins in primary cultures of mouse brain. *Dev Neurosci, 12*(4-5), 263-272.

Armendariz, B. G., Bribian, A., Perez-Martinez, E., Martinez, A., de Castro, F., Soriano, E., & Burgaya, F. (2012). Expression of Semaphorin 4F in neurons and brain oligodendrocytes and the regulation of oligodendrocyte precursor migration in the optic nerve. *Mol Cell Neurosci, 49*(1), 54-67.

Armstrong, R. C., Dorn, H. H., Kufta, C. V., Friedman, E., & Dubois-Dalcq, M. E. (1992). Pre-oligodendrocytes from adult human CNS. *J Neurosci, 12*(4), 1538-1547.

Azevedo, M. M., Domingues, H. S., Cordelières, F. P., Sampaio, P., Seixas, A. I., & Relvas, J. B. (2018). Jmy regulates oligodendrocyte differentiation via modulation of actin cytoskeleton dynamics. *Glia*, 1-19.

Bacon, C., Lakics, V., Machesky, L., & Rumsby, M. (2007). N-WASP regulates extension of filopodia and processes by oligodendrocyte progenitors, oligodendrocytes, and Schwann cells-implications for axon ensheathment at myelination. *Glia, 55*(8), 844-858.

Baer, A. S., Syed, Y. A., Kang, S. U., Mitteregger, D., Vig, R., Ffrench-Constant, C., Franklin, R. J., Altmann, F., Lubec, G., & Kotter, M. R. (2009). Myelin-mediated inhibition of oligodendrocyte precursor differentiation can be overcome by pharmacological modulation of Fyn-RhoA and protein kinase C signalling. *Brain, 132*(Pt 2), 465-481.

Barateiro, A., Miron, V. E., Santos, S. D., Relvas, J. B., Fernandes, A., Ffrench-Constant, C., & Brites, D. (2013). Unconjugated bilirubin restricts oligodendrocyte differentiation and axonal myelination. *Mol Neurobiol, 47*(2), 632-644.

Baron, W., & Hoekstra, D. (2010). On the biogenesis of myelin membranes: sorting, trafficking and cell polarity. *FEBS Lett, 584*(9), 1760-1770.

Barry, D. J., Durkin, C. H., Abella, J. V., & Way, M. (2015). Open source software for quantification of cell migration, protrusions, and fluorescence intensities. *J Cell Biol, 209*(1), 163-180.

Bauer, N. G., Richter-Landsberg, C., & Ffrench-Constant, C. (2009). Role of the oligodendroglial cytoskeleton in differentiation and myelination. *Glia, 57*(16), 1691-1705.

Bauer, N. G., Richter-Landsberg, C., & Ffrench-Constant, C. (2009). Role of the oligodendroglial cytoskeleton in differentiation and myelination. *Glia, 57*(16), 1691-1705.

Baumann, N., & Pham-Dinh, D. (2001). Biology of oligodendrocyte and myelin in the mammalian central nervous system. *Physiol Rev, 81*(2), 871-927.

Bendix, P. M., Koenderink, G. H., Cuvelier, D., Dogic, Z., Koeleman, B. N., Brieher, W. M., Field, C. M., Mahadevan, L., & Weitz, D. A. (2008). A quantitative analysis of contractility in active cytoskeletal protein networks. *Biophys J, 94*(8), 3126-3136.

Bentley, D., & Toroian-Raymond, A. (1986). Disoriented pathfinding by pioneer neurone growth cones deprived of filopodia by cytochalasin treatment. *Nature, 323*(6090), 712-715.

Bergles, D. E., Jabs, R., & Steinhauser, C. (2010). Neuron-glia synapses in the brain. *Brain Res Rev, 63*(1-2), 130-137.

Bezanilla, M., Gladfelter, A. S., Kovar, D. R., & Lee, W. L. (2015). Cytoskeletal dynamics: a view from the membrane. *J Cell Biol, 209*(3), 329-337.

Bhat, N. R., & Zhang, P. (1996). Activation of mitogen-activated protein kinases in oligodendrocytes. *J Neurochem, 66*(5), 1986-1994.

Billeci, L., Magliaro, C., Pioggia, G., & Ahluwalia, A. (2013). NEuronMOrphological analysis tool: open-source software for quantitative morphometrics. *Front Neuroinform, 7*, 2.

Blakemore, W. F. (1974). Pattern of remyelination in the CNS. *Nature, 249*(457), 577-578.

Blanchoin, L., Amann, K. J., Higgs, H. N., Marchand, J. B., Kaiser, D. A., & Pollard, T. D. (2000). Direct observation of dendritic actin filament networks nucleated by Arp2/3 complex and WASP/Scar proteins. *Nature, 404*(6781), 1007-1011.

Blanchoin, L., Boujemaa-Paterski, R., Sykes, C., & Plastino, J. (2014). Actin dynamics, architecture, and mechanics in cell motility. *Physiol Rev, 94*(1), 235-263.

Boda, E., Vigano, F., Rosa, P., Fumagalli, M., Labat-Gest, V., Tempia, F., Abbracchio, M. P., Dimou, L., & Buffo, A. (2011). The GPR17 receptor in NG2 expressing cells: focus on in vivo cell maturation and participation in acute trauma and chronic damage. *Glia, 59*(12), 1958-1973.

Bogdan, S., Schultz, J., & Grosshans, J. (2013). Formin' cellular structures: Physiological roles of Diaphanous (Dia) in actin dynamics. *Commun Integr Biol, 6*(6), e27634.

Boggs, J. M., Homchaudhuri, L., Ranagaraj, G., Liu, Y., Smith, G. S., & Harauz, G. (2014). Interaction of myelin basic protein with cytoskeletal and signaling proteins in cultured primary oligodendrocytes and N19 oligodendroglial cells. *BMC Res Notes, 7*, 387.

Boggs, J. M., Rangaraj, G., Heng, Y. M., Liu, Y., & Harauz, G. (2011). Myelin basic protein binds microtubules to a membrane surface and to actin filaments in vitro: effect of phosphorylation and deimination. *Biochim Biophys Acta, 1808*(3), 761-773.

Boggs, J. M., & Wang, H. (2001). Effect of liposomes containing cerebroside and cerebroside sulfate on cytoskeleton of cultured oligodendrocytes. *J Neurosci Res, 66*(2), 242-253.

Bosco, E. E., Mulloy, J. C., & Zheng, Y. (2009). Rac1 GTPase: a "Rac" of all trades. *Cell Mol Life Sci, 66*(3), 370-374.

Brakebusch, C., & Fassler, R. (2003). The integrin-actin connection, an eternal love affair. *EMBO J, 22*(10), 2324-2333.

Breitsprecher, D., & Goode, B. L. (2013). Formins at a glance. *J Cell Sci, 126*(Pt 1), 1-7.

Bunge, M. B., Bunge, R. P., & Ris, H. (1961). Ultrastructural study of remyelination in an experimental lesion in adult cat spinal cord. *J Biophys Biochem Cytol, 10*, 67-94.

Butt, A. M., & Ransom, B. R. (1989). Visualization of oligodendrocytes and astrocytes in the intact rat optic nerve by intracellular injection of lucifer yellow and horseradish peroxidase. *Glia, 2*(6), 470-475.

Buttery, P. C., & ffrench-Constant, C. (2001). Process extension and myelin sheet formation in maturing oligodendrocytes. *Prog Brain Res, 132*, 115-130.

Cahoy, J. D., Emery, B., Kaushal, A., Foo, L. C., Zamanian, J. L., Christopherson, K. S., Xing, Y., Lubischer, J. L., Krieg, P. A., Krupenko, S. A., Thompson, W. J., & Barres, B. A. (2008). A transcriptome database for astrocytes, neurons, and oligodendrocytes: a new resource for understanding brain development and function. *The Journal of Neuroscience, 28*(1), 264-278.

Calver, A. R., Hall, A. C., Yu, W. P., Walsh, F. S., Heath, J. K., Betsholtz, C., & Richardson, W. D. (1998). Oligodendrocyte population dynamics and the role of PDGF in vivo. *Neuron, 20*(5), 869-882.

Campellone, K. G., Webb, N. J., Znameroski, E. A., & Welch, M. D. (2008). WHAMM is an Arp2/3 complex activator that binds microtubules and functions in ER to Golgi transport. *Cell, 134*(1), 148-161.

Campellone, K. G., & Welch, M. D. (2010). A nucleator arms race: cellular control of actin assembly. *Nat Rev Mol Cell Biol, 11*(4), 237-251.

Caprariello, A. V., Mangla, S., Miller, R. H., & Selkirk, S. M. (2012). Apoptosis of oligodendrocytes in the central nervous system results in rapid focal demyelination. *Ann Neurol, 72*(3), 395-405.

Carlier, M. F., Pantaloni, D., & Korn, E. D. (1987). The mechanisms of ATP hydrolysis accompanying the polymerization of Mg-actin and Ca-actin. *J Biol Chem, 262*(7), 3052-3059.

Carpenter, A. E., Jones, T. R., Lamprecht, M. R., Clarke, C., Kang, I. H., Friman, O., Guertin, D. A., Chang, J. H., Lindquist, R. A., Moffat, J., Golland, P., & Sabatini, D. M. (2006). CellProfiler: image analysis software for identifying and quantifying cell phenotypes. *Genome Biol, 7*(10), R100.

Carson, J. H., Worboys, K., Ainger, K., & Barbarese, E. (1997). Translocation of myelin basic protein mRNA in oligodendrocytes requires microtubules and kinesin. *Cell Motil Cytoskeleton, 38*(4), 318-328.

Chang, A., Nishiyama, A., Peterson, J., Prineas, J., & Trapp, B. D. (2000). NG2-positive oligodendrocyte progenitor cells in adult human brain and multiple sclerosis lesions. *J Neurosci, 20*(17), 6404-6412.

Chang, A., Tourtellotte, W. W., Rudick, R., & Trapp, B. D. (2002). Premyelinating oligodendrocytes in chronic lesions of multiple sclerosis. *N Engl J Med, 346*(3), 165-173.

Chang, K. J., Redmond, S. A., & Chan, J. R. (2016). Remodeling myelination: implications for mechanisms of neural plasticity. *Nat Neurosci, 19*(2), 190-197.

Charras, G. T., Coughlin, M., Mitchison, T. J., & Mahadevan, L. (2008). Life and times of a cellular bleb. *Biophys J, 94*(5), 1836-1853.

Charras, G. T., Yarrow, J. C., Horton, M. A., Mahadevan, L., & Mitchison, T. J. (2005). Non-equilibration of hydrostatic pressure in blebbing cells. *Nature, 435*(7040), 365-369.

Chen, Y., Balasubramaniyan, V., Peng, J., Hurlock, E. C., Tallquist, M., Li, J., & Lu, R. Q. (2007). Isolation and culture of rat and mouse oligodendrocyte precursor cells. *Nature Protocols, 2*(5), 1044-1051.

Chen, Z., Borek, D., Padrick, S. B., Gomez, T. S., Metlagel, Z., Ismail, A. M., Umetani, J., Billadeau, D. D., Otwinowski, Z., & Rosen, M. K. (2010). Structure and control of the actin regulatory WAVE complex. *Nature, 468*(7323), 533-538.

Chenouard, N., Smal, I., de Chaumont, F., Maska, M., Sbalzarini, I. F., Gong, Y., Cardinale, J., Carthel, C., Coraluppi, S., Winter, M., Cohen, A. R., Godinez, W. J., Rohr, K., Kalaidzidis, Y., Liang, L., Duncan, J., Shen, H., Xu, Y., Magnusson, K. E., Jalden, J., Blau, H. M., Paul-Gilloteaux, P., Roudot, P., Kervrann, C., Waharte, F., Tinevez, J. Y., Shorte, S. L., Willemse, J., Celler, K., van Wezel, G. P., Dan, H. W., Tsai, Y. S., Ortiz de Solorzano, C., Olivo-Marin, J. C., & Meijering, E. (2014). Objective comparison of particle tracking methods. *Nat Methods, 11*(3), 281-289.

Chernoff, G. F. (1981). Shiverer: an autosomal recessive mutant mouse with myelin deficiency. *J Hered, 72*(2), 128.

Chesarone, M. A., DuPage, A. G., & Goode, B. L. (2010). Unleashing formins to remodel the actin and microtubule cytoskeletons. *Nat Rev Mol Cell Biol, 11*(1), 62-74.

Chesarone, M. A., & Goode, B. L. (2009). Actin nucleation and elongation factors: mechanisms and interplay. *Curr Opin Cell Biol, 21*(1), 28-37.

Chien, C. B., Rosenthal, D. E., Harris, W. A., & Holt, C. E. (1993). Navigational errors made by growth cones without filopodia in the embryonic Xenopus brain. *Neuron, 11*(2), 237-251.

Chittajallu, R., Aguirre, A., & Gallo, V. (2004). NG2-positive cells in the mouse white and grey matter display distinct physiological properties. *J Physiol, 561*(Pt 1), 109-122.

Choe, Y., Huynh, T., & Pleasure, S. J. (2014). Migration of oligodendrocyte progenitor cells is controlled by transforming growth factor beta family proteins during corticogenesis. *J Neurosci, 34*(45), 14973-14983.

Colman, D. R., Kreibich, G., Frey, A. B., & Sabatini, D. D. (1982). Synthesis and incorporation of myelin polypeptides into CNS myelin. *J Cell Biol, 95*(2 Pt 1), 598-608.

Correia, A. S., Augusto, L., Meireles, J., Pinto, J., & Sousa, A. P. (2016). Pediatric Multiple Sclerosis in Portugal: A Multicentre Study. *Acta Med Port, 29*(7-8), 425-431.

Coutts, A. S., Boulahbel, H., Graham, A., & La Thangue, N. B. (2007). Mdm2 targets the p53 transcription cofactor JMY for degradation. *EMBO Rep, 8*(1), 84-90.

Coutts, A. S., Weston, L., & La Thangue, N. B. (2009). A transcription co-factor integrates cell adhesion and motility with the p53 response. *Proc Natl Acad Sci U S A, 106*(47), 19872-19877.

Dahl, J. P., Wang-Dunlop, J., Gonzales, C., Goad, M. E., Mark, R. J., & Kwak, S. P. (2003). Characterization of the WAVE1 knock-out mouse: implications for CNS development. *J Neurosci, 23*(8), 3343-3352.

Dancker, P., Low, I., Hasselbach, W., & Wieland, T. (1975). Interaction of actin with phalloidin: polymerization and stabilization of F-actin. *Biochim Biophys Acta, 400*(2), 407-414.

Dangata, Y. Y., & Kaufman, M. H. (1997). Myelinogenesis in the optic nerve of (C57BL x CBA) F1 hybrid mice: a morphometric analysis. *Eur J Morphol, 35*(1), 3-17.

De Robertis, E., Gerschenfeld, H. M., & Wald, F. (1958). Cellular mechanism of myelination in the central nervous system. *J Biophys Biochem Cytol, 4*(5), 651-656.

Decker, L., Avellana-Adalid, V., Nait-Oumesmar, B., Durbec, P., & Baron-Van Evercooren, A. (2000). Oligodendrocyte precursor migration and differentiation: combined effects of PSA residues, growth factors, and substrates. *Mol Cell Neurosci, 16*(4), 422-439.

Derivery, E., Sousa, C., Gautier, J. J., Lombard, B., Loew, D., & Gautreau, A. (2009). The Arp2/3 activator WASH controls the fission of endosomes through a large multiprotein complex. *Dev Cell, 17*(5), 712-723.

Desouza, M., Gunning, P. W., & Stehn, J. R. (2012). The actin cytoskeleton as a sensor and mediator of apoptosis. *BioArchitecture, 2*(3), 75-87.

DiMilla, P. A., Stone, J. A., Quinn, J. A., Albelda, S. M., & Lauffenburger, D. A. (1993). Maximal migration of human smooth muscle cells on fibronectin and type IV collagen occurs at an intermediate attachment strength. *J Cell Biol, 122*(3), 729-737.

dos Remedios, C. G., Chhabra, D., Kekic, M., Dedova, I. V., Tsubakihara, M., Berry, D. A., & Nosworthy, N. J. (2003). Actin binding proteins: regulation of cytoskeletal microfilaments. *Physiol Rev, 83*(2), 433-473.

Dubois, C., Manuguerra, J. C., Hauttecoeur, B., & Maze, J. (1990). Monoclonal antibody A2B5, which detects cell surface antigens, binds to ganglioside GT3 (II3 (NeuAc)3LacCer) and to its 9-O-acetylated derivative. *J Biol Chem, 265*(5), 2797-2803.

Dubois-Dalcq, M., & Murray, K. (2000). Why are growth factors important in oligodendrocyte physiology? *Pathol Biol (Paris), 48*(1), 80-86.

Dugas, J. C., Tai, Y. C., Speed, T. P., Ngai, J., & Barres, B. A. (2006). Functional genomic analysis of oligodendrocyte differentiation. *J Neurosci, 26*(43), 10967-10983.

Duleh, S. N., & Welch, M. D. (2010). WASH and the Arp2/3 complex regulate endosome shape and trafficking. *Cytoskeleton (Hoboken), 67*(3), 193-206.

Duncan, I. D., Marik, R. L., Broman, A. T., & Heidari, M. (2017). Thin myelin sheaths as the hallmark of remyelination persist over time and preserve axon function. *Proc Natl Acad Sci U S A, 114*(45), E9685-E9691.

Dyer, C. A., & Benjamins, J. A. (1989). Organization of oligodendroglial membrane sheets: II. Galactocerebroside:antibody interactions signal changes in cytoskeleton and myelin basic protein. *J Neurosci Res, 24*(2), 212-221.

Dyer, C. A., Philibotte, T. M., Billings-Gagliardi, S., & Wolf, M. K. (1995). Cytoskeleton in myelin-basic-protein-deficient shiverer oligodendrocytes. *Dev Neurosci, 17*(1), 53-62.

Dyer, C. A., Phillbotte, T., Wolf, M. K., & Billings-Gagliardi, S. (1997). Regulation of cytoskeleton by myelin components: studies on shiverer oligodendrocytes carrying an Mbp transgene. *Dev Neurosci, 19*(5), 395-409.

Emery, B. (2010). Regulation of oligodendrocyte differentiation and myelination. *Science, 330*(6005), 779-782.

Engqvist-Goldstein, A. E., & Drubin, D. G. (2003). Actin assembly and endocytosis: from yeast to mammals. *Annu Rev Cell Dev Biol, 19*, 287-332.

Ferreira, T. A., Blackman, A. V., Oyrer, J., Jayabal, S., Chung, A. J., Watt, A. J., Sjostrom, P. J., & van Meyel, D. J. (2014). Neuronal morphometry directly from bitmap images. *Nat Methods, 11*(10), 982-984.

Ffrench-Constant, C., Miller, R. H., Burne, J. F., & Raff, M. C. (1988). Evidence that migratory oligodendrocyte-type-2 astrocyte (O-2A) progenitor cells are kept out of the rat retina by a barrier at the eye-end of the optic nerve. *J Neurocytol, 17*(1), 13-25.

Firat-Karalar, E. N., Hsiue, P. P., & Welch, M. D. (2011). The actin nucleation factor JMY is a negative regulator of neuritogenesis. *Mol Biol Cell, 22*(23), 4563-4574.

Firat-Karalar, E. N., & Welch, M. D. (2011). New mechanisms and functions of actin nucleation. *Curr Opin Cell Biol, 23*(1), 4-13.

Fitzner, D., Schneider, A., Kippert, A., Mobius, W., Willig, K. I., Hell, S. W., Bunt, G., Gaus, K., & Simons, M. (2006). Myelin basic protein-dependent plasma membrane reorganization in the formation of myelin. *EMBO J, 25*(21), 5037-5048.

Fletcher, D. A., & Mullins, R. D. (2010). Cell mechanics and the cytoskeleton. *Nature, 463*(7280), 485-492.

Fogarty, C. E., & Bergmann, A. (2017). Killers creating new life: caspases drive apoptosis-induced proliferation in tissue repair and disease. *Cell Death Differ, 24*(8), 1390-1400.

Fogarty, M., Richardson, W. D., & Kessaris, N. (2005). A subset of oligodendrocytes generated from radial glia in the dorsal spinal cord. *Development, 132*(8), 1951-1959.

Foran, D. R., & Peterson, A. C. (1992). Myelin acquisition in the central nervous system of the mouse revealed by an MBP-Lac Z transgene. *J Neurosci, 12*(12), 4890-4897.

Fox, M. A., Afshari, F. S., Alexander, J. K., Colello, R. J., & Fuss, B. (2006). Growth conelike sensorimotor structures are characteristic features of postmigratory, premyelinating oligodendrocytes. *Glia, 53*(5), 563-566.

Franklin, R. J., & Ffrench-Constant, C. (2008). Remyelination in the CNS: from biology to therapy. *Nat Rev Neurosci, 9*(11), 839-855.

Franklin-Tong, V. E., & Gourlay, C. W. (2008). A role for actin in regulating apoptosis/programmed cell death: evidence spanning yeast, plants and animals. *Biochem J, 413*(3), 389-404.

Fritzsche, M., Lewalle, A., Duke, T., Kruse, K., & Charras, G. (2013). Analysis of turnover dynamics of the submembranous actin cortex. *Mol Biol Cell, 24*(6), 757-767.

Fruttiger, M., Karlsson, L., Hall, A. C., Abramsson, A., Calver, A. R., Bostrom, H., Willetts, K., Bertold, C. H., Heath, J. K., Betsholtz, C., & Richardson, W. D. (1999). Defective oligodendrocyte development and severe hypomyelination in PDGF-A knockout mice. *Development, 126*(3), 457-467.

Funfschilling, U., Supplie, L. M., Mahad, D., Boretius, S., Saab, A. S., Edgar, J., Brinkmann, B. G., Kassmann, C. M., Tzvetanova, I. D., Mobius, W., Diaz, F., Meijer, D., Suter, U., Hamprecht, B., Sereda, M. W., Moraes, C. T., Frahm, J., Goebbels, S., & Nave, K. A. (2012). Glycolytic oligodendrocytes maintain myelin and long-term axonal integrity. *Nature, 485*(7399), 517-521.

Gard, A. L., & Pfeiffer, S. E. (1989). Oligodendrocyte progenitors isolated directly from developing telencephalon at a specific phenotypic stage: myelinogenic potential in a defined environment. *Development, 106*(1), 119-132.

Gielen, E., Baron, W., Vandeven, M., Steels, P., Hoekstra, D., & Ameloot, M. (2006). Rafts in oligodendrocytes: evidence and structure-function relationship. *Glia, 54*(6), 499-512.

Gomez, T. M., & Letourneau, P. C. (2014). Actin dynamics in growth cone motility and navigation. *J Neurochem, 129*(2), 221-234.

Griffiths, I. (1998). Axonal Swellings and Degeneration in Mice Lacking the Major Proteolipid of Myelin. *Science, 280*(5369), 1610-1613.

Hall, A. (1998). Rho GTPases and the actin cytoskeleton. *Science, 279*(5350), 509-514.

Hand, R., Bortone, D., Mattar, P., Nguyen, L., Heng, J. I., Guerrier, S., Boutt, E., Peters, E., Barnes, A. P., Parras, C., Schuurmans, C., Guillemot, F., & Polleux, F. (2005). Phosphorylation of Neurogenin2 specifies the migration properties and the dendritic morphology of pyramidal neurons in the neocortex. *Neuron, 48*(1), 45-62.

Hannigan, G. E., Leung-Hagesteijn, C., Fitz-Gibbon, L., Coppolino, M. G., Radeva, G., Filmus, J., Bell, J. C., & Dedhar, S. (1996). Regulation of cell adhesion and anchorage-dependent growth by a new beta 1-integrin-linked protein kinase. *Nature, 379*(6560), 91-96.

Hayakawa, K., Seo, J. H., Pham, L. D., Miyamoto, N., Som, A. T., Guo, S., Kim, K. W., Lo, E. H., & Arai, K. (2012). Cerebral endothelial derived vascular endothelial growth factor promotes the migration but not the proliferation of oligodendrocyte precursor cells in vitro. *Neurosci Lett, 513*(1), 42-46.

Heng, Y. W., & Koh, C. G. (2010). Actin cytoskeleton dynamics and the cell division cycle. *Int J Biochem Cell Biol, 42*(10), 1622-1633.

Higgs, H. N., & Pollard, T. D. (2000). Activation by Cdc42 and Pip2of Wiskott-Aldrich Syndrome Protein (Wasp) Stimulates Actin Nucleation by Arp2/3 Complex. *The Journal of Cell Biology, 150*(6), 1311-1320.

Hildebrand, C., Remahl, S., Persson, H., & Bjartmar, C. (1993). Myelinated nerve fibres in the CNS. *Prog Neurobiol, 40*(3), 319-384.

Hilpela, P., Vartiainen, M. K., & Lappalainen, P. (2004). Regulation of the actin cytoskeleton by PI(4,5)P2 and PI(3,4,5)P3. *Curr Top Microbiol Immunol, 282*, 117-163.

Hu, K., Ji, L., Applegate, K. T., Danuser, G., & Waterman-Storer, C. M. (2007). Differential transmission of actin motion within focal adhesions. *Science, 315*(5808), 111-115.

Hughes, E. G., Kang, S. H., Fukaya, M., & Bergles, D. E. (2013). Oligodendrocyte progenitors balance growth with self-repulsion to achieve homeostasis in the adult brain. *Nat Neurosci, 16*(6), 668-676.

Ioannidou, K., Anderson, K. I., Strachan, D., Edgar, J. M., & Barnett, S. C. (2012). Time-lapse imaging of the dynamics of CNS glial-axonal interactions in vitro and ex vivo. *PLoS One, 7*(1), e30775.

Jacquemet, G., Paatero, I., Carisey, A. F., Padzik, A., Orange, J. S., Hamidi, H., & Ivaska, J. (2017). FiloQuant reveals increased filopodia density during breast cancer progression. *J Cell Biol, 216*(10), 3387-3403.

Jahn, O., Tenzer, S., & Werner, H. B. (2009). Myelin proteomics: molecular anatomy of an insulating sheath. *Mol Neurobiol, 40*(1), 55-72.

Jain, N., Kalailingam, P., Tan, K. W., Tan, H. B., Sng, M. K., Chan, J. S., Tan, N. S., & Thanabalu, T. (2016). Conditional knockout of N-WASP in mouse fibroblast caused keratinocyte hyper proliferation and enhanced wound closure. *Sci Rep, 6*, 38109.

Jarjour, A. A., Boyd, A., Dow, L. E., Holloway, R. K., Goebbels, S., Humbert, P. O., Williams, A., & ffrench-Constant, C. (2015). The polarity protein Scribble regulates myelination and remyelination in the central nervous system. *PLoS Biol, 13*(3), e1002107.

Jontes, J. D., & Smith, S. J. (2000). Filopodia, spines, and the generation of synaptic diversity. *Neuron, 27*(1), 11-14.

Kachar, B., Behar, T., & Dubois-Dalcq, M. (1986). Cell shape and motility of oligodendrocytes cultured without neurons. *Cell Tissue Res, 244*(1), 27-38.

Kachar, B., Behar, T., & Duboisdalcq, M. (1986). Cell-Shape and Motility of Oligodendrocytes Cultured without Neurons. *Cell and Tissue Research, 244*(1), 27-38.

Kanchanawong, P., Shtengel, G., Pasapera, A. M., Ramko, E. B., Davidson, M. W., Hess, H. F., & Waterman, C. M. (2010). Nanoscale architecture of integrin-based cell adhesions. *Nature, 468*(7323), 580-584.

Karp, G. C., & Solursh, M. (1985). Dynamic activity of the filopodia of sea urchin embryonic cells and their role in directed migration of the primary mesenchyme in vitro. *Developmental Biology, 112*(2), 276-283.

Kessaris, N., Fogarty, M., Iannarelli, P., Grist, M., Wegner, M., & Richardson, W. D. (2006). Competing waves of oligodendrocytes in the forebrain and postnatal elimination of an embryonic lineage. *Nat Neurosci, 9*(2), 173-179.

Kessaris, N., Pringle, N., & Richardson, W. D. (2008). Specification of CNS glia from neural stem cells in the embryonic neuroepithelium. *Philos Trans R Soc Lond B Biol Sci, 363*(1489), 71-85.

Kierdorf, K., & Prinz, M. (2017). Microglia in steady state. *J Clin Invest, 127*(9), 3201-3209.

Kim, A. S., Kakalis, L. T., Abdul-Manan, N., Liu, G. A., & Rosen, M. K. (2000). Autoinhibition and activation mechanisms of the Wiskott-Aldrich syndrome protein. *Nature, 404*(6774), 151-158.

Kim, H. J., DiBernardo, A. B., Sloane, J. A., Rasband, M. N., Solomon, D., Kosaras, B., Kwak, S. P., & Vartanian, T. K. (2006). WAVE1 is required for oligodendrocyte morphogenesis and normal CNS myelination. *J Neurosci, 26*(21), 5849-5859.

Kirby, B. B., Takada, N., Latimer, A. J., Shin, J., Carney, T. J., Kelsh, R. N., & Appel, B. (2006). In vivo time-lapse imaging shows dynamic oligodendrocyte progenitor behavior during zebrafish development. *Nat Neurosci, 9*(12), 1506-1511.

Kolodny, E. H. (1993). Dysmyelinating and demyelinating conditions in infancy. *Curr Opin Neurol Neurosurg, 6*(3), 379-386.

Korn, E. D., Carlier, M. F., & Pantaloni, D. (1987). Actin polymerization and ATP hydrolysis. *Science, 238*(4827), 638-644.

Korobova, F., & Svitkina, T. (2008). Arp2/3 complex is important for filopodia formation, growth cone motility, and neuritogenesis in neuronal cells. *Mol Biol Cell, 19*(4), 1561-1574.

Kuhlmann, T., Miron, V., Cui, Q., Wegner, C., Antel, J., & Bruck, W. (2008). Differentiation block of oligodendroglial progenitor cells as a cause for remyelination failure in chronic multiple sclerosis. *Brain, 131*(Pt 7), 1749-1758.

Kuhnert, F., Mancuso, M. R., Shamloo, A., Wang, H. T., Choksi, V., Florek, M., Su, H., Fruttiger, M., Young, W. L., Heilshorn, S. C., & Kuo, C. J. (2010). Essential regulation of CNS angiogenesis by the orphan G protein-coupled receptor GPR124. *Science, 330*(6006), 985-989.

Kustermans, G., Piette, J., & Legrand-Poels, S. (2008). Actin-targeting natural compounds as tools to study the role of actin cytoskeleton in signal transduction. *Biochem Pharmacol, 76*(11), 1310-1322.

Kyrylkova, K., Kyryachenko, S., Leid, M., & Kioussi, C. (2012). Detection of apoptosis by TUNEL assay. *Methods Mol Biol, 887*, 41-47.

Laursen, L. S., Chan, C. W., & Ffrench-Constant, C. (2011). Translation of myelin basic protein mRNA in oligodendrocytes is regulated by integrin activation and hnRNP-K. *J Cell Biol, 192*(5), 797-811.

Lazzarini, R. A. (2003). *Myelin Biology and Disorders* (E. A. Press Ed. Vol. 1).

Lecuit, T., Lenne, P. F., & Munro, E. (2011). Force generation, transmission, and integration during cell and tissue morphogenesis. *Annu Rev Cell Dev Biol, 27*, 157-184.

Legate, K. R., Montanez, E., Kudlacek, O., & Fassler, R. (2006). ILK, PINCH and parvin: the tIPP of integrin signalling. *Nat Rev Mol Cell Biol, 7*(1), 20-31.

Leray, E., Moreau, T., Fromont, A., & Edan, G. (2016). Epidemiology of multiple sclerosis. *Rev Neurol (Paris), 172*(1), 3-13.

Levine, J. M., Stincone, F., & Lee, Y. S. (1993). Development and differentiation of glial precursor cells in the rat cerebellum. *Glia, 7*(4), 307-321.

Lewis, A. K., & Bridgman, P. C. (1992). Nerve growth cone lamellipodia contain two populations of actin filaments that differ in organization and polarity. *J Cell Biol, 119*(5), 1219-1243.

Li, C., Tropak, M. B., Gerlai, R., Clapoff, S., Abramow-Newerly, W., Trapp, B., Peterson, A., & Roder, J. (1994). Myelination in the absence of myelin-associated glycoprotein. *Nature, 369*(6483), 747-750.

Li, H., He, Y., Richardson, W. D., & Casaccia, P. (2009). Two-tier transcriptional control of oligodendrocyte differentiation. *Curr Opin Neurobiol, 19*(5), 479-485.

Liang, X., Draghi, N. A., & Resh, M. D. (2004). Signaling from integrins to Fyn to Rho family GTPases regulates morphologic differentiation of oligodendrocytes. *J Neurosci, 24*(32), 7140-7149.

Longhurst, C. M., & Jennings, L. K. (1998). Integrin-mediated signal transduction. *Cell Mol Life Sci, 54*(6), 514-526.

Lukinavicius, G., Reymond, L., D'Este, E., Masharina, A., Gottfert, F., Ta, H., Guther, A., Fournier, M., Rizzo, S., Waldmann, H., Blaukopf, C., Sommer, C., Gerlich, D. W., Arndt, H. D., Hell, S. W., & Johnsson, K. (2014). Fluorogenic probes for live-cell imaging of the cytoskeleton. *Nat Methods, 11*(7), 731-733.

Lunn, K. F., Baas, P. W., & Duncan, I. D. (1997). Microtubule organization and stability in the oligodendrocyte. *J Neurosci, 17*(13), 4921-4932.

Luse, S. A. (1956). Formation of Myelin in the Central Nervous System of Mice and Rats, as Studied with the Electron Microscope. *The Journal of Cell Biology, 2*(6), 777-784.

Machesky, L. M. (2008). Lamellipodia and filopodia in metastasis and invasion. *FEBS Lett, 582*(14), 2102-2111.

Machesky, L. M., Atkinson, S. J., Ampe, C., Vandekerckhove, J., & Pollard, T. D. (1994). Purification of a cortical complex containing two unconventional actins from Acanthamoeba by affinity chromatography on profilin-agarose. *J Cell Biol, 127*(1), 107-115.

Machesky, M. L., Reeves, E., Wientjes, F., Mattheyse, J. F., Grogan, A., Totty, F. N., Burlingame, L. A., Hsuan, J. J., & Segal, W. A. (1997). Mammalian actin-related protein 2/3 complex localizes to regions of lamellipodial protrusion and is composed of evolutionarily conserved proteins. *Biochemical Journal, 328*(1), 105-112.

Malinda, K. M., Fisher, G. W., & Ettensohn, C. A. (1995). Four-dimensional microscopic analysis of the filopodial behavior of primary mesenchyme cells during gastrulation in the sea urchin embryo. *Dev Biol, 172*(2), 552-566.

McCarthy, K. D., & de Vellis, J. (1980). Preparation of separate astroglial and oligodendroglial cell cultures from rat cerebral tissue. *J Cell Biol, 85*(3), 890-902.

McConnell, R. E., Edward van Veen, J., Vidaki, M., Kwiatkowski, A. V., Meyer, A. S., & Gertler, F. B. (2016). A requirement for filopodia extension toward Slit during Robo-mediated axon repulsion. *J Cell Biol, 213*(2), 261-274.

McKinnon, R. D., Matsui, T., Dubois-Dalcq, M., & Aaronson, S. A. (1990). FGF modulates the PDGF-driven pathway of oligodendrocyte development. *Neuron, 5*(5), 603-614.

Mellor, H. (2010). The role of formins in filopodia formation. *Biochim Biophys Acta, 1803*(2), 191-200.

Michalski, J. P., Cummings, S. E., O'Meara, R. W., & Kothary, R. (2016). Integrin-linked kinase regulates oligodendrocyte cytoskeleton, growth cone, and adhesion dynamics. *J Neurochem, 136*(3), 536-549.

Miki, H., Sasaki, T., Takai, Y., & Takenawa, T. (1998). Induction of filopodium formation by a WASP-related actin-depolymerizing protein N-WASP. *Nature, 391*(6662), 93-96.

Miki, H., Suetsugu, S., & Takenawa, T. (1998). WAVE, a novel WASP-family protein involved in actin reorganization induced by Rac. *EMBO J, 17*(23), 6932-6941.

Miller, R. H. (2002). Regulation of oligodendrocyte development in the vertebrate CNS. *Prog Neurobiol, 67*(6), 451-467.

Milner, R., & Ffrench-Constant, C. (1994). A developmental analysis of oligodendroglial integrins in primary cells: changes in alpha v-associated beta subunits during differentiation. *Development, 120*(12), 3497-3506.

Mitchison, T. J., & Cramer, L. P. (1996). Actin-based cell motility and cell locomotion. *Cell, 84*(3), 371-379.

Mollereau, B., Perez-Garijo, A., Bergmann, A., Miura, M., Gerlitz, O., Ryoo, H. D., Steller, H., & Morata, G. (2013). Compensatory proliferation and apoptosis-induced proliferation: a need for clarification. *Cell Death Differ, 20*(1), 181.

Moore, C. B., Guthrie, E. H., Huang, M. T., & Taxman, D. J. (2010). Short hairpin RNA (shRNA): design, delivery, and assessment of gene knockdown. *Methods Mol Biol, 629*, 141-158.

Mooren, O. L., Galletta, B. J., & Cooper, J. A. (2012). Roles for actin assembly in endocytosis. *Annu Rev Biochem, 81*, 661-686.

Morita, J., Kano, K., Kato, K., Takita, H., Sakagami, H., Yamamoto, Y., Mihara, E., Ueda, H., Sato, T., Tokuyama, H., Arai, H., Asou, H., Takagi, J., Ishitani, R., Nishimasu, H., Nureki, O., & Aoki, J. (2016). Structure and biological function of ENPP6, a choline-specific glycerophosphodiester-phosphodiesterase. *Sci Rep, 6*, 20995.

Morrison, B. M., Lee, Y., & Rothstein, J. D. (2013). Oligodendroglia: metabolic supporters of axons. *Trends Cell Biol, 23*(12), 644-651.

Mullins, R. D., Stafford, W. F., & Pollard, T. D. (1997). Structure, subunit topology, and actin-binding activity of the Arp2/3 complex from Acanthamoeba. *J Cell Biol, 136*(2), 331-343.

Nave, K. A. (2010). Myelination and the trophic support of long axons. *Nat Rev Neurosci, 11*(4), 275-283.

Nave, K. A., & Trapp, B. D. (2008). Axon-glial signaling and the glial support of axon function. *Annu Rev Neurosci, 31*, 535-561.

Nawaz, S., Kippert, A., Saab, A. S., Werner, H. B., Lang, T., Nave, K. A., & Simons, M. (2009). Phosphatidylinositol 4,5-bisphosphate-dependent interaction of myelin basic protein with the plasma membrane in oligodendroglial cells and its rapid perturbation by elevated calcium. *J Neurosci, 29*(15), 4794-4807.

Nawaz, S., Sanchez, P., Schmitt, S., Snaidero, N., Mitkovski, M., Velte, C., Bruckner, B. R., Alexopoulos, I., Czopka, T., Jung, S. Y., Rhee, J. S., Janshoff, A., Witke, W., Schaap, I. A. T.,

Lyons, D. A., & Simons, M. (2015). Actin filament turnover drives leading edge growth during myelin sheath formation in the central nervous system. *Dev Cell, 34*(2), 139-151.

Nayak, D., Roth, T. L., & McGavern, D. B. (2014). Microglia development and function. *Annu Rev Immunol, 32*, 367-402.

Nielsen, J. A., Maric, D., Lau, P., Barker, J. L., & Hudson, L. D. (2006). Identification of a novel oligodendrocyte cell adhesion protein using gene expression profiling. *J Neurosci, 26*(39), 9881-9891.

Nimmerjahn, A., Kirchhoff, F., & Helmchen, F. (2005). Resting microglial cells are highly dynamic surveillants of brain parenchyma in vivo. *Science, 308*(5726), 1314-1318.

Nishiyama, A., Lin, X. H., Giese, N., Heldin, C. H., & Stallcup, W. B. (1996). Interaction between NG2 proteoglycan and PDGF alpha-receptor on O2A progenitor cells is required for optimal response to PDGF. *J Neurosci Res, 43*(3), 315-330.

Nobes, C. D., & Hall, A. (1995). Rho, rac, and cdc42 GTPases regulate the assembly of multimolecular focal complexes associated with actin stress fibers, lamellipodia, and filopodia. *Cell, 81*(1), 53-62.

Noble, M., Murray, K., Stroobant, P., Waterfield, M. D., & Riddle, P. (1988). Platelet-derived growth factor promotes division and motility and inhibits premature differentiation of the oligodendrocyte/type-2 astrocyte progenitor cell. *Nature, 333*(6173), 560-562.

O'Connor, T. P., Duerr, J. S., & Bentley, D. (1990). Pioneer growth cone steering decisions mediated by single filopodial contacts in situ. *J Neurosci, 10*(12), 3935-3946.

O'Meara, R. W., Michalski, J. P., Anderson, C., Bhanot, K., Rippstein, P., & Kothary, R. (2013). Integrin-linked kinase regulates process extension in oligodendrocytes via control of actin cytoskeletal dynamics. *J Neurosci, 33*(23), 9781-9793.

Odaka, C., Sanders, M. L., & Crews, P. (2000). Jasplakinolide induces apoptosis in various transformed cell lines by a caspase-3-like protease-dependent pathway. *Clin Diagn Lab Immunol, 7*(6), 947-952.

Ono, K., Hirahara, Y., Gotoh, H., Nomura, T., Takebayashi, H., Yamada, H., & Ikenaka, K. (2017). Origin of Oligodendrocytes in the Vertebrate Optic Nerve: A Review. *Neurochem Res*.

Ozcelik, M., Cotter, L., Jacob, C., Pereira, J. A., Relvas, J. B., Suter, U., & Tricaud, N. (2010). Pals1 is a major regulator of the epithelial-like polarization and the extension of the myelin sheath in peripheral nerves. *J Neurosci, 30*(11), 4120-4131.

Pacary, E., Heng, J., Azzarelli, R., Riou, P., Castro, D., Lebel-Potter, M., Parras, C., Bell, D. M., Ridley, A. J., Parsons, M., & Guillemot, F. (2011). Proneural transcription factors regulate different steps of cortical neuron migration through Rnd-mediated inhibition of RhoA signaling. *Neuron, 69*(6), 1069-1084.

Palecek, S. P., Loftus, J. C., Ginsberg, M. H., Lauffenburger, D. A., & Horwitz, A. F. (1997). Integrin-ligand binding properties govern cell migration speed through cell-substratum adhesiveness. *Nature, 385*(6616), 537-540.

Payne, H. R., Hemperly, J. J., & Lemmon, V. (1996). N-cadherin expression and function in cultured oligodendrocytes. *Brain Res Dev Brain Res, 97*(1), 9-15.

Pedraza, L., Huang, J. K., & Colman, D. (2009). Disposition of axonal caspr with respect to glial cell membranes: Implications for the process of myelination. *J Neurosci Res, 87*(15), 3480-3491.

Peters, A. (1964). Observations on the Connexions between Myelin Sheaths and Glial Cells in the Optic Nerves of Young Rats. *J Anat, 98*, 125-134.

Plopper, G., Plopper, S. L. A. R. S. B. A. H. G., Sharp, D., & Sikorski, E. (2013). *Lewin's Cells*: Jones & Bartlett Learning, LLC.

Pollard, T. D., Blanchoin, L., & Mullins, R. D. (2000). Molecular mechanisms controlling actin filament dynamics in nonmuscle cells. *Annu Rev Biophys Biomol Struct, 29*, 545-576.

Pollard, T. D., & Borisy, G. G. (2003). Cellular motility driven by assembly and disassembly of actin filaments. *Cell, 112*(4), 453-465.

Pollard, T. D., & Cooper, J. A. (2009). Actin, a central player in cell shape and movement. *Science, 326*(5957), 1208-1212.

Posey, S. C., & Bierer, B. E. (1999). Actin stabilization by jasplakinolide enhances apoptosis induced by cytokine deprivation. *J Biol Chem, 274*(7), 4259-4265.

Prehoda, K. E., Scott, J. A., Mullins, R. D., & Lim, W. A. (2000). Integration of multiple signals through cooperative regulation of the N-WASP-Arp2/3 complex. *Science, 290*(5492), 801-806.

Pringle, N. P., Mudhar, H. S., Collarini, E. J., & Richardson, W. D. (1992). PDGF receptors in the rat CNS: during late neurogenesis, PDGF alpha-receptor expression appears to be restricted to glial cells of the oligodendrocyte lineage. *Development, 115*(2), 535-551.

Rafelski, S. M., & Theriot, J. A. (2004). Crawling toward a unified model of cell mobility: spatial and temporal regulation of actin dynamics. *Annu Rev Biochem, 73*, 209-239.

Raff, M. C., Lillien, L. E., Richardson, W. D., Burne, J. F., & Noble, M. D. (1988). Platelet-derived growth factor from astrocytes drives the clock that times oligodendrocyte development in culture. *Nature, 333*(6173), 562-565.

Rajasekharan, S., Bin, J. M., Antel, J. P., & Kennedy, T. E. (2010). A central role for RhoA during oligodendroglial maturation in the switch from netrin-1-mediated chemorepulsion to process elaboration. *J Neurochem, 113*(6), 1589-1597.

Rao, J. Y., Jin, Y. S., Zheng, Q., Cheng, J., Tai, J., & Hemstreet, G. P., 3rd. (1999). Alterations of the actin polymerization status as an apoptotic morphological effector in HL-60 cells. *J Cell Biochem, 75*(4), 686-697.

Readhead, C., Popko, B., Takahashi, N., Shine, H. D., Saavedra, R. A., Sidman, R. L., & Hood, L. (1987). Expression of a myelin basic protein gene in transgenic shiverer mice: correction of the dysmyelinating phenotype. *Cell, 48*(4), 703-712.

Relvas, J. B., Setzu, A., Baron, W., Buttery, P. C., LaFlamme, S. E., Franklin, R. J., & ffrench-Constant, C. (2001). Expression of dominant-negative and chimeric subunits reveals an essential role for beta1 integrin during myelination. *Curr Biol, 11*(13), 1039-1043.

Renault, L., Bugyi, B., & Carlier, M. F. (2008). Spire and Cordon-bleu: multifunctional regulators of actin dynamics. *Trends Cell Biol, 18*(10), 494-504.

Reynolds, R., & Wilkin, G. P. (1988). Development of macroglial cells in rat cerebellum. II. An in situ immunohistochemical study of oligodendroglial lineage from precursor to mature myelinating cell. *Development, 102*(2), 409-425.

Richard H. Quarles, P. M. (2005). Myelin Formation, Structure and Biochemistry. In B. W. A. George J. Siegel (Ed.), *Basic Neurochemistry: Molecular, Cellular, and Medical Aspects* (pp. 51-71): Lippincott Williams & Wilkins.

Richardson, W. D., Kessaris, N., & Pringle, N. (2006). Oligodendrocyte wars. *Nat Rev Neurosci, 7*(1), 11-18.

Richardson, W. D., Pringle, N., Mosley, M. J., Westermark, B., & Dubois-Dalcq, M. (1988). A role for platelet-derived growth factor in normal gliogenesis in the central nervous system. *Cell, 53*(2), 309-319.

Richter-Landsberg, C., & Heinrich, M. (1996). OLN-93: a new permanent oligodendroglia cell line derived from primary rat brain glial cultures. *J Neurosci Res, 45*(2), 161-173.

Ridley, A. J. (2006). Rho GTPases and actin dynamics in membrane protrusions and vesicle trafficking. *Trends Cell Biol, 16*(10), 522-529.

Ridley, A. J., & Hall, A. (1992). The small GTP-binding protein rho regulates the assembly of focal adhesions and actin stress fibers in response to growth factors. *Cell, 70*(3), 389-399.

Ridley, A. J., Paterson, H. F., Johnston, C. L., Diekmann, D., & Hall, A. (1992). The small GTP-binding protein rac regulates growth factor-induced membrane ruffling. *Cell, 70*(3), 401-410.

Ridley, A. J., Schwartz, M. A., Burridge, K., Firtel, R. A., Ginsberg, M. H., Borisy, G., Parsons, J. T., & Horwitz, A. R. (2003). Cell migration: integrating signals from front to back. *Science, 302*(5651), 1704-1709.

Robinson, R. C., Turbedsky, K., Kaiser, D. A., Marchand, J. B., Higgs, H. N., Choe, S., & Pollard, T. D. (2001). Crystal structure of Arp2/3 complex. *Science, 294*(5547), 1679-1684.

Rogister, B., Ben-Hur, T., & Dubois-Dalcq, M. (1999). From neural stem cells to myelinating oligodendrocytes. *Mol Cell Neurosci, 14*(4-5), 287-300.

Rohatgi, R., Ho, H. Y., & Kirschner, M. W. (2000). Mechanism of N-WASP activation by CDC42 and phosphatidylinositol 4, 5-bisphosphate. *J Cell Biol, 150*(6), 1299-1310.

Rohatgi, R., Ma, L., Miki, H., Lopez, M., Kirchhausen, T., Takenawa, T., & Kirschner, M. W. (1999). The interaction between N-WASP and the Arp2/3 complex links Cdc42-dependent signals to actin assembly. *Cell, 97*(2), 221-231.

Rushton, W. A. (1951). A theory of the effects of fibre size in medullated nerve. *J Physiol, 115*(1), 101-122.

Ryoo, H. D., & Bergmann, A. (2012). The role of apoptosis-induced proliferation for regeneration and cancer. *Cold Spring Harb Perspect Biol, 4*(8), a008797.

Schindelin, J., Arganda-Carreras, I., Frise, E., Kaynig, V., Longair, M., Pietzsch, T., Preibisch, S., Rueden, C., Saalfeld, S., Schmid, B., Tinevez, J. Y., White, D. J., Hartenstein, V., Eliceiri, K., Tomancak, P., & Cardona, A. (2012). Fiji: an open-source platform for biological-image analysis. *Nat Methods, 9*(7), 676-682.

Schluter, K., Waschbusch, D., Anft, M., Hugging, D., Kind, S., Hanisch, J., Lakisic, G., Gautreau, A., Barnekow, A., & Stradal, T. E. (2014). JMY is involved in anterograde vesicle trafficking from the trans-Golgi network. *Eur J Cell Biol, 93*(5-6), 194-204.

Schneider, C. A., Rasband, W. S., & Eliceiri, K. W. (2012). NIH Image to ImageJ: 25 years of image analysis. *Nat Methods, 9*(7), 671-675.

Scolding, N. (2004). Myelin biology and its disorders: two-volume set. * Edited by Robert A. Lazzarini 2004. San Diego: Elsevier Academic Press Price 340.00. ISBN 0-12-439510-4. *Brain, 127*(9), 2144-2147.

Scolding, N. J., Frith, S., Linington, C., Morgan, B. P., Campbell, A. K., & Compston, D. A. (1989). Myelin-oligodendrocyte glycoprotein (MOG) is a surface marker of oligodendrocyte maturation. *J Neuroimmunol, 22*(3), 169-176.

Semple, B. D., Blomgren, K., Gimlin, K., Ferriero, D. M., & Noble-Haeusslein, L. J. (2013). Brain development in rodents and humans: Identifying benchmarks of maturation and vulnerability to injury across species. *Prog Neurobiol, 106-107*, 1-16.

Shao, X., Li, Q., Mogilner, A., Bershadsky, A. D., & Shivashankar, G. V. (2015). Mechanical stimulation induces formin-dependent assembly of a perinuclear actin rim. *Proc Natl Acad Sci U S A, 112*(20), E2595-2601.

Sherman, D. L., & Brophy, P. J. (2005). Mechanisms of axon ensheathment and myelin growth. *Nat Rev Neurosci, 6*(9), 683-690.

Shikama, N., Lee, C. W., France, S., Delavaine, L., Lyon, J., Krstic-Demonacos, M., & La Thangue, N. B. (1999). A novel cofactor for p300 that regulates the p53 response. *Mol Cell, 4*(3), 365-376.

Sim, F. J., Zhao, C., Penderis, J., & Franklin, R. J. (2002). The age-related decrease in CNS remyelination efficiency is attributable to an impairment of both oligodendrocyte progenitor recruitment and differentiation. *J Neurosci, 22*(7), 2451-2459.

Simons, M., & Nave, K. A. (2015). Oligodendrocytes: Myelination and Axonal Support. *Cold Spring Harb Perspect Biol, 8*(1), a020479.

Simpson, P. B., & Armstrong, R. C. (1999). Intracellular signals and cytoskeletal elements involved in oligodendrocyte progenitor migration. *Glia, 26*(1), 22-35.

Siton-Mendelson, O., & Bernheim-Groswasser, A. (2017). Functional Actin Networks under Construction: The Cooperative Action of Actin Nucleation and Elongation Factors. *Trends Biochem Sci, 42*(6), 414-430.

Skau, C. T., Fischer, R. S., Gurel, P., Thiam, H. R., Tubbs, A., Baird, M. A., Davidson, M. W., Piel, M., Alushin, G. M., Nussenzweig, A., Steeg, P. S., & Waterman, C. M. (2016). FMN2 Makes Perinuclear Actin to Protect Nuclei during Confined Migration and Promote Metastasis. *Cell, 167*(6), 1571-1585 e1518.

Small, R. K., Riddle, P., & Noble, M. (1987). Evidence for migration of oligodendrocyte--type-2 astrocyte progenitor cells into the developing rat optic nerve. *Nature, 328*(6126), 155-157.

Smith, L. G., & Li, R. (2004). Actin Polymerization: Riding the Wave. *Current Biology, 14*(3), R109-R111.

Smith, R. S., & Koles, Z. J. (1970). Myelinated nerve fibers: computed effect of myelin thickness on conduction velocity. *Am J Physiol, 219*(5), 1256-1258.

Snaidero, N., Mobius, W., Czopka, T., Hekking, L. H., Mathisen, C., Verkleij, D., Goebbels, S., Edgar, J., Merkler, D., Lyons, D. A., Nave, K. A., & Simons, M. (2014). Myelin membrane wrapping of CNS axons by PI(3,4,5)P3-dependent polarized growth at the inner tongue. *Cell, 156*(1-2), 277-290.

Snaidero, N., & Simons, M. (2017). The logistics of myelin biogenesis in the central nervous system. *Glia, 65*(7), 1021-1031.

Sobottka, B., Ziegler, U., Kaech, A., Becher, B., & Goebels, N. (2011). CNS live imaging reveals a new mechanism of myelination: the liquid croissant model. *Glia, 59*(12), 1841-1849.

Soderling, S. H., Guire, E. S., Kaech, S., White, J., Zhang, F., Schutz, K., Langeberg, L. K., Banker, G., Raber, J., & Scott, J. D. (2007). A WAVE-1 and WRP signaling complex regulates spine density, synaptic plasticity, and memory. *J Neurosci, 27*(2), 355-365.

Sofroniew, M. V., & Vinters, H. V. (2010). Astrocytes: biology and pathology. *Acta Neuropathol, 119*(1), 7-35.

Somjen, G. G. (1988). Nervenkitt: notes on the history of the concept of neuroglia. *Glia, 1*(1), 2-9.

Sommer, I., & Schachner, M. (1981). Monoclonal antibodies (O1 to O4) to oligodendrocyte cell surfaces: an immunocytological study in the central nervous system. *Dev Biol, 83*(2), 311-327.

Song, J., Goetz, B. D., Baas, P. W., & Duncan, I. D. (2001). Cytoskeletal reorganization during the formation of oligodendrocyte processes and branches. *Mol Cell Neurosci, 17*(4), 624-636.

Sossey-Alaoui, K., Ranalli, T. A., Li, X., Bakin, A. V., & Cowell, J. K. (2005). WAVE3 promotes cell motility and invasion through the regulation of MMP-1, MMP-3, and MMP-9 expression. *Exp Cell Res, 308*(1), 135-145.

Stewart, M. P., Helenius, J., Toyoda, Y., Ramanathan, S. P., Muller, D. J., & Hyman, A. A. (2011). Hydrostatic pressure and the actomyosin cortex drive mitotic cell rounding. *Nature, 469*(7329), 226-230.

Suetsugu, S., Yamazaki, D., Kurisu, S., & Takenawa, T. (2003). Differential Roles of WAVE1 and WAVE2 in Dorsal and Peripheral Ruffle Formation for Fibroblast Cell Migration. *Developmental Cell, 5*(4), 595-609.

Sugiarto, S., Persson, A. I., Munoz, E. G., Waldhuber, M., Lamagna, C., Andor, N., Hanecker, P., Ayers-Ringler, J., Phillips, J., Siu, J., Lim, D. A., Vandenberg, S., Stallcup, W., Berger, M. S., Bergers, G., Weiss, W. A., & Petritsch, C. (2011). Asymmetry-defective oligodendrocyte progenitors are glioma precursors. *Cancer Cell, 20*(3), 328-340.

Sugimoto, Y., Taniguchi, M., Yagi, T., Akagi, Y., Nojyo, Y., & Tamamaki, N. (2001). Guidance of glial precursor cell migration by secreted cues in the developing optic nerve. *Development, 128*(17), 3321-3330.

Sun, S. C., Sun, Q. Y., & Kim, N. H. (2011). JMY is required for asymmetric division and cytokinesis in mouse oocytes. *Mol Hum Reprod, 17*(5), 296-304.

Suzuki, N., Sekimoto, K., Hayashi, C., Mabuchi, Y., Nakamura, T., & Akazawa, C. (2017). Differentiation of Oligodendrocyte Precursor Cells from Sox10-Venus Mice to Oligodendrocytes and Astrocytes. *Sci Rep, 7*(1), 14133.

Tasaki, I. (1939). The electro-saltatory transmission of the nerve impulse and the effect of narcosis upon the nerve fiber. *American Journal of Physiology, 127*(2), 211-227.

Team, R. D. C. (2011). R: A Language and Environment for Statistical Computing.

Theriot, J. A., & Mitchison, T. J. (1991). Actin microfilament dynamics in locomoting cells. *Nature, 352*(6331), 126-131.

Thiam, H. R., Vargas, P., Carpi, N., Crespo, C. L., Raab, M., Terriac, E., King, M. C., Jacobelli, J., Alberts, A. S., Stradal, T., Lennon-Dumenil, A. M., & Piel, M. (2016). Perinuclear Arp2/3-driven actin polymerization enables nuclear deformation to facilitate cell migration through complex environments. *Nat Commun, 7*, 10997.

Thurnherr, T., Benninger, Y., Wu, X., Chrostek, A., Krause, S. M., Nave, K. A., Franklin, R. J., Brakebusch, C., Suter, U., & Relvas, J. B. (2006). Cdc42 and Rac1 signaling are both required for and act synergistically in the correct formation of myelin sheaths in the CNS. *J Neurosci, 26*(40), 10110-10119.

Tiscornia, G., Singer, O., & Verma, I. M. (2006). Production and purification of lentiviral vectors. *Nat Protoc, 1*(1), 241-245.

Tojkander, S., Gateva, G., Schevzov, G., Hotulainen, P., Naumanen, P., Martin, C., Gunning, P. W., & Lappalainen, P. (2011). A molecular pathway for myosin II recruitment to stress fibers. *Curr Biol, 21*(7), 539-550.

Tomasevic, N., Jia, Z., Russell, A., Fujii, T., Hartman, J. J., Clancy, S., Wang, M., Beraud, C., Wood, K. W., & Sakowicz, R. (2007). Differential regulation of WASP and N-WASP by Cdc42, Rac1, Nck, and PI(4,5)P2. *Biochemistry, 46*(11), 3494-3502.

Tripathi, R. B., Clarke, L. E., Burzomato, V., Kessaris, N., Anderson, P. N., Attwell, D., & Richardson, W. D. (2011). Dorsally and ventrally derived oligodendrocytes have similar electrical properties but myelinate preferred tracts. *J Neurosci, 31*(18), 6809-6819.

Tsai, H. H., Niu, J., Munji, R., Davalos, D., Chang, J., Zhang, H., Tien, A. C., Kuo, C. J., Chan, J. R., Daneman, R., & Fancy, S. P. (2016). Oligodendrocyte precursors migrate along vasculature in the developing nervous system. *Science, 351*(6271), 379-384.

Tsygankov, D., Bilancia, C. G., Vitriol, E. A., Hahn, K. M., Peifer, M., & Elston, T. C. (2014). CellGeo: a computational platform for the analysis of shape changes in cells with complex geometries. *J Cell Biol, 204*(3), 443-460.

Urbancic, V., Butler, R., Richier, B., Peter, M., Mason, J., Livesey, F. J., Holt, C. E., & Gallop, J. L. (2017). Filopodyan: An open-source pipeline for the analysis of filopodia. *J Cell Biol, 216*(10), 3405-3422.

Vallstedt, A., Klos, J. M., & Ericson, J. (2005). Multiple dorsoventral origins of oligodendrocyte generation in the spinal cord and hindbrain. *Neuron, 45*(1), 55-67.

Ventura, A., Meissner, A., Dillon, C. P., McManus, M., Sharp, P. A., Van Parijs, L., Jaenisch, R., & Jacks, T. (2004). Cre-lox-regulated conditional RNA interference from transgenes. *Proc Natl Acad Sci U S A, 101*(28), 10380-10385.

Vinzenz, M., Nemethova, M., Schur, F., Mueller, J., Narita, A., Urban, E., Winkler, C., Schmeiser, C., Koestler, S. A., Rottner, K., Resch, G. P., Maeda, Y., & Small, J. V. (2012). Actin branching in the initiation and maintenance of lamellipodia. *J Cell Sci, 125*(Pt 11), 2775-2785.

Wang, H., Rusielewicz, T., Tewari, A., Leitman, E. M., Einheber, S., & Melendez-Vasquez, C. V. (2012). Myosin II is a negative regulator of oligodendrocyte morphological differentiation. *J Neurosci Res, 90*(8), 1547-1556.

Wang, P. S., Chou, F. S., Ramachandran, S., Xia, S., Chen, H. Y., Guo, F., Suraneni, P., Maher, B. J., & Li, R. (2016). Crucial roles of the Arp2/3 complex during mammalian corticogenesis. *Development, 143*(15), 2741-2752.

Wang, Y. (2010). JimMY on the stage: Linking DNA damage with cell adhesion and motility. *Cell Adh Migr, 4*(2), 166-168.

Welch, M. D., DePace, A. H., Verma, S., Iwamatsu, A., & Mitchison, T. J. (1997). The Human Arp2/3 Complex Is Composed of Evolutionarily Conserved Subunits and Is Localized to Cellular Regions of Dynamic Actin Filament Assembly. *The Journal of Cell Biology, 138*(2), 375-384.

Welch, M. D., Iwamatsu, A., & Mitchison, T. J. (1997). Actin polymerization is induced by Arp2/3 protein complex at the surface of Listeria monocytogenes. *Nature, 385*(6613), 265-269.

Welch, M. D., & Mullins, R. D. (2002). Cellular control of actin nucleation. *Annu Rev Cell Dev Biol, 18*, 247-288.

Williams, K. A., & Deber, C. M. (1993). The structure and function of central nervous system myelin. *Crit Rev Clin Lab Sci, 30*(1), 29-64.

Wilson, R., & Brophy, P. J. (1989). Role for the oligodendrocyte cytoskeleton in myelination. *J Neurosci Res, 22*(4), 439-448.

Witte, H., & Bradke, F. (2008). The role of the cytoskeleton during neuronal polarization. *Curr Opin Neurobiol, 18*(5), 479-487.

Wolf, R. M., Wilkes, J. J., Chao, M. V., & Resh, M. D. (2001). Tyrosine phosphorylation of p190 RhoGAP by Fyn regulates oligodendrocyte differentiation. *J Neurobiol, 49*(1), 62-78.

Wolswijk, G. (1998). Chronic stage multiple sclerosis lesions contain a relatively quiescent population of oligodendrocyte precursor cells. *J Neurosci, 18*(2), 601-609.

Xiao, L., Ohayon, D., McKenzie, I. A., Sinclair-Wilson, A., Wright, J. L., Fudge, A. D., Emery, B., Li, H., & Richardson, W. D. (2016). Rapid production of new oligodendrocytes is required in the earliest stages of motor-skill learning. *Nat Neurosci, 19*(9), 1210-1217.

Yakovlev, P. I., & Lecours, A. R. (1967). The myelogenetic cycles of regional maturation of the brain. In O. Blackwell (Ed.), *Regional Development of the Brain in Early Life* (pp. 3-70).

Yamazaki, D., Fujiwara, T., Suetsugu, S., & Takenawa, T. (2005). A novel function of WAVE in lamellipodia: WAVE1 is required for stabilization of lamellipodial protrusions during cell spreading. *Genes Cells, 10*(5), 381-392.

Young, K. M., Psachoulia, K., Tripathi, R. B., Dunn, S. J., Cossell, L., Attwell, D., Tohyama, K., & Richardson, W. D. (2013). Oligodendrocyte dynamics in the healthy adult CNS: evidence for myelin remodeling. *Neuron, 77*(5), 873-885.

Yu, W., Lee, H. K., Hariharan, S., Bu, W., & Ahmed, S. (2009). Quantitative neurite outgrowth measurement based on image segmentation with topological dependence. *Cytometry A, 75*(4), 289-297.

Yu, W. P., Collarini, E. J., Pringle, N. P., & Richardson, W. D. (1994). Embryonic expression of myelin genes: evidence for a focal source of oligodendrocyte precursors in the ventricular zone of the neural tube. *Neuron, 12*(6), 1353-1362.

Zeng, C., Pan, F., Jones, L. A., Lim, M. M., Griffin, E. A., Sheline, Y. I., Mintun, M. A., Holtzman, D. M., & Mach, R. H. (2010). Evaluation of 5-ethynyl-2'-deoxyuridine staining as a sensitive and reliable method for studying cell proliferation in the adult nervous system. *Brain Res, 1319*, 21-32.

Zhang, H., & Miller, R. H. (1996). Density-dependent feedback inhibition of oligodendrocyte precursor expansion. *J Neurosci, 16*(21), 6886-6895.

Zhang, L., & Goldman, J. E. (1996). Developmental fates and migratory pathways of dividing progenitors in the postnatal rat cerebellum. *J Comp Neurol, 370*(4), 536-550.

Zhang, Y., Chen, K., Sloan, S. A., Bennett, M. L., Scholze, A. R., O'Keeffe, S., Phatnani, H. P., Guarnieri, P., Caneda, C., Ruderisch, N., Deng, S., Liddelow, S. A., Zhang, C., Daneman, R., Maniatis, T., Barres, B. A., & Wu, J. Q. (2014). An RNA-sequencing transcriptome and splicing database of glia, neurons, and vascular cells of the cerebral cortex. *J Neurosci, 34*(36), 11929-11947.

Zheng, J. Q., Wan, J. J., & Poo, M. M. (1996). Essential role of filopodia in chemotropic turning of nerve growth cone induced by a glutamate gradient. *J Neurosci, 16*(3), 1140-1149.

Zhuravlev, P. I., Lan, Y., Minakova, M. S., & Papoian, G. A. (2012). Theory of active transport in filopodia and stereocilia. *Proc Natl Acad Sci U S A, 109*(27), 10849-10854.

Zigmond, S. H. (2004). Beginning and ending an actin filament: control at the barbed end. *Curr Top Dev Biol, 63*, 145-188.

Zuchero, J. B., Belin, B., & Mullins, R. D. (2012). Actin binding to WH2 domains regulates nuclear import of the multifunctional actin regulator JMY. *Mol Biol Cell, 23*(5), 853-863.

Zuchero, J. B., Coutts, A. S., Quinlan, M. E., Thangue, N. B., & Mullins, R. D. (2009). p53-cofactor JMY is a multifunctional actin nucleation factor. *Nat Cell Biol, 11*(4), 451-459.

Zuchero, J. B., Fu, M. M., Sloan, S. A., Ibrahim, A., Olson, A., Zaremba, A., Dugas, J. C., Wienbar, S., Caprariello, A. V., Kantor, C., Leonoudakis, D., Lariosa-Willingham, K., Kronenberg, G., Gertz, K., Soderling, S. H., Miller, R. H., & Barres, B. A. (2015). CNS myelin wrapping is driven by actin disassembly. *Dev Cell, 34*(2), 152-167.

APPENDIX I

Supporting Information

Movie captions:

Supporting Information Movie S1. Timelapse microscopy of oligodendrocytes during protrusion extension and remodeling.

Supporting Information Movie S2. Timelapse microscopy of oligodendrocytes with deposition of lamellar sheets.

Supporting Information Movie S3. Timelapse microscopy of Jmy-depleted oligodendrocytes during protrusion extension and remodeling.

Supporting Information Movie S4. Timelapse microscopy with fluorescent labeling of F-actin in oligodendrocytes during protrusion extension and remodeling.

Supporting Information Movie S5. Timelapse microscopy with fluorescent labeling of F-actin in Jmy-depleted oligodendrocytes during protrusion extension and remodeling.

Supporting Information Movie S6. Timelapse microscopy with fluorescent labeling of F-actin in oligodendrocytes with deposition of lamellar sheets.

Supporting Information Movie S7. Timelapse microscopy of early (first 16h) neurite-oligodendrocyte interaction in culture.

Supporting Information Movie S8. Timelapse microscopy of oligodendrocytes contacting neurites in culture.

Supporting Information Movie S9. Timelapse microscopy of early neurite-oligodendrocyte interaction after Jmy depletion.

APPENDIX II

Article Published

Received: 13 December 2017 | Revised: 26 March 2018 | Accepted: 5 April 2018

DOI: 10.1002/glia.23342

GLIA
WILEY

RESEARCH ARTICLE

Jmy regulates oligodendrocyte differentiation via modulation of actin cytoskeleton dynamics

Maria M. Azevedo[1,2] | Helena S. Domingues[1,2] | Fabrice P. Cordelières[3] | Paula Sampaio[1,2] | Ana I. Seixas[1,2] | João B. Relvas[1,2,4]

[1]i3S – Instituto de Investigação e Inovação em Saúde, Universidade do Porto, Porto, Portugal

[2]IBMC – Instituto de Biologia Molecular e Celular, Porto, Portugal

[3]Bordeaux Imaging Centre, UMS 3420 CNRS, CNRS-INSERM, University of Bordeaux, Bordeaux, France

[4]The Discoveries Centre for Regeneration and Precision Medicine, Porto campus, Porto, Portugal

Correspondence
Ana I. Seixas and João B. Relvas, Rua Alfredo Allen, 208 I 4200-135 Porto, Portugal.
Emails: aseixas@ibmc.up.pt and jrelvas@ibmc.up.pt

Present address
Helena S. Domingues, INL – International Iberian Nanotechnology Laboratory, Braga, Portugal

Funding information
FEDER funds through the Operational Competitiveness Programme – COMPETE – and by National Funds through FCT – Fundação para a Ciência e a Tecnologia, Grant/Award Numbers: FCOMP-01-0124-FEDER 021333, NORTE-01-0145-FEDER-000008, and PTDC/SAU/NMC/119937/2010; FCT, Grant/Award Number: SFRH/BD/90301/2012; Marie Curie Actions, Grant/Award Number: IEF 2010, #276322; Postdoctoral fellowship, Grant/Award Number: SFRH/BPD/90268/2012; FCT postdoctoral fellowship, Grant/Award Number: SFRH/BPD/79417/2011

Abstract

During central nervous system development, oligodendrocytes form structurally and functionally distinct actin-rich protrusions that contact and wrap around axons to assemble myelin sheaths. Establishment of axonal contact is a limiting step in myelination that relies on the oligodendrocyte's ability to locally coordinate cytoskeletal rearrangements with myelin production, under the control of a transcriptional differentiation program. The molecules that provide fine-tuning of actin dynamics during oligodendrocyte differentiation and axon ensheathment remain largely unidentified. We performed transcriptomics analysis of soma and protrusion fractions from rat brain oligodendrocyte progenitors and found a subcellular enrichment of mRNAs in newly-formed protrusions. Approximately 30% of protrusion-enriched transcripts encode proteins related to cytoskeleton dynamics, including the junction mediating and regulatory protein Jmy, a multifunctional regulator of actin polymerization. Here, we show that expression of Jmy is upregulated during myelination and is required for the assembly of actin filaments and protrusion formation during oligodendrocyte differentiation. Quantitative morphodynamics analysis of live oligodendrocytes showed that differentiation is driven by a stereotypical actin network-dependent "cellular shaping" program. Disruption of actin dynamics via knockdown of Jmy leads to a program fail resulting in oligodendrocytes that do not acquire an arborized morphology and are less efficient in contacting neurites and forming myelin wraps in co-cultures with neurons. Our findings provide new mechanistic insight into the relationship between cell shape dynamics and differentiation in development.

KEYWORDS
actin cytoskeleton, ImageJ macro, Jmy, live imaging, oligodendrocyte differentiation

1 | INTRODUCTION

In eukaryotic cells, the actin cytoskeleton defines shape and is critical for many cellular functions requiring membrane deformation. In the central nervous system (CNS), regulation of morphological plasticity is a feature of oligodendrocytes (OLs) (Hughes & Appel, 2016), myelinating glia cells initially noted for their abundant fine processes (Hortega, 1928) that were later characterized as actin-rich membrane protrusions (Song, Goetz, Baas, & Duncan, 2001; Wilson & Brophy, 1989).

Assembling myelin, the insulator membrane that allows for fast saltatory conduction in the vertebrate nervous system, is a remarkable example of cell specialization in development. During differentiation, OLs integrate extracellular and axon-derived cues to change their morphology while simultaneously activating a transcriptional program to express myelin genes that give rise to the structural components of

Maria M. Azevedo and Helena S. Domingues are co-first authors.

Ana I. Seixas and João B. Relvas are co-senior authors.

mature sheaths (Simons & Nave, 2015). Formation of myelin membranes relies on extraordinary morphological plasticity as cells change from immature and migratory oligodendrocyte progenitor cells (OPCs) with mostly bipolar/multipolar shape, to a highly arborized structure seen in pre-myelinating OLs (Buttery & ffrench-Constant, 2001). One single OL can myelinate several axons with its membranous extensions formed by the protrusive forces of F-actin polymerization at the leading edge. Upon axonal contact, these lamellipodia-like structures continue to wrap while simultaneously extending laterally in an adhesion-independent manner that is driven by actin depolymerization (Nawaz et al., 2015; Zuchero et al., 2015).

The program that governs OL differentiation has been extensively characterized by transcriptomics studies (Cahoy et al., 2008; Dugas, Tai, Speed, Ngai, & Barres, 2006; Nielsen, Maric, Lau, Barker, & Hudson, 2006; Zhang et al., 2014). Among the most heavily regulated genes, aside from those encoding myelin proteins, are ones involved in cell cycle and motility, adhesion, and cytoskeletal remodeling. An important question is how the differentiation program connects with the signaling pathways controlling morphological plasticity. It has been shown that myelin basic protein (MBP) triggers actin depolymerization by promoting the release of actin disassembly proteins (Zuchero et al., 2015). It is likely that different actin regulators have distinct roles in myelination: WASP-family verprolin-homologous protein (WAVE) and integrin-linked kinase (ILK) regulate OL differentiation and axon ensheathment (Kim et al., 2006; O'Meara et al., 2013), while the Arp2/3 complex, a major actin nucleator, is required for initiation of myelination *in vivo* (Zuchero et al., 2015), and Rho GTPases Cdc42 and Rac1 regulate myelin sheath formation (Thurnherr et al., 2006).

The junction-mediating and regulatory protein (Jmy) is a multifunctional actin regulator, acting as a pro-nucleating factor for the Arp2/3 complex to form branched actin filaments or nucleating unbranched filaments by itself (Zuchero, Coutts, Quinlan, Thangue, & Mullins, 2009). In different cell lines Jmy regulates fast actin rearrangements at the leading edge, important for cell migration (Zuchero et al., 2009), while in neuroblastoma cells it acts as a negative regulator of neuritogenesis (Firat-Karalar, Hsiue, & Welch, 2011). Jmy is ubiquitously expressed and, in isolated brain cells from mouse, has its highest expression in newly formed OLs and endothelial cells (Zhang et al., 2014).

Spatial organization of mRNAs is a biological phenomenon reported in various eukaryote cells regulating, for example, local protein synthesis important for polarity and for general cell development (Holt & Schuman, 2013). Myelination relies on local control of protein production and transduction of extracellularly-derived signals at the tip of OL protrusions and we hypothesized that coordinating these events requires compartmentalized organization of specific mRNAs. A whole-transcriptome analysis of OPC membrane protrusions that were physically separated from their soma revealed an enrichment of transcripts related to cytoskeleton dynamics. One of such transcripts encodes the actin-related protein Jmy, which we found to be highly expressed in pro-myelinating OLs in the mouse CNS and upregulated during OL differentiation. Using morphodynamic analysis from time lapse images, we show that Jmy is required for OLs to acquire a complex arborized morphology, a feature that is critical for efficient formation of MBP membrane sheets and the establishment of proper OL-neurite contact in myelinating co-cultures.

2 | MATERIALS AND METHODS

2.1 | Animals

Wistar rats were used for primary cultures of mixed glial cells (MGCs) and embryonic dorsal root ganglia (DRG). For immunohistochemistry (IHC) analysis, CNS tissue was obtained from wild type C57BL/6 mice transcardially perfused with 4% paraformaldehyde-PBS. All animal experiments were performed with the approval and in accordance with the IBMC/i3S Animal Ethics Committee, the Portuguese Veterinary Office and the European Union animal welfare laws and guidelines.

2.2 | Primary cultures of OPCs from rat brain

OPCs were isolated from MGCs of postnatal day 0–2 (P0–P2) rat brains (Chen et al., 2007; McCarthy & de Vellis, 1980). Briefly, 10–12 dissected brain cortices were freed of meninges, mechanically homogenized and enzymatically treated for 15 min with DNase I (0.1 mg/ml, Sigma, Madrid, Spain) and 0.25% Trypsin-EDTA (Gibco, Scotland, UK)). The dissociated tissue was resuspended in C-DMEM (Gibco), filtered through a 100 μm nylon cell strainer (BD Falcon), and plated on poly-D-lysine (PDL)-coated (Sigma) flasks at density of ~2 brains/75 cm^2. To prepare pure OPCs, 10–12-day-old MGCs were pre-shaken at 220 rpm for 2 hr in a INFORS HT Minitron incubator with a radius of 2.5 cm at 37°C, followed by an overnight shake at 240 rpm. The cell suspension obtained after differential adhesion was passed through a 40 μm nylon cell strainer (BD Falcon, USA) and plated onto coated glass coverslips (14 mm) at a density of 45,000 cells, or on 6-well plates with ~3×10^5 cells/well, in Sato medium. To induce differentiation, mitogens were replaced by 0.5% of FBS.

2.3 | A modified Boyden chamber system for physical separation of OPC soma and membrane protrusions

Approximately 2.5×10^5 OPCs were plated in the upper compartment of a Boyden chamber insert, consisting of a permeable PET membrane with 1-μm pore size (BD Falcon) coated with 10 μg/ml of PDL and human placental laminin-2 (Millipore, France) on the bottom side to create an haptotactic gradient. To promote extension of OPC protrusions across the pores, a chemotactic gradient was established by adding human PDGF and FGF2 (Peprotech; both at 10 ng/ml) to the lower chamber, and the chemorepulsive netrin-1 (R&D Systems; 25 ng/ml) to the upper chamber. OPCs were cultured for 24 hr in Sato proliferating medium.

2.4 | Isolation of total RNA

Total RNA from OPC soma or membrane protrusions was isolated using the Quick-RNA MicroPrep kit (Zymo Research, USA) according with manufacturer's instructions. The OPC soma fraction was isolated by scrapping the upper side of the insert with a cotton swab that was then dipped in ZR RNA lysis buffer. RNA from membrane protrusions

was collected from the bottom side of the insert, which was pushed down into a well containing lysis buffer. RNA from different experiments was pooled and concentrated using the RNA Clean & Concentrator-5 kit (Zymo Research).

2.5 | Bioinformatics analysis

Reads were mapped to the rat genome assembly for Rnor_5.0 with TopHat using the transcript set from Ensembl v69 to provide splicing information. Raw read counts for the Ensembl v69 transcripts were calculated in SeqMonk and differential expression was determined using DESeq (Anders & Huber, 2010) with $p < .05$ after multiple testing correction with no hit count optimization applied. Hits were further filtered for size of change using the SeqMonk intensity difference filter where only genes with a change significantly different ($p < .05$ after Benjamini and Hochberg multiple testing correction) to a normal distribution modeled over the log2 fold change of the 1% of genes with the most similar average expression to the gene being tested were kept. The complete RNA-Seq results dataset is available through the Gene Expression Omnibus (GEO) repository (accession number GSE106862).

2.6 | Myelinating co-cultures of rat DRG neurons

Myelinating co-cultures were performed according to Laursen et al., with minor modifications (Laursen, Chan, & Ffrench-Constant, 2011). Briefly, DRG were isolated from spinal cords of E15 rat embryos and digested with 0.05% Trypsin/EDTA and DNase I (0.4 mg/ml) for 90 min at 37°C. Dissociated neurons were plated on growth factor-reduced matrigel (BD Bioscience) coated coverslips (14 mm, 90,000 cells/coverslip). DRG neurons were grown for 21 days *in vitro* (DIV) in C-DMEM supplemented with NGF (100 ng/ml). Cells were treated at 1 and 6 DIV for 48 hr with 5-fluoro-2′-deoxyuridine (FUrd, 20 μM). After 3 DIV, FBS was replaced with B27. After 21 DIV, transduced OPCs were seeded on top of neurons (8,000 cells per coverslip) and myelinating medium was added. Co-cultures were maintained for 18 DIV with media changes every 2–3 days.

2.7 | Lentiviral transduction of OPCs

shRNAs specific for *Jmy* (sh1–5′-GAAGGCAAGTTTGCTATAA-3′ and sh2–5′-GGACCTCACTGTCAAATAT-3′) were designed with PSICOLIGOMAKER 1.5 software. Oligonucleotides containing the shRNA sequence were synthesized, annealed and cloned into the pSicoR vector (a gift from Tyler Jacks – Addgene plasmid # 11579; Ventura et al., 2004). Lentivirus containing a shRNA sequence (5′-AGTTCCAGTACGGCTCCAA-3′) targeting DsRed2, which is not found in mammals (Ozcelik et al., 2010), was used as an experimental control. Transduction of OPCs was performed with a MOI of 3 at the time of seeding.

2.8 | Time-lapse microscopy

Live cell imaging of OLs was performed with phase contrast microscopy. Cells were plated on 24-well-PDL-coated plastic bottom dishes after sorting and imaged with 5-min frame rates for 3.5^{+} days. For visualization of F-actin in live cells, OPCs were plated on PDL-BAB-matrigel-coated glass bottom 2-well u-Slides (Ibidi, Germany) and imaged with Sir-Actin (Spirochrome AG, Switzerland) added to the medium at 100 nM. Images were acquired with 15-min intervals. For live-cell imaging of co-cultures, images were acquired at a frame rate of 10 min. All imaging was done under a controlled environment (37°C, 5% CO2) with a Leica DMI6000 epifluorescence microscope (Germany) equipped with an Orca Flash 4.0v2.0 camera (Hamamatsu, Japan). At least 30 fields of view were set for each condition.

2.9 | Image and quantitative morphodynamics analysis

For categorization of OL morphology, Olig2-positive cells were grouped according to their complexity (Baer et al., 2009) using phase-contrast and F-actin images. For Sholl analysis, Olig2-positive cells were analyzed using the Sholl analysis tool (Ferreira et al., 2014) for ImageJ (Schneider, Rasband, & Eliceiri, 2012) with the following parameters: 10 μm starting radius and 4 μm step size. The total area occupied by F-actin was determined using ImageJ tools and a home-made macro. Measurement of MBP-segment length in co-cultures was performed using the "segmented line" tool from ImageJ. For semiautomated analysis of phase-contrast live imaging of OL differentiation, we developed "OligoMacro", an ImageJ toolset (extended information available in Supporting Information, Text S1 and S2).

2.10 | Statistical analysis

Statistical analysis was performed using GraphPad Prism or SPSS software. Data distribution was tested for normality using the Shapiro–Wilk test. Comparisons between groups of measurements that follow a normal distribution and pass the F test of variances were performed using the one-sample *t* test, unpaired two-tailed Student's *t* test, or ANOVA followed by the recommended post hoc test. For non-normal data, non-parametric tests were applied. Analysis of distribution of categorical variables was performed with Pearson's chi-squared (χ^2) test. Significance was set as $^{*}p < .05$, $^{**}p < .01$, or $^{***}p < .001$.

3 | RESULTS

3.1 | Transcriptomic profiling of OPC membrane protrusions versus soma

Similarly to other cells with elaborate morphology (Holt & Schuman, 2013), OLs probably require asymmetrical spatial regulation of biological processes. Formation of specialized membrane domains is critical for OL development and for contacting axons, and we hypothesized that the enrichment of specific mRNAs in protrusions of OPCs is important for morphological differentiation, thus having an impact in myelination. To explore this hypothesis, we established a modified Boyden chamber system to physically separate soma from membrane protrusions of rat primary OPCs cultured *in vitro* for 24 hr (Figure 1a) and isolated total RNA from each fraction. Next, we performed a whole-transcriptome analysis by RNA sequencing to identify and characterize mRNAs specifically enriched in the membrane protrusions of OPCs. Due to the very low amounts of RNA recovered from the OPC

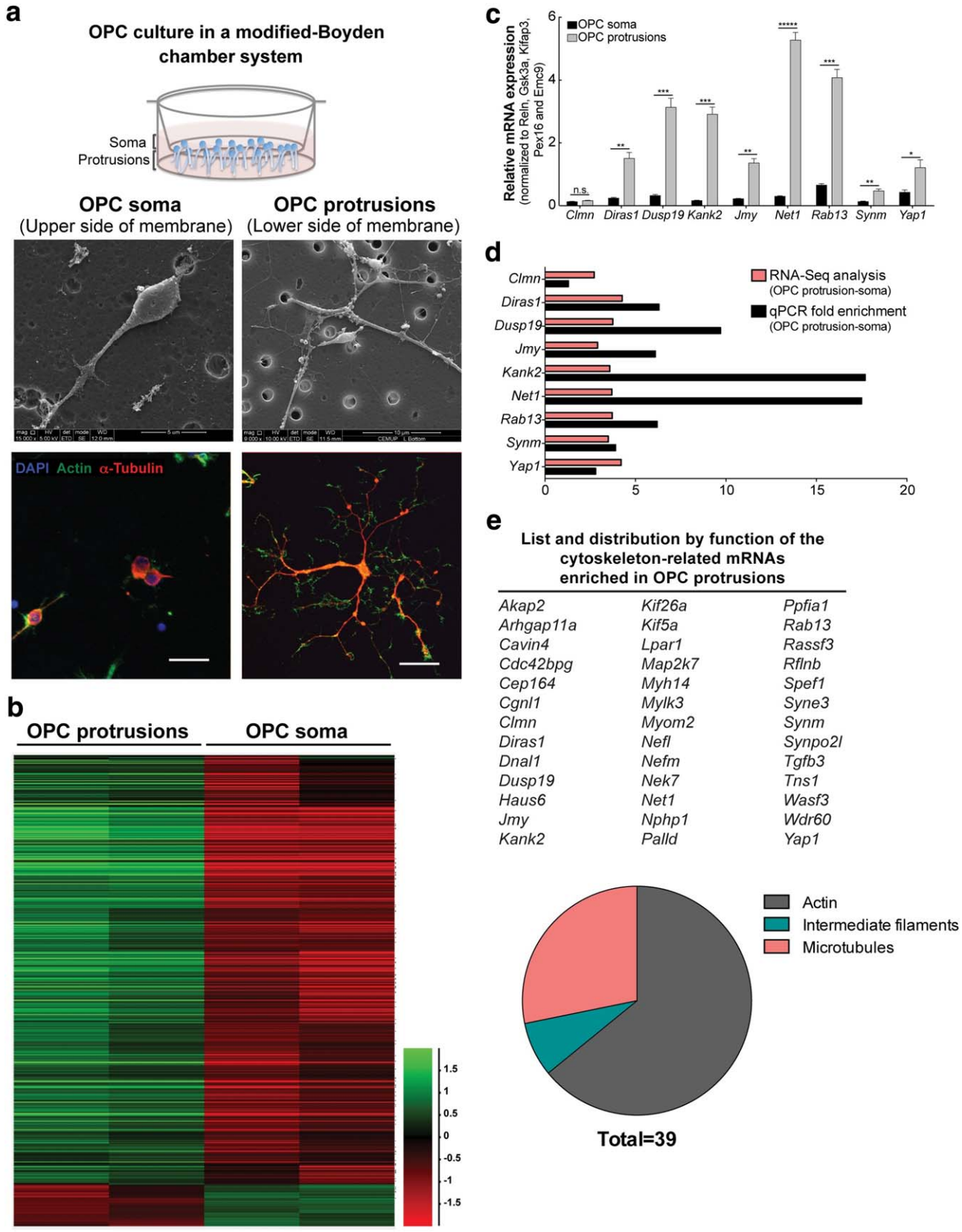
a
OPC culture in a modified-Boyden chamber system
Soma
Protrusions
OPC soma
(Upper side of membrane)
OPC protrusions
(Lower side of membrane)
DAPI Actin α-Tubulin
b
OPC protrusions
OPC soma
1.5
1
0.5
0
-0.5
-1
-1.5
c
Relative mRNA expression
(normalized to Rein, Gsk3a, Kifap3, Pex16 and Emc9)
OPC soma
OPC protrusions
n.s.
Clmn
Diras1
Dusp19
Kank2
Jmy
Net1
Rab13
Synm
Yap1
d
RNA-Seq analysis
(OPC protrusion-soma)
qPCR fold enrichment
(OPC protrusion-soma)
e
List and distribution by function of the cytoskeleton-related mRNAs enriched in OPC protrusions
Akap2
Arhgap11a
Cavin4
Cdc42bpg
Cep164
Cgnl1
Clmn
Diras1
Dnal1
Dusp19
Haus6
Jmy
Kank2
Kif26a
Kif5a
Lpar1
Map2k7
Myh14
Mylk3
Myom2
Nefl
Nefm
Nek7
Net1
Nphp1
Palld
Ppfia1
Rab13
Rassf3
Rflnb
Spef1
Syne3
Synm
Synpo2l
Tgfb3
Tns1
Wasf3
Wdr60
Yap1
Actin
Intermediate filaments
Microtubules
Total=39

FIGURE 1.

protrusion fraction (~9 ng of RNA per 6-well insert), each replicate consisted of pools from several experiments. Transcript expression for each individual replicate of OPC soma versus membrane protrusions fractions was grouped to determine the average expression level, followed by differential expression (DESeq) analysis that showed a subcellular enrichment of 951 transcripts (Figure 1b). Significance of these differentially expressed hits was assessed by correcting for intensity differences, which revealed that 116 transcripts are significantly enriched in OPC protrusions (Supporting Information, Table S2). Next, we selected 9 *genes—Clmn*, *Diras1*, *Dusp19*, *Kank2*, *Jmy*, *Net1*, *Rab13*, *Synm*, *and Yap1*—and assessed their expression profiles in OPC soma vs. membrane protrusions fractions by qPCR with normalization to five genes with variable abundances that were selected from a list of transcripts found in equal ratios in both fractions (Supporting Information, Table S3). We confirmed that, with the exception of Clmn, these transcripts were significantly enriched in membrane protrusion fraction of OPCs (Figure 1c), thus validating the RNA-Seq analysis top hits for protrusion-enriched mRNAs (Figure 1d). To better understand which biological processes are being spatially regulated in the OPC membrane protrusions, we initially performed a gene ontology (GO)-term enrichment analysis using G:profiler (Reimand et al., 2016). The analysis showed a significant enrichment of GO terms associated with cellular component assembly, organelle organization, actin filament-based process, cytoskeleton organization, and supramolecular fiber organization (Supporting Information, Table S4). We further refined the functional analysis by manually searching the literature or GO annotations using databases such as EMBL QuickGO (https://www.ebi.ac.uk/QuickGO/) and Gene Cards (http://www.genecards.org). Remarkably, ~30% of the protrusion-enriched transcripts have annotations and/or functions related to the cytoskeleton (Figure 1e). This list of top cytoskeleton hits includes transcripts that are functionally related to the actin network (64%) and microtubule function (28%; Figure 1e). Comparing our top hits list with other previously published RNA-Seq studies of mRNAs enriched in protrusion-like structures in fibroblast pseudopodia (Mili, Moissoglu, & Macara, 2008), axons (Gumy et al., 2011; Zivraj et al., 2010), and neurites (Feltrin et al., 2012), we observed that more than 70% of the transcripts identified in our study are OPC-specific (Supporting Information, Table S5). Altogether, our analysis of the OPC subcellular transcriptome, comparing cell soma with membrane protrusions that contact axons and later form the myelin wraps, revealed a substantial and cell-specific enrichment of mRNAs in protrusions, especially of transcripts associated to cytoskeleton dynamics and in particular with the actin network.

3.2 | Jmy is expressed in oligodendrocytes and upregulated during developmental CNS myelination

Control of F-actin assembly is known to play an essential role in OL differentiation and initiation of myelination (O'Meara et al., 2013; Zuchero et al., 2015) but the details of the molecular network that links actin dynamics to function in OLs are not fully characterized. With this in mind, we chose to study the recently identified multifunctional actin assembly factor Jmy, which came up in our RNA-Seq screening as an mRNA that is asymmetrically distributed in OPCs during initial extension of membrane protrusions (Figure 1c,d). Of note, Jmy was not found to be enriched in the protrusions of other cells (Supporting Information, Table S5), suggesting that the subcellular organization of its transcripts is important in OPCs specifically. Firstly, we assessed the *in vivo* expression of Jmy in myelin-rich areas of the mouse CNS during developmental myelination, which occurs during the early postnatal period. Double immunohistochemistry analysis showed that, in that time window, expression of Jmy is predominantly found in cells that are positive for CC1 (Figure 2a, c, d), a marker of pro-myelinating and mature OLs (Bhat & Zhang, 1996). The number of cells positive for both Jmy and CC1 increases significantly during active myelination in the mouse spinal cord (at P5), cerebellum (from P5 to P14) and optic nerve (around P14; Figure 2b, d, e). Interestingly, we observed differences in temporal co-expression of Jmy and CC1 among the various white matter tracts analyzed—earlier in spinal cord and later in optic nerve and cerebellum—which is in accordance with different rates of OL lineage progression and myelination in distinct regions of the developing CNS (Foran & Peterson, 1992). On average, about 25%–30% of CC1-posititve OLs transiently co-express Jmy in the first 14 postnatal days (Figure 2), a developmental time window that for example in the optic nerve spans the period of axon ensheathment (Dangata & Kaufman, 1997), suggesting that Jmy plays a role during a specific temporally-regulated differentiation state in pro-myelinating and/or myelinating OLs.

To further characterize the expression profile of Jmy during OL differentiation, we used *in vitro* cultures of OPCs from neonate rat brains. Primary cultures of OPCs can be induced to differentiate into mature OLs by a cell-autonomous transcriptional program that recapitulates several aspects of OL differentiation *in vivo*, including the morphological changes and the expression of myelin proteins (Kachar, Behar, & Dubois-Dalcq, 1986). qPCR analysis showed that transcript levels of *Jmy* are upregulated during OL differentiation (Figure 3a), and its

FIGURE 1 The oligodendrocyte "protrusiosome". (a) Rat OPCs were plated for 24 hr on a modified Boyden chamber system, consisting of a transwell with 1 μm pore size with chemo- and haptotactic gradients, to physically separate OPC soma and protrusion fractions for RNA sequencing. Efficient separation of OPC soma (top surface) and protrusions (bottom surface) was confirmed by scanning electron microscopy (upper panels) and confocal microscopy (lower panels). (b) Heatmap displaying 951 differentially expressed genes in individual biological replicates of OPC soma and protrusion fractions. (c and d). Validation by qPCR of a subset of transcripts significantly enriched in OPC protrusions; shown in (c) as relative mRNA expression of Clmn, Diras1, Dusp19, Kank2, Jmy, Net1, Rab13, Synm, and Yap1 in OPC protrusion and soma fractions normalized to five genes that are equally expressed in both fractions (Reln, Gsk3a, Kifap3, Pex16, and Emc9), and in (d) represented as fold enrichment in OPC protrusions/soma, plotted together with the results from RNA-Seq. Data represented as mean ± *SEM* of $n = 3$ biological replicates collected from independent experiments (n.s. = not significant, $^{*}p < .05$, $^{**}p < .01$, $^{***}p < .001$, $^{****}p < .0001$, calculated using the unpaired *t* test). (e) Top transcripts significantly enriched in OPC protrusions with GO terms related to cytoskeletal dynamics, distributed into lower-hierarchical functional groups [Color figure can be viewed at wileyonlinelibrary.com]

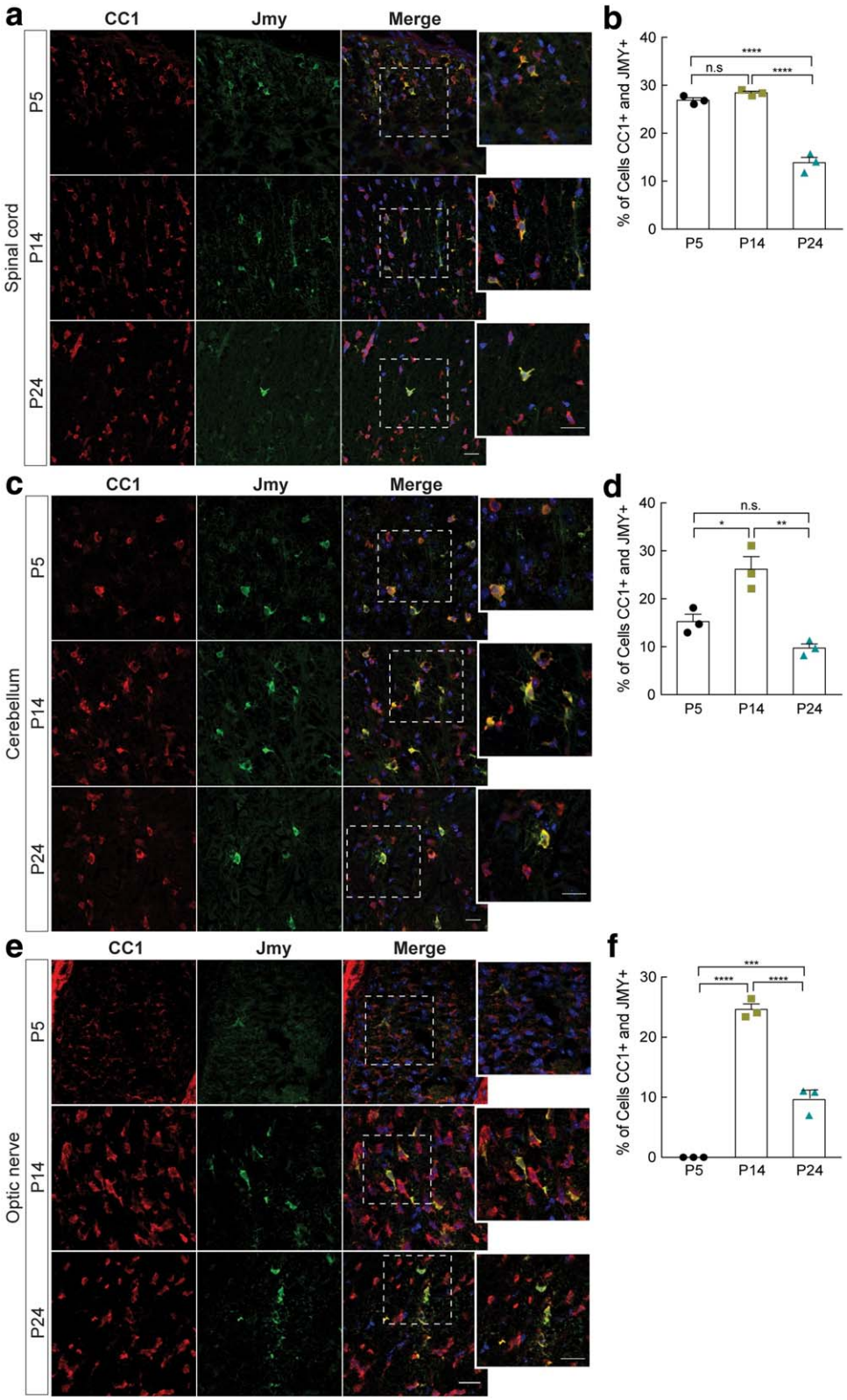

FIGURE 2 Jmy is predominantly expressed in oligodendroglia during postnatal development in the mouse CNS. Representative single plane confocal images of IHC of transversal sections of mouse (a) spinal cord, (c) cerebellum and (e) optic nerve to label oligodendrocytes (CC1, red), Jmy (green) and nuclei (DAPI, blue), with zoomed in detail of the areas indicated by the white frames. Scale bar is 20 μm. Quantification of OLs co-expressing CC1 and Jmy in CNS regions (b, d, and f, correspond to spinal cord, cerebellum and optic nerve, respectively). Three whole, non-consecutive sections per animal were used for quantification. Data represented as mean ± SEM of three animals (n.s. = not significant, $^{*}p < .05$, $^{**}p < .01$, $^{***}p < .001$, $^{****}p < .0001$, calculated using one-way ANOVA followed by Tukey's multiple comparisons test) [Color figure can be viewed at wileyonlinelibrary.com]

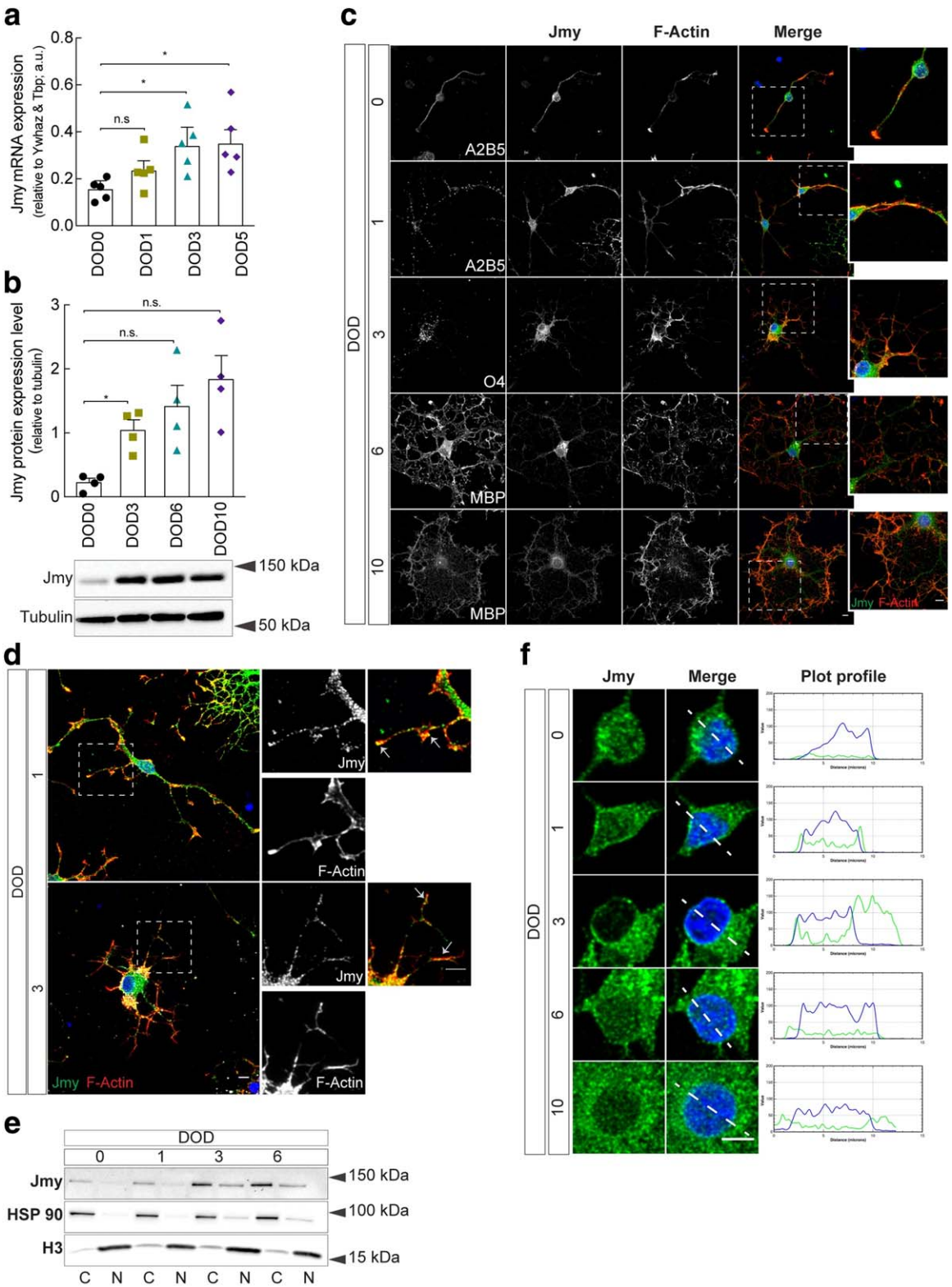

FIGURE 3.

protein levels rise by approximately four-fold in the first 3 days of differentiation (DOD), an increase that is sustained as OLs differentiate further (Figure 3b). Jmy was initially described as a p300 transcription cofactor, active in the p53 response to cellular stress (Shikama et al., 1999). It localizes to both the nucleus and the cytosol in various cell types (Coutts, Weston, & La Thangue, 2009; Firat-Karalar et al., 2011), but is enriched in the cytosol and its actin nucleation activity in motile cells requires translocation to the cytoplasm where it is seen at the leading edge (Zuchero et al., 2009). We assessed the subcellular localization of Jmy in OLs at different stages of differentiation by

immunofluorescence analysis. Jmy was mainly detected in the cytoplasm, as a punctate staining pattern with widespread cytosolic distribution in both OPCs and OLs, and a prominent localization in the perinuclear region of the cell soma (Figure 3c). We also noticed that during early differentiation (at DOD1 to 3), when OLs are undergoing extension and branching of membrane protrusions, Jmy was seen in discrete sites of strong F-actin labeling throughout the protrusion structures (Figure 3c,d).

To further investigate if in OLs Jmy is regulated by nuclear versus cytoplasmic localization, we performed western blot analysis of subcellular fractions of OLs at different stages of differentiation. Jmy was mainly detected in cytoplasm-enriched fractions containing Hsp90, a predominantly cytosolic protein, compared with nuclear-enriched fractions, containing histone H3, a nuclear protein (Figure 3e). Additionally, measurement of relative intensities of Jmy and DAPI across the nucleus showed little overlap of fluorescence signals (Figure 3f). Together, these observations suggest that Jmy is expressed and transcriptionally upregulated during OL differentiation, particularly during stages of intense actin filament assembly. Furthermore, its role in OL biology is probably independent of its nuclear function as a transcription co-factor: although Jmy was not completely excluded from the nucleus, we found significant enrichment in the cytoplasm during all stages of OL differentiation.

3.3 | Jmy regulates the morphological differentiation of oligodendrocytes

We next performed a functional analysis study of Jmy in OLs during differentiation by knocking down its expression by RNAi. We designed two shRNAs, *Jmy* shRNA construct #1 and #2, for cloning into the lentiviral pSicoR vector (Ventura et al., 2004) and tested their knockdown efficiency by western blot analysis, which was similar between both constructs (Supporting Information, Figure S1a). All experiments reported here were conducted using *Jmy* shRNA construct #1, which provided an average knockdown efficiency of 55%. pSicoR has a second promoter driving expression of EGFP that was used as a marker of lentiviral transduction in cells. We performed an initial morphological assessment of OLs transduced with *Jmy* shRNA (sh*Jmy*-OLs) or a non-targeting shRNA (shCtr-OLs) using phalloidin staining to visualize the entire F-actin skeleton of the cell and follow fine changes in cell shape. As expected, shCtr-OLs underwent a dramatic morphological transformation during differentiation, from a multipolar state at DOD3 with extension of new protrusions and branching, to a highly arborized morphology that culminates with the flattening of protrusions to form membranous sheets characteristic of mature OLs *in vitro* (Figure 4a). Differentiating sh*Jmy*-OLs however, presented with less membrane protrusions and markedly decreased branching, with a noticeable impairment in the acquisition of complex arborization (Figure 4a). Another particular feature of sh*Jmy*-OLs was their abnormally small size. Measurement of the total cell area using F-actin staining showed that, when compared with shCtr-OLs, sh*Jmy*-OLs were overall smaller at all stages of differentiation, although the difference in cell area did not reach statistical significance at DOD10 (Figure 4b). Next, we classified OLs in different morphological branching categories, which correlate with their degree of differentiation (Bauer, Richter-Landsberg, & Ffrench-Constant, 2009; Thurnherr et al., 2006). Morphological categorization showed that, during differentiation, sh*Jmy*-OLs display a less complex morphology when compared with shCtr-OLs, retaining a more immature morphology with mostly primary branches in the initial stages of differentiation (DOD3; Figure 4c). In line with this, Sholl analysis at DOD3 showed that sh*Jmy*-OLs contained significantly less intersections compared with branches in shCtr-OLs (Figure 4d), suggesting that Jmy is required for the extension and branching of new protrusions. At DOD6, sh*Jmy*-OLs remained as multipolar or arborized cells, and very few formed lamellar structures or membranous sheets, when compared with shCtr-OLs (Figure 4c). Importantly, even after 10 days of differentiation most sh*Jmy*-OLs persisted in a less mature morphological state, indicating that defects in branching earlier in differentiation lead to a partial arrest, and not a delay, in the timing of morphological differentiation.

Given that Jmy functions as an actin nucleator and/or pro-nucleating factor, we next asked whether knocking down expression of Jmy would affect F-actin polymerization during early OL differentiation. Using super-resolution microscopy and the fluorogenic probe SiR-actin, we performed live imaging of differentiating OLs. At DOD1 and 3, respectively, star-shaped and arborized shCtr-OLs show abundant

FIGURE 3 Jmy localizes to the perinuclear region and membrane protrusion of OLs, and its expression is upregulated during differentiation. Expression levels of Jmy mRNA (a) and protein (b) were assessed by qPCR and immunoblotting, respectively, in primary rat OPCs (DOD0) and differentiating OLs (DOD3, 5, 6, and 10). (a) Relative transcript expression levels calculated as $2^{-\Delta Ct}$ (**$p < .01$, calculated using one-way ANOVA followed by Tukey's multiple comparisons test on $2^{-\Delta Ct}$ values of $n = 5$ biological replicates collected from independent experiments). (b) Data represented as mean of the normalized relative densities ± *SEM* of $n = 4$ biological replicates collected from independent experiments (*$p < .05$, calculated using one-way ANOVA followed by Tukey's multiple comparisons test). Tubulin was found to be stably expressed during OL differentiation and was used as a loading control in all immunoblots performed. (c) Representative images of confocal deconvoluted Z-projections showing the cellular distribution of Jmy at different stages of OL differentiation. IF labeling was performed for an OL lineage marker (A2B5, O4, or MBP), Jmy (green), F-actin (phalloidin, red), and nuclei (DAPI, blue). Scale bar is 5 μm. (d) Representative images of confocal deconvoluted Z-projections showing Jmy in sites of F-actin enrichment in OL protrusions (arrows) at DOD1 and DOD3. IF labeling was performed for an OL lineage marker (A2B5 or O4), Jmy (green), F-actin (phalloidin, red), and nuclei (DAPI, blue). Scale bar is 5 μm. (e and f) Relative subcellular distribution of Jmy in oligodendrocytes assessed by (e) immunoblotting of subfractionated OPC and OL lysates collected during differentiation. Both cytoplasmic and nuclear samples were immunoblotted against Jmy, HSP90 (a cytoplasmic-enriched protein) and histone H3 (a nuclear protein). Ponceau S staining of blotted membrane is shown in Supporting Information, Figure S1b. (f) Middle plane representative images of high magnification detail of the OL soma that were used to determine DAPI and Jmy intensities that were plotted as a function of position across a line (shown in the images as an overlay). Scale bar is 5 μm [Color figure can be viewed at wileyonlinelibrary.com]

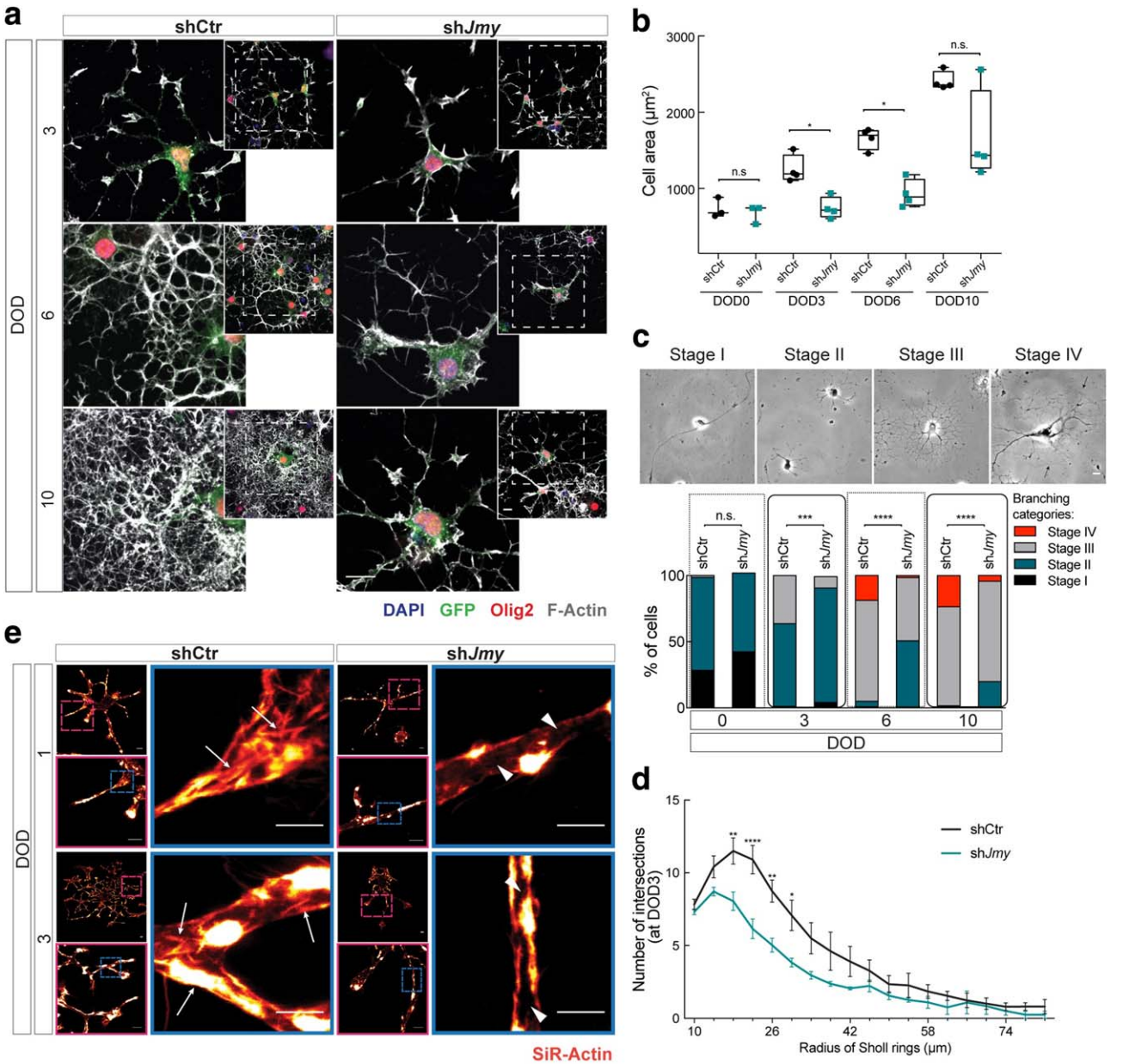

FIGURE 4 Morphological differentiation of oligodendrocytes requires Jmy-dependent assembly of F-actin. (a) Representative single plane confocal images showing morphological differentiation of transduced shCtr- or sh*Jmy*-OLs. IF labeling was performed for an OL lineage marker (Olig2, red), F-actin (phalloidin, gray), and nuclei (DAPI, blue), and GFP was used as a reporter of transduction. A zoomed out view of the framed areas is shown for each image. Scale bar is 20 μm. (b) F-actin staining of $GFP^+/Olig2^+$ cells was used to determine the total area of the cell. Data represented as median area±min and max values of $n = 4$ independent experiments, with at least 30 $GFP^+/Olig2^+$ cells in each condition analyzed per experiment (n.s. = not significant; $^{**}p < .01$, calculated using the Mann-Whitney test). (c) Representative phase-contrast images of OL morphological categories during differentiation, which were used to classify the differentiation stage of shCtr- and sh*Jmy*-OLs. Morphology of $GFP^+/Olig2^+$ cells was assessed using images of stained F-actin and phase contrast. Data are represented as the percentage of cells counted in each morphological category at different times of differentiation. The total cells analyzed were pooled from three independent experiments, with at least 70 $GFP^+/Olig2^+$ cells in each condition collected per experiment. A significant association was found at DOD3 ($\chi^2_{(2,\ N=700)} = 17.42$, $^{***}p < .001$), DOD6 ($\chi^2_{(2,\ N=827)} = 50.83$, $^{****}p < .0001$) and DOD10 ($\chi^2_{(2,\ N=695)} = 30.51$, $^{****}p < .0001$), calculated using the Chi-square test. (d) Sholl analysis was performed in shCtr- and sh*Jmy*-OLs to measure complexity and length of protrusions at DOD3. The analysis was performed using images of stained F-actin. The number of intersections between protrusions and the concentric rings was determined and plotted as a function of distance from the cell body. Data represented as mean ± *SEM* of $n = 4$ independent experiments, with at least 40 $GFP^+/Olig2^+$ cells in each condition analyzed per experiment ($^*p < .05$, $^{**}p < .01$ $^{****}p < .0001$, calculated using two-way ANOVA followed by Sidak's multiple comparisons test). (e) Representative live STED super resolution microscopy images of shCtr- and sh*Jmy*-OLs at DOD1 and 3. Shown are thick bundles of F-actin (arrows) found in protrusions of shCtr-OLs, which are not seen in the "hollow" protrusions (arrowheads) of sh*Jmy*-OLs. Scale bar is 5 μm on the left upper and lower panels, and 2 μm on the panels to the right [Color figure can be viewed at wileyonlinelibrary.com]

thick bundles of F-actin in the protrusions (Figure 4e, arrows). sh*Jmy*-OLs showed "hollow" protrusions (Figure 4e, arrowheads) void of actin trails, indicating that less F-actin was present in these structures.

Since Jmy can promote nucleation of actin by itself or activate Arp2/3 (Zuchero et al., 2009) we next investigated if disrupting the expression of Jmy would result in altered levels of Arp2/3 complex. We found that expression of Arp3, an essential subunit of the complex, shows slightly increased levels, a difference that is not statistically significant, in sh*Jmy*-OLs during differentiation when compared with shCtr-OLs (Supporting Information, Figure S2). Altogether, our observations suggest that an impairment in F-actin polymerization in sh*Jmy*-OLs is associated with decreased protrusion formation and branching, resulting in overall smaller cells that do not differentiate into mature OLs.

3.4 | A stereotypical cellular shaping program, dependent of actin dynamics, directs distinct steps of oligodendrocyte differentiation

The widely-reported analyses of OL morphology during differentiation are greatly limited by the use of fixed cells at pre-established timepoints, missing important details on the dynamics of morphological differentiation. In other cell types, the combination of time-lapse microscopy, genetically encoded fluorescent proteins and computational image analysis has provided powerful ways to use robust quantitative morphometrics to study cell behavior (Barry, Durkin, Abella, & Way, 2015; Tsygankov et al., 2014). However, in cells with elaborate morphology, unbiased automated image analysis correlating morphodynamics and cell behavior remains very challenging. Moreover, in OLs, studying the real-time dynamics of morphological differentiation is made particularly difficult by the demanding experimental conditions required for *in vitro* cultures of primary OPCs and limited availability of effective gene transfer techniques. With this in mind, we devised a live-cell imaging and computational analysis setup to address two important aspects of OL biology: first, assess if morphological differentiation follows a specific pattern that can be extracted by morphometric analysis; and second, how the differentiation program is affected by the disruption of actin dynamics. We designed an ImageJ (Schindelin et al., 2012) workflow, which we called OligoMacro, to perform semi-automated analysis of large image datasets generated from live cell imaging of OLs. Cytometry-sorted EGFP-positive sh*Jmy*- and shCtr-OLs were imaged by phase contrast microscopy over a time course of 3.5 days, with a 5-min time frame. An initial qualitative assessment of the movies showed that OL differentiation is an extremely dynamic process requiring high protrusion remodeling, with cells undergoing profound cytoskeleton rearrangements that follow a stereotypical "cellular shaping" program (Figure 5a,b; Supporting Information, Movie S1). Quantitative image analysis using OligoMacro revealed that shCtr-OLs undergo an initial phase of intense addition of new protrusions that slows down after 48 hr into differentiation (Figure 5c). After 24 hr of differentiation, we detected a rapid increase in the addition of branching points (Figure 5d), corresponding to secondary and tertiary branches resulting in widespread arborization of the cells. Arborization is followed by retraction/collapse of membrane protrusions, corresponding to a plateau or even a decrease in the number of added protrusion or branches (Figure 5c,d), and maintenance of a steady morphology roughly after day 3. We could occasionally observe some lamellipodial structures, characteristic of pro-myelinating OLs, in sites where retraction of secondary OL protrusions occurred (Supporting Information, Movie S2). In contrast, we found that OLs with reduced levels of Jmy are, in general, less dynamic (Supporting Information, Movie S3), showing impairment in the formation of protrusions (Figure 5c) and in the addition of new branching points (Figure 5d). Moreover, sh*Jmy*-OLs are not able to acquire complex arborization (Figure 5a,b) and do not follow the "cellular shaping program" timeline that we identified in shCtr-OLs (Figure 5a,b). Running the OligoMacro requires the user to define the "cell body" area, which is tracked during the analysis and provides quantitative extraction of OLs movement. Analysis of the total distance covered along time showed that sh*Jmy*-OLs move significantly slower than shCtr-OLs (Figure 5e) but with larger displacement from their point of origin, as seen in the plot of the individual trajectories of cells (Figure 5f).

Live imaging of the actin cytoskeleton dynamics using SiR-Actin showed that during the initial extension of protrusions, levels of F-actin in shCtr-OLs were highly increased at the leading edge of the growth cone-like structures (Figure 6a and Supporting Information, Movie S4). As the OLs progress to the stage of arborization, high levels of F-actin are seen in newly-formed secondary and tertiary branches, away from primary processes and the cell body (Figure 6a and Supporting Information, Movie S4). This is in stark contrast with what was seen in sh*Jmy*-OLs, which exhibit a permanent strong labeling of F-actin around the cell body and in primary protrusions, and very little F-actin in the protrusion tips (Figure 6a and Supporting Information, Movie S5). As previously mentioned, some shCtr-OLs occasionally formed membranous sheets and we used SiR-actin to follow actin cytoskeleton dynamics during this process. Formation of this specialized structure, limited in its border by an actin ring, is accompanied by a drastic decrease in F-actin levels in the inner region of the forming lamella, which occurs simultaneously with the collapse of secondary and tertiary protrusions (Figure 6b and Supporting Information, Movie S6). As differentiation progresses, sh*Jmy*-OLs were not able to remodel protrusions and arborize, and failed to redistribute F-actin away from the cell soma (Figure 6b and Supporting Information, Movie S7).

Altogether, our morphodynamics analysis suggest that Jmy is necessary for the precise organization and displacement of actin filaments during OL differentiation, and for the timely acquisition of the different morphological states that direct OL maturation

3.5 | Jmy is required for the assembly of MBP sheets

Functional decoupling of morphological differentiation and expression of myelin-specific proteins by mature OLs is difficult, as both events are timely coordinated and essential for myelination. We questioned whether Jmy was required for OLs to progress to a myelination phenotype and analyzed expression of MBP, one of the earliest myelin-specific components to arise and a marker of mature OLs. Immunofluorescence analysis showed that comparable numbers of sh*Jmy*- and shCtr-OLs expressed MBP, both at DOD 6 and 10 (Figure 7a,b). In line with this, no changes were observed in the percentage of NG2- (a

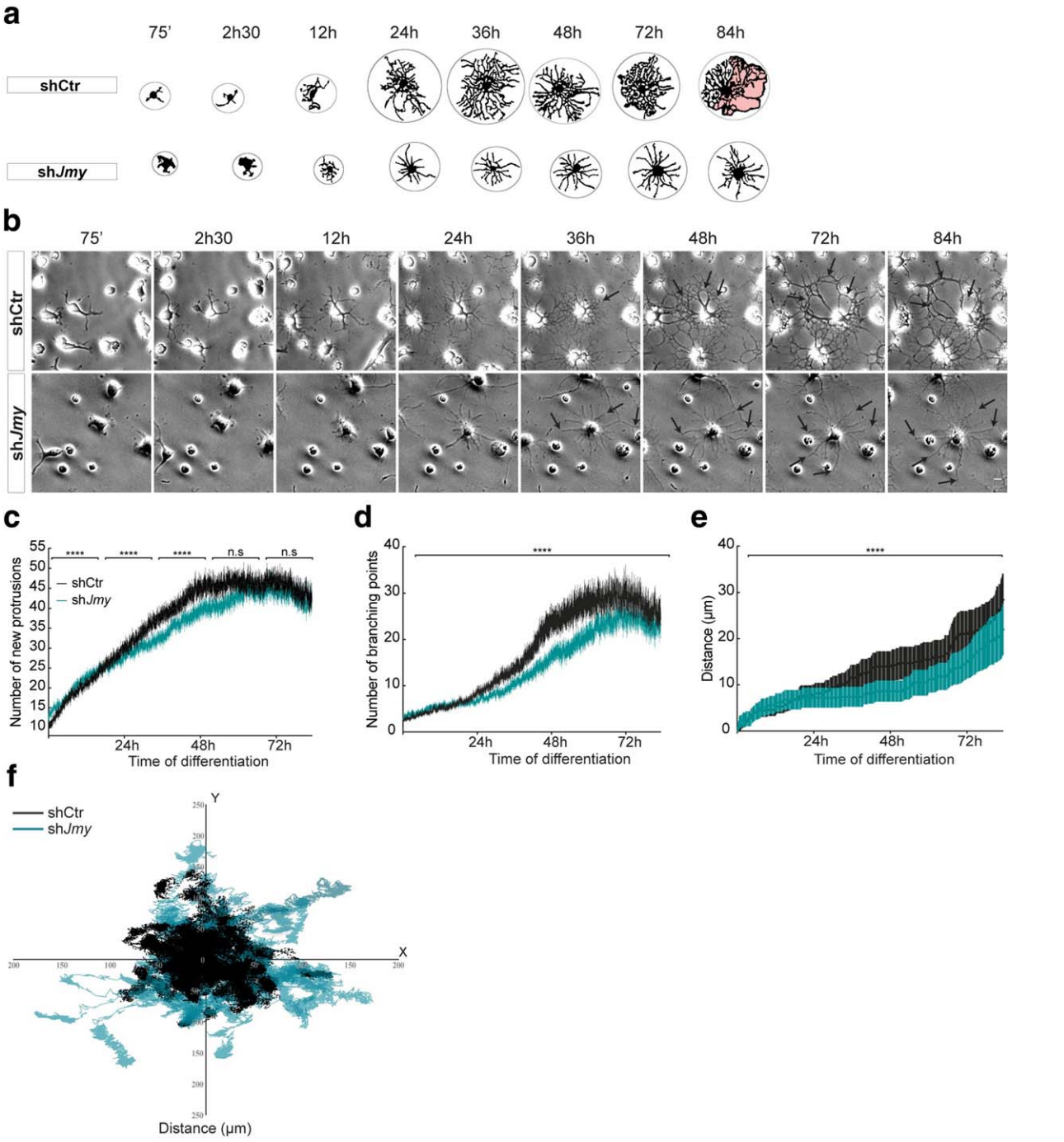

FIGURE 5.

marker of immature OLs) and O4-expressing cells during differentiation (data not shown), suggesting that antigenic differentiation is unaffected by the depletion of Jmy. However, significantly less sh*Jmy*-OLs formed MBP^+ sheets after 6 and 10 days of differentiation (Figure 7a, arrows, and 7c), which is in line with the decreased total levels of MBP assayed by western blot (Figure 7d). Interestingly, we observed comparable levels of expression of MAG, a component of periaxonal myelin that is not required for initial myelination (Li et al., 1994), in both conditions (Figure 7d). These results suggest that Jmy-dependent regulation of OL differentiation does not affect the developmental expression timing of maturity markers but impairs the extension of MBP membranous sheets *in vitro*.

3.6 | Jmy is necessary for the assembly of myelin segments in myelinating co-cultures

Our observations that Jmy is required for the acquisition of an arborized morphology in OLs and assembly of lamellar sheets posed the question of whether protrusion complexity directly correlates with myelination. Using an *in vitro* model of myelination consisting of co-

cultures of purified OPCs and DRG neurons, we analyzed the initial establishment of OL-neurite contact, neurite wrapping and deposition of myelin sheets. After 18 days of co-culture, less than 60% of MBP^+ sh*Jmy*-OLs had formed myelin segments, compared with 80% of MBP^+ shCtr-OLs (Figure 8a). sh*Jmy*-OLs were less efficient at contacting and ensheathing neurites and most cells extended membrane protrusions that were not contacting neurites (Figure 8a). Measurement of myelin segments deposited on neurites showed that sh*Jmy*-OLs formed shorter internodes (Figure 8b). As decreased levels of Jmy did not affect the developmental onset of MBP expression (Figure 7a,b), the shorter segments observed in co-cultures with sh*Jmy*-OLs likely result from either a delay in the initiation of myelination, or an impairment in lateral membrane extension during wrapping (Figure 8b).

To assess in real-time the dynamics of early OL interaction with neurites, we performed live imaging of myelinating co-cultures. We observed that shCtr-OLs actively surveyed the neighboring neurites by rapidly extending and retracting membrane protrusions (Supporting Information, Movie S8, initial 16 hr in co-culture). shCtr-OLs often formed membranous lamellipodia-like structures to stabilize the interaction with neurites (Supporting Information, Movie S9, 16–68 hr in co-culture). In contrast, sh*Jmy*-OLs sustained a constant and almost stochastic extension and retraction of their membrane protrusions, only forming short-lasting neurite-OL contacts (Supporting Information, Movie S10, 46 hr in co-culture). Additionally, we also observed that a significantly higher number of MBP-positive sh*Jmy*-OLs had multiple, dispersed and aberrant accumulations of MBP that appear to overlap with neurites, when compared with shCtr-OLs (Figure 8c).

4 | DISCUSSION

Morphological plasticity driven by rearrangements of the actin cytoskeleton is an essential feature of oligodendrocyte biology (Song et al., 2001), important for migration trajectory choice in progenitor cells and axonal contact (Kirby et al., 2006), and formation of lamellipodia-like structures that initiate wrapping during myelination (Nawaz et al., 2015; Zuchero et al., 2015). However, the details of how formation of these specialized actin-rich structures acts synergistically with the differentiation program in OLs to promote myelination are not entirely known. Here, we present a transcriptomic analysis of isolated membrane protrusions from primary cultures of OPCs and show that, in the very initial stage of protrusion extension, there is a significant subcellular enrichment of transcripts encoding proteins related to cellular component assembly and cytoskeleton organization, particularly of actin-related molecules. This suggests that the regulation of the cytoskeleton dynamics may be locally controlled in OPCs and probably relevant for their differentiation program. One of those transcripts encodes Jmy, a multifunctional actin polymerization factor that we found to be enriched in pro-myelinating OLs in the mouse CNS during developmental myelination. Moreover, Jmy is upregulated during OL differentiation *in vitro* and is necessary for the assembly of actin filaments and morphological differentiation. Live-imaging analysis of OLs during early differentiation showed that these cells follow a stereotypical "cellular shaping" program. They undergo intensive protrusion remodeling and branching to acquire a large arborized shape that lays the foundation for the deposition of specialized membranous sheets on sites where protrusion retraction/collapse occurs. We speculate that this morphological phenomenon of arborization and process retraction in OLs directly correlates with their pro-myelinating potential and is dependent on actin dynamics: in the absence of Jmy, OLs fail to timely acquire a complex arborized morphology and are not able to form membranous lamellae, which renders them less efficient at depositing MBP sheets *in vitro* and myelinating neurites in a co-culture system.

"Omics" analyses have shown that, in polarized cells, subcellular compartmentalization of transcripts or proteins is important for

FIGURE 5 Time-lapse imaging and quantitative morphodynamics analysis of early oligodendrocyte differentiation. (a) Cartoon depicting the morphological states that characterize a stereotypical "cellular shaping" program in shCtr-OLs: protrusion formation, extension and remodeling, arborization (secondary branching), and retraction on sites where lamellar sheets will begin to assemble (shown as a pink shade). sh*Jmy*-OLs remain in an immature morphology, with fewer and unbranched protrusions, and do not arborize. The circle lines denote the total space occupied by the cell's protrusion network, sketched after thresholded representative images of shCtr- and sh*Jmy*-OLs from the time-lapse videomicroscopy, shown in (b). Scale bar is 10 μm. Quantitative analysis of morphological complexity in OLs performed with OligoMacro on 5,000 images acquired by videomicroscopy of shCtr- and sh*Jmy*-OLs, measuring the: (c) number of new protrusions. A two-way ANOVA to examine the effect of time of differentiation and knockdown showed a statistically significant interaction between both factors on the number of new protrusions ($F_{4,1990} = 84.97$, $^{****}p < .0001$). shCtr-OLs formed significantly more new protrusions than shJmy-OLs during differentiation ($F_{1,1990} = 370.83$, $^{****}p < .0001$). A multiple comparisons analysis of time intervals followed by Tukey's test showed a significant effect of time on the number of new protrusions only during the first 50 hr of differentiation ($^{****}p < .0001$). Data represented as mean ± *SEM* of $n = 55$ cells per condition, randomly sampled from three independent experiments; and (d) branching points per cell. A two-way ANOVA showed a statistically significant interaction between time of differentiation and knockdown on the number of branching points ($F_{4,1990} = 198.94$, $^{****}p < .0001$). sh*Jmy*-OLs had decreased ability to form protrusion branches during differentiation when compared with shCtr-OLs ($F_{1,1990} = 1331.91$, $^{****}p < .0001$). A multiple comparisons analysis of time intervals followed by Tukey's test showed a significant effect of time on formation on branching points during differentiation ($^{****}p < .0001$). Data represented as mean ± *SEM* of $n = 55$ cells per condition, randomly sampled from three independent experiments. (e) Plot of the cumulative cell body movement in time. A two-way ANOVA showed a statistically significant interaction between time of differentiation and knockdown on the movement of the cell body ($F_{4,1992} = 331.454$, $^{****}p < .0001$). A multiple comparisons analysis of time intervals followed by Tukey's test showed a significant effect of time on the cells travelled distance during differentiation ($^{****}p < .0001$). Data represented as mean ± *SEM* of $n = 55$ cells per condition, randomly sampled from three independent experiments. (f) Individual trajectories of shCtr- and sh*Jmy*-OLs from their point of origin at the start of differentiation ($n = 55$ in each group) [Color figure can be viewed at wileyonlinelibrary.com]

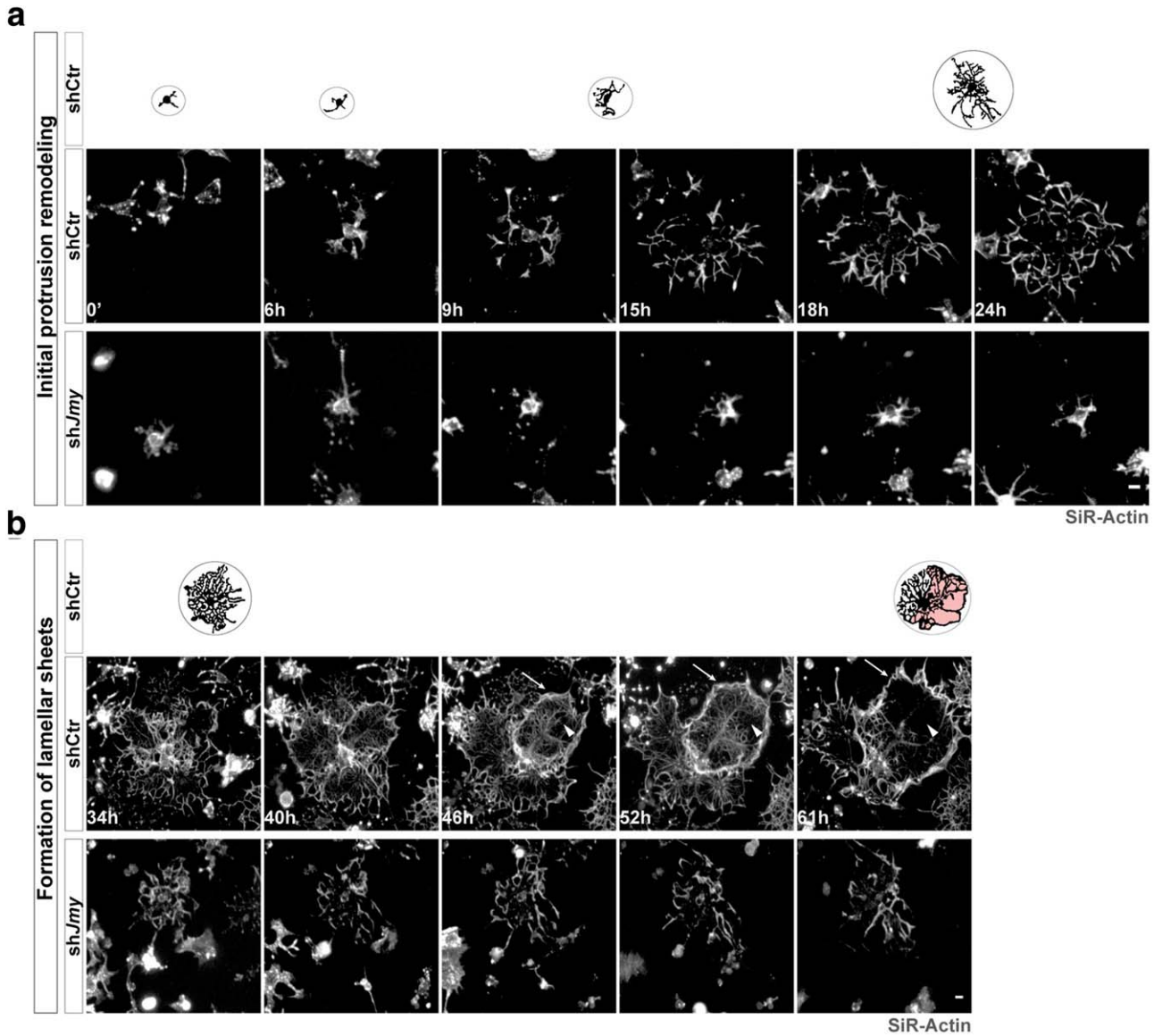

FIGURE 6 Live actin dynamics of OL differentiation. Representative images of shCtr and sh*Jmy*-OLs from time-lapse videomicroscopy using SiR-Actin. Depicted are also the cartoon representations of morphological states typical of OL differentiation. (a) In shCtr-OLs, top row, there is active extension and remodeling of actin-rich protrusions during the initial phase of differentiation as the cell arborizes. sh*Jmy*-OLs display an aberrant distribution of F-actin toward the cell soma. (b) Top row shows pro-myelinating OLs forming lamellar sheets, delimited by an actin ring (arrows) that grows simultaneously with retraction of fine protrusions in the inner area (arrowheads). Differentiating sh*Jmy*-OLs have shorter and thinner protrusions, and an overall abnormal actin profile. Images were processed using a nonlinear gamma change of 0.45. Scale bar is 10 μm [Color figure can be viewed at wileyonlinelibrary.com]

function and cell-cell interactions (Feltrin et al., 2012; Holt & Schuman, 2013; Mili et al., 2008; Poitelon et al., 2015). Although ours and other published data suggest that the same functional classes of molecules are polarized in specialized cellular compartments, we identified an OPC-specific signature of transcripts enriched in membrane protrusion. It is possible that the asymmetrical cellular distribution of these transcripts allows for local regulation of their expression and function in OL differentiation and myelination of axons. Accordingly, *MOBP* (myelin-associated oligodendrocyte basic protein), which encodes a myelin-specific protein only found in mature OLs and known to be locally translated (Schafer, Muller, Luhmann, & White, 2016), is in the top hit list of 116 OPC protrusion-enriched mRNAs. Altogether, asymmetrical enrichment of specific cytoskeleton and myelin transcripts as early as the OPC stage suggests that the localized transcriptome is probably a primary feature of the cell-autonomous program that governs OL differentiation and production of myelin. Future studies should address if, like in other cells, local translation of actin regulatory proteins (Mingle et al., 2005; Piper et al., 2006), and of actin itself (Lawrence & Singer, 1986), in the OPC/OL protrusion plays a role in signal reception to control cell behavior and myelin sheath formation.

It has been long recognized that the actin network constitutes a major cytoskeletal element at the leading edge of the OPC protrusive

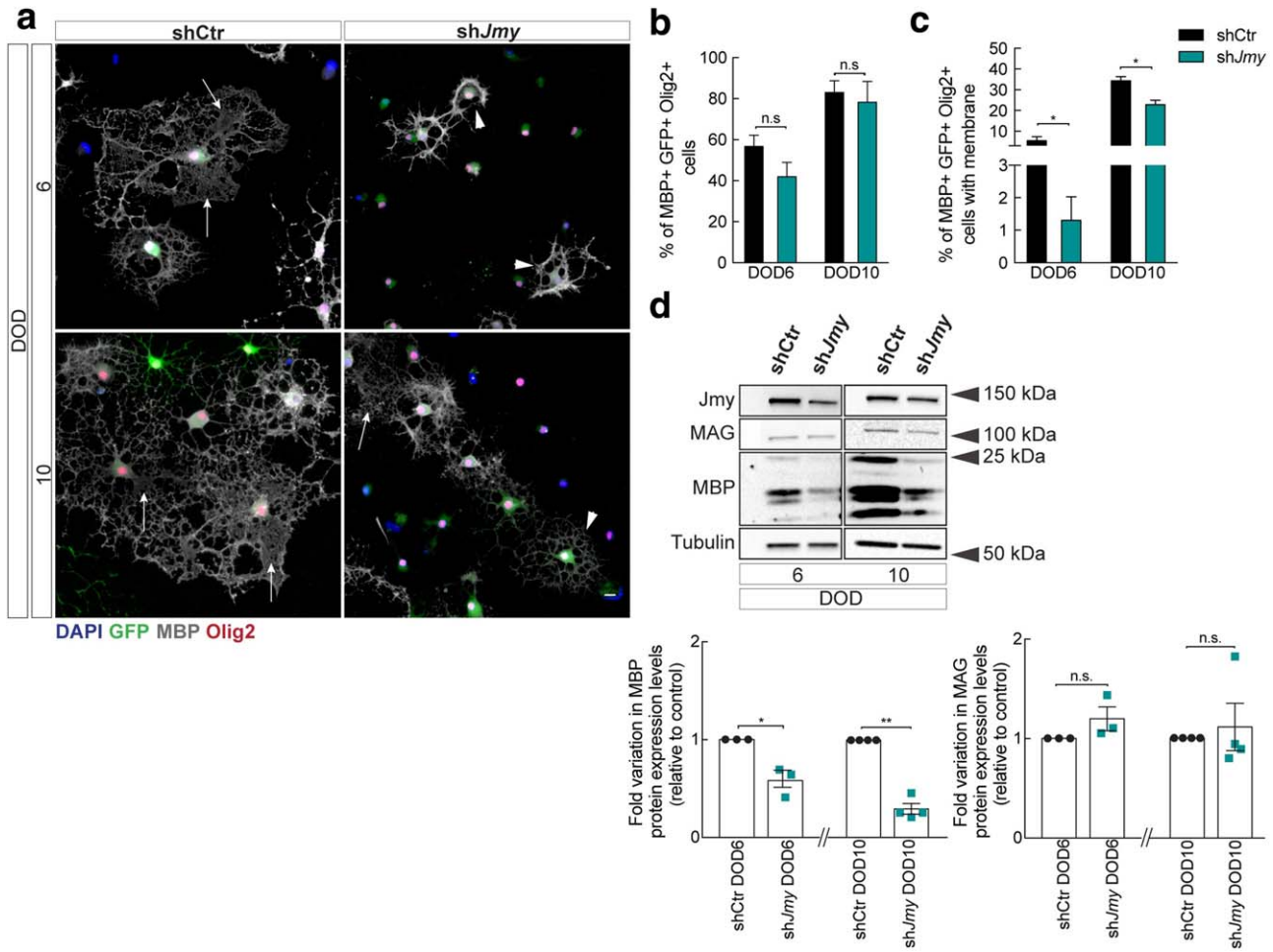

FIGURE 7 Jmy is required for the formation of MBP sheets by mature OLs. (a) Representative widefield images of ICC on shCtr- and sh*Jmy*-OLs during differentiation, labeled for MBP (red), Olig2 (gray) and nuclei (DAPI, blue). Mature OLs (seen at DOD 6 and 10) form membranous sheets containing MBP (arrows) that are rarely seen in sh*Jmy*-OLs, which display an immature morphology with a simple protrusion network (arrowheads). Images were processed using a nonlinear gamma change of 0.5. Scale bar is 10 μm. (b and c) Percentage of $MBP^+/GFP^+/Olig2^+$ cells (b) and sheet-forming OLs (c) was determined at DOD 6 or 10. Cells were labeled for MBP (red), Olig2 (gray), and nuclei (DAPI, blue). Data represented as mean ± *SEM* of $n = 6$ or $n = 3$ independent experiments for DOD6 and DOD10, respectively (n.s. = not significant, $^*p < .05$, calculated using unpaired *t* test). (d) Immunoblot analysis of MBP and MAG expression in total extracts from shCtr- and sh*Jmy*-OLs after 6 and 10 DODs. Data represented as mean of the fold variation to control of the relative densities ± *SEM* of $n = 3$ or $n = 4$ independent experiments for DOD6 and DOD10, respectively (n.s. = not significant, $^*p < .05$, $^{**}p < .001$, calculated using one-sample *t* test [for MBP] or Wilcoxon signed rank test [for MAG]) [Color figure can be viewed at wileyonlinelibrary.com]

structures (Simpson & Armstrong, 1999; Song et al., 2001). In addition to the large proteomics and transcriptomics screenings, recent studies have provided compelling evidence that actin dynamics directs myelination (Nawaz et al., 2015; Zuchero et al., 2015). A two-step model has emerged proposing that in the initial stages of myelination, actin polymerization is strong at the leading edge of the OL protrusion, as a crucial force-generating mechanism for extension of membrane protrusions in an adhesion-independent manner (Nawaz et al., 2015). We speculate that Jmy may be a key player in this process in two different ways. First, its intrinsic or complex-dependent actin nucleation activity is necessary for F-actin assembly in OLs, as seen in the STED analysis, driving protrusion formation and branching. Secondly, we observed that Jmy localizes to discrete areas of the cell, including in protrusions, with high concentration of F-actin. Knocking down levels of Jmy leads to an aberrant displacement of F-actin to the cell soma during OL differentiation, seen in the live-imaging experiments with Sir-Actin. Furthermore, the live-imaging and immunofluorescence analysis of axo-glia interaction in co-culture showed that OLs depleted of Jmy are less efficient at forming persistent OL-neurite contacts. These observations led us to consider the hypothesis that Jmy may be involved in the architecture of a specific actin network that creates cellular tension gradients in OLs, important for membrane deformation (Bovellan et al., 2014).

In a second phase during myelination, F-actin depolymerization reduces cell surface tension, allowing for lateral membrane spreading (Nawaz et al., 2015; Zuchero et al., 2015). Because OLs without Jmy fail to build a F-actin network at the leading edge of protrusions, this active process of depolymerization probably occurs to a lesser extent,

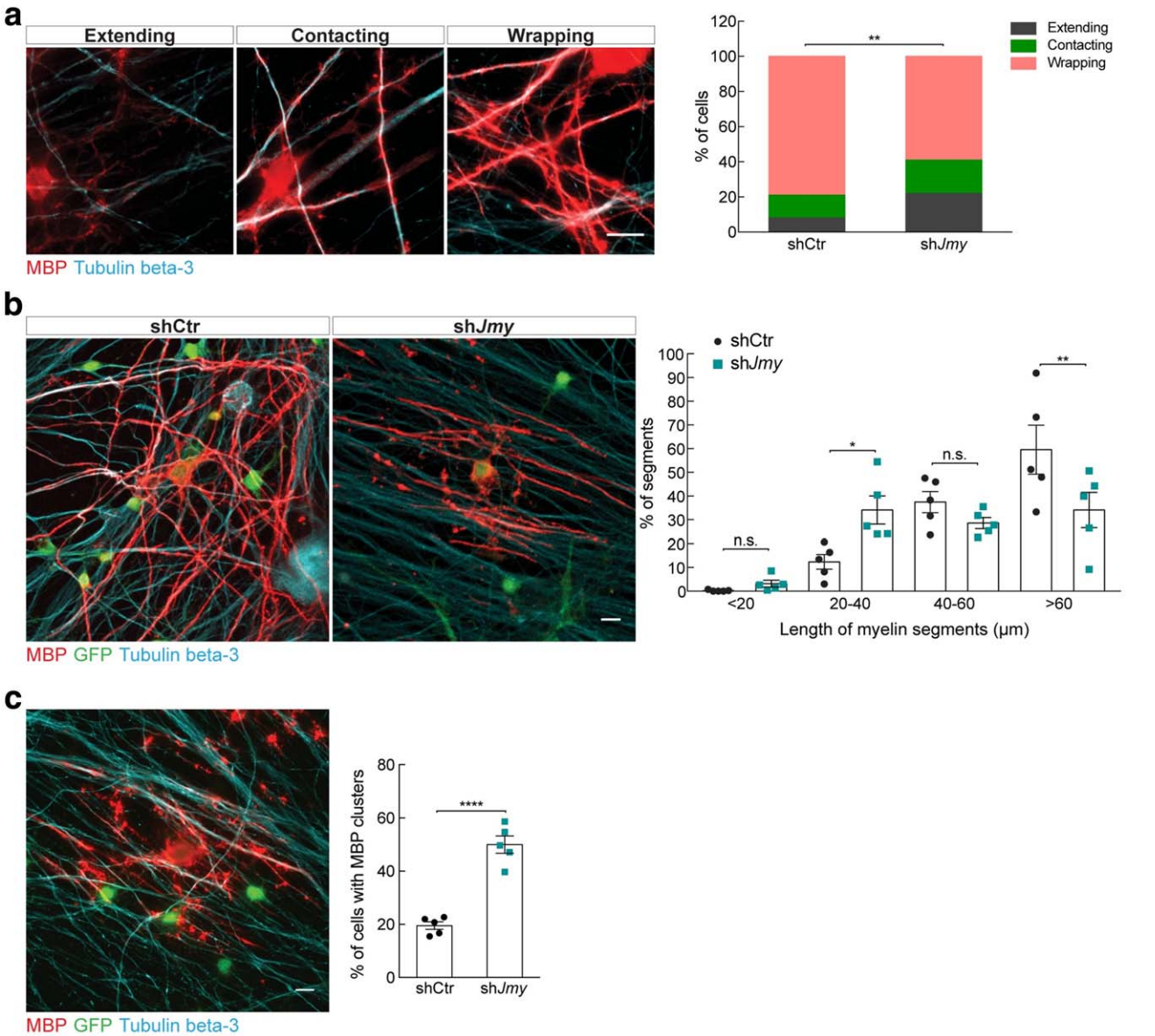

FIGURE 8 Jmy is required for neurite wrapping and formation of MBP segments in a myelinating co-culture. (a) Myelinating co-cultures of DRG neurons and shCtr- or sh*Jmy*-OLs. MBP$^+$ OLs were grouped into three different categories of morphological maturity, as shown in the representative images. After 18 days, co-cultures were fixed and ICC was performed for MBP (red), and Tubulin beta-3 (cyan), a neuronal marker. Data are represented as the percentage of cells counted in each category. The total cells analyzed were pooled from five independent experiments, with an average of 100 MBP$^+$ cells in each condition collected per experiment. A significant association was found between the shRNA and the stage of OL-neurite interaction ($\chi^2_{(2,\ N=1062)} = 10.56$, $p = .0051$, calculated using the Chi-square test). Scale bar is 10 μm. (b) Length distribution of MBP segments used as a readout for the ability of OLs to form internodes in a myelinating co-culture. Length measurement was performed in co-cultures of shCtr- or sh*Jmy*-OLs and binned into four groups. Data represented as mean ± *SEM* of $n = 5$ independent experiments (n.s. = not significant, $^{**}p < .01$, calculated using one-way ANOVA followed by Sidak's multiple comparisons test). Scale bar is 10 μm. (c) Percentage of shCtr- or sh*Jmy*-OLs in co-culture with aberrant MBP clusters. Data represented as mean ± *SEM* of $n = 5$ independent experiments ($^{****}p < .0001$, calculated using the unpaired *t* test). Scale bar is 10 μm [Color figure can be viewed at wileyonlinelibrary.com]

explaining why OLs form fewer membranous sheets *in vitro*, and shorter MBP segments in co-culture with neurites. Future studies *in vivo* will help to clarify which aspects of myelination are dependent of Jmy's function. For example, it is known that neuronal activity modulates protrusion formation in OLs and axon ensheathment (Hines, Ravanelli, Schwindt, Scott, & Appel, 2015; Mensch et al., 2015), the same way that the biophysical properties of axons or inert fibers do (Lee et al., 2012; Voyvodic, 1989). In this regard, it would be of particular interest to understand if these mechanical and electrochemical axon-derived cues regulate actin dynamics locally in the protrusions of OLs to influence the choice of axons to be myelinated during CNS development.

Actin nucleation is a feature of membrane projections in any cell, where these structures control, for example, movement, sensing, morphogenesis, and cell:cell interaction. While the machinery that regulates F-actin dynamics is generally well conserved from yeast to mammals (Campellone & Welch, 2010), Jmy is only found in vertebrates (Zuchero et al., 2009). Moreover, the precise role of actin regulators is somewhat cell context-dependent: the Arp2/3 complex, a key nucleator of actin networks found in lamellipodia, is required for the formation of filopodia in neurons (Korobova & Svitkina, 2008) but not in melanoma cells (Steffen et al., 2006; reviewed in Firat-Karalar & Welch, 2011); and different diaphanous-related formins, which nucleate linear actin filaments in filopodial protrusions, are required for the assembly of lamellipodia in specific cell types (reviewed in Bogdan, Schultz, & Grosshans, 2013). In what concerns Jmy, it is described as an inhibitor of neuritogenesis in a neuroblastoma cell line (Firat-Karalar et al., 2011), while in primary OLs we found it to be necessary for protrusion extension and branching. Even in the control of cell behavior, the function of Jmy is not identical in all cell types: it plays a role in migration of U2OS epithelial cells (Coutts et al., 2009; Zuchero et al., 2009), but migration defects are not seen in mouse embryonic and NIH3T3 fibroblasts upon its depletion (Firat-Karalar et al., 2011), despite the fact that in these cells Jmy also localizes to membrane ruffles. In conclusion, a unifying view of how similar actin-based protrusions are formed is still under investigation and assuming that, for example, a basic set of actin regulators play the same static role in protrusion formation in any cell is rather limiting. So, what makes the oligodendrocyte context special? First, the function of a membrane protrusion in immature OLs is unique in the sense that they have to contact, "survey" and in the end, choose which axons will be myelinated. Second, myelin thickness is regulated locally in response to variable axonal caliber (Waxman & Sims, 1984), implying that one single OL can perhaps adapt to sustain different specialized membranes with varying myelin content at the same time (Almeida, Czopka, Ffrench-Constant, & Lyons, 2011). In spite of this remarkable paradigm of "form follows function" in development, the molecular machinery that regulates actin dynamics in OLs remains poorly characterized. Future experimental studies are required to determine how different actin regulators work together to locally remodel the actin cytoskeleton in the protrusive structures of OLs.

Our findings suggest that Jmy may be a major regulator of actin polymerization in pro-myelinating OLs, either by its intrinsic activity of nucleating actin monomers into linear filaments, or by promoting the assembly of branched filaments via Arp2/3. Jmy is a unique actin-related protein, since it also acts as a transcriptional co-activator in the p53 response to cellular stress. The nuclear localization signal and actin nucleation domains overlap in Jmy and, after DNA damage, translocation of Jmy to the nucleus occurs in response to actin polymerization in the cytoplasm (Zuchero, Belin, & Mullins, 2012). But unlike in other cells, Jmy appears not to localize in the nucleus of OPCs or OLs and it is improbable that shuttling between the nucleus and the cytoplasm is a primary mechanism of regulating its function in these cells. Moreover, our subcellular fractionation shows that Jmy is not redistributed between the two compartments upon differentiation, and it localizes to sites of active F-actin assembly in the protrusions of pro-myelinating OLs. In light of our transcriptomics data, we speculate that, in OLs, Jmy may be regulated by local translation in specific cellular structures. However, one cannot exclude the possibility that, even if present in the nucleus at low levels, Jmy may have a nuclear role in OL differentiation. Because growth factor-induced differentiation of OLs activates a specific transcriptional program, it is tempting to hypothesize that Jmy could be involved in this process, either by directly regulating actin polymerization in the nucleus or by binding to its transcriptional co-activation partners. An interesting question that remains to be investigated is which upstream signaling molecules drive expression and activity of Jmy.

In the developing zebrafish, high protrusion dynamics is a feature of migratory OPCs and axon-contacting pre-myelinating OLs (Kirby et al., 2006). Our time-lapse imaging experiments and quantitative morphodynamics analysis show that, early in differentiation, OLs must undergo a specific program of stereotypical "cellular shaping" to mature and later assemble myelin-sheath like structures. After an initial period of fast protrusion remodeling, pre-myelinating OLs acquire a densely-arborized morphology with thin branches. This arborization is impaired in OLs with decreased levels of Jmy, which translates into deficient formation of sheets and arrested maturation. Our results suggest that the arborization step is a pre-requisite for the extension of myelin-like membranes in pro-myelinating OLs, since these specialized structures start to be formed in sites where protrusion retraction occurs. Accordingly, targeting of MBP in newly formed myelin sheaths results from the disassembly of actin in the cytoplasmic membrane (Nawaz et al., 2015).

OligoMacro is an open source ImageJ macro-toolset that was developed to analyze OL morphology during differentiation. It is a semi-automated tool that uses phase contrast microscopy time-lapse datasets to easily isolate, track and characterize the morphology of a large number of cells in time. OligoMacro benefits from ImageJ built-in functions to process images and extract data, and relies on the R software to generate plots. The vast majority of the tools available to perform semi-automated or full-automated analyses of cellular morphology require the use of fluorescence microscopy time-lapse datasets and are specifically designed or adapted to work with cells that present a less complex morphology (Carpenter et al., 2006; Tsygankov et al., 2014). We consider that OligoMacro can be a powerful tool to be used in different contexts because it can easily be improved and adapted to other cell types or to analyze fluorescence images and it does not require the user to master any particular programming language. OligoMacro is the first semi-automated tool specifically designed to study OLs behavior at the spatiotemporal scale.

In conclusion, we identified a protrusion-specific transcriptome in OLs that probably allows for local regulation of protrusion extension and myelin sheet assembly. One of those molecules is Jmy, an important regulator of actin cytoskeleton dynamics in oligodendrocytes, enabling morphological differentiation to be timely coordinated with myelin production.

ACKNOWLEDGMENT

We want to thank Dr. Joana Paes de Faria for helpful discussions and critical reading of the manuscript; Dr. Carolina Lemos for

assistance with statistical analyses; and Dr. António Pereira for helping with STED microscopy. The authors acknowledge the support of i3S Scientific Platforms: Advanced Light Microscopy, member of the national infrastructure PPBI-Portuguese Platform of BioImaging (supported by POCI-01–0145-FEDER-022122), the Translational Cytometry Unit and the Animal Facility. We also acknowledge the support of the Bordeaux Imaging Center, a service unit of CNRS-INSERM and Bordeaux University, member of the national infrastructure France BioImaging supported by the French National Research Agency (ANR-10-INBS-04). We also thank the Centro de Materiais da Universidade do Porto (CEMUP), the High-Throughput Genomics Group at the Wellcome Trust Centre for Human Genetics and the Bioinformatics Group of the Babraham Institute. This work was funded by FEDER funds through the Operational Competitiveness Programme – COMPETE – and by National Funds through FCT – Fundação para a Ciência e a Tecnologia – under the projects FCOMP-01–0124-FEDER 021333, NORTE-01–0145-FEDER-000008, and PTDC/SAU/NMC/119937/2010. M. A. is the recipient of a PhD scholarship from FCT (SFRH/BD/90301/2012), H. S. D. was supported by Marie Curie Actions (IEF 2010, #276322) and a FCT post-doctoral fellowship (reference SFRH/BPD/90268/2012), and A. I. S. is the recipient of a FCT postdoctoral fellowship (SFRH/BPD/79417/2011).

ORCID

Maria M. Azevedo http://orcid.org/0000-0001-7316-8283
Helena S. Domingues http://orcid.org/0000-0003-1230-2682
Ana I. Seixas http://orcid.org/0000-0003-3237-777X
João B. Relvas http://orcid.org/0000-0001-7636-0924

REFERENCES

Almeida, R. G., Czopka, T., Ffrench-Constant, C., & Lyons, D. A. (2011). Individual axons regulate the myelinating potential of single oligodendrocytes in vivo. *Development*, *138*(20), 4443–4450. https://doi.org/10.1242/dev.071001

Anders, S., & Huber, W. (2010). Differential expression analysis for sequence count data. *Genome Biology*, *11*(10), R106. https://doi.org/10.1186/gb-2010-11-10-r106

Baer, A. S., Syed, Y. A., Kang, S. U., Mitteregger, D., Vig, R., Ffrench-Constant, C., … Kotter, M. R. (2009). Myelin-mediated inhibition of oligodendrocyte precursor differentiation can be overcome by pharmacological modulation of Fyn-RhoA and protein kinase C signalling. *Brain*, *132*(2), 465–481. https://doi.org/10.1093/brain/awn334

Barry, D. J., Durkin, C. H., Abella, J. V., & Way, M. (2015). Open source software for quantification of cell migration, protrusions, and fluorescence intensities. *The Journal of Cell Biology*, *209*(1), 163–180. https://doi.org/10.1083/jcb.201501081

Bauer, N. G., Richter-Landsberg, C., & Ffrench-Constant, C. (2009). Role of the oligodendroglial cytoskeleton in differentiation and myelination. *Glia*, *57*(16), 1691–1705. https://doi.org/10.1002/glia.20885

Bhat, N. R., & Zhang, P. (1996). Activation of mitogen-activated protein kinases in oligodendrocytes. *J Neurochem*, *66*(5), 1986–1994.

Bogdan, S., Schultz, J., & Grosshans, J. (2013). Formin' cellular structures: Physiological roles of Diaphanous (Dia) in actin dynamics. *Communicative & Integrative Biology*, *6*(6), e27634. https://doi.org/10.4161/cib.27634

Bovellan, M., Romeo, Y., Biro, M., Boden, A., Chugh, P., Yonis, A., … Charras, G. (2014). Cellular control of cortical actin nucleation. *Current Biology*, *24*(14), 1628–1635. https://doi.org/10.1016/j.cub.2014.05.069

Buttery, P. C., & Ffrench-Constant, C. (2001). Process extension and myelin sheet formation in maturing oligodendrocytes. *Progress in Brain Research*, *132*, 115–130. https://doi.org/10.1016/S0079-6123(01)32070-8

Cahoy, J. D., Emery, B., Kaushal, A., Foo, L. C., Zamanian, J. L., Christopherson, K. S., … Barres, B. A. (2008). A transcriptome database for astrocytes, neurons, and oligodendrocytes: a new resource for understanding brain development and function. *The Journal of Neuroscience*, *28*(1), 264–278. https://doi.org/10.1523/JNEUROSCI.4178-07.2008

Campellone, K. G., & Welch, M. D. (2010). A nucleator arms race: cellular control of actin assembly. *Nature Reviews Molecular Cell Biology*, *11*(4), 237–251. https://doi.org/10.1038/nrm2867

Carpenter, A. E., Jones, T. R., Lamprecht, M. R., Clarke, C., Kang, I., Friman, O., … Sabatini, D. M. (2006). CellProfiler: image analysis software for identifying and quantifying cell phenotypes. *Genome Biology*, *7*(10), R100. https://doi.org/10.1186/gb-2006-7-10-r100

Chen, Y., Balasubramaniyan, V., Peng, J., Hurlock, E. C., Tallquist, M., Li, J., & Lu, R. Q. (2007). Isolation and culture of rat and mouse oligodendrocyte precursor cells. *Nature Protocols*, *2*(5), 1044–1051. https://doi.org/10.1038/nprot.2007.149

Coutts, A. S., Weston, L., & La Thangue, N. B. (2009). A transcription co-factor integrates cell adhesion and motility with the p53 response. *Proceedings of the National Academy of Sciences of the United States of America*, *106*(47), 19872–19877. https://doi.org/10.1073/pnas.0906785106

Dangata, Y. Y., & Kaufman, M. H. (1997). Myelinogenesis in the optic nerve of (C57BL x CBA) F1 hybrid mice: a morphometric analysis. *European Journal of Morphology*, *35*(1), 3–17.

Dugas, J. C., Tai, Y. C., Speed, T. P., Ngai, J., & Barres, B. A. (2006). Functional genomic analysis of oligodendrocyte differentiation. *Journal of Neuroscience*, *26*(43), 10967–10983. https://doi.org/10.1523/JNEUROSCI.2572-06.2006

Feltrin, D., Fusco, L., Witte, H., Moretti, F., Martin, K., Letzelter, M., … Pertz, O. (2012). Growth cone MKK7 mRNA targeting regulates MAP1b-dependent microtubule bundling to control neurite elongation. *PLoS Biology*, *10*(12), e1001439. https://doi.org/10.1371/journal.pbio.1001439

Ferreira, T. A., Blackman, A. V., Oyrer, J., Jayabal, S., Chung, A. J., Watt, A. J., … van Meyel, D. J. (2014). Neuronal morphometry directly from bitmap images. *Nature Methods*, *11*(10), 982–984. https://doi.org/10.1038/nmeth.3125

Firat-Karalar, E. N., Hsiue, P. P., & Welch, M. D. (2011). The actin nucleation factor JMY is a negative regulator of neuritogenesis. *Molecular Biology of the Cell*, *22*(23), 4563–4574. https://doi.org/10.1091/mbc.E11-06-0585

Firat-Karalar, E. N., & Welch, M. D. (2011). New mechanisms and functions of actin nucleation. *Current Opinion in Cell Biology*, *23*(1), 4–13. https://doi.org/10.1016/j.ceb.2010.10.007

Foran, D. R., & Peterson, A. C. (1992). Myelin acquisition in the central nervous system of the mouse revealed by an MBP-Lac Z transgene. *The Journal of Neuroscience*, *12*(12), 4890–4897.

Gumy, L. F., Yeo, G. S. H., Tung, Y.-C. L., Zivraj, K. H., Willis, D., Coppola, G., … Fawcett, J. W. (2011). Transcriptome analysis of embryonic and adult sensory axons reveals changes in mRNA repertoire localization. *RNA*, *17*(1), 85–98. https://doi.org/10.1261/rna.2386111

Hines, J. H., Ravanelli, A. M., Schwindt, R., Scott, E. K., & Appel, B. (2015). Neuronal activity biases axon selection for myelination in

vivo. *Nature Neuroscience*, *18*(5), 683–689. https://doi.org/10.1038/nn.3992

Holt, C. E., & Schuman, E. M. (2013). The central dogma decentralized: new perspectives on RNA function and local translation in neurons. *Neuron*, *80*(3), 648–657. https://doi.org/10.1016/j.neuron.2013.10.036

Hortega, P. R. (1928). *Tercera aportación al conocimiento morfológico e interpretación funcional de la oligodendroglía*: Museo Nacional de Ciencias Naturales.

Hughes, E. G., & Appel, B. (2016). The cell biology of CNS myelination. *Current Opinion in Neurobiology*, *39*, 93–100. https://doi.org/10.1016/j.conb.2016.04.013

Kachar, B., Behar, T., & Dubois-Dalcq, M. (1986). Cell shape and motility of oligodendrocytes cultured without neurons. *Cell and Tissue Research*, *244*(1), 27–38.

Kim, H. J., DiBernardo, A. B., Sloane, J. A., Rasband, M. N., Solomon, D., Kosaras, B., … Vartanian, T. K. (2006). WAVE1 is required for oligodendrocyte morphogenesis and normal CNS myelination. *Journal of Neuroscience*, *26*(21), 5849–5859. https://doi.org/10.1523/JNEUROSCI.4921-05.2006

Kirby, B. B., Takada, N., Latimer, A. J., Shin, J., Carney, T. J., Kelsh, R. N., & Appel, B. (2006). In vivo time-lapse imaging shows dynamic oligodendrocyte progenitor behavior during zebrafish development. *Nature Neuroscience*, *9*(12), 1506–1511. https://doi.org/10.1038/nn1803

Korobova, F., & Svitkina, T. (2008). Arp2/3 complex is important for filopodia formation, growth cone motility, and neuritogenesis in neuronal cells. *Molecular Biology of the Cell*, *19*(4), 1561–1574. https://doi.org/10.1091/mbc.E07-09-0964

Laursen, L. S., Chan, C. W., & Ffrench-Constant, C. (2011). Translation of myelin basic protein mRNA in oligodendrocytes is regulated by integrin activation and hnRNP-K. *The Journal of Cell Biology*, *192*(5), 797–811. https://doi.org/10.1083/jcb.201007014

Lawrence, J. B., & Singer, R. H. (1986). Intracellular localization of messenger RNAs for cytoskeletal proteins. *Cell*, *45*(3), 407–415.

Lee, S., Leach, M. K., Redmond, S. A., Chong, S. Y. C., Mellon, S. H., Tuck, S. J., … Chan, J. R. (2012). A culture system to study oligodendrocyte myelination processes using engineered nanofibers. *Nature Methods*, *9*(9), 917–922. https://doi.org/10.1038/nmeth.2105

Li, C., Tropak, M. B., Gerlai, R., Clapoff, S., Abramow-Newerly, W., Trapp, B., … Roder, J. (1994). Myelination in the absence of myelin-associated glycoprotein. *Nature*, *369*(6483), 747–750. https://doi.org/10.1038/369747a0

McCarthy, K. D., & de Vellis, J. (1980). Preparation of separate astroglial and oligodendroglial cell cultures from rat cerebral tissue. *Journal of Cell Biology*, *85*(3), 890–902.

Mensch, S., Baraban, M., Almeida, R., Czopka, T., Ausborn, J., El Manira, A., & Lyons, D. A. (2015). Synaptic vesicle release regulates myelin sheath number of individual oligodendrocytes in vivo. *Nature Neuroscience*, *18*(5), 628–630. https://doi.org/10.1038/nn.3991

Mili, S., Moissoglu, K., & Macara, I. G. (2008). Genome-wide screen reveals APC-associated RNAs enriched in cell protrusions. *Nature*, *453*(7191), 115–119. https://doi.org/10.1038/nature06888

Mingle, L. A., Okuhama, N. N., Shi, J., Singer, R. H., Condeelis, J., & Liu, G. (2005). Localization of all seven messenger RNAs for the actin-polymerization nucleator Arp2/3 complex in the protrusions of fibroblasts. *Journal of Cell Science*, *118*(11), 2425–2433. https://doi.org/10.1242/jcs.02371

Nawaz, S., Sánchez, P., Schmitt, S., Snaidero, N., Mitkovski, M., Velte, C., … Simons, M. IKAEL. (2015). Actin filament turnover drives leading edge growth during myelin sheath formation in the central nervous system. *Developmental Cell*, *34*(2), 139–151. https://doi.org/10.1016/j.devcel.2015.05.013

Nielsen, J. A., Maric, D., Lau, P., Barker, J. L., & Hudson, L. D. (2006). Identification of a novel oligodendrocyte cell adhesion protein using gene expression profiling. *The Journal of Neuroscience*, *26*(39), 9881–9891. https://doi.org/10.1523/JNEUROSCI.2246-06.2006

O'Meara, R. W., Michalski, J.-P., Anderson, C., Bhanot, K., Rippstein, P., & Kothary, R. (2013). Integrin-linked kinase regulates process extension in oligodendrocytes via control of actin cytoskeletal dynamics. *The Journal of Neuroscience*, *33*(23), 9781–9793. https://doi.org/10.1523/JNEUROSCI.5582-12.2013

Ozcelik, M., Cotter, L., Jacob, C., Pereira, J. A., Relvas, J. B., Suter, U., & Tricaud, N. (2010). Pals1 is a major regulator of the epithelial-like polarization and the extension of the myelin sheath in peripheral nerves. *Journal of Neuroscience*, *30*(11), 4120–4131. https://doi.org/10.1523/JNEUROSCI.5185-09.2010

Piper, M., Anderson, R., Dwivedy, A., Weinl, C., van Horck, F., Leung, K. M., … Holt, C. (2006). Signaling mechanisms underlying Slit2-induced collapse of Xenopus retinal growth cones. *Neuron*, *49*(2), 215–228. https://doi.org/10.1016/j.neuron.2005.12.008

Poitelon, Y., Bogni, S., Matafora, V., Della-Flora Nunes, G., Hurley, E., Ghidinelli, M., … Feltri, M. L. (2015). Spatial mapping of juxtacrine axo-glial interactions identifies novel molecules in peripheral myelination. *Nature Communications*, *6*(1), 8303. https://doi.org/10.1038/ncomms9303

Reimand, J., Arak, T., Adler, P., Kolberg, L., Reisberg, S., Peterson, H., & Vilo, J. (2016). g:Profiler-a web server for functional interpretation of gene lists (2016 update). *Nucleic Acids Research*, *44*(W1), W83–W89. https://doi.org/10.1093/nar/gkw199

Schafer, I., Muller, C., Luhmann, H. J., & White, R. (2016). MOBP levels are regulated by Fyn kinase and affect the morphological differentiation of oligodendrocytes. *Journal of Cell Science*, *129*(5), 930–942. https://doi.org/10.1242/jcs.172148

Schindelin, J., Arganda-Carreras, I., Frise, E., Kaynig, V., Longair, M., Pietzsch, T., … Cardona, A. (2012). Fiji: an open-source platform for biological-image analysis. *Nature Methods*, *9*(7), 676–682. https://doi.org/10.1038/nmeth.2019

Schneider, C. A., Rasband, W. S., & Eliceiri, K. W. (2012). NIH Image to ImageJ: 25 years of image analysis. *Nature Methods*, *9*(7), 671–675.

Shikama, N., Lee, C. W., France, S., Delavaine, L., Lyon, J., Krstic-Demonacos, M., & La Thangue, N. B. (1999). A novel cofactor for p300 that regulates the p53 response. *Molecular Cell*, *4*(3), 365–376.

Simons, M., & Nave, K. A. (2015). Oligodendrocytes: Myelination and Axonal Support. *Cold Spring Harb Perspect Biol*, *8*(1), a020479. https://doi.org/10.1101/cshperspect.a020479

Simpson, P. B., & Armstrong, R. C. (1999). Intracellular signals and cytoskeletal elements involved in oligodendrocyte progenitor migration. *Glia*, *26*(1), 22–35.

Song, J., Goetz, B. D., Baas, P. W., & Duncan, I. D. (2001). Cytoskeletal reorganization during the formation of oligodendrocyte processes and branches. *Molecular and Cellular Neuroscience*, *s*, *17*(4), 624–636. https://doi.org/10.1006/mcne.2001.0974

Steffen, A., Faix, J., Resch, G. P., Linkner, J., Wehland, J., Small, J. V., … Stradal, T. E. (2006). Filopodia formation in the absence of functional WAVE- and Arp2/3-complexes. *Molecular Biology of the Cell*, *17*(6), 2581–2591. https://doi.org/10.1091/mbc.E05-11-1088

Thurnherr, T., Benninger, Y., Wu, X., Chrostek, A., Krause, S. M., Nave, K.-A., … Relvas, J. B. (2006). Cdc42 and Rac1 signaling are both required for and act synergistically in the correct formation of myelin sheaths in the CNS. *Journal of Neuroscience*, *26*(40), 10110–10119. https://doi.org/10.1523/JNEUROSCI.2158-06.2006

Tsygankov, D., Bilancia, C. G., Vitriol, E. A., Hahn, K. M., Peifer, M., & Elston, T. C. (2014). CellGeo: a computational platform for the analysis

of shape changes in cells with complex geometries. *The Journal of Cell Biology*, *204*(3), 443–460. https://doi.org/10.1083/jcb.201306067

Ventura, A., Meissner, A., Dillon, C. P., McManus, M., Sharp, P. A., Van Parijs, L., … Jacks, T. (2004). Cre-lox-regulated conditional RNA interference from transgenes. *Proceedings of the National Academy of Sciences of the United States of America*, *101*(28), 10380–10385. https://doi.org/10.1073/pnas.0403954101

Voyvodic, J. T. (1989). Target size regulates calibre and myelination of sympathetic axons. *Nature*, *342*(6248), 430–433. https://doi.org/10.1038/342430a0

Waxman, S. G., & Sims, T. J. (1984). Specificity in central myelination: evidence for local regulation of myelin thickness. *Brain Research*, *292*(1), 179–185.

Wilson, R., & Brophy, P. J. (1989). Role for the oligodendrocyte cytoskeleton in myelination. *Journal of Neuroscience Research*, *22*(4), 439–448. https://doi.org/10.1002/jnr.490220409

Zhang, Y., Chen, K., Sloan, S. A., Bennett, M. L., Scholze, A. R., O'Keeffe, S., … Wu, J. Q. (2014). An RNA-sequencing transcriptome and splicing database of glia, neurons, and vascular cells of the cerebral cortex. *The Journal of Neuroscience*, *34*(36), 11929–11947. https://doi.org/10.1523/JNEUROSCI.1860-14.2014

Zivraj, K. H., Tung, Y. C., Piper, M., Gumy, L., Fawcett, J. W., Yeo, G. S., & Holt, C. E. (2010). Subcellular profiling reveals distinct and developmentally regulated repertoire of growth cone mRNAs. *Journal of Neuroscience*, *30*(46), 15464–15478. https://doi.org/10.1523/JNEUROSCI.1800-10.2010

Zuchero, J. B., Belin, B., & Mullins, R. D. (2012). Actin binding to WH2 domains regulates nuclear import of the multifunctional actin regulator JMY. *Molecular Biology of the Cell*, *23*(5), 853–863. https://doi.org/10.1091/mbc.E11-12-0992

Zuchero, J. B., Coutts, A. S., Quinlan, M. E., Thangue, N. B., & Mullins, R. D. (2009). p53-cofactor JMY is a multifunctional actin nucleation factor. *Nature Cell Biology*, *11*(4), 451–459. https://doi.org/10.1038/ncb1852

Zuchero, J. B., Fu, M. -M., Sloan, S. A., Ibrahim, A., Olson, A., Zaremba, A., … Barres, B. A. (2015). CNS myelin wrapping is driven by actin disassembly. *Developmental Cell*, *34*(2), 152–167. https://doi.org/10.1016/j.devcel.2015.06.011

SUPPORTING INFORMATION

Additional Supporting Information may be found online in the supporting information tab for this article.

How to cite this article: Azevedo MM, Domingues HS, Cordelières FP, Sampaio P, Seixas AI, Relvas JB. Jmy regulates oligodendrocyte differentiation via modulation of actin cytoskeleton dynamics. *Glia*. 2018;00:1–19. https://doi.org/10.1002/glia.23342